

Optimal Control Design  
for a  
Solar Greenhouse

Rachel Joanna Catharina van Ooteghem

*Promotor*

PROF.DR.IR. G. VAN STRATEN  
hoogleraar Meet-, Regel- en Systeemtechniek

*Co-promotor*

DR.IR. L.G. VAN WILLIGENBURG  
universitair docent, leerstoelgroep Meet-, Regel- en Systeemtechniek

*Leden van de promotiecommissie*

PROF.DR.IR. P.M.J. VAN DEN HOF  
Technische Universiteit Delft, Delft, Nederland

PROF.DR.IR. E.J. VAN HENTEN  
Wageningen Universiteit, Wageningen, Nederland

PROF.DR. O. VAN KOOTEN  
Wageningen Universiteit, Wageningen, Nederland

DR.IR. T.A. RIESWIJK  
PRIVA B.V., De Lier, Nederland

PROF.DR.IR. G.P.A. BOT  
Wageningen Universiteit, Wageningen, Nederland

Dit onderzoek is uitgevoerd binnen de onderzoekschool  
PE&RC (Production Ecology and Resource Conservation).

Optimal Control Design

for a

Solar Greenhouse

Rachel Joanna Catharina van Ooteghem

PROEFSCHRIFT

TER VERKRIJGING VAN DE GRAAD VAN DOCTOR

OP GEZAG VAN DE RECTOR MAGNIFICUS

VAN WAGENINGEN UNIVERSITEIT

PROF.DR. M.J. KROPFF

IN HET OPENBAAR TE VERDEDIGEN

OP WOENSDAG 10 JANUARI 2007

DES NAMIDDAGS OM VIER UUR IN DE AULA

CIP gegevens Koninklijke Bibliotheek, Den Haag

R.J.C. van Ooteghem, 2007,  
Optimal control design for a solar greenhouse  
Ph.D. thesis Wageningen University  
with summaries in English and Dutch.

Keywords: greenhouse, solar greenhouse,  
greenhouse model, model validation,  
optimal control, crop biophysics

ISBN 90-8504-569-x

# Abstract

The research of this thesis was part of a larger project aiming at the design of a greenhouse and an associated climate control that achieves optimal crop production with sustainable instead of fossil energy. This so called solar greenhouse design extends a conventional greenhouse with an improved roof cover, ventilation with heat recovery, a heat pump, a heat exchanger and an aquifer. This thesis describes the design of an optimal control strategy for the solar greenhouse, to ensure that the benefits of this innovative greenhouse are exploited in the best possible way.

The ingredients of an optimal control design are a dynamic model for greenhouse and crop, an explicitly formulated cost function, and a solution method. The advantages of this systematic approach are that scientific knowledge concerning the greenhouse and the crop is fully exploited, and with a goal that is stated in clear and transparent quantitative terms, it computes the best possible control. Furthermore it gives flexibility because the control is automatically adjusted when economic or other factors determining the cost function are changed. The control objectives used here are: minimize gas use and maximize crop yield, development and quality. Since the optimal control fully relies on the cost function and the dynamic model, this model must give a good description of the system response for a wide range of temperature and humidity conditions.

The first major contribution of this thesis is the development of a comprehensive, science-based, dynamic model of the greenhouse-with-crop system in a form that is suitable for optimal control purposes. The model describes the temperature, the carbondioxide balance and the water vapour balance in the greenhouse, as a function of the external inputs (i.e. the outdoor weather conditions) and the control inputs (e.g. valve positions and window apertures). This model has been validated with data, and was found to give a good description of reality.

The second major contribution of this thesis is the design of the optimal controller, including an efficient solution technique. A conjugate gradient search is used as the ultimate fine-tuning method, but it has the risk of achieving local minima, and it is time consuming. Therefore, a grid search method has been designed to provide a good initial guess for the gradient search method. This method uses only a small number of discrete constant control trajectories, which are then modified with rule based state dependent control input bounds to obtain initial control trajectories.

Receding horizon optimal control has been used for year-round computations of the solar greenhouse with crop. Extensive analyses have been made of the effect of various components of the solar greenhouse system and of the uncertainty in weather. Growers should be aware that setting tighter humidity bounds increases energy use. It was found that in the optimally controlled solar greenhouse, gas use can be seriously reduced (by 52%), while the crop production is significantly increased (by 39%), as compared to an optimally controlled conventional greenhouse without the solar greenhouse elements.

# Index

<b>Abstract</b>	<b>v</b>
<b>1 Introduction</b>	<b>1</b>
1.1 The solar greenhouse project . . . . .	1
1.2 Optimal control . . . . .	3
1.3 The greenhouse-with-crop model . . . . .	5
1.4 Outline of this thesis . . . . .	6
References . . . . .	7
Appendix . . . . .	10
1.A Smoothing function . . . . .	10
<b>2 Model of crop biophysics</b>	<b>13</b>
2.1 Introduction . . . . .	13
2.2 Evapotranspiration . . . . .	15
2.3 Crop photosynthesis and respiration . . . . .	18
2.4 Temperature integration . . . . .	34
References . . . . .	38
Appendices . . . . .	41
2.A Photosynthesis models . . . . .	41
2.B Solar radiation parameters . . . . .	43
2.C Humidity parameters . . . . .	51
<b>3 Solar greenhouse model</b>	<b>55</b>
3.1 Introduction . . . . .	55
3.2 System description . . . . .	58
3.3 Carbondioxide model . . . . .	67
3.4 Water vapour model . . . . .	70
3.5 Thermal model . . . . .	74
3.6 Modelling the screen . . . . .	96
3.7 Modelling ventilation . . . . .	100

3.8	Modelling the heating and the cooling system . . . . .	102
3.9	Validation conventional greenhouse model . . . . .	114
	References . . . . .	125
	Appendices . . . . .	127
3.A	View factors . . . . .	127
3.B	Derivation temperature leaving heating or cooling net . . . . .	131
3.C	Derivation temperature soil . . . . .	133
3.D	Derivation temperature roof outdoor side . . . . .	135
3.E	Derivation heat pump equations . . . . .	139
3.F	Derivation heat exchanger equations . . . . .	144
3.G	Sensitivity analysis and Fisher information matrix . . . . .	145
<b>4</b>	<b>Optimal control of a solar greenhouse</b>	<b>149</b>
4.1	Introduction . . . . .	149
4.2	Greenhouse-with-crop model . . . . .	151
4.3	The RHOC controller: methodology and implementation . . . . .	152
4.4	Open loop optimal control ( $\mathcal{PI}$ ) . . . . .	177
4.5	Open loop optimal control ( $TI$ ) . . . . .	188
4.6	Receding horizon optimal control, grid search ( $TI$ ) . . . . .	199
4.7	Receding horizon optimal control, gradient search ( $TI$ ) . . . . .	204
4.8	Comparisons . . . . .	214
4.9	Conclusions and discussion . . . . .	225
	References . . . . .	237
	<b>Summary</b>	<b>241</b>
	<b>Samenvatting</b>	<b>251</b>
	<b>Dankwoord</b>	<b>261</b>
	<b>Curriculum Vitae</b>	<b>263</b>
	<b>References</b>	<b>267</b>
	<b>Appendices</b>	<b>275</b>
<b>A</b>	<b>List of figures and tables</b>	<b>275</b>
	List of figures . . . . .	275
	List of tables . . . . .	277
<b>B</b>	<b>List of variables and parameters</b>	<b>279</b>

# Chapter 1

## Introduction

Greenhouse horticulture is an important branch of industry for the Dutch economy. The Dutch climate with cool summers and mild winters is favourable for greenhouse crop production. The intensive crop production however involves high input of fossil energy, pesticides and nutrients. Without proper precautions this will lead to unacceptable emissions to groundwater and atmosphere. Agreements have been made with the government to reduce these emissions. Solutions are being developed in practice and in research. Pest management is being performed in a biological way where possible, and water recycling systems for nutrient dosage are being used to strongly reduce emission.

According to an agreement between the government and the greenhouse industry, the energy efficiency index must be decreased by 65% in 2010 compared to 1980. The energy efficiency index is a measure for the primary gas use per unit product, defined relative to the year 1980. The consumption of natural gas in greenhouse horticulture was about 10% of the total national consumption in 2004. The natural gas consumption per unit product has decreased. The total usage per unit greenhouse area however, has increased during the past years, and is now stabilizing (see figure 1.1).

### 1.1 The solar greenhouse project

The goal of the ‘solar greenhouse project’ was to come to a greenhouse that makes better use of the (sustainable) solar radiation energy, to obtain a major reduction of the total energy use, while the fossil energy use is reduced

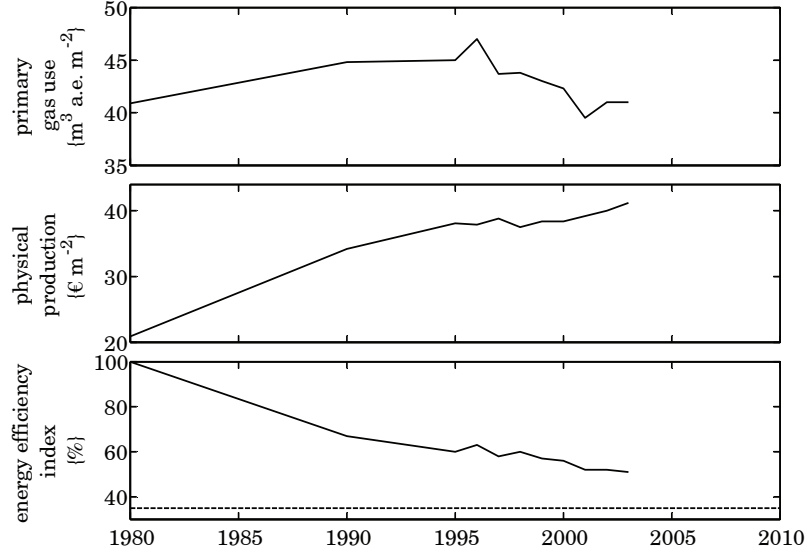


Figure 1.1: Gas use  $\{\text{m}^3 \text{ a.e. m}^{-2}[\text{soil}]\}$ , production  $\{\text{€ m}^{-2}[\text{soil}]\}$  and energy efficiency index  $\{\%\}$  (van der Knijff et al., 2006) a.e. = natural gas equivalent

(preferably to zero). This would also lead to a substantial reduction of the  $\text{CO}_2$  exhaust.

The following project parts were defined:

1. Lower the energy demand of the greenhouse
2. Balance the energy requirement of the greenhouse to the supply of sustainable energy
3. Use optimal control to control the resulting complex production system

Part 1 and 2 were concerned with the design and dimensioning of the solar greenhouse and the exploration of the crop tolerances for temperature and humidity (Körner, 2003). These parts of the project were conducted by other project partners.

This thesis describes part 3, where the control strategy is designed for the new greenhouse. The solar greenhouse project was set up as a feasibility study to investigate the possibilities for energy reduction. No actual greenhouse was built. While experimental work was done to test some of the system components and concepts for the project parts 1 and 2 (e.g., ventilation with heat recovery, heat pump and temperature integration), project part 3 had to be done entirely ‘in silico’.

The new greenhouse design proposed maximizes solar energy use and minimizes fossil energy consumption. The solar greenhouse has the following extensions compared to a conventional greenhouse:

- A heat pump and a heat exchanger to withdraw and store heat in the aquifer.
- Ventilation with heat recovery to be used to reduce humidity with less heat loss than regular ventilation through the windows.
- CO<sub>2</sub> supply independent of boiler operation. Since the goal is to minimize the fossil energy use, CO<sub>2</sub> must be retrieved from another source.
- Roof cover material with an improved insulation value and improved light transmission. More light means more crop yield, and better insulation means less heat loss, so lower energy consumption.

Although these extensions make the solar greenhouse more complex, they also provide us with additional possibilities for control.

In this thesis, this so called solar greenhouse design is integrated with climate control to obtain optimal crop growth conditions. Model based receding horizon optimal control is used to maximize solar energy use, minimize fossil energy consumption and obtain a high quality crop yield. Optimal control in combination with temperature integration allows the greenhouse temperature to vary over a wider range than is commonly used in order to minimize energy use.

## 1.2 Optimal control

The setting and tuning of conventional greenhouse climate controllers is by no means an easy or standard procedure. The large number of greenhouse controller settings (up to a few hundred) and weather dependant corrections on these settings make it difficult to foresee the influence on the results and the costs involved.

Greenhouse climate management can be significantly improved by implementing advanced controllers designed by using optimal control theory (van Henten, 1994; Tap, 2000; de Graaf, 2006). The performance improvements mainly concern energy efficiency and profit. Another important advantage of optimal controllers is their small number of settings (in the order of 10), which are very transparent.

With a dynamic model that describes the behaviour of the greenhouse-with-crop in time plus a weather prediction, the influence of control adjustments can be simulated over a specific time horizon. A goal is formulated in the form of a cost function that describes the energy cost and the crop yield.

With a search procedure the control inputs are computed that minimize this cost function. Feedback is achieved by repeating this procedure at a next time point with the incorporation of new measurement data. Feedback is necessary to correct for differences between model predictions and reality. This form of optimal control with feedback is called ‘receding horizon optimal control’ (RHOC), which is a special form of ‘model predictive control’ (MPC).

The performance improvements realized by optimal greenhouse climate controllers relate to the explicit detailed quantitative scientific knowledge they exploit. This knowledge concerns the behaviour of the crop in relation to the greenhouse climate and the behaviour of the greenhouse climate in relation to the outside weather conditions and the controls, which is incorporated in the dynamic model. It also concerns the costs associated to greenhouse climate management and control like heating and CO<sub>2</sub> supply, as well as the yield obtained from selling the crops, which are incorporated in the cost function. Current greenhouse climate control systems have to be set and tuned regularly by the growers. When setting and tuning the controllers, growers focus mainly on the quality of the crops and less on the costs of the control actions involved.

Although, in principal, optimal control has the above mentioned huge advantages, the improvements that will be obtained in practice depend critically on the accuracy and validity of the dynamic model and the cost function. Together the dynamic model and the cost function make up an optimal control problem. Within this thesis this optimal control problem will be solved numerically.

The formulation of the cost function is an important part of the optimal control system design, since it heavily influences the performance of the optimal control system. Especially for the solar greenhouse, which contains additional equipment when compared to a conventional greenhouse, the influence and complications of these additional elements has to be studied carefully.

Receding horizon optimal controllers and their simulation are known to be computationally ‘expensive’ because during every sampling period an optimal control problem must be solved. To relax the computational burden a highly simplified grid search method is developed in this thesis. This method is used to simulate the year-round receding horizon optimal control of the greenhouse-with-crop within 8 hours. The grid search method computes a suboptimal control using only a few discrete control input values and some a priori knowledge of the optimal control problem.

It was found that the conjugate gradient search procedure used in this research to compute the ‘true’ optimal control tends to get stuck in local minima. A

wisely chosen starting point for the control input values increases the probability that the global minimum is found. The results of the grid search method are therefore also used as a starting point for this minimization. The conjugate gradient search method can perform the full year-round computation in 8 days.

Optimal control further requires the model to be smooth. This implies that no transitions or switches are allowed within the model description. Since most models do include non-smooth relations, which are described by case structures (if/else) or min/max functions, a smoothing function is introduced to smooth these relations. This smoothing function is described in §1.A. It is important to note that for reasons of readability in the model equations given throughout this thesis the non-smooth functions are listed.

### 1.3 The greenhouse-with-crop model

A major contribution of this thesis is the construction and comprehensive documentation of a detailed, accurate and mainly first principles dynamic model for a greenhouse with crop. This model can be used for the solar greenhouse as well as for a conventional greenhouse. Although several publications have appeared in the past decades on optimal greenhouse climate control, these publications use models that are very much simplified, under assumptions that deteriorate their accuracy in actual practice (Ioslovich and Seginer, 1998; Udink ten Cate, 1983; Tap, 2000). The more detailed models that exist (Bot, 1983; de Zwart, 1996) are not directly suitable for optimal control purposes because they hold too many states. Therefore existing models (van Henten, 1994; de Zwart, 1996; Bot, 1983; de Jong, 1990) for conventional greenhouses were combined and were simplified to obtain a model suitable for optimal control. People concerned with modelling crop behaviour generally focused only on a part of this behaviour (Farquhar et al., 1980; Farquhar and von Caemmerer, 1982; Farquhar, 1988; Gijzen, 1994; Nederhoff, 1994; Stanghellini, 1987). For optimal control purposes the model must describe the full behaviour of the greenhouse climate and the crop. Furthermore the model must hold under all practical circumstances. To develop such a model turned out to be a real challenge.

The dynamic models presented in this thesis are the outcome of extensive literature research and the verification against several data sets containing realistic data. Large parts of the greenhouse-with-crop model are based on research of other scientists, who studied a part of the greenhouse or the crop

behaviour. A careful selection has been made to find the most suitable information. Some model parts had to be simplified, because the original description was too detailed or demanded too much computation time. Not surprisingly, in the course of this process several errors and inconsistencies have also been remedied. Other parts of the model were designed specifically for this research since no models were readily available. Care was taken to describe the model over a wide temperature and humidity range, since these ranges may not be as restricted in the solar greenhouse as in a conventional greenhouse. This research finally resulted in an accurate, detailed dynamic model of the (conventional or solar) greenhouse with crop.

The crop model should describe the crop growth and development. Particularly for crop development no simple accurate models exist. More elaborate models do exist, but they work on a large timescale compared to the horizon of the optimal controller, hold many crop development stages or are too crop specific. A simple approach to describe these long(er) term effects is temperature integration, which is used by many growers. Therefore a temperature integral concept was specifically designed for the solar greenhouse (Körner et al., 2002; Körner and Challa, 2003) to describe the long-term effects of the indoor temperature on crop growth and development. In combination with the wider range for the greenhouse temperature, the temperature integral is meant to ensure that a specific average temperature is attained, which should be a measure for good crop development.

Because for engineering and optimal control purposes it is very important to fully document the model and the underlying reasoning, the presentation of the model will be complete and therefore detailed and is motivated whenever necessary.

## 1.4 Outline of this thesis

The model of the crop biophysics is developed in chapter 2. The crop biophysics model holds submodels for: photosynthesis, respiration, evapotranspiration and temperature integration. This model has been developed based on research by Farquhar (1988), Goudriaan (1987), Heuvelink (1996), Gijzen (1994), Stanghellini (1987) and Körner (2003).

The solar greenhouse model is described in chapter 3. This model has been developed based on research by Van Henten (1994), De Zwart (1996), Bot (1983) and De Jong (1990), as far as it is describing the conventional greenhouse. Submodels had to be designed specifically for this research for the solar

greenhouse extensions, such as the heat pump and the heat exchanger. Some of the model parts by De Zwart (1996) were too elaborate or called for too many states in the dynamic model, and were therefore simplified to decrease computation time. The model of the conventional greenhouse with crop is validated with data to ensure that the model gives an accurate description of reality.

A full list of variables and parameters is given in appendix B.

The optimal control of the solar greenhouse is described in chapter 4. It presents a feasibility study of the optimal control of the solar greenhouse, since unfortunately the solar greenhouse only exists on paper. In the simulations it is attempted to approach reality as closely as possible. Small time scale computations (1 day) were done to test the optimal controller settings. Then year-round computations were performed for the solar greenhouse, as well as for a non-solar greenhouse (without solar greenhouse extensions). It will be shown that a 50% gas use reduction can be obtained using the solar greenhouse compared to a non-solar greenhouse with the same crop yield.

## References

- R. Baldick, A. Kahng, A. Kennings, and I. Markov (1999). Function smoothing with applications to VLSI layout. In: *ASP-DAC*, pp. 225–228, IEEE Computer Society, Los Alamitos, CA, USA. Asia and South Pacific Design Automation Conference 1999 (ASP-DAC 99).
- G.P.A. Bot (1983). *Greenhouse climate: from physical processes to a dynamic model*. Ph.D. thesis, Wageningen Agricultural University, Wageningen, The Netherlands. 240 p.
- S.C. de Graaf (2006). *Low nitrate lettuce cultivations in greenhouses: optimal control in the presence of measurable disturbances*. Ph.D. thesis, Wageningen Agricultural University, Wageningen, The Netherlands. 138 p.
- T. de Jong (1990). *Natural ventilation of large multi-span greenhouses*. Ph.D. thesis, Wageningen Agricultural University, Wageningen, The Netherlands.
- H.F. de Zwart (1996). *Analyzing energy-saving options in greenhouse cultivation using a simulation model*. Ph.D. thesis, Wageningen Agricultural University, Wageningen, The Netherlands. 236 p.
- G.D. Farquhar (1988). Models relating subcellular effects of temperature to whole plant responses. In: *Plants and temperature*, vol. 42, pp. 395–409. Society for experimental biology; Editors: S.P. Long and F.I. Woodward.

- G.D. Farquhar and S. von Caemmerer (1982). Modelling of photosynthetic response to environmental conditions. In: *Encyclopedia of plant physiology, New series; Physiological Plant Ecology II*, vol. 12B, pp. 549–587, Springer-Verlag, Heidelberg, Germany. Editors: O.L. Lange, P.S. Nobel, and H. Ziegler.
- G.D. Farquhar, S. von Caemmerer, and J.A. Berry (1980). A biochemical model of photosynthetic CO<sub>2</sub> assimilation in leaves of C<sub>3</sub> species. *Planta*, 149, pp. 78–90.
- J. Goudriaan (1987). *Simulatie van gewasgroei*. Wageningen Agricultural University, the Netherlands. (in Dutch).
- H. Gijzen (1994). Ontwikkeling van een simulatiemodel voor transpiratie en wateropname en van een integraal gewasmodel. AB-DLO, rapport 18, Wageningen, The Netherlands. (in Dutch).
- E. Heuvelink (1996). *Tomato growth and yield: quantitative analysis and synthesis*. Ph.D. thesis, Wageningen Agricultural University, Wageningen, The Netherlands. 326 p.
- I. Ioslovich and I. Seginer (1998). Approximate seasonal optimization of the greenhouse environment for a mulit-state-variable tomato model. *Transactions of the ASAE*, 41(4), pp. 1139–1149.
- O. Körner (2003). *Crop based climate regimes for energy saving in greenhouse cultivation*. Ph.D. thesis, Wageningen University, Wageningen, The Netherlands.
- O. Körner and H. Challa (2003). Design for an improved temperature integration concept in greenhouse cultivation. *Computers and Electronics in Agriculture*, 39(1), pp. 39–59.
- O. Körner, H. Challa, and R.J.C. van Ooteghem (2002). Modelling temperature effects on crop photosynthesis at high radiation in a solar greenhouse. *Acta Horticulturae*, 593, pp. 137–144.
- E.M. Nederhoff (1994). *Effects of CO<sub>2</sub> concentration on photosynthesis, transpiration and production of greenhouse fruit vegetable crops*. Ph.D. thesis, Wageningen Agricultural University, Wageningen, The Netherlands. 213 p.
- C. Stanghellini (1987). *Transpiration of greenhouse crops — an aid to climate management*. Ph.D. thesis, Wageningen Agricultural University, Wageningen, The Netherlands. 150 p.
- R.F. Tap (2000). *Economics-based optimal control of greenhouse tomato crop production*. Ph.D. thesis, Wageningen Agricultural University, Wageningen, The Netherlands.
- A.J. Udink ten Cate (1983). *Modeling and (adaptive) control of greenhouse climates*. Ph.D. thesis, Wageningen Agricultural University, Wageningen, The Netherlands.

- A. van der Knijff, J. Benninga, C. Reijnders, and J. Nienhuis (2006). Energie in de glastuinbouw van nederland; ontwikkelingen in de sector en op de bedrijven tot en met 2004. Rapport 3.06.02, LEI, Den Haag, The Netherlands. (in Dutch), 77 p.
- E.J. van Henten (1994). *Greenhouse climate management: an optimal control approach*. Ph.D. thesis, Wageningen Agricultural University, Wageningen, The Netherlands. 329 p.

## Appendix chapter 1

### 1.A Smoothing function

In the model description, case structures like

$$Y = \begin{cases} 2.8 + 1.2 X & \forall X < 4 \\ 2.5 X^{0.8} & \forall X \geq 4 \end{cases} \quad (1.1)$$

(heat transfer coefficient  $\alpha_{ro,o}$ ) occur.

These structures lead to a discontinuity in the derivative of the variable  $Y$  (here even in the variable  $Y$  itself) at the switch value  $X = 4$ . The same problem is found in equations where a minimum or a maximum value is used. For optimal control purposes these equations should be smoothed. All equations containing case structures (if/else), min- or max-functions are therefore smoothed.

The general case structure is smoothed using the following sigmoid equation

$$\Sigma(\Delta X, \varsigma) = \frac{1}{1 + 10^{-\varsigma \cdot \Delta X}} \quad (1.2)$$

where  $\varsigma$  is the slope and  $\Delta X = X - X_s$ , in which  $X_s$  is the switch value for  $X$ . The function  $\Sigma$  is equal to 0 when  $\Delta X \ll 0$ , equal to 1 when  $\Delta X \gg 0$  and a smooth function from 0 to 1 in between. In figure 1.2 the smoothing function  $\Sigma$  is given for a number of values for the slope  $\varsigma$ . In this thesis the value  $\varsigma = 10$  is used.

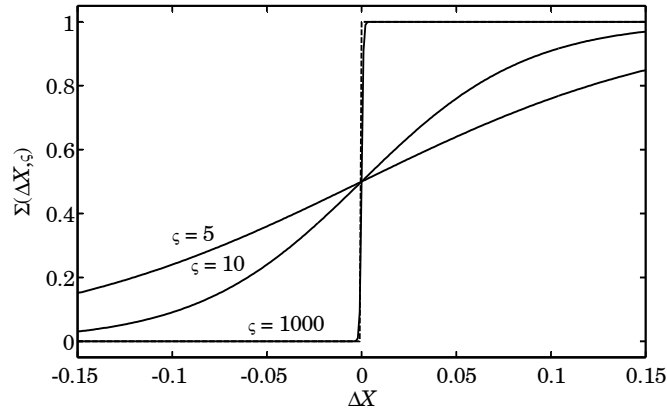


Figure 1.2: Smoothing function, original (—) and smoothed (—) functions

The case structure in eqn. 1.1 is then smoothed with

$$Y^* = (2.8 + 1.2 X) \cdot (1 - \Sigma(X - 4, \varsigma)) + (2.5 X^{0.8}) \cdot \Sigma(X - 4, \varsigma) \quad (1.3)$$

in which  $\varsigma = 10$ .

The min-function can be described as

$$Y = \min(Y, \max Y) \quad (1.4)$$

$$= 0.5 (Y + \max Y - |Y - \max Y|) \quad (1.5)$$

which is then smoothed with

$$Y^* = 0.5 \left( Y + \max Y - \sqrt[p]{|Y - \max Y|^p + \beta} \right) \quad (1.6)$$

in which  $p = 2$  and  $\beta = 1 \cdot 10^{-7}$ .

In a similar way the max-function can be described as

$$Y = \max(Y, \min Y) \quad (1.7)$$

$$= 0.5 (Y + \min Y + |Y - \min Y|) \quad (1.8)$$

which is then smoothed with

$$Y^* = 0.5 \left( Y + \min Y + \sqrt[p]{|Y - \min Y|^p + \beta} \right) \quad (1.9)$$

in which  $p = 2$  and  $\beta = 1 \cdot 10^{-7}$ .

Furthermore a penalty function is used in the optimal control. The penalty function is given by

$$L_x(x, u, t) = \begin{cases} c_x \cdot |x_{\min} - x(t)| & x_{\min} > x(t) \\ 0 & x_{\min} \leq x(t) \leq x_{\max} \\ c_x \cdot |x_{\max} - x(t)| & x(t) > x_{\max} \end{cases} \quad (1.10)$$

which can be written as

$$L_x^*(x, u, t) = \frac{c_x}{2} \cdot (|x_{\min} - x(t)| + |x_{\max} - x(t)| - (x_{\max} - x_{\min})) \quad (1.11)$$

which is then smoothed with

$$L_x^*(x, u, t) = \frac{c_x}{2} \cdot \left( \sqrt{(x_{\min} - x(t))^2 + \beta} + \sqrt{(x_{\max} - x(t))^2 + \beta} - (x_{\max} - x_{\min}) \right) \quad (1.12)$$

in which  $\beta = 1 \cdot 10^{-3}$ .

The smoothing functions used in eqns. 1.6, 1.9 and 1.12 are defined in Baldick et al. (1999). The smoothing functions defined here are demonstrated in table 1.1 and figure 1.3. In figure 1.3 the dashed lines are the original functions and the solid lines are the smoothed functions. For reasons of readability the non-smooth functions are given throughout the remainder of this thesis.

Table 1.1: Examples smoothing function

original	smoothed
$Y = \begin{cases} 2.8 + 1.2 X & \forall X < 4 \\ 2.5 X^{0.8} & \forall X \geq 4 \end{cases}$	$Y^* = (2.8 + 1.2 X) \cdot (1 - \Sigma(X - 4, 10)) + (2.5 X^{0.8}) \cdot \Sigma(X - 4, 10)$
$\Phi = \max(m_\Phi, 10 \Delta C)$	$\Phi^* = 0.5 \left( 10 \Delta C + m_\Phi + \sqrt{ 10 \Delta C - m_\Phi ^2 + 1 \cdot 10^{-7}} \right)$
$L_x = \begin{cases} c_x \cdot (x_{\min} - x) & \forall x_{\min} > x \\ 0 & \forall x_{\min} \leq x \leq x_{\max} \\ c_x \cdot (x - x_{\max}) & \forall x > x_{\max} \end{cases}$	$L_x^* = \frac{c_x}{2} \cdot \left( \sqrt{(x_{\min} - x(t))^2 + \beta} + \sqrt{(x_{\max} - x(t))^2 + \beta} - (x_{\max} - x_{\min}) \right)$

in which  $m_\Phi = 0$ ,  $c_x = 2$ ,  $x_{\min} = 19$  and  $x_{\max} = 21$

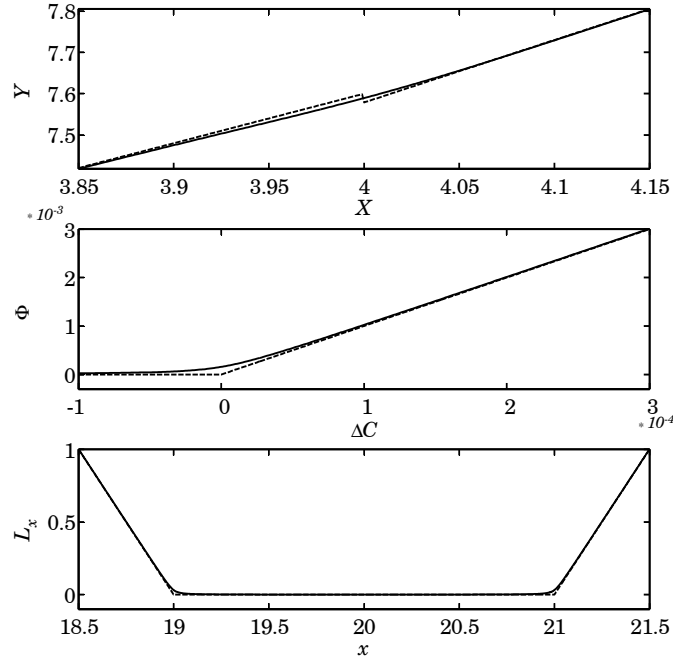


Figure 1.3: Examples smoothing function, original (---) and smoothed (—) function

## Chapter 2

# Model of crop biophysics

### 2.1 Introduction

The Dutch solar greenhouse design aims at reducing fossil energy use in Dutch horticulture (Bot, 2001). It reduces the required heating while maintaining or increasing crop yield and quality. It is therefore beneficial if larger temperature fluctuations are allowed compared to conventional greenhouses. This may lead to temperature and humidity extremes that are beyond the range for which the current crop models are designed and tested. It is important that the crop model gives an accurate description of the relevant crop processes also for these extreme values for temperature and humidity.

In literature many models are given for various parts of the crop growth process. To limit the on-line computational load in the optimal control computation, the model should be sufficiently small with respect to the number of differential equations. It should however also be sufficiently accurate. The time scale considered is also important, since a longer time scale requires a longer prediction horizon in the optimal control context.

The crop processes considered in this thesis are the rates of photosynthesis, dark respiration and evapotranspiration. The description of the evapotranspiration process is based on the resistances for  $\text{H}_2\text{O}$  diffusion. These resistances are closely related to the resistances for  $\text{CO}_2$  diffusion, which are important for the photosynthesis rate. From the photosynthesis and dark respiration the crop total biomass is obtained. It is assumed that the photosynthesis and respiration directly affect the biomass weight. No subdivision into vegetative and generative state or partitioning into fruit and leaves are taken into account.

Temperature integration is used as a descriptive method for long-term temperature effects on crop development. It is assumed that the grower is able to set optimal control values for the greenhouse temperature and humidity and for the temperature integration such that proper crop development is ensured during all its development stages. The crop is grown on substrate, which is placed in a gutter, covered with white plastic. It is assumed that water and nutrient supply is well-controlled and not limiting crop photosynthesis and evaporation.

Various models are available in the literature for the simulation of crop and leaf photosynthesis. These models describe the photosynthesis process in a various ways, e.g., leaf photosynthesis or crop photosynthesis. The literature is not always as transparent, since some models are made with different goals and time scales, therefore a thorough study is made. Terms will be clearly defined and literature models will be compared. The findings are unified in a new model to get an accurate description of the crop gross photosynthesis rate as a function of light intensity, CO<sub>2</sub> concentration and temperature.

Most models found in the literature are incomplete and so is their motivation. Therefore they are unsuitable for optimal control purposes, which requires a complete model of sufficient accuracy over the full range of working conditions.

Since our aim is to use an optimal control approach, it is important to have an accurate description of the effect of the control and external inputs on the crop processes<sup>⓪</sup>. Furthermore it is favourable to have a limited number of differential equations (lower order model) to limit the on-line computation time.

A complete and detailed description of a new crop processes model that is suitable for optimal control purposes is given in this chapter. The different physical and physiological processes that together make up the model are described in different sections.

The outline of this chapter is as follows. The evapotranspiration process is described in §2.2. In §2.3 the crop photosynthesis and respiration are described. A number of models from the literature are compared. The temperature integration is given in §2.4. In appendix B a list of variables and parameters used in the new crop processes model is given for easy reference.

---

<sup>⓪</sup> All non-smooth equations are smoothed according to the smoothing functions described in appendix 1.A.

## 2.2 Evapotranspiration

The evapotranspiration process concerns the evaporation of water from the leaf to the greenhouse air. This process is important for the water and nutrient transport from roots to leaves and fruits. It is also important to decrease the temperature of the crop. Water is mainly evaporated through the leaf stomata. The canopy transpiration is thus a function of the resistance of the stomata and the leaf boundary layer. In the literature these resistances are often assumed to be constant. Since we want to use the crop model for extreme temperature and humidity values, we are not in the domain where these constant resistances apply. We therefore use a model to compute the leaf resistances.

The model by Stanghellini (1987) is used for the evaporation process. This model is an adaptation of the Penman-Monteith-Rijtema method (the combination method) to determine the actual instead of the potential transpiration rate in a greenhouse. The transpiration rate depends on light intensity, CO<sub>2</sub> concentration, temperature and humidity. All relations — if not otherwise noted — are taken from Stanghellini (1987).

The canopy transpiration  $\Phi_{m.c.a.H_2O}$  or the mass flow rate of water vapour from crop to indoor air is

$$\Phi_{m.c.a.H_2O} = \max(A_c \cdot k_{c.a.H_2O} \cdot (C_{c.H_2O_s} - C_{a.H_2O}), 0) \{ \text{kg[H}_2\text{O] s}^{-1} \} \quad (2.1)$$

where  $A_c \{ \text{m}^2[\text{leaf}] \}$  is surface area of the canopy,  $k_{c.a.H_2O} \{ \text{m s}^{-1} \}$  is the mass transfer coefficient of water vapour from the crop to the indoor air,  $C_{c.H_2O_s} \{ \text{kg[H}_2\text{O] m}^{-3}[\text{air}] \}$  is the saturation concentration of water vapour at the temperature of the crop (see §2.C.1) and  $C_{a.H_2O} \{ \text{kg[H}_2\text{O] m}^{-3}[\text{air}] \}$  is the concentration water vapour at the temperature of the indoor air. If  $C_{c.H_2O_s} \leq C_{a.H_2O_s}$ , then  $\Phi_{m.c.a.H_2O} = 0$  (no evapotranspiration).

Bot (1983) describes the total resistance to diffusion of water as the boundary layer resistance in series with the cuticular resistance parallel to the stomatal resistance. From this the mass transfer coefficient  $k_{c.a.H_2O}$  from crop to indoor air is derived as

$$k_{c.a.H_2O} = \frac{1}{R_{b.H_2O} + \frac{R_{cut} \cdot R_{s.H_2O}}{R_{cut} + R_{s.H_2O}}} \{ \text{m s}^{-1} \} \quad (2.2)$$

in which the leaf cuticular resistance  $R_{cut} = 2000 \text{ s m}^{-1}$ , where  $R_{s.H_2O} \{ \text{s m}^{-1} \}$  is the stomatal resistance to diffusion of water and  $R_{b.H_2O} \{ \text{s m}^{-1} \}$  is the boundary layer resistance to diffusion of water.

The stomatal resistance to diffusion of water  $R_{s\_H2O}$  is described by

$$R_{s\_H2O} = R_{\min} \cdot f_I \cdot f_{Tc} \cdot f_{CO2} \cdot f_{H2O} \quad \{\text{sm}^{-1}\} \quad (2.3)$$

in which the radiation dependency  $f_I$  is given by

$$f_I = \frac{\frac{I_{c\_s}}{2 LAI} + 4.3}{\frac{I_{c\_s}}{2 LAI} + 0.54} \quad \{-\} \quad (2.4)$$

the temperature dependency  $f_{Tc}$  is given by

$$f_{Tc} = \begin{cases} 1 + 0.5 \cdot 10^{-2} \cdot (T_c - T_0 - 33.6)^2 & \text{if } I_{c\_s} \leq 3 \\ 1 + 2.2593 \cdot 10^{-2} \cdot (T_c - T_0 - 24.512)^2 & \text{if } I_{c\_s} > 3 \end{cases} \quad \{-\} \quad (2.5)$$

the  $\text{CO}_2$  dependency  $f_{CO2}$  is given by

$$f_{CO2} = \begin{cases} 1 & \text{if } I_{c\_s} \leq 3 \\ 1 + 6.08 \cdot 10^{-7} \cdot (CO_{2a} - 200)^2 & \text{if } I_{c\_s} > 3 \\ 1.49 & \text{if } CO_{2a} \geq 1100 \end{cases} \quad \{-\} \quad (2.6)$$

the humidity dependency  $f_{H2O}$  is given by

$$f_{H2O} = \frac{4}{\sqrt[4]{1 + 255 e^{-0.5427 \Delta p_{c\_H2O_m}}}} \quad \{-\} \quad (2.7)$$

and the minimum internal crop resistance  $R_{\min} = 82.003 \text{ s m}^{-1}$  (Jarvis' model). The term  $\frac{I_{c\_s}}{2 LAI} \{\text{W m}^{-2}[\text{leaf}]\}$  determines the leaf shortwave radiation absorption from the heat absorbed by the canopy  $I_{c\_s} = \eta_{c\_Is} \cdot I_o \{\text{W m}^{-2}[\text{soil}]\}$  and the leaf area index  $LAI \{\text{m}^{-2}[\text{leaf}] \text{m}^{-2}[\text{soil}]\}$ .  $T_c \{\text{K}\}$  is the temperature of the crop,  $T_0 = 273.15 \text{ K}$ ,  $CO_{2a} \{\mu\text{mol}[\text{CO}_2] \text{mol}^{-1}[\text{air}]\}$  is the  $\text{CO}_2$  concentration of the indoor air and  $\Delta p_{c\_H2O_m} \{\text{mbar}\}$  is the crop saturation deficit. All numbers in eqns. (2.3) to (2.7) are model parameters, determined by Stanghellini for tomato. De Zwart (1996) also gives values for roses.

The dependencies of the stomatal resistance to diffusion of water  $R_{s\_H2O} \{\text{sm}^{-1}\}$  are given in figure 2.1. The radiation dependency  $f_I$  decreases from 8 to 1 for increasing values of radiation, which indicates that radiation only influences the resistance at low light intensities. The temperature dependency  $f_{Tc}$  is parabolic with a minimum at  $24.5^\circ\text{C}$ . The humidity dependency  $f_{H2O}$  is constant at a maximum of 4 for vapour pressure differences above about 15 mbar and decreases at lower vapour pressure differences. This is due to stomata closure at low humidity values to prevent dehydration. The  $\text{CO}_2$  dependency  $f_{CO2}$  increases to 1.5 if the  $\text{CO}_2$  concentration increases.

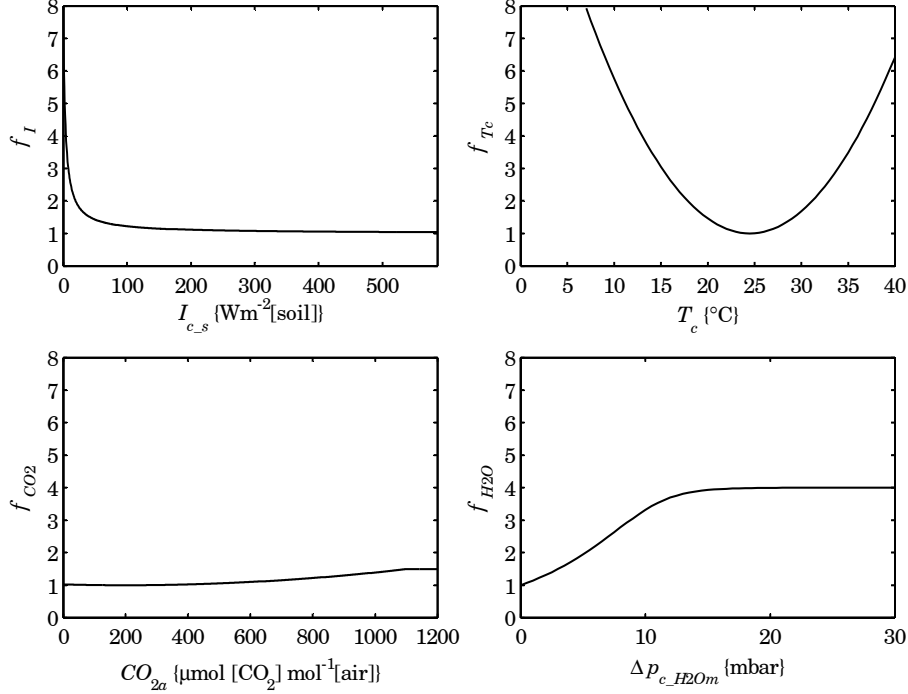


Figure 2.1: Stomatal resistance parameters  $f_I$ ,  $f_{T_c}$ ,  $f_{CO_2}$  and  $f_{H_2O}$ . Default values parameters — if not varied — are:  $I_{c-s} = 293.06 \text{ W m}^{-2}\text{[soil]}$  ( $I_o = 500 \text{ W m}^{-2}\text{[soil]}$ ,  $\eta_{c-I_s} = 0.586$ ),  $T_c = 20^\circ\text{C}^\dagger$ ,  $\Delta p_{c-H_2O} = 3.51 \text{ mbar}$  ( $RH_a = 85\%$ ),  $CO_{2a} = 1000 \mu\text{mol[CO}_2\text{] mol}^{-1}\text{[air]}$  and  $T_a = 20^\circ\text{C}^\dagger$ .

$^\dagger T_a$  and  $T_c$  in {K} in computations, in  $\{^\circ\text{C}\}$  here for readability

The boundary layer resistance to diffusion of water  $R_{b-H_2O}$  is described by Monteith and Unsworth (1990) as

$$R_{b-H_2O} = Le^{\frac{2}{3}} \cdot R_{b-heat} \quad \{\text{s m}^{-1}\} \quad (2.8)$$

where  $R_{b-heat} \{\text{s m}^{-1}\}$  is the boundary layer resistance to convective heat transfer and  $Le = 0.89 \{-\}$  is the Lewis number for water vapour in air.

The boundary layer resistance to convective heat transfer  $R_{b-heat}$  is given by

$$R_{b-heat} = \frac{1174 \sqrt{l_f}}{(l_f \cdot |T_c - T_a| + 207 v_a^2)^{\frac{1}{4}}} \quad \{\text{s m}^{-1}\} \quad (2.9)$$

in which the mean leaf width  $l_f = 0.035 \text{ m}$  and the wind speed (in the greenhouse)  $v_a = 0.09 \text{ m s}^{-1}$ , where  $|T_c - T_a| \{\text{K}\}$  is the temperature difference between the crop and the greenhouse air.

## 2.3 Crop photosynthesis and respiration

The photosynthesis process concerns the chemical assimilation of  $\text{CO}_2$  and water to assimilate for maintenance, growth and development. The canopy extracts  $\text{CO}_2$  from its environment. The photosynthesis rate is mainly influenced by light intensity,  $\text{CO}_2$  concentration and temperature. The photosynthesis rate increases with the radiation intensity and  $\text{CO}_2$  concentration. Furthermore the photosynthesis rate increases with temperature to a maximum value, and then decreases at higher temperatures. Since the solar greenhouse may have lower and higher temperatures than a conventional greenhouse, the photosynthesis model must describe the photosynthesis process well over a wide temperature range.

Various models are available for the simulation of crop and leaf photosynthesis. These models describe the photosynthesis process in different ways. There are two mainstream approaches to photosynthesis modelling. Leaf photosynthesis describes the photosynthesis rate of a single leaf. Crop photosynthesis describes the overall photosynthesis rate of the canopy as a whole. In principle, crop photosynthesis can be obtained from leaf photosynthesis by some form of spatial integration over the canopy.

The models considered here are:

- CG1 General Farquhar model** This is a leaf photosynthesis model (Farquhar et al., 1980) that describes the leaf biochemical processes. A detailed description of the biochemical processes is used.
- CG2 Big leaf Farquhar model** This is a crop photosynthesis model (Gijzen, 1994) that assumes that the crop can be interpreted as one big leaf. The description of the biochemical processes is extremely simplified. The light interception in the layers of the crop is simplified to yield the light interception for a big leaf.
- CG3 Goudriaan model** This is a (SUCROS related) crop photosynthesis model (Goudriaan and van Laar, 1994) with Gaussian integration over the crop depth. The description of the biochemical processes is simplified. A detailed description is given for the light interception in the layers of the crop height. Gaussian integration is used to integrate over the crop depth. This model has been successfully validated under normal temperature and humidity conditions for a tomato crop by Heuvelink (1996).

The models are compared, and from these models a new model is formed, to give an accurate description of the crop gross photosynthesis rate as a function of light intensity, CO<sub>2</sub> concentration and temperature.

**CG4 New photosynthesis model** This is a crop photosynthesis model. It is based on the models *CG1* and *CG3*. For the description of the biochemical processes on a leaf level, model *CG1* (Farquhar et al., 1980) is used, since it gives the most detailed description from the models selected here. The light interception in the crop layers and the Gaussian integration from model *CG3* (Goudriaan and van Laar, 1994; Heuvelink, 1996) is used, since we need a crop and not a leaf photosynthesis model.

The photosynthesis rate can be limited by the stomatal and boundary layer resistances to CO<sub>2</sub> diffusion, which are a function of the resistances to H<sub>2</sub>O diffusion. In the models *CG1*, *CG2* and *CG3*, constant resistances to CO<sub>2</sub> diffusion are used. Since we are not working in the temperature and humidity ranges where these constant resistances apply, the resistances found from §2.2 by Stanghellini (1987) are used.

All models are summarized in §2.A. The model *CG4* is described here in detail. This model has been validated by Körner and van Oorteghem (Körner and van Oorteghem, 2003; Körner et al., 2001a,b, 2002, 2003, 2007a,b). It was found that the model showed good accordance with measured data. The resistances computed with the evaporation model resulted in better results in most cases compared to constant resistances.

### 2.3.1 Photosynthesis model

This paragraph describes the new photosynthesis model *CG4*. A number of parameters used are general for all models considered here, and their values are given in table 2.1. The purpose of the model is to describe the CO<sub>2</sub> assimilation rate of the canopy (expressed in {mg[CO<sub>2</sub>] m<sup>-2</sup>[soil] s<sup>-1</sup>}) as a function of the outdoor shortwave solar radiation  $I_o$  {W m<sup>-2</sup>[soil]}, the CO<sub>2</sub> concentration  $CO_{2a}$  {μmol[CO<sub>2</sub>] mol<sup>-1</sup>[air]}, the temperature of the crop  $T_c$  {K} and the relative humidity  $RH_a$  {%}.

Table 2.1: Photosynthesis model, general parameters

name	value	unit	contents
Constants			
$R_g$	8.314	$\text{J mol}^{-1} \text{K}^{-1}$	gas constant
$\rho_{CO_2}$	1.98	$\text{kg}[\text{CO}_2] \text{m}^{-3}[\text{CO}_2]$	$\text{CO}_2$ density at $T_0$
$M_{CO_2}$	$44 \cdot 10^{-3}$	$\text{kg}[\text{CO}_2] \text{mol}^{-1}[\text{CO}_2]$	molar mass $\text{CO}_2$
$T_0$	273.15	K	273.15 K = 0°C
$T_{25}$	$T_0 + 25$	K	273.15 + 25 K = 25°C
$\zeta$	4.59	$\mu\text{mol}[\text{photons}] \text{J}^{-1}$	conversion factor, J to photons
$\rho_{Chl}$	0.45	$\text{g}[\text{Chl}] \text{m}^{-2}[\text{leaf}]$	Ⓢ superficial chlorophyll density
Constants at 25°C			
$p_{O_2i}$	210	mbar	ⓈⓈ $\text{O}_2$ partial pressure inside stomata
$K_{C25}$	310	$\mu\text{bar}$	Ⓢ Michaelis Menten constant Rubisco carboxylation ( $\text{CO}_2$ )
$K_{O25}$	155	mbar	Ⓢ Michaelis Menten constant Rubisco oxygenation ( $\text{O}_2$ )
$k_C$	2.5	$\text{s}^{-1}$	Ⓢ turnover number of RuP2 (carboxylase)
$E_t$	87.0	$\mu\text{mol}[\text{CO}_2] \text{g}^{-1}[\text{Chl}]$	Ⓢ total concentration of enzyme sites
$V_{C \max 25}$	$\rho_{Chl} \cdot k_C \cdot E_t$	$\mu\text{mol}[\text{CO}_2] \text{m}^{-2}[\text{leaf}] \text{s}^{-1}$	Ⓢ maximum carboxylation rate at 25°C
$r_{D25-uL}$	1.1	$\mu\text{mol}[\text{CO}_2] \text{m}^{-2}[\text{leaf}] \text{s}^{-1}$	Ⓢ dark respiration at 25°C
$J_{\max 25}$	$467 \rho_{Chl}$	$\mu\text{mol}[\text{e}^-] \text{m}^{-2}[\text{leaf}] \text{s}^{-1}$	Ⓢ maximum electron transport rate at 25°C
Radiation parameters			
$slo$	0.5	—	Ⓢ specific leaf orientation
$\delta$	0.15	—	Ⓢ scattering coefficient
$k_{difBL}$	0.8	—	Ⓢ extinction coefficient diffuse PAR and black leaves
$k_{dif}$	$k_{difBL} \cdot \sqrt{1 - \delta}$	—	Ⓢ extinction coefficient diffuse PAR
$k_{dirBL}$	$\frac{slo}{\sin \beta}$	—	Ⓢ extinction coefficient direct PAR and black leaves
$k_{dir}$	$k_{dirBL} \cdot \sqrt{1 - \delta}$	—	Ⓢ extinction coefficient direct PAR
$\tau_{dif}$	$e^{-k_{dif} \cdot LAI}$	—	Ⓢ transmittance diffuse PAR
$\tau_{dirBL}$	$e^{-k_{dirBL} \cdot LAI}$	—	Ⓢ transmittance direct PAR and black leaves
$\tau_{dir}$	$e^{-k_{dir} \cdot LAI}$	—	Ⓢ transmittance direct PAR total
$\beta_{dif}$	$\frac{1 - \sqrt{1 - \delta}}{1 + \sqrt{1 - \delta}}$	—	Ⓢ reflection coefficient canopy diffuse PAR
$\beta_{dir}$	$\frac{2}{1 + \frac{k_{difBL}}{k_{dirBL}}} \cdot \beta_{dif}$	—	Ⓢ reflection coefficient canopy direct PAR
$I_{P-o}$	$f_{par} \cdot I_o$	$\text{W m}^{-2}[\text{soil}]$	Ⓢ PAR outside greenhouse
$I_{P-dif-o}$	$f_{dif} f_{par} \cdot I_{P-o}$	$\text{W m}^{-2}[\text{soil}]$	Ⓢ diffuse PAR outside greenhouse
$I_{P-dir-o}$	$I_{P-o} - I_{P-dif-o}$	$\text{W m}^{-2}[\text{soil}]$	Ⓢ direct PAR outside greenhouse
$I_{P-dif}$	$\tau_{dif} R \cdot \tau_{sc-Is} \cdot I_{P-dif-o}$	$\text{W m}^{-2}[\text{soil}]$	diffuse PAR inside greenhouse
$I_{P-dir}$	$\tau_{dir} R \cdot \tau_{sc-Is} \cdot I_{P-dir-o}$	$\text{W m}^{-2}[\text{soil}]$	direct PAR inside greenhouse
$I_P$	$f_{par} \cdot \tau_{dif} R \cdot \tau_{sc-Is} \cdot I_o$	$\text{W m}^{-2}[\text{soil}]$	PAR inside greenhouse

Ⓢ Gijzen (1994); Ⓢ Farquhar et al. (1980); Ⓢ Goudriaan and van Laar (1994); Ⓢ Spitters (1986); Ⓢ Heuvelink (1996)

Table 2.1: Photosynthesis model, general parameters (continued)

name	value	unit	contents
Temperature parameters, Arrhenius function			
$E_C$	59356	$\text{J mol}^{-1}$	© activation energy $K_C$ Rubisco carboxylation
$E_O$	35948	$\text{J mol}^{-1}$	© activation energy $K_O$ Rubisco oxygenation
$E_M$	39017	$\text{J mol}^{-1}$	activation energy $K_M$ Michaelis Menten constant
$E_{VC}$	58520	$\text{J mol}^{-1}$	© activation energy $V_{C \max}$ maximum carboxylation rate
$E_D$	66405	$\text{J mol}^{-1}$	© activation energy $r_D$ dark respiration rate
$E_J$	37000	$\text{J mol}^{-1}$	© activation energy $J_{\max}$ maximum electron transport rate
Temperature parameters, $Q_{10}$ function			
$Q_{10KM}$	$e^{13.6 \cdot 10^{-6} E_M} \approx 1.7$	–	$Q_{10}$ value $K_M$
$Q_{10VC}$	$e^{13.6 \cdot 10^{-6} E_{VC}} \approx 2.2$	–	© $Q_{10}$ value $V_{C \max}$
$Q_{10rD}$	$e^{13.6 \cdot 10^{-6} E_{rD}} \approx 2.5$	–	© $Q_{10}$ value $r_D$

©Farquhar et al. (1980)

### 2.3.1.1 Gross assimilation and dark respiration

The gross canopy assimilation rate  $P_g$  is found by multiplying the gross leaf assimilation rate  $P_{g,L}$  by the leaf area index  $LAI$

$$P_g = P_{g,L} \cdot LAI \quad \{\text{mg}[\text{CO}_2] \text{ m}^{-2}[\text{soil}] \text{ s}^{-1}\} \quad (2.10)$$

The canopy dark respiration rate  $r_D$  is equal to

$$r_D = M_{CO2} \cdot r_{D,uL} \cdot LAI \quad \{\text{mg}[\text{CO}_2] \text{ m}^{-2}[\text{soil}] \text{ s}^{-1}\} \quad (2.11)$$

where  $r_{D,uL}$   $\{\mu\text{mol}[\text{CO}_2] \text{ m}^{-2}[\text{leaf}] \text{ s}^{-1}\}$  is the leaf dark respiration rate.

In general, the gross leaf assimilation rate  $P_{g,L}$  is determined from the negative exponential light-response curve (Goudriaan and van Laar, 1994)

$$P_{g,L} = P_{g \max} \cdot \left(1 - e^{-\frac{\varepsilon \cdot I_A}{P_{g \max}}}\right) \quad \{\text{mg}[\text{CO}_2] \text{ m}^{-2}[\text{leaf}] \text{ s}^{-1}\} \quad (2.12)$$

where  $P_{g \max}$   $\{\text{mg}[\text{CO}_2] \text{ m}^{-2}[\text{leaf}] \text{ s}^{-1}\}$  is the maximum gross assimilation rate,  $\varepsilon$   $\{\text{mg}[\text{CO}_2] \text{ J}^{-1}\}$  is the light use efficiency by photorespiration and  $I_A$   $\{\text{W m}^{-2}[\text{soil}]\}$  is the absorbed radiation.

The absorbed radiation  $I_A$  depends on the position of a leaf in the canopy. It is determined by the gradual extinction of radiation with canopy depth as a whole and by the leaves being either sunlit or shaded at any single level in the canopy. Therefore the assimilation rate is computed through a three-point Gaussian integration over the crop depth. The Gaussian integration determines the canopy assimilation rate from the average assimilation rate for three layers in the canopy. Two summation counters are used:  $l_1 \in \{1, 2, 3\}$  for the integration over the canopy depth, and  $l_2 \in \{1, 2, 3\}$  for the correction of  $I_{A\_ppd}$  for the canopy depth.

The values of the relative depth  $X_g$  of the canopy and the weight factor  $W_g$  needed for the three-point Gaussian integration are

$$\begin{aligned} X_g &= \{0.5 - \sqrt{0.15} \quad 0.5 \quad 0.5 + \sqrt{0.15}\} \\ &= \{0.1127 \quad 0.5 \quad 0.8873\} \end{aligned} \quad \{-\} \quad (2.13)$$

$$\begin{aligned} W_g &= \left\{ \frac{1}{3.6} \quad \frac{1.6}{3.6} \quad \frac{1}{3.6} \right\} \\ &= \{0.2778 \quad 0.4444 \quad 0.2778\} \end{aligned} \quad \{-\} \quad (2.14)$$

Note: if  $LAI$  is higher than 3, a five-point Gaussian integration should be used for accuracy.

The leaf area index  $LAI_l$  at layer  $l_1$  — used to determine the transmittance  $\tau_{dif}$  and  $\tau_{dir}$  — is a function of the depth in the canopy

$$LAI_l(l_1) = LAI \cdot X_g(l_1) \quad \{\text{m}^2[\text{leaf}] \text{m}^{-2}[\text{soil}]\} \quad (2.15)$$

The gross leaf assimilation rate  $P_{g-L}$  is computed from the assimilation rate of the sunlit and the shaded part with the fraction sunlit leaf area  $f_{SLA}$   $\{-\}$

$$\begin{aligned} P_{g-L} &= \sum_{l_1=1}^3 W_g(l_1) \cdot (f_{SLA} \cdot P_{g-sun}(l_1) + (1 - f_{SLA}) \cdot P_{g-shd}(l_1)) \\ &\quad \{\text{mg}[\text{CO}_2] \text{m}^{-2}[\text{leaf}] \text{s}^{-1}\} \end{aligned} \quad (2.16)$$

in which the fraction sunlit leaf area  $f_{SLA} = \tau_{dirBL}(l_1)$ . This summation moves through the crop layers from top to bottom.

The gross assimilation rates  $P_{g-sun}$  of the sunlit part and  $P_{g-shd}$  of the shaded part at layer  $l_1$  are defined by

$$\begin{aligned} P_{g-sun}(l_1) &= P_{g\max} \cdot \sum_{l_2=1}^3 W_g(l_2) \cdot \left( 1 - e^{-\frac{\varepsilon \cdot I_{A-sun}(l_1, l_2)}{P_{g\max}}} \right) \\ &\quad \{\text{mg}[\text{CO}_2] \text{m}^{-2}[\text{leaf}] \text{s}^{-1}\} \end{aligned} \quad (2.17)$$

$$P_{g-shd}(l_1) = P_{g\max} \cdot \left( 1 - e^{-\frac{\varepsilon \cdot I_{A-shd}(l_1)}{P_{g\max}}} \right) \quad \{\text{mg}[\text{CO}_2] \text{m}^{-2}[\text{leaf}] \text{s}^{-1}\} \quad (2.18)$$

The absorbed radiation  $I_{A-sun}$  of the sunlit part and  $I_{A-shd}$  of the shaded part of the canopy can be defined as a function of various absorbed radiation terms (Spitters, 1986; Goudriaan and van Laar, 1994)

$$I_{A-sun}(l_1, l_2) = I_{A-shd}(l_1) + I_{A-ppd}(l_1) \cdot X_g(l_2) \quad \{\text{W m}^{-2}[\text{leaf}]\} \quad (2.19)$$

$$I_{A-shd}(l_1) = I_{A-dif}(l_1) + I_{A-tdir}(l_1) - I_{A-dir}(l_1) \quad \{\text{W m}^{-2}[\text{leaf}]\} \quad (2.20)$$

in which the diffuse flux  $I_{A\_dif}$ , the total direct flux  $I_{A\_tdir}$ , the direct flux  $I_{A\_dir}$  and the direct flux of leaves perpendicular on the direct beam  $I_{A\_ppd}$  are given by

$$I_{A\_dif}(l_1) = (1 - \beta_{dif}) \cdot I_{P\_dif} \cdot k_{dif} \cdot \tau_{dif}(l_1) \quad \{\text{W m}^{-2}[\text{leaf}]\} \quad (2.21)$$

$$I_{A\_tdir}(l_1) = (1 - \beta_{dir}) \cdot I_{P\_dir} \cdot k_{dir} \cdot \tau_{dir}(l_1) \quad \{\text{W m}^{-2}[\text{leaf}]\} \quad (2.22)$$

$$I_{A\_dir}(l_1) = (1 - \delta) \cdot I_{P\_dir} \cdot k_{dirBL} \cdot \tau_{dirBL}(l_1) \quad \{\text{W m}^{-2}[\text{leaf}]\} \quad (2.23)$$

$$I_{A\_ppd}(l_1) = \frac{1 - \delta}{\sin \beta} \cdot I_{P\_dir} \quad \{\text{W m}^{-2}[\text{leaf}]\} \quad (2.24)$$

The summation in eqn. 2.17 is needed for the sunlit leaves. The sunlit part  $I_{A\_sun}$  of the absorbed radiation gives an average value over all sines of incidence of the direct beam on the leaves. Since in principle any sine of incidence can occur, this part has to be integrated separately.

### 2.3.1.2 Photosynthesis parameters

The light use efficiency by photorespiration  $\varepsilon$   $\{\text{mg}[\text{CO}_2] \text{J}^{-1}\}$  and the maximum gross assimilation rate  $P_{g\max}$   $\{\text{mg}[\text{CO}_2] \text{m}^{-2}[\text{leaf}] \text{s}^{-1}\}$  depend on the photosynthesis parameters. The photosynthesis parameters depend on the  $\text{CO}_2$  concentration  $CO_{2a}$   $\{\mu\text{mol}[\text{CO}_2] \text{mol}^{-1}[\text{air}]\}$  in the greenhouse and the temperature of the crop  $T_c$   $\{\text{K}\}$ .

The light use efficiency by photorespiration  $\varepsilon$  (Goudriaan and van Laar, 1994) is given by

$$\varepsilon = \psi \cdot \frac{M_{CO_2}}{4} \cdot \frac{\max(CO_{2a}, \Gamma) - \Gamma}{\max(CO_{2a}, \Gamma) + 2\Gamma} \quad \{\text{mg}[\text{CO}_2] \text{J}^{-1}\} \quad (2.25)$$

in which the number of electrons ( $e^-$ ) per fixed  $\text{CO}_2$  is 4, where  $CO_{2a}$   $\{\mu\text{mol}[\text{CO}_2] \text{mol}^{-1}[\text{air}]\}$  is the  $\text{CO}_2$  concentration in the greenhouse,  $\Gamma$   $\{\mu\text{mol}[\text{CO}_2] \text{mol}^{-1}[\text{air}]\}$  is the  $\text{CO}_2$  compensation concentration,  $M_{CO_2}$   $\{\text{mg}[\text{CO}_2] \mu\text{mol}^{-1}[\text{CO}_2]\}$  is the molar mass of  $\text{CO}_2$  and  $\psi$   $\{\mu\text{mol}[e^-] \text{J}^{-1}\}$  is the conversion factor from  $\{\text{J}\}$  to  $\{\mu\text{mol}[e^-]\}$ .

The conversion factor  $\psi$  is

$$\psi = \frac{1 - F_p}{2} \cdot \zeta \quad \{\mu\text{mol}[e^-] \text{J}^{-1}\} \quad (2.26)$$

in which the fraction PAR (photosynthesis active radiation) absorbed by non-photosynthetic tissues  $F_p = 0.3$ , the number of electrons ( $e^-$ ) per absorbed photon is 2 and the conversion factor  $\zeta = 4.59 \mu\text{mol}[\text{photons}] \text{J}^{-1}$ .

The  $\text{CO}_2$  compensation concentration  $\Gamma$  in the absence of dark respiration (Farquhar et al., 1980) is defined by

$$\Gamma = \frac{K_C}{2K_O} \cdot p_{O2i} \cdot f_{OC} \quad \{\mu\text{mol}[\text{CO}_2] \text{ mol}^{-1}[\text{air}]\} \quad (2.27)$$

in which the  $\text{O}_2$  partial pressure inside the stomata  $p_{O2i} = 210$  mbar and the ratio of  $V_{O\max}$  (maximum oxygenation rate) to  $V_{C\max}$  (maximum carboxylation rate)  $f_{OC} = \frac{V_{O\max}}{V_{C\max}} = 0.21$  (which is assumed constant). The Michaelis Menten constants  $K_C$  for Rubisco carboxylation and  $K_O$  for Rubisco oxygenation are given by

$$K_C = K_{C25} \cdot e^{E_C \cdot \frac{T_c - T_{25}}{T_c \cdot R_g \cdot T_{25}}} \quad \{\mu\text{bar}\} \quad (2.28)$$

$$K_O = K_{O25} \cdot e^{E_O \cdot \frac{T_c - T_{25}}{T_c \cdot R_g \cdot T_{25}}} \quad \{\text{mbar}\} \quad (2.29)$$

where  $T_c$  {K} is the temperature of the crop.

The maximum gross assimilation rate  $P_{g\max}$  is determined by adding the maximum net assimilation rate and the leaf dark respiration rate

$$P_{g\max} = P_{n\max} + M_{CO2} \cdot r_{D,uL} \quad \{\text{mg}[\text{CO}_2] \text{ m}^{-2}[\text{leaf}] \text{ s}^{-1}\} \quad (2.30)$$

The leaf dark respiration rate  $r_{D,uL}$  (Farquhar et al., 1980) is given by

$$r_{D,uL} = r_{D25,uL} \cdot e^{E_D \cdot \frac{T_c - T_{25}}{T_c \cdot R_g \cdot T_{25}}} \quad \{\mu\text{mol}[\text{CO}_2] \text{ m}^{-2}[\text{leaf}] \text{ s}^{-1}\} \quad (2.31)$$

The maximum (light saturated) net assimilation rate  $P_{n\max}$  is a function of the maximum net assimilation rate  $P_{nc}$  limited by  $\text{CO}_2$ , the maximum endogenous photosynthetic capacity  $P_{mm}$  and a factor  $\Theta$  for the degree of curvature (Goudriaan and van Laar, 1994)

$$P_{n\max} = \frac{P_{mm} + P_{nc} - \sqrt{(P_{mm} + P_{nc})^2 - 4\Theta \cdot P_{mm} \cdot P_{nc}}}{2\Theta} \quad \{\text{mg}[\text{CO}_2] \text{ m}^{-2}[\text{leaf}] \text{ s}^{-1}\} \quad (2.32)$$

in which  $\Theta = 0.7$ . The rate  $P_{n\max}$  is the solution of the non-rectangular hyperbola  $\Theta \cdot P_{n\max}^2 - (P_{mm} + P_{nc}) \cdot P_{n\max} + P_{mm} \cdot P_{nc} = 0$ . This function gives a close approximation of the negative exponential function.

The maximum endogenous photosynthetic capacity  $P_{mm}$  is defined by

$$P_{mm} = \frac{M_{CO2}}{4} \cdot J_{\max} \quad \{\text{mg}[\text{CO}_2] \text{ m}^{-2}[\text{leaf}] \text{ s}^{-1}\} \quad (2.33)$$

in which the maximum electron transport rate  $J_{\max}$  (Farquhar et al., 1980; Gijzen, 1994) is given by

$$J_{\max} = J_{\max 25} \cdot e^{E_J \cdot \frac{T_c - T_{25}}{T_c \cdot R_g \cdot T_{25}}} \cdot \frac{1 + e^{\frac{S \cdot T_{25} - H}{R_g \cdot T_{25}}}}{1 + e^{\frac{S \cdot T_c - H}{R_g \cdot T_c}}} \quad \{\mu\text{mol}[\text{e}^-] \text{m}^{-2}[\text{leaf}] \text{s}^{-1}\} \quad (2.34)$$

and the constants  $S = 710 \text{ J mol}^{-1} \text{ K}^{-1}$  and  $H = 220000 \text{ J mol}^{-1}$ .

The  $\text{CO}_2$  limited rate  $P_{nc}$  of net photosynthesis (Goudriaan and van Laar, 1994) is defined by

$$P_{nc} = \frac{\rho_{CO_2 T}}{R_{tot\_CO_2}} \cdot (\max(CO_{2a}, \Gamma) - \Gamma) \quad \{\text{mg}[\text{CO}_2] \text{m}^{-2}[\text{leaf}] \text{s}^{-1}\} \quad (2.35)$$

where  $\Gamma$   $\{\mu\text{mol}[\text{CO}_2] \text{mol}^{-1}[\text{air}]\}$  is the  $\text{CO}_2$  compensation concentration in absence of dark respiration,  $CO_{2a}$   $\{\mu\text{mol}[\text{CO}_2] \text{mol}^{-1}[\text{air}]\}$  is the  $\text{CO}_2$  concentration in the greenhouse,  $R_{tot\_CO_2}$   $\{\text{s m}^{-1}\}$  is the total resistance to  $\text{CO}_2$  diffusion and  $\rho_{CO_2 T}$   $\{\text{kg}[\text{CO}_2] \text{m}^{-3}[\text{CO}_2]\}$  is the  $\text{CO}_2$  density at temperature  $T_c$ .

The  $\text{CO}_2$  density  $\rho_{CO_2 T}$  at temperature  $T_c$   $\{\text{K}\}$  is defined by the law for ideal gas as

$$\rho_{CO_2 T} = \rho_{CO_2} \cdot \frac{T_0}{T_c} \quad \{\text{kg}[\text{CO}_2] \text{m}^{-3}[\text{CO}_2]\} \quad (2.36)$$

where  $\rho_{CO_2}$  is the  $\text{CO}_2$  density at  $T_0$ .

The total resistance to  $\text{CO}_2$  diffusion  $R_{tot\_CO_2}$  is determined by adding stomatal, boundary layer and carboxylation resistance

$$R_{tot\_CO_2} = R_{s\_CO_2} + R_{b\_CO_2} + R_{c\_CO_2} \quad \{\text{s m}^{-1}\} \quad (2.37)$$

The stomatal and boundary layer resistance to  $\text{CO}_2$  diffusion  $R_{s\_CO_2}$  and  $R_{b\_CO_2}$  are computed from the stomatal and boundary layer resistance to  $\text{H}_2\text{O}$  diffusion  $R_{s\_H_2O}$  (eqn. 2.3) and  $R_{b\_H_2O}$  (eqn. 2.8) from §2.2. For  $\text{CO}_2$  these resistances are larger than for water vapour because the diffusion coefficient is lower (Monteith and Unsworth, 1990).

$$R_{s\_CO_2} = 1.6 R_{s\_H_2O} \quad \{\text{s m}^{-1}\} \quad (2.38)$$

$$R_{b\_CO_2} = 1.37 R_{b\_H_2O} \quad \{\text{s m}^{-1}\} \quad (2.39)$$

The carboxylation resistance  $R_{c\_CO_2}$  (Goudriaan and van Laar, 1994; Gijzen, 1994) is given by

$$R_{c\_CO_2} = \frac{K_M}{V_{C\max}} \cdot \frac{\rho_{CO_2 T}}{M_{CO_2}} \quad \{\text{s m}^{-1}\} \quad (2.40)$$

where  $K_M$  is the effective Michaelis Menten constant for carboxylation and  $V_{C\max}$  is the maximum carboxylation rate (Farquhar et al., 1980)

$$K_M = K_C \cdot \left(1 + \frac{pO_2 i}{K_O}\right) \quad \{\mu\text{bar}\} \quad (2.41)$$

$$V_{C\max} = V_{C\max 25} \cdot e^{\frac{E_{VC} \cdot (T_c - T_{25})}{T_c \cdot R_g \cdot T_{25}}} \quad \{\mu\text{mol}[\text{CO}_2] \text{ m}^{-2} [\text{leaf}] \text{ s}^{-1}\} \quad (2.42)$$

### 2.3.2 Comparison photosynthesis models

The main differences between the photosynthesis models *CG1* to *CG3* relate to the following terms:

- The photosynthesis parameters  $J_{\max}$  and  $\Gamma$  as a function of  $T_c$ .
- The stomatal and boundary layer resistance as a function of  $I_o$ ,  $CO_{2a}$ ,  $T_c$  and  $RH_a$ .
- The photosynthesis and respiration rate as a function of  $I_o$ ,  $CO_{2a}$  and  $T_c$ .

In this paragraph these differences are investigated, discussed and evaluated, resulting in the selection of the equations for model *CG4*.

#### 2.3.2.1 Photosynthesis parameters

The main difference between the models *CG1*, *CG2*, *CG3* and *CG4* in the photosynthesis parameters is found in the parameters  $J_{\max}$  and  $\Gamma$  as a function of the temperature of the crop  $T_c$ . The corresponding equations are given in table 2.2. These parameters are graphically displayed in figure 2.2.

The same relation is used for the maximum electron transport rate  $J_{\max}$  in model *CG1* and *CG4*. In model *CG2* it is described by a linear relation, which does not hold for temperatures  $T_c$  above 30°C. In model *CG3* it is described by a trapezium shape, which is a simplified form of the equation used in Farquhar et al. (1980) from model *CG1*.

The same relation is used for the  $\text{CO}_2$  compensation concentration  $\Gamma$  in absence of dark respiration in model *CG1* and *CG4*. In model *CG2* it is described by a linear relation and in model *CG3* by a quadratic equation as proposed in Farquhar (1988).

Table 2.2: Photosynthesis parameters  $J_{\max}$  and  $\Gamma$ 

model	maximum electron transport rate $J_{\max}$ $\{\mu\text{mol}[\text{e}^-] \text{m}^{-2}[\text{leaf}] \text{s}^{-1}\}$	ref.	CO <sub>2</sub> compensation concentration $\Gamma$ $\{\mu\text{mol}[\text{CO}_2] \text{mol}^{-1}[\text{air}]\}$	ref.
CG1 CG4	$J_{\max} = J_{\max 25} \cdot e^{\frac{E \cdot J \cdot \frac{T_c - T_{25}}{T_c \cdot R_g \cdot T_{25}}}{1 + e^{\frac{S \cdot T_{25} - H}{R_g \cdot T_{25}}}} \cdot \frac{1 + e^{\frac{S \cdot T_c - H}{R_g \cdot T_c}}}{1 + e^{\frac{S \cdot T_c - H}{R_g \cdot T_c}}}$	Ⓐ Ⓒ	$\Gamma = \frac{K_C}{2 K_O} \cdot p_{O_2 i} \cdot f_{OC}$	Ⓒ
CG2	$J_{\max} = J_{\max 25} \cdot \frac{T_c - T_0}{25}$	Ⓒ	$\Gamma = 1.7 (T_c - T_0)$	Ⓒ
CG3	$J_{\max} = \begin{cases} 0 & \text{if } T_c - T_0 \in \langle -, 5 \rangle \\ J_{\max 25} \cdot \frac{T_c - T_0 - 5}{20} & \text{if } T_c - T_0 \in [5, 25 \rangle \\ J_{\max 25} & \text{if } T_c - T_0 \in [25, 35 \rangle \\ J_{\max 25} \cdot \left(1 - \frac{(T_c - T_0 - 35)}{10}\right) & \text{if } T_c - T_0 \in [35, 45 \rangle \\ 0 & \text{if } T_c - T_0 \in [45, \rightarrow \rangle \end{cases}$	Ⓐ	$\Gamma = 42.7 + 1.68 (T_c - T_{25}) + 0.012 (T_c - T_{25})^2$	Ⓒ

Ⓐ Gijzen (1994); Ⓒ Farquhar et al. (1980); Ⓐ Farquhar (1988); Ⓒ Heuvelink (1996)

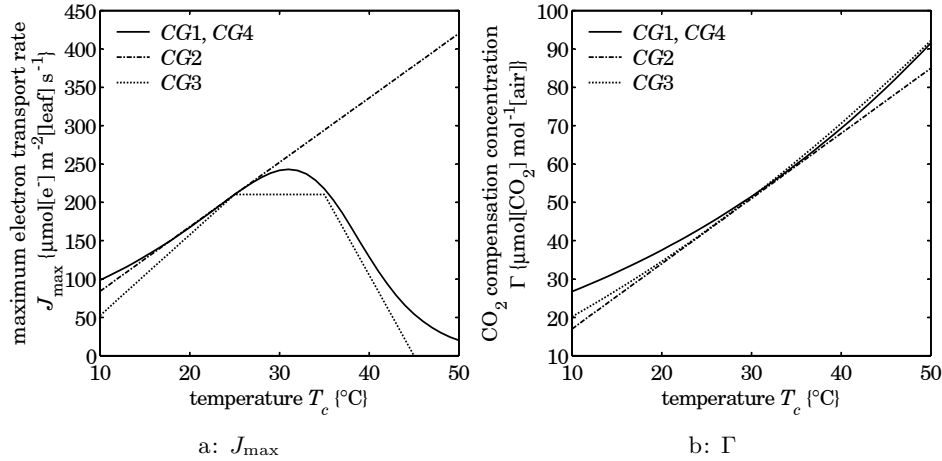


Figure 2.2: Photosynthesis parameters  $J_{\max}$  and  $\Gamma$  as a function of crop temperature  $T_c$  <sup>†</sup>  $T_c$  in {K} in computations, in {°C} here for readability

In figure 2.2 it can be seen that model CG2 gives an oversimplified view of both parameters, since it estimates them by straight lines. These estimates approximate the parameters given by model CG1 for values close to 25°C for  $J_{\max}$  and for values close to 30°C for  $\Gamma$ . Model CG3 gives a relatively good approximation of  $J_{\max}$  from model CG1. The maximum value of  $J_{\max}$  is the same however for all temperatures between 25°C and 35°C. This can be an important factor in the photosynthesis rate. The relations for  $\Gamma$  in models

CG3 and CG1 give approximately the same responses for high temperatures, while for temperatures below 30°C model CG3 gives lower values, up to 25% lower than with model CG1.

### 2.3.2.2 Stomatal and boundary layer resistance

In most photosynthesis models, the stomatal and boundary layer resistances to  $H_2O$  are assumed constant, with typical values of 50 and 100  $s\ m^{-1}$  respectively (Heuvelink, 1996). Stanghellini (1987) defined a model for crop evaporation (see §2.2) that holds equations for the stomatal and boundary layer resistance to  $H_2O$ . From these resistances, the resistances to  $CO_2$  can be computed with eqns. (2.38) and (2.39). The influence of various environmental variables on these resistances to  $CO_2$  are investigated in this paragraph.

According to Stanghellini (1987) the leaf stomatal resistance  $R_{s,CO_2}$  [ $s\ m^{-1}$ ] to  $CO_2$  is a function of the temperature of the crop  $T_c$  [K], the  $CO_2$  concentration  $CO_{2a}$  [ $\mu mol[CO_2]\ mol^{-1}[air]$ ], the outdoor shortwave solar radiation  $I_o$  [ $W\ m^{-2}[soil]$ ] and the relative humidity  $RH_a$  [%]. It is assumed that the leaf area index  $LAI = 3\ m^{-2}[leaf]\ m^{-2}[soil]$ . The relations are shown in figure 2.3.

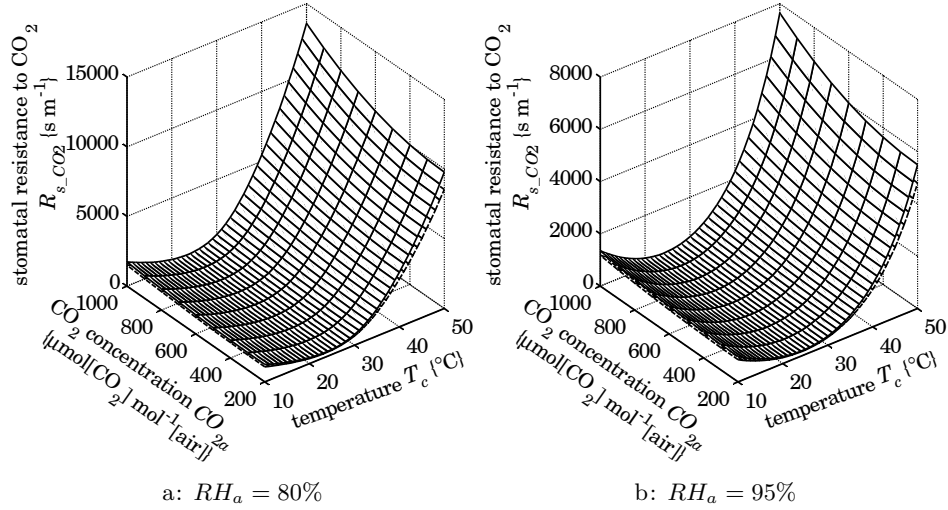


Figure 2.3: Leaf stomatal resistance to  $CO_2$   $R_{s,CO_2}$  as a function of  $T_c^\dagger$ ,  $CO_{2a}$ ,  $I_o$  and  $RH_a$ , with  $I_o = 200\ W\ m^{-2}[soil]$  (—) and  $1000\ W\ m^{-2}[soil]$  (---)  
 $^\dagger T_c$  in [K] in computations, in [°C] here for readability

From figure 2.3 it can be seen that the leaf stomatal resistance to  $CO_2$   $R_{s,CO_2}$  increases with the  $CO_2$  concentration  $CO_{2a}$ , decreases slightly with outdoor

shortwave solar radiation  $I_o$  and significantly with relative humidity  $RH_a$  and has a minimum for the temperature  $T_c$  of the crop. For the ranges chosen for  $CO_{2a}$  and  $T_c$  in figure 2.3, the value of  $R_{s\_CO2}$  ranges from 301 to  $13568 \text{ s m}^{-1}$ . The resistance  $R_{s\_CO2}$  can be as low as  $134 \text{ s m}^{-1}$  (with  $I_o = 1000 \text{ W m}^{-2}$ [soil],  $CO_{2a} = 200 \text{ } \mu\text{mol}[\text{CO}_2] \text{ mol}^{-1}[\text{air}]$ ,  $RH_a = 100\%$  and  $T_c = 25^\circ\text{C}$ ) and as high as  $49590 \text{ s m}^{-1}$  (with  $I_o = 6 \text{ W m}^{-2}$ [soil],  $CO_{2a} = 1000 \text{ } \mu\text{mol}[\text{CO}_2] \text{ mol}^{-1}[\text{air}]$ ,  $RH_a = 20\%$  and  $T_c = 50^\circ\text{C}$ ).

The leaf boundary layer resistance to  $\text{CO}_2$   $R_{b\_CO2} \{\text{s m}^{-1}\}$  is a function of the wind speed  $v_a \{\text{m s}^{-1}\}$ , the temperature difference between crop and greenhouse air  $|T_c - T_a| \{\text{K}\}$  and the mean leaf width  $l_f \{\text{m}\}$ . The relation is shown in figure 2.4.

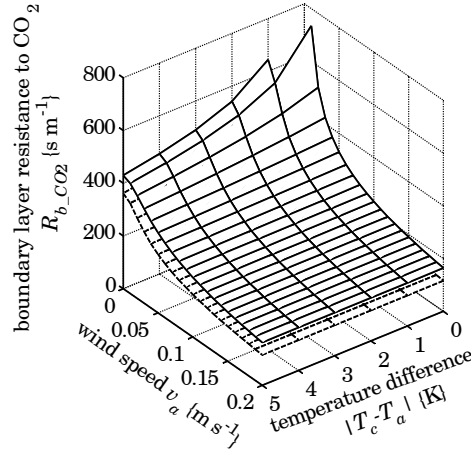


Figure 2.4: Leaf boundary layer resistance to  $\text{CO}_2$   $R_{b\_CO2}$  as a function of  $v_a$ ,  $|T_c - T_a|$  and  $l_f$ , with  $l_f = 0.0175 \text{ m}$  (---) and  $l_f = 0.035 \text{ m}$  (—)

From figure 2.4 it can be seen that the leaf boundary layer resistance to  $\text{CO}_2$   $R_{b\_CO2}$  decreases with the wind speed  $v_a$  and the temperature difference  $|T_c - T_a|$  and increases with the mean leaf width  $l_f$ . For the ranges chosen for  $v_a$  and  $|T_c - T_a|$  in figure 2.4, the value of  $R_{b\_CO2}$  ranges from 116 to  $\infty \text{ s m}^{-1}$  (if  $v_a = 0 \text{ m s}^{-1}$  and  $|T_c - T_a| = 0 \text{ K}$ ).

Stanghellini (1987) stated that the temperature difference  $(T_c - T_a)$  is in the range of 0 to 2 K. With the chosen values for the mean leaf width  $l_f = 0.035 \text{ m}$  and the wind speed  $v_a = 0.09 \text{ m s}^{-1}$ , the value of the resistance  $R_{b\_CO2}$  ranges from  $245 \text{ s m}^{-1}$  ( $|T_c - T_a| = 0 \text{ K}$ ) to  $242 \text{ s m}^{-1}$  ( $|T_c - T_a| = 2 \text{ K}$ ).

The results of this investigation are used in §2.3.2.3 to study the influence of these resistances on the photosynthesis rate.

### 2.3.2.3 Photosynthesis rate

To compare the photosynthesis models, they are tested with steady state conditions for the outdoor shortwave solar radiation  $I_o$ , the  $\text{CO}_2$  concentration  $\text{CO}_{2a}$  and the temperature  $T_c$  of the crop. It is clear from §2.3.2.2 that the values for the leaf resistances to  $\text{CO}_2$  are not constant, but vary with the crop environmental conditions. These resistances are part of the photosynthesis model, so they influence the result of the photosynthesis rate computation. To test this influence, the photosynthesis models are tested with constant resistances against the resistances determined with the evaporation model by Stanghellini (1987) as given in §2.3.2.2.

Simulations are made for 1 May at 12 o'clock at a latitude of  $52^\circ$  and a longitude of  $4.2^\circ$ . This influences the solar parameters specified in §2.B, such as the sine of the solar elevation (inclination)  $\sin\beta \{-\}$ , the transmittance  $\tau_{dirR} \{-\}$  of the roof for direct PAR radiation and the fractions PAR  $f_{par}$  and diffuse PAR  $f_{difpar} \{-\}$  in outdoor shortwave solar radiation. The following assumptions are made:

- The greenhouse air temperature  $T_a$  is equal to the temperature  $T_c$  of the crop. This implies that the boundary layer resistance to  $\text{CO}_2$   $R_{b\text{CO}_2}$  is constant.
- The relative humidity of the greenhouse air  $RH_a = 80\%$ .

Further general greenhouse and crop relations and parameters are given in table 2.3.

In figure 2.5 the photosynthesis rate  $P_g$  is given as a function of  $I_o$ ,  $\text{CO}_{2a}$  and  $T_c$  for models *CG1*, *CG2*, *CG3* and *CG4*. The stomatal and boundary layer resistances to  $\text{H}_2\text{O}$  are computed as described in §2.3.2.2.

From figure 2.5 it can be seen that:

- Model *CG1* gives a higher photosynthesis rate compared to *CG4*. In model *CG1* the gross canopy assimilation rate is computed from the gross leaf photosynthesis rate. This is done by simple multiplication of the leaf photosynthesis with an extinction coefficient. It is assumed that model *CG4* gives a better description than *CG1*, since it uses a three-layer Gaussian integration for the light interception in the crop layers instead of one-layer.
- Model *CG2* gives a higher photosynthesis rate for temperatures above  $30^\circ\text{C}$ . This is due to the equation for the maximum electron transport rate  $J_{\max}$ , which does not hold for temperatures above  $30^\circ\text{C}$  (see table 2.2 and figure 2.2). It is therefore assumed that the values found with model *CG2* for temperatures above  $30^\circ\text{C}$  are not correct.

Table 2.3: Greenhouse and crop parameters

name	value	unit	contents
Greenhouse parameters			
$\tau_{r-Is}$	$f_{dif} \cdot \tau_{difR} + (1 - f_{dif}) \cdot \tau_{dirR}$	—	Ⓔ transmittance shortwave radiation by roof
$\tau_{difR}$	0.78	—	transmittance diffuse PAR radiation by roof
$\tau_{dirR}$	(see §2.B)	—	transmittance direct PAR radiation by roof
$\beta_{s-Is}$	0.58	—	shortwave radiation coefficient, reflection by soil (white foil)
$p_{a-H2O}$	$p_{a-H2Os} \cdot \frac{RH_a}{100}$	$N m^{-2}$	vapour pressure air
$p_{a-H2Os}$	(see §2.C)	$N m^{-2}$	saturation vapour pressure air
Crop parameters			
$LAI$	3	$m^{-2}[\text{leaf}] m^{-2}[\text{soil}]$	leaf area index
$R_{cut}$	2000	$s m^{-1}$	cuticular resistance
$R_{min}$	82.003	$s m^{-1}$	minimum internal resistance crop (Jarvis' model)
$\rho_c$	700	$kg[b.m.] m^{-3}[b.m.]$	crop density
$k_{c-Il}$	0.64	—	Ⓔ extinction coefficient longwave radiation by crop
$k_{c-Is}$	0.48	—	Ⓔ extinction coefficient shortwave radiation by crop
$\beta_{c-Is\infty}$	0.12	—	shortwave radiation coefficient, reflection by crop (dense stand)
$\beta_{c-Is}$	$(1 - \tau_{c-Il}) \cdot \beta_{c-Is\infty}$	—	shortwave radiation coefficient, reflection by crop
$\tau_{c-Il}$	$e^{-k_{c-Il} \cdot LAI}$	—	Ⓔ transmittance longwave radiation by crop
$\tau_{c-Is}$	$e^{-k_{c-Is} \cdot LAI}$	—	transmittance shortwave radiation by crop
$\eta_{c-Is}$	$\tau_{r-Is} \cdot \tau_{sc-Is} \cdot (1 + \tau_{c-Is} \cdot \beta_{s-Is}) \cdot (1 - \tau_{c-Is} - \beta_{c-Is})$	—	shortwave radiation coefficient, absorption by canopy
$I_{c-s}$	$\eta_{c-Is} \cdot I_o = \frac{Q_{rd-c}}{A_s}$	$W m^{-2}[\text{soil}]$	shortwave radiation absorption by crop
$\Delta p_{c-H2Om}$	$0.01(p_{c-H2Os} - p_{a-H2O})$	mbar	saturation deficit crop
$p_{c-H2Os}$	(see §2.C)	$N m^{-2}$	saturation vapour pressure crop

ⒺDe Zwart (1996); ⒺAcock et al. (1978); ⒺGoudriaan (1987)

- Model *CG3* shows a strange dent at a temperature of 45°C. This is due to the equation for the maximum electron transport rate  $J_{max}$ , which is a trapezium shape that equals zero for temperatures above 45°C (see table 2.2 and figure 2.2). The discontinuity in the response makes it less suitable for optimal control.

Next the stomatal and boundary layer resistances to  $H_2O$  are assumed constant, with values of 50 and  $100 s m^{-1}$  respectively. In figure 2.6 the responses of the photosynthesis rate  $P_g$  are given as a function of  $I_o$ ,  $CO_{2a}$  and  $T_c$  for models *CG1*, *CG2*, *CG3* and *CG4*.

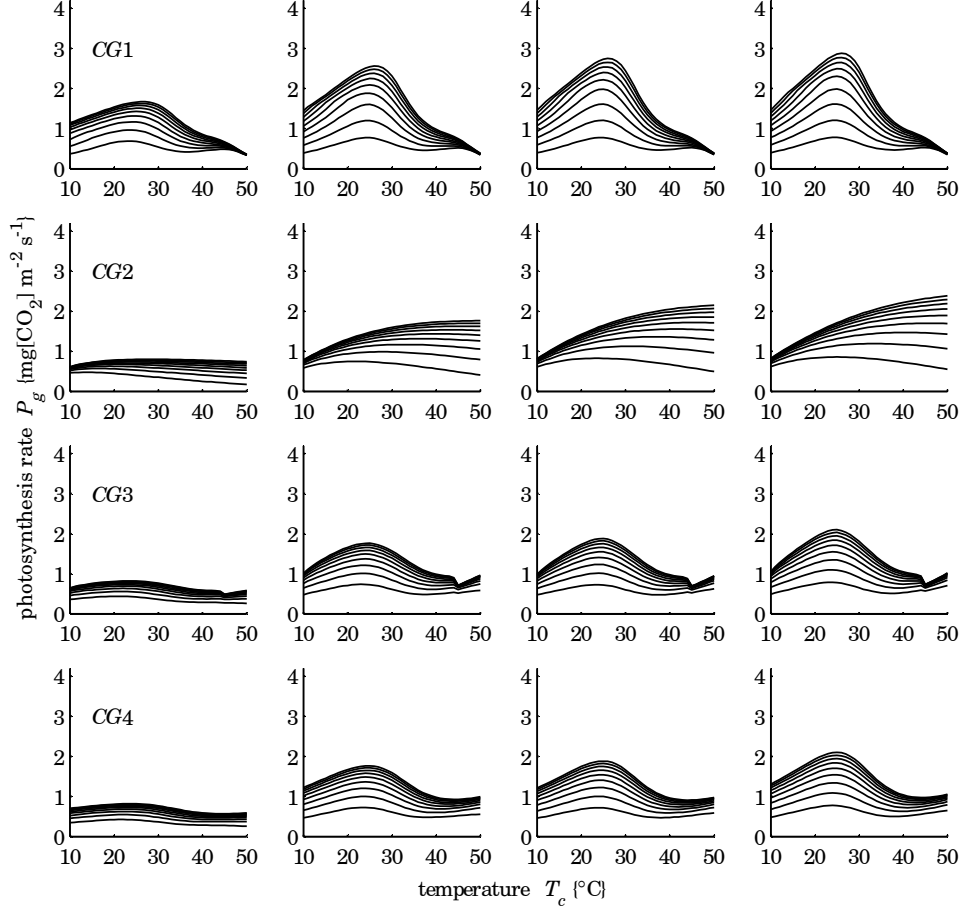


Figure 2.5: Photosynthesis rate  $P_g$  with variable resistances  $R_{s\_CO2}$  and  $R_{b\_CO2}$  for models  $CG1$ ,  $CG2$ ,  $CG3$  and  $CG4$  as a function of  $I_o$ ,  $CO_{2a}$  and  $T_c^\dagger$ , with from left to right  $I_o = 200, 600, 800, 1000 \text{ W m}^{-2}[\text{soil}]$  and from bottom to top  $CO_{2a} = 200, 300, 400, \dots, 1000 \mu\text{mol}[\text{CO}_2] \text{ mol}^{-1}[\text{air}]$

$^\dagger T_c$  in {K} in computations, in {°C} here for readability

From figure 2.6 compared to figure 2.5 it can be seen that:

- Model  $CG2$  gives the same response, since it does not use the resistances.
- Model  $CG3$  gets a more trapezium-like shape.
- Models  $CG1$  and  $CG4$  show about the same form. The photosynthesis rate is increased and the temperature where the highest photosynthesis rate is found is increased.

It is known that the leaf boundary resistances are not constant, especially at extreme temperatures and humidities, which are expected to occur in the solar

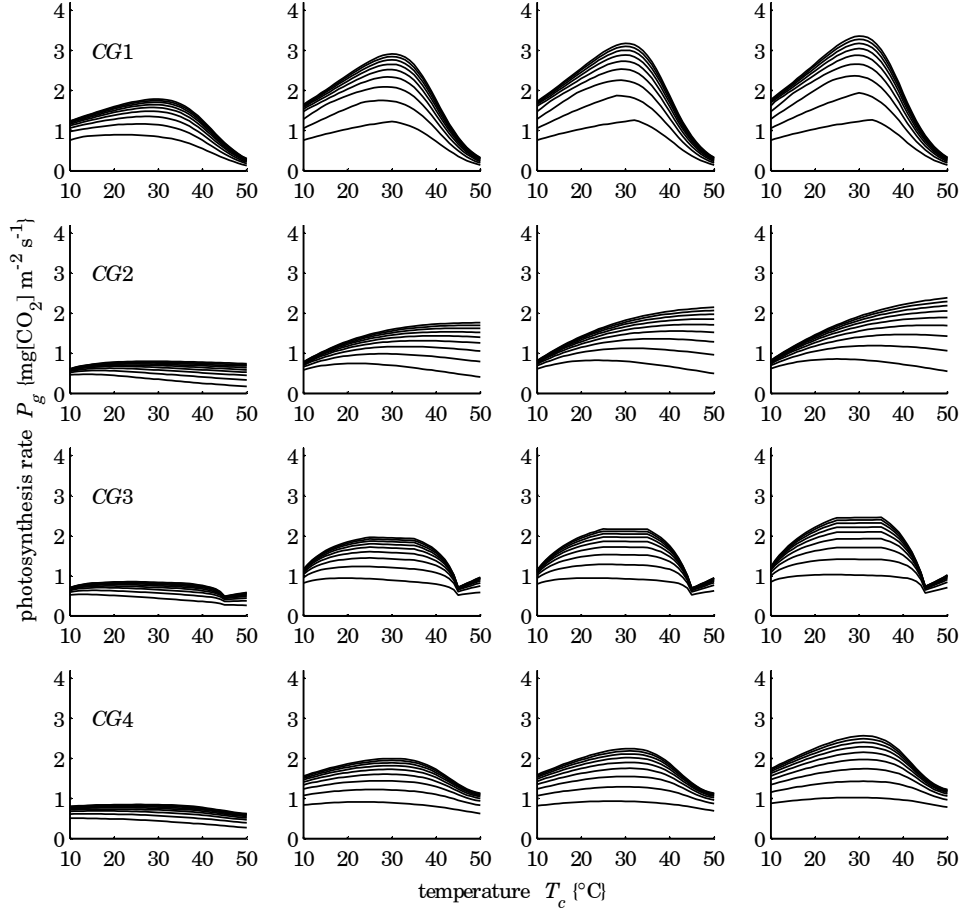


Figure 2.6: Photosynthesis rate  $P_g$  with fixed resistances  $R_{s,CO_2}$  and  $R_{b,CO_2}$  for models  $CG1$ ,  $CG2$ ,  $CG3$  and  $CG4$  as a function of  $I_o$ ,  $CO_{2a}$  and  $T_c^\dagger$ , with from left to right  $I_o = 200, 600, 800, 1000 \text{ W m}^{-2}[\text{soil}]$  and from bottom to top  $CO_{2a} = 200, 300, 400, \dots, 1000 \mu\text{mol}[\text{CO}_2] \text{ mol}^{-1}[\text{air}]$

$^\dagger T_c$  in {K} in computations, in {°C} here for readability

greenhouse. It is therefore assumed here that the model by Stanghellini (1987) gives a better description than constant resistances.

In model  $CG4$  the detailed description of the photosynthesis parameters from model  $CG1$  is combined with the Gaussian integration over the crop height from model  $CG3$  and the equations for the resistances from Stanghellini (1987). Based on the comparison of the simulated responses in figures 2.5 and 2.6 it is assumed that model  $CG4$  gives the most accurate description of the

photosynthesis rate, because it describes the known photosynthesis behaviour over a wider range of conditions.

#### 2.3.2.4 Respiration rate

The dark respiration rate  $r_D$   $\{\text{mg}[\text{CO}_2] \text{ m}^{-2}[\text{soil}] \text{ s}^{-1}\}$  is a function of the temperature  $T_c$   $\{\text{K}\}$  of the crop. In figure 2.7 the response of the dark respiration rate  $r_D$  is given as a function of  $T_c$  for models *CG1*, *CG2*, *CG3* and *CG4*.

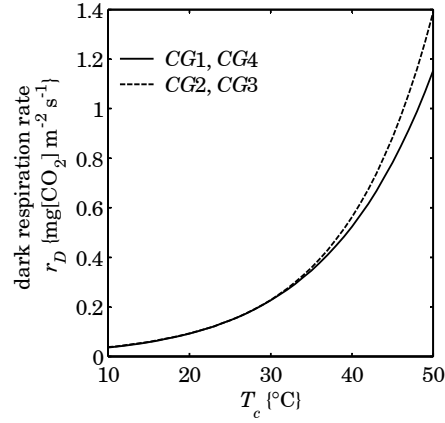


Figure 2.7: Dark respiration rate  $r_D$  for models *CG1*, *CG2*, *CG3* and *CG4* as a function of  $T_c$  <sup>†</sup>  $T_c$  in  $\{\text{K}\}$  in computations, in  $\{\text{°C}\}$  here for readability

Only a small difference is found between the models, which is due to the fact that the models *CG2* and *CG3* use a  $Q_{10}$  function (Gijzen, 1994; Goudriaan and van Laar, 1994) and *CG1* and *CG4* use an Arrhenius function (Farquhar et al., 1980). The description by the Arrhenius function is preferred over the  $Q_{10}$  function, since it is more physical and detailed.

## 2.4 Temperature integration

Temperature integration is used as a descriptive method for long-term temperature effects on crop development. A descriptive method is used since — to our best knowledge — no simple accurate models for crop development exist. More elaborate models for crop development do exist. These models however work on a larger timescale (days, up to 10-day periods), are too detailed (many crop development stages), are too crop specific or are not developed

for greenhouse climate but for the open field (different temperature, humidity and CO<sub>2</sub> conditions).

The temperature integration concept is based on the results of horticultural research, which indicates that crop growth responds to long-term average temperatures rather than specific day and night temperature profiles (Sigrimis et al., 2000). Photosynthesis is an almost instantaneous process, while the processing of the assimilates is a slower, dynamical process. It can be assumed that the crop stores the assimilates in a carbohydrate pool (Seginer et al., 1994). The capacity of the assimilate pool is crop specific and it probably differs for each development stage. Temperature integration is a simplified approach to the same theory. The buffering capacity is not specified in this concept, but it is assumed sufficient over a period of several days (de Koning, 1988). The concept is mainly based on empirical observations.

Much research has been done on temperature integration to describe crop development (Körner and Challa, 2003; van den Bosch, 1998; Gijzen et al., 1998; Elings et al., 2005), and it is already in use by many commercial greenhouse horticulturists. The duration of the temperature integration and the boundary values described here are based on the research by Körner and Challa (2003), who developed temperature integration rules specifically for the solar greenhouse. The underlying assumption is that crop development is determined by an average temperature, rather than the actual temperature. In addition it is assumed that temperature deviations that occurred long ago can no longer be compensated for — as far as their influence on crop development is concerned — and should therefore not be taken into account.

For the temperature integral used in this thesis a time period of six days is considered. From these six days, five days ( $t_p$  {s}) are in the past, and one day ( $t_f$  {s}) is used to correct for this past.

The temperature integral is determined from the temperature of the indoor air  $T_a$ . An example is given in figure 2.8. The average temperature of the indoor air  $\bar{T}_{a.ts}$  (dashed) is saved at every sampling interval  $t_s$  (1800 s) for the days in the past ( $t_p$ ). The predicted temperature course  $\hat{T}_a$  for the day in the future ( $t_f$ ) is found by simulating the greenhouse-with-crop model during the next day. The temperature  $T_{aref} = T_0 + 19$  K (dotted) is the reference temperature for the temperature integral.

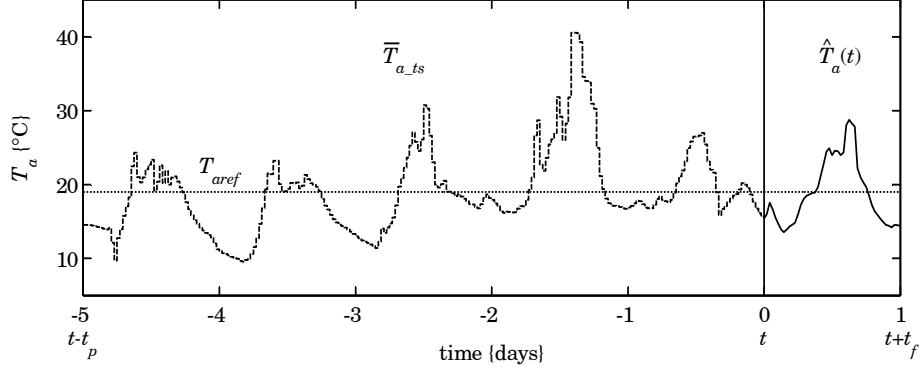


Figure 2.8: Temperature trajectory  $T_a^\dagger$  for temperature integral  $^\dagger T_a$ ,  $\bar{T}_{a\_ts}$ ,  $\hat{T}_a$  and  $T_{aref}$  in {K} in computations, in {°C} here for readability

The temperature integral trajectory  $S_T$  at time  $t$  is described by

$$S_T(t, \tau) = \frac{1}{n_{secs}} \cdot \int_0^\tau (\hat{T}_a(t, \nu) - T_{aref}) d\nu + S_{T0}(t) \quad \forall 0 \leq \tau \leq t_f$$

{K day} (2.43)

in which  $t_f = 1 n_{secs}$  s (1 day)<sup>⊙</sup> is the future horizon, where  $t$  {s} is the current time and  $\hat{T}_a(t, \tau)$  {K} is the predicted temperature of the indoor air at time  $\nu$  based on information until time  $t$ . This gives a trajectory  $S_T(t, \tau)$  for every time  $t$  where  $\tau$  runs from 0 to  $t_f$  (see figure 2.9).

The initial value  $S_{T0}(t)$  of the temperature integral is defined so that temperature deviations that occurred more than five days ago are not taken into account. The initial value of the temperature integral  $S_{T0}(t)$  at time  $t$  {s} is therefore computed over the past horizon  $t_p$  {s}

$$S_{T0}(t) = \frac{1}{n_{secs}} \cdot \int_{t-t_p}^t (T_a(\nu) - T_{aref}) d\nu$$

{K day} (2.44)

in which  $t_p = 5 n_{secs}$  s (5 days) is the past horizon, where  $T_a$  {K} is the temperature of the indoor air.

<sup>⊙</sup> Since the unit of the temperature integral is {K day}, time has to be converted from {s} to {day} with the number of seconds in a day  $n_{secs} = 86400 \text{ s day}^{-1}$ .

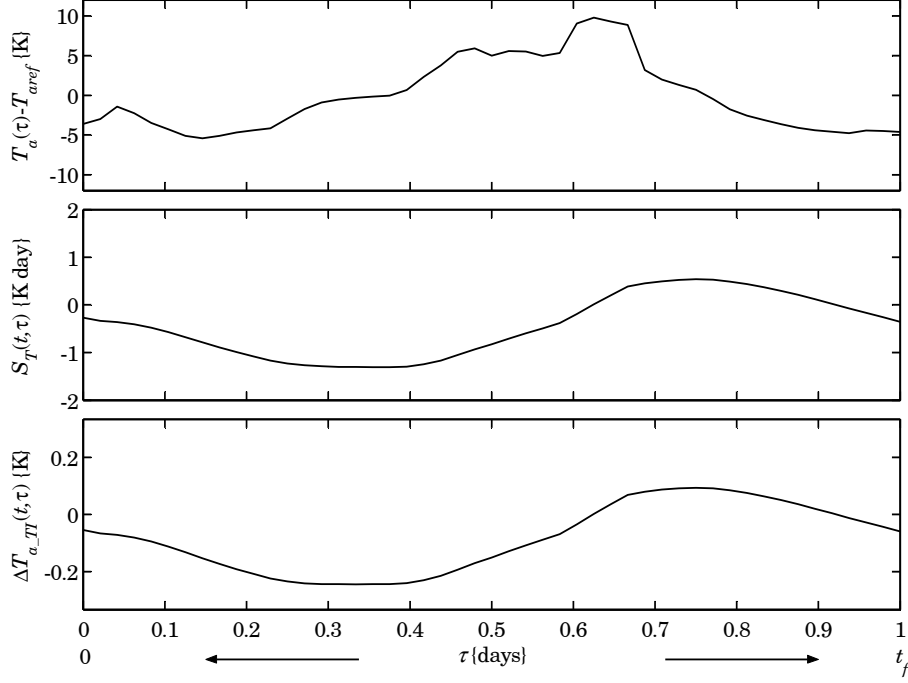


Figure 2.9: Temperature deviation  $T_a - T_{aref}$ , temperature integral  $S_T$  and predicted average temperature deviation  $\Delta T_{a\_TI}$  at time  $t$

This integral is approximated numerically by a summation, where the average temperature of the indoor air  $\bar{T}_{a\_ts}$  is saved at every sampling interval  $t_s$  (1800 s)

$$S_{T0}(t) = \frac{1}{n_{secs}} \cdot \sum_{k_\nu = \frac{t-t_p}{t_s}}^{\frac{t}{t_s}} (\bar{T}_{a\_ts}(k_\nu) - T_{aref}) \cdot t_s \quad \{\text{K day}\} \quad (2.45)$$

where  $k_\nu$  is the discrete time step. In the example given in figure 2.9 the initial value  $S_{T0}(t) = -0.194$  K day. The initial value  $S_{T0}(t)$  of the temperature integral is recomputed (and thus changed) at every time interval  $t_s$ .

The predicted average temperature deviation trajectory  $\Delta T_{a\_TI}(t, \tau)$  at time  $t$  is given by

$$\Delta T_{a\_TI}(t, \tau) = \frac{S_T(t, \tau)}{\frac{t_p + \tau}{n_{secs}}} \quad \forall 0 \leq \tau \leq t_f \quad \{\text{K}\} \quad (2.46)$$

This describes the average deviation between the past and forecasted temperatures  $T_a$  and  $\hat{T}_a$  and the reference temperature  $T_{aref}$  (see figure 2.9).

The aims for the temperature integral are to keep the average temperature deviation  $\Delta T_{a\_TI}$  within the boundary values of  $\pm 6$  K (see table 4.1) and to obtain an average temperature deviation of zero at the end of the control horizon of one day

$$\begin{aligned} -6 \leq \Delta T_{a\_TI}(t, \tau) \leq 6 & \quad \forall 0 \leq \tau \leq t_f \\ \Delta T_{a\_TI}(t_f) &= 0 \end{aligned} \quad \{\text{K}\} \quad (2.47)$$

These aims will be implemented as receding horizon optimal control objectives in chapter 4. In the example in figure 2.9 the average temperature deviation  $\Delta T_{a\_TI}$  ranges from  $-0.25$  to  $0.09$  K, while its value at the end of the day  $\Delta T_{a\_TI}(t_f) = -0.06$  K.

## References

- B. Acock, D.A. Charles-Edwards, D.J. Fitter, D.W. Hand, L.J. Ludwig, J.W. Wilson, and A.C. Withers (1978). The contribution of leaves from different levels within a tomato crop to canopy net photosynthesis: an experimental examination of two canopy models. *Journal of experimental botany*, 29, pp. 815–827.
- G.P.A. Bot (1983). *Greenhouse climate: from physical processes to a dynamic model*. Ph.D. thesis, Wageningen Agricultural University, Wageningen, The Netherlands. 240 p.
- G.P.A. Bot (2001). Developments in indoor sustainable plant production with emphasis on energy saving. *Computers and Electronics in Agriculture*, 30, pp. 151–165.
- A.N.M. de Koning (1988). More efficient use of base load heating with a temperature integrating control programme; effect on development, growth and production of tomato. *Acta Horticulturae*, 229, pp. 233–237.
- H.F. de Zwart (1996). *Analyzing energy-saving options in greenhouse cultivation using a simulation model*. Ph.D. thesis, Wageningen Agricultural University, Wageningen, The Netherlands. 236 p.
- A. Defant and F. Defant (1958). *Physikalische Dynamik der Atmosphäre*. Akademische Verlagsgesellschaft, Frankfurt, Germany. (in German).
- A. Elings, F.L.K. Kempkes, R.C. Kaarsemaker, M.N.A. Ruijs, N.J. van de Braak, and T.A. Dueck (2005). The energy balance and energy-saving measures in greenhouse tomato cultivation. *Acta Horticulturae (ISHS)*, 691, pp. 67–74.

- J.R. Evans and G.D. Farquhar (1991). *Modeling crop photosynthesis: from biochemistry to canopy*, chapter 1: Modelling canopy photosynthesis from the biochemistry of the C<sub>3</sub> chloroplast, pp. 1–15. Madison, Wisconsin, USA. Editors: K.J. Boote and R.S. Loomis, CSSA special publication no. 19.
- G.D. Farquhar (1988). Models relating subcellular effects of temperature to whole plant responses. In: *Plants and temperature*, vol. 42, pp. 395–409. Society for experimental biology; Editors: S.P. Long and F.I. Woodward.
- G.D. Farquhar and S. von Caemmerer (1982). Modelling of photosynthetic response to environmental conditions. In: *Encyclopedia of plant physiology, New series; Physiological Plant Ecology II*, vol. 12B, pp. 549–587, Springer-Verlag, Heidelberg, Germany. Editors: O.L. Lange, P.S. Nobel, and H. Ziegler.
- G.D. Farquhar, S. von Caemmerer, and J.A. Berry (1980). A biochemical model of photosynthetic CO<sub>2</sub> assimilation in leaves of C<sub>3</sub> species. *Planta*, 149, pp. 78–90.
- W. Ferrel (1885). Annual report of the chief signal officer of the army to the secretary of war for the year 1886. Appendix 24, Washington DC.
- J. Goudriaan (1987). *Simulatie van gewasgroei*. Wageningen Agricultural University, the Netherlands. (in Dutch).
- J. Goudriaan and H.H. van Laar (1994). *Modelling potential crop growth process*, vol. 2. Kluwer academic publishers, Dordrecht, the Netherlands. 238 p.
- H. Gijzen (1994). Ontwikkeling van een simulatiemodel voor transpiratie en wateropname en van een integraal gewasmodel. AB-DLO, rapport 18, Wageningen, The Netherlands. (in Dutch).
- H. Gijzen, E. Heuvelink, H. Challa, E. Dayan, L.F.M. Marcelis, S. Cohen, and M. Fuchs (1998). Hortisim: a model for greenhouse crops and greenhouse climate. *Acta Horticulturae*, 456, pp. 441–450.
- E. Heuvelink (1996). *Tomato growth and yield: quantitative analysis and synthesis*. Ph.D. thesis, Wageningen Agricultural University, Wageningen, The Netherlands. 326 p.
- O. Körner and H. Challa (2003). Design for an improved temperature integration concept in greenhouse cultivation. *Computers and Electronics in Agriculture*, 39(1), pp. 39–59.
- O. Körner, H. Challa, and R.J.C. van Oorteghem (2001a). Modelling temperature effects on crop photosynthesis at high radiation in a solar greenhouse. In: *Joint meeting on modeling for the 21<sup>st</sup> century: Agronomic and greenhouse crop models; ISHS symposium*.
- O. Körner, H. Challa, and R.J.C. van Oorteghem (2001b). Modelling temperature effects on crop photosynthesis at high radiation in a solar greenhouse.

- In: *Workshop Modelling for the 21st century: Agronomic and greenhouse crop models; Joined meeting of International Society of Horticultural Science (ISHS) and Biological Systems Simulation Group (BSSG)*, Beltsville, Maryland, USA. March 25–29.
- O. Körner, H. Challa, and R.J.C. van Oorteghem (2002). Modelling temperature effects on crop photosynthesis at high radiation in a solar greenhouse. *Acta Horticulturae*, 593, pp. 137–144.
- O. Körner, H. Challa, and R.J.C. van Oorteghem (2003). Chapter 2.1: Modelling temperature effects on crop photosynthesis. In: *Crop based climate regimes for energy saving in greenhouse cultivation*, pp. 29–36, Ph.D. thesis, Wageningen University, Wageningen, The Netherlands.
- O. Körner, Q. Niu, and E. Heuvelink (2007a). Quantification of temperature and CO<sub>2</sub> effects on crop photosynthesis. In preparation.
- O. Körner, Q. Niu, and R.J.C. van Oorteghem (2007b). Simulations of high temperature and CO<sub>2</sub> effects on greenhouse crop photosynthesis. In preparation.
- O. Körner and R.J.C. van Oorteghem (2003). Chapter 2.4: Simulating crop gross photosynthesis at high temperatures. In: *Crop based climate regimes for energy saving in greenhouse cultivation*, pp. 75–90, Ph.D. thesis, Wageningen University, Wageningen, The Netherlands.
- J.L. Monteith and M.H. Unsworth (1990). *Principles of environmental physics*. Edward Arnold, London, United Kingdom, 2<sup>nd</sup> edition. 291 p.
- I. Seginer, C. Gary, and M. Tchamitchian (1994). Optimal temperature regimes for a greenhouse crop with a carbohydrate pool: a modelling study. *Scientia Horticulturae*, 60, pp. 55–80.
- N. Sigrimis, A. Anastasiou, and N. Rerras (2000). Energy saving in greenhouses using temperature integration: a simulation survey. *Computers and Electronics in Agriculture*, 26(1), pp. 321–341.
- Smithsonian Meteorological Tables (1966). Washington D.C., 6<sup>th</sup> (revised) edition. Editor: R.J. List.
- C.J.T. Spitters (1986). Separating the diffuse and direct component of global radiation and its implications for modeling canopy photosynthesis. Part II. Calculation of canopy photosynthesis. *Agricultural and forest meteorology*, 38, pp. 231–242.
- C. Stanghellini (1987). *Transpiration of greenhouse crops — an aid to climate management*. Ph.D. thesis, Wageningen Agricultural University, Wageningen, The Netherlands. 150 p.
- J.A.M. van den Bosch (1998). Opportunities and bottlenecks for model applications in practice. *Acta Horticulturae*, 456, pp. 505–508.

## Appendices chapter 2

### 2.A Photosynthesis models

In this appendix the photosynthesis models, compared in §2.3.2 are given. A comprehensive list of variables and parameters is given in appendix B. Some general photosynthesis parameters are given in table 2.1.

#### 2.A.1 CG1 General Farquhar model

This model is based on Farquhar et al. (1980). The model uses a detailed description of the biochemical processes. This model is a leaf photosynthesis model. The gross canopy photosynthesis rate is computed from the gross leaf photosynthesis rate by simple multiplication with an extinction coefficient. The photosynthesis parameters specific for model *CG1* are given in table 2.4 and the equations for the computation of gross assimilation and dark respiration rate are given in table 2.4.

#### 2.A.2 CG2 Big leaf Farquhar model

This model is based on Gijzen (1994), which is a further development of Evans and Farquhar (1991). In the big leaf model, the canopy is treated as one big leaf. This assumption is made based on the hypothesis that all leaves have the same curvature in the photosynthesis-light response curve. The photosynthesis parameters specific for model *CG2* are given in table 2.5 and the equations for the computation of gross assimilation and dark respiration rate are given in table 2.5.

#### 2.A.3 CG3 Goudriaan model

This model is based on Goudriaan and van Laar (1994). The model uses a simplified description of the biochemical processes. Gaussian integration is used to integrate the light interception in the layers of the crop over the crop height according to Goudriaan and van Laar (1994). This model has been successfully validated under normal temperature and humidity conditions for a tomato crop by Heuvelink (1996). The photosynthesis parameters specific for model *CG3* are given in table 2.6 and the equations for the computation of gross assimilation and dark respiration rate are given in table 2.6.

Table 2.4: Model CG1

a: photosynthesis parameters

name	value	unit	contents
$f_{OC}$	0.21	—	⊙ $f_{OC} = \frac{V_{O\max}}{V_{C\max}} = \frac{ko}{kc} = \text{constant}$
$\gamma$	2.1	$\mu\text{mol}[\text{photons}] \mu\text{mol}^{-1}[\text{e}^-]$	Ⓣ conversion factor, $\text{e}^-$ to photons
$\psi$	$\frac{\zeta}{\gamma}$	$\mu\text{mol}[\text{e}^-] \text{J}^{-1}$	Ⓣ conversion factor, J to $\text{e}^-$
Temperature dependencies			
$\rho_{CO2T}$	$\rho_{CO2} \cdot \frac{T_0}{T_c}$	$\text{kg}[\text{CO}_2] \text{m}^{-3}[\text{CO}_2]$	$\text{CO}_2$ density at $T_c$ (gaslaw)
$X$	$\frac{T_c - T_{25}}{T_c \cdot R_g \cdot T_{25}}$	$\text{mol} \text{J}^{-1}$	⊙ intermediate variable
$K_C$	$K_{C25} \cdot e^{E_C \cdot X}$	$\mu\text{bar}$	⊙ Michaelis Menten constant Rubisco carboxylation ( $\text{CO}_2$ )
$K_O$	$K_{O25} \cdot e^{E_O \cdot X}$	$\text{mbar}$	⊙ Michaelis Menten constant Rubisco oxygenation ( $\text{O}_2$ )
$K_M$	$K_C \cdot \left(1 + \frac{p_{O2i}}{K_O}\right)$	$\mu\text{bar}$	Ⓜ effective Michaelis Menten constant ( $\text{CO}_2$ )
$V_{C\max}$	$V_{C\max 25} \cdot e^{E_{VC} \cdot X}$	$\mu\text{mol}[\text{CO}_2] \text{m}^{-2}[\text{leaf}] \text{s}^{-1}$	⊙ maximum carboxylation rate
$r_{D-uL}$	$r_{D25-uL} \cdot e^{E_D \cdot X}$	$\mu\text{mol}[\text{CO}_2] \text{m}^{-2}[\text{leaf}] \text{s}^{-1}$	⊙ dark respiration rate leaves
$S$	710	$\text{J} \text{mol}^{-1} \text{K}^{-1}$	⊙ constant for optimum curve temperature dependent electron transport rate
$H$	220000	$\text{J} \text{mol}^{-1}$	⊙ constant for optimum curve temperature dependent electron transport rate
$D$	$\frac{1 + e^{\frac{S \cdot T_c - H}{R_g \cdot T_c}}}{1 + e^{\frac{S \cdot T_{25} - H}{R_g \cdot T_{25}}}}$	—	ⓂⓉ intermediate variable
$J_{\max}$	$J_{\max 25} \cdot \frac{e^{E_J \cdot X}}{D}$	$\mu\text{mol}[\text{e}^-] \text{m}^{-2}[\text{leaf}] \text{s}^{-1}$	Ⓜ⊙ maximum electron transport rate
$\Gamma$	$\frac{K_C}{2 K_O} \cdot p_{O2i} \cdot f_{OC}$	$\mu\text{mol}[\text{CO}_2] \text{mol}^{-1}[\text{air}]$	⊙ $\text{CO}_2$ compensation concentration in absence of dark respiration

Ⓜ Gijzen (1994); Ⓣ Farquhar and von Caemmerer (1982); ⊙ Farquhar et al. (1980)

b: gross assimilation and dark respiration

name	value	unit	contents
$I_{P\psi}$	$\psi \cdot I_P$	$\mu\text{mol}[\text{e}^-] \text{m}^{-2}[\text{soil}] \text{s}^{-1}$	absorbed PAR
$J_C$	$\frac{J_{\max} \cdot I_{P\psi}}{I_{P\psi} + J_{\max}}$	$\mu\text{mol}[\text{e}^-] \text{m}^{-2}[\text{leaf}] \text{s}^{-1}$	Ⓣ electron transport rate carboxylation
$R_{CO2}$	$R_{b,CO2} + R_{s,CO2}$	$\text{s} \text{m}^{-1}$	stomatal resistance + boundary layer resistance to $\text{CO}_2$ diffusion
$CO_{2i}$	$CO_{2a} - \frac{R_{CO2}}{\rho_{CO2T}} \cdot M_{CO2} \cdot (P_{g-uL} - r_{D-uL})$	$\mu\text{mol}[\text{CO}_2] \text{mol}^{-1}[\text{air}]$	$\text{CO}_2$ concentration inside stomata, determined by recursive computation since $P_{g-uL} = f(CO_{2i})$
$P_c$	$V_{C\max} \cdot \frac{CO_{2i} - \Gamma}{CO_{2i} + K_M}$	$\mu\text{mol}[\text{CO}_2] \text{m}^{-2}[\text{leaf}] \text{s}^{-1}$	Ⓣ carboxylation rate, Rubisco limited
$P_j$	$J_C \cdot \frac{CO_{2i} - \Gamma}{4.5 CO_{2i} + 10.5 \Gamma}$	$\mu\text{mol}[\text{CO}_2] \text{m}^{-2}[\text{leaf}] \text{s}^{-1}$	Ⓣ carboxylation rate, RuP2 limited
$P_{g-uL}$	$\min(P_c, P_j)$	$\mu\text{mol}[\text{CO}_2] \text{m}^{-2}[\text{leaf}] \text{s}^{-1}$	Ⓣ gross assimilation rate leaves
$\eta$	$1 - e^{-k_{cis} \cdot LAI}$	—	Ⓣ absorption coefficient canopy
$P_g$	$M_{CO2} \cdot P_{g-uL} \cdot LAI \cdot \eta$	$\text{mg}[\text{CO}_2] \text{m}^{-2}[\text{soil}] \text{s}^{-1}$	gross assimilation rate canopy
$r_D$	$M_{CO2} \cdot r_{D-uL} \cdot LAI$	$\text{mg}[\text{CO}_2] \text{m}^{-2}[\text{soil}] \text{s}^{-1}$	dark respiration rate canopy

Ⓣ Farquhar and von Caemmerer (1982); Ⓣ Stanghellini (2005, personal communication)

Table 2.5: Model *CG2*  
a: photosynthesis parameters

name	value	unit	contents
Temperature dependencies			
$r_{D_{uL}}$	$r_{D25_{uL}} \cdot Q_{10rD}^{0.1(T_c - T_{25})}$	$\mu\text{mol}[\text{CO}_2] \text{ m}^{-2}[\text{leaf}] \text{ s}^{-1}$	dark respiration rate leaves
$J_{\max}$	$J_{\max 25} \cdot \frac{T_c - T_0}{25}$	$\mu\text{mol}[\text{e}^-] \text{ m}^{-2}[\text{leaf}] \text{ s}^{-1}$	Ⓐ maximum electron transport rate; for $T_c < 30^\circ\text{C}$
$\Gamma$	$1.7 (T_c - T_0)$	$\mu\text{mol}[\text{CO}_2] \text{ mol}^{-1}[\text{air}]$	Ⓑ $\text{CO}_2$ compensation concentration in absence of dark respiration
Radiation parameters			
$f_{SLA}$	$\frac{1 - \tau_{dirBL}}{k_{dirBL}}$	—	Ⓐ fraction sunlit leaf area
$F_p$	0.3	—	Ⓐ fraction PAR absorbed by non-photosynthetic tissues
$\Theta$	0.7	—	Ⓐ Ⓑ degree of curvature of $\text{CO}_2$ response of light saturated net photosynthesis
$\psi$	$\frac{1 - F_p}{2} \cdot \zeta$	$\mu\text{mol}[\text{e}^-] \text{ J}^{-1}$	Ⓑ conversion factor, J to $\text{e}^-$
$f_{CO2ia}$	0.67	—	Ⓐ fraction $\text{CO}_2$ inside compared to outside stomata
$CO_{2i}$	$f_{CO2ia} \cdot CO_{2a}$	$\mu\text{mol}[\text{CO}_2] \text{ mol}^{-1}[\text{air}]$	Ⓐ $\text{CO}_2$ concentration inside stomata

Ⓐ Gijzen (1994); Ⓑ Farquhar and von Caemmerer (1982); Ⓒ Farquhar (1988)

#### 2.A.4 CG4 New photosynthesis model

This model combines the detailed description of the biochemical processes from Farquhar et al. (1980) with the description by Goudriaan and van Laar (1994). Gaussian integration is used to integrate the light interception in the layers of the crop over the crop height according to Goudriaan and van Laar (1994). This model is described in §2.3.1. The photosynthesis parameters are given in table 2.7 and the equations for gross assimilation and dark respiration rate are given in table 2.7.

### 2.B Solar radiation parameters

In most cases the measured data only holds the outdoor shortwave solar radiation  $I_o$   $\{\text{W m}^{-2}\}$ . The fractions PAR  $f_{par}$  and diffuse PAR  $f_{difpar}$   $\{-\}$  in the outdoor shortwave solar radiation, and other terms like the transmittance  $\tau_{dirR}$  of the roof for direct radiation have to be computed. These parameters depend on the position of the sun in relation to the location of the greenhouse (Goudriaan and van Laar, 1994) and on time.

Table 2.5: Model *CG2* (continued)

b: gross assimilation and dark respiration

name	value	unit	contents
Absorbed radiation			
$I_{A\_dif t}$	$(1 - \beta_{dif}) \cdot I_{P\_dif} \cdot (1 - \tau_{dif})$	$\text{W m}^{-2} [\text{soil}]$	Ⓐ total diffuse flux, excl. ground reflected
$I_{A\_dif r}$	$\beta_{s\_Is} \cdot ((1 - \beta_{dif}) \cdot I_{P\_dif} \cdot \tau_{dif} + (1 - \beta_{dir}) \cdot I_{P\_dir} \cdot \tau_{dir})$	$\text{W m}^{-2} [\text{soil}]$	Ⓐ ground reflected diffuse flux
$I_{A\_dif}$	$I_{A\_dif t} + I_{A\_dif r} \cdot (1 - \tau_{dif})$	$\text{W m}^{-2} [\text{soil}]$	Ⓐ total diffuse flux, incl. ground reflected
$I_{A\_tdir}$	$(1 - \beta_{dir}) \cdot I_{P\_dir} \cdot (1 - \tau_{dir})$	$\text{W m}^{-2} [\text{soil}]$	Ⓐ total direct flux, incl. secondary diffuse
$I_{A\_dir}$	$(1 - \delta) \cdot I_{P\_dir} \cdot (1 - \tau_{dirBL})$	$\text{W m}^{-2} [\text{soil}]$	Ⓐ direct flux (not scattered)
$I_{A\_ppd}$	$(1 - \delta) \cdot k_{dirBL} \cdot I_{P\_dir}$	$\text{W m}^{-2} [\text{soil}]$	Ⓐ direct flux leaves perpendicular on direct beam
$I_{A\_shd}$	$I_{A\_dif} + I_{A\_tdir} - I_{A\_dir}$	$\text{W m}^{-2} [\text{soil}]$	Ⓐ flux shaded part of big leaf
$I_{A\_sun}$	$I_{A\_shd} + I_{A\_ppd}$	$\text{W m}^{-2} [\text{soil}]$	Ⓐ flux sunlit part of big leaf
$I_{P\psi\_shd}$	$\psi \cdot I_{A\_shd}$	$\mu\text{mol}[\text{e}^-] \text{m}^{-2} [\text{soil}] \text{s}^{-1}$	Ⓐ absorbed PAR, shaded leaves
$I_{P\psi\_sun}$	$\psi \cdot I_{A\_sun}$	$\mu\text{mol}[\text{e}^-] \text{m}^{-2} [\text{soil}] \text{s}^{-1}$	Ⓐ absorbed PAR, sunlit leaves
$J_{C\_shd}$	$\left( J_{\max} + I_{P\psi\_shd} - \left( (J_{\max} + I_{P\psi\_shd})^2 - 4 \Theta \cdot J_{\max} \cdot I_{P\psi\_shd} \right)^{\frac{1}{2}} \right) / (2 \Theta)$	$\mu\text{mol}[\text{e}^-] \text{m}^{-2} [\text{soil}] \text{s}^{-1}$	Ⓐ electron transport rate carboxylation, shaded part
$J_{C\_sun}$	$\left( J_{\max} + I_{P\psi\_sun} - \left( (J_{\max} + I_{P\psi\_sun})^2 - 4 \Theta \cdot J_{\max} \cdot I_{P\psi\_sun} \right)^{\frac{1}{2}} \right) / (2 \Theta)$	$\mu\text{mol}[\text{e}^-] \text{m}^{-2} [\text{soil}] \text{s}^{-1}$	Ⓐ electron transport rate carboxylation, sunlit part
$P_{g\_shd}$	$J_{C\_shd} \cdot \frac{CO_{2i} - \Gamma}{4 CO_{2i} + 8 \Gamma}$	$\mu\text{mol}[\text{CO}_2] \text{m}^{-2} [\text{soil}] \text{s}^{-1}$	Ⓐ Ⓔ gross assimilation rate canopy shaded part
$P_{g\_sun}$	$J_{C\_sun} \cdot \frac{CO_{2i} - \Gamma}{4 CO_{2i} + 8 \Gamma}$	$\mu\text{mol}[\text{CO}_2] \text{m}^{-2} [\text{soil}] \text{s}^{-1}$	Ⓐ Ⓔ gross assimilation rate canopy shaded part
$P_{g\_u}$	$f_{SLA} \cdot P_{g\_sun} + (1 - f_{SLA}) \cdot P_{g\_shd}$	$\mu\text{mol}[\text{CO}_2] \text{m}^{-2} [\text{soil}] \text{s}^{-1}$	Ⓐ gross assimilation rate canopy
$P_g$	$M_{CO_2} \cdot P_{g\_u}$	$\text{mg}[\text{CO}_2] \text{m}^{-2} [\text{soil}] \text{s}^{-1}$	Ⓐ gross assimilation rate canopy
$r_D$	$M_{CO_2} \cdot r_{D\_uL} \cdot LAI$	$\text{mg}[\text{CO}_2] \text{m}^{-2} [\text{soil}] \text{s}^{-1}$	dark respiration rate canopy

Ⓐ Gijzen (1994); Ⓔ Farquhar and von Caemmerer (1982)

The location of our greenhouse is given by its latitude  $\lambda_{gh} = 52^\circ$  and longitude  $\varphi_{gh} = 4.2^\circ$ . With the day number  $day_{NR}$  [1,365] and the hour of the day  $hour$  [0,23], the solar parameters, such as the position of the sun (azimuth  $\alpha_{sun}$  and elevation  $\beta_{sun}$ ), the sine of the solar elevation  $\sin\beta$  and the solar constant  $solar_C$  can be determined.

Table 2.6: Model CG3  
a: photosynthesis parameters

name	value	unit	contents
Temperature dependencies			
$\rho_{CO2-25}$	$\rho_{CO2} \cdot \frac{T_0}{T_{25}}$	$\text{kg}[\text{CO}_2] \text{ m}^{-3}[\text{CO}_2]$	$\text{CO}_2$ density at $T_{25}$
$\rho_{CO2T}$	$\rho_{CO2} \cdot \frac{T_0}{T_c}$	$\text{kg}[\text{CO}_2] \text{ m}^{-3}[\text{CO}_2]$	$\text{CO}_2$ density at $T_c$ (gaslaw)
$K_{M25}$	$K_{C25} \cdot \left(1 + \frac{p_{O2i}}{K_{O25}}\right)$	$\mu\text{bar}$	Ⓐ Ⓒ effective Michaelis Menten constant ( $\text{CO}_2$ )
$K_M$	$K_{M25} \cdot Q_{10KM}^{0.1(T_c - T_{25})}$	$\mu\text{bar}$	Ⓐ effective Michaelis Menten constant ( $\text{CO}_2$ )
$V_{C \max}$	$V_{C \max 25} \cdot Q_{10VC}^{0.1(T_c - T_{25})}$	$\mu\text{mol}[\text{CO}_2] \text{ m}^{-2}[\text{leaf}] \text{ s}^{-1}$	maximum carboxylation rate
$r_{D-uL}$	$r_{D25-uL} \cdot Q_{10rD}^{0.1(T_c - T_{25})}$	$\mu\text{mol}[\text{CO}_2] \text{ m}^{-2}[\text{leaf}] \text{ s}^{-1}$	dark respiration rate leaves
$J_{\max}$	$\begin{cases} 0 & \text{if } T_c - T_0 \in \leftarrow, 5 > \\ J_{\max 25} \cdot \frac{T_c - T_0 - 5}{20} & \text{if } T_c - T_0 \in [5, 25 > \\ J_{\max 25} & \text{if } T_c - T_0 \in [25, 35 > \\ J_{\max 25} \cdot \left(1 - \frac{(T_c - T_0 - 35)}{10}\right) & \text{if } T_c - T_0 \in [35, 45 > \\ 0 & \text{if } T_c - T_0 \in [45, \rightarrow > \end{cases}$	$\mu\text{mol}[\text{e}^-] \text{ m}^{-2}[\text{leaf}] \text{ s}^{-1}$	Ⓔ maximum electron transport rate
$\Gamma$	$42.7 + 1.68 (T_c - T_{25}) + 0.012 (T_c - T_{25})^2$	$\mu\text{mol}[\text{CO}_2] \text{ mol}^{-1}[\text{air}]$	Ⓒ $\text{CO}_2$ compensation concentration in absence of dark respiration
Radiation parameters			
$f_{SLA}$	$\tau_{dirBL}(l_1)$	—	Ⓐ fraction sunlit leaf area
$F_p$	0.3	—	Ⓐ fraction PAR absorbed by non-photosynthetic tissues
$\Theta$	0.7	—	Ⓐ Ⓒ degree of curvature of $\text{CO}_2$ response of light saturated net photosynthesis
$\psi$	$\frac{1 - F_p}{2} \cdot \zeta$	$\mu\text{mol}[\text{e}^-] \text{ J}^{-1}$	Ⓔ conversion factor, J to $\text{e}^-$
$\varepsilon$	$\psi \cdot M_{CO2} \cdot \frac{\max(CO_{2a}, \Gamma) - \Gamma}{4 \max(CO_{2a}, \Gamma) + 8 \Gamma}$	$\text{mg}[\text{CO}_2] \text{ J}^{-1}$	Ⓐ light use efficiency by photorespiration
$R_{c-CO2}$	$\frac{K_M}{V_{C \max}} \cdot \frac{\rho_{CO2-25}}{M_{CO2}}$	$\text{s m}^{-1}$	Ⓐ Ⓓ carboxylation resistance
$R_{CO2}$	$R_{b-CO2} + R_{s-CO2}$	$\text{s m}^{-1}$	stomatal resistance + boundary layer resistance to $\text{CO}_2$ diffusion
$R_{tot-CO2}$	$R_{CO2} + R_{c-CO2}$	$\text{s m}^{-1}$	Ⓐ total resistance to $\text{CO}_2$ diffusion
$P_{mm}$	$\frac{M_{CO2}}{4} \cdot J_{\max}$	$\text{mg}[\text{CO}_2] \text{ m}^{-2}[\text{leaf}] \text{ s}^{-1}$	maximum endogenous photosynthetic capacity
$P_{nc}$	$\frac{\rho_{CO2T}}{R_{tot-CO2}} \cdot (\max(CO_{2a}, \Gamma) - \Gamma)$	$\text{mg}[\text{CO}_2] \text{ m}^{-2}[\text{leaf}] \text{ s}^{-1}$	Ⓐ $\text{CO}_2$ limited rate of net photosynthesis
$P_{n \max}$	$\left( P_{mm} + P_{nc} - \left( (P_{mm} + P_{nc})^2 - 4 \Theta \cdot P_{mm} \cdot P_{nc} \right)^{\frac{1}{2}} \right) / (2 \Theta)$	$\text{mg}[\text{CO}_2] \text{ m}^{-2}[\text{leaf}] \text{ s}^{-1}$	Ⓐ Ⓓ maximum net assimilation rate
$P_{g \max}$	$P_{n \max} + r_{D-uL} \cdot M_{CO2}$	$\text{mg}[\text{CO}_2] \text{ m}^{-2}[\text{leaf}] \text{ s}^{-1}$	Ⓐ Ⓓ maximum gross assimilation rate leaves (light saturation)

Ⓐ Gijzen (1994); Ⓔ Farquhar and von Caemmerer (1982); Ⓒ Farquhar et al. (1980); Ⓓ Goudriaan and van Laar (1994); Ⓒ Farquhar (1988); Ⓔ Heuvelink (1996)

Table 2.6: Model *CG3* (continued)

b: gross assimilation and dark respiration

name	value	unit	contents
Three layer Gaussian integration			
$X_g$	{0.1127, 0.5, 0.8873}	—	Ⓓ relative depth canopy
$W_g$	{0.2778, 0.4444, 0.2778}	—	Ⓓ weight factor
$l_1$	{1, 2, 3}	—	Ⓓ first counter
$l_2$	{1, 2, 3}	—	Ⓓ second counter
$LAI_l(l_1)$	$LAI \cdot X_g(l_1)$	$\text{m}^2[\text{leaf}] \text{m}^{-2}[\text{soil}]$	Ⓓ leaf area index, layer $l_1$
Absorbed radiation			
$I_{A\_dif}(l_1)$	$(1 - \beta_{dif}) \cdot I_{P\_dif} \cdot k_{dif} \cdot \tau_{dif}(l_1)$	$\text{W m}^{-2}[\text{leaf}]$	Ⓓ Ⓓ diffuse flux
$I_{A\_tdir}(l_1)$	$(1 - \beta_{dir}) \cdot I_{P\_dir} \cdot k_{dir} \cdot \tau_{dir}(l_1)$	$\text{W m}^{-2}[\text{leaf}]$	Ⓓ Ⓓ total direct flux
$I_{A\_dir}(l_1)$	$(1 - \delta) \cdot I_{P\_dir} \cdot k_{dirBL} \cdot \tau_{dirBL}(l_1)$	$\text{W m}^{-2}[\text{leaf}]$	Ⓓ Ⓓ direct flux
$I_{A\_ppd}(l_1)$	$\frac{1 - \delta}{\sin \beta} \cdot I_{P\_dir}$	$\text{W m}^{-2}[\text{leaf}]$	Ⓓ Ⓓ direct flux leaves perpendicular on direct beam
$I_{A\_shd}(l_1)$	$I_{A\_dif}(l_1) + I_{A\_tdir}(l_1) - I_{A\_dir}(l_1)$	$\text{W m}^{-2}[\text{leaf}]$	Ⓓ Ⓓ flux shaded part of canopy
$I_{A\_sun}(l_1, l_2)$	$I_{A\_shd}(l_1) + I_{A\_ppd}(l_1) \cdot X_g(l_2)$	$\text{W m}^{-2}[\text{leaf}]$	Ⓓ Ⓓ flux sunlit part of canopy
$P_{g\_sun}(l_1)$	$P_{g \max} \cdot \sum_{l_2=1}^3 W_g(l_2) \cdot \left(1 - e^{-\frac{\varepsilon \cdot I_{A\_sun}(l_1, l_2)}{P_{g \max}}}\right)$	$\text{mg}[\text{CO}_2] \text{m}^{-2}[\text{leaf}] \text{s}^{-1}$	Ⓓ gross assimilation rate leaves sunlit part
$P_{g\_shd}(l_1)$	$P_{g \max} \cdot \left(1 - e^{-\frac{\varepsilon \cdot I_{A\_shd}(l_1)}{P_{g \max}}}\right)$	$\text{mg}[\text{CO}_2] \text{m}^{-2}[\text{leaf}] \text{s}^{-1}$	Ⓓ gross assimilation rate leaves shaded part
$P_{g\_L}$	$\sum_{l_1=1}^3 W_g(l_1) \cdot \left(f_{SLA} \cdot P_{g\_sun}(l_1) + (1 - f_{SLA}) \cdot P_{g\_shd}(l_1)\right)$	$\text{mg}[\text{CO}_2] \text{m}^{-2}[\text{leaf}] \text{s}^{-1}$	Ⓓ gross assimilation rate leaves
$P_g$	$P_{g\_L} \cdot LAI$	$\text{mg}[\text{CO}_2] \text{m}^{-2}[\text{soil}] \text{s}^{-1}$	gross assimilation rate canopy
$r_D$	$M_{CO_2} \cdot r_{D\_uL} \cdot LAI$	$\text{mg}[\text{CO}_2] \text{m}^{-2}[\text{soil}] \text{s}^{-1}$	dark respiration rate canopy

ⒹGoudriaan and van Laar (1994); ⒹSpitters (1986)

### 2.B.1 Solar parameters

The declination of the sun  $\delta_{sun}$  with respect to the equator is given by

$$\delta_{sun} = -\arcsin\left(\sin\left(2\pi \cdot \frac{23.45}{360}\right) \cdot \cos\left(2\pi \cdot \frac{day_{NR} + 10}{365}\right)\right) \quad \{\text{rad}\} \quad (2.48)$$

where  $day_{NR}$  [1,365] is the day number. The angle of  $23.45^\circ$  is the tilt of the earth axis with regard to the plane in which the earth moves around the sun.

Table 2.7: Model CG4  
a: photosynthesis parameters

name	value	unit	contents
Temperature dependencies			
$f_{OC}$	0.21	—	Ⓢ $f_{OC} = \frac{V_{O\max}}{V_{C\max}} = \frac{k_o}{k_c} = \text{constant}$
$\rho_{CO_2T}$	$\rho_{CO_2} \cdot \frac{T_0}{T_c}$	$\text{kg}[\text{CO}_2] \text{ m}^{-3}[\text{CO}_2]$	$\text{CO}_2$ density at $T_c$ (gaslaw)
$X$	$\frac{T_c - T_{25}}{T_c \cdot R_g \cdot T_{25}}$	$\text{mol J}^{-1}$	Ⓢ intermediate variable
$K_C$	$K_{C25} \cdot e^{E_C \cdot X}$	$\mu\text{bar}$	Ⓢ Michaelis Menten constant Rubisco carboxylation ( $\text{CO}_2$ )
$K_O$	$K_{O25} \cdot e^{E_O \cdot X}$	$\text{mbar}$	Ⓢ Michaelis Menten constant Rubisco oxygenation ( $\text{O}_2$ )
$K_M$	$K_C \cdot \left(1 + \frac{\rho_{CO_2i}}{K_O}\right)$	$\mu\text{bar}$	Ⓢ Ⓢ effective Michaelis Menten constant ( $\text{CO}_2$ )
$V_{C\max}$	$V_{C\max 25} \cdot e^{E_{VC} \cdot X}$	$\mu\text{mol}[\text{CO}_2] \text{ m}^{-2}[\text{leaf}] \text{ s}^{-1}$	Ⓢ maximum carboxylation rate
$r_{D-uL}$	$r_{D25-uL} \cdot e^{E_D \cdot X}$	$\mu\text{mol}[\text{CO}_2] \text{ m}^{-2}[\text{leaf}] \text{ s}^{-1}$	Ⓢ dark respiration rate leaves
$S$	710	$\text{J mol}^{-1} \text{ K}^{-1}$	Ⓢ constant for optimum curve temperature dependent electron transport rate
$H$	220000	$\text{J mol}^{-1}$	Ⓢ constant for optimum curve temperature dependent electron transport rate
$D$	$\frac{1 + e^{\frac{S \cdot T_c - H}{R_g \cdot T_c}}}{1 + e^{\frac{S \cdot T_{25} - H}{R_g \cdot T_{25}}}}$	—	Ⓢ Ⓢ intermediate variable
$J_{\max}$	$J_{\max 25} \cdot \frac{e^{E_J \cdot X}}{D}$	$\mu\text{mol}[\text{e}^-] \text{ m}^{-2}[\text{leaf}] \text{ s}^{-1}$	Ⓢ Ⓢ maximum electron transport rate
$\Gamma$	$\frac{K_C}{2 K_O} \cdot \rho_{CO_2i} \cdot f_{OC}$	$\mu\text{mol}[\text{CO}_2] \text{ mol}^{-1}[\text{air}]$	Ⓢ $\text{CO}_2$ compensation concentration in absence of dark respiration
Radiation parameters			
$f_{SLA}$	$\tau_{dirBL}(l_1)$	—	Ⓢ fraction sunlit leaf area
$F_p$	0.3	—	Ⓢ fraction PAR absorbed by non-photosynthetic tissues
$\Theta$	0.7	—	Ⓢ Ⓢ degree of curvature of $\text{CO}_2$ response of light saturated net photosynthesis
$\psi$	$\frac{1 - F_p}{2} \cdot \zeta$	$\mu\text{mol}[\text{e}^-] \text{ J}^{-1}$	Ⓢ conversion factor, J to $\text{e}^-$
$\varepsilon$	$\psi \cdot M_{CO_2} \cdot \frac{\max(\text{CO}_{2a}, \Gamma) - \Gamma}{4 \max(\text{CO}_{2a}, \Gamma) + 8 \Gamma}$	$\text{mg}[\text{CO}_2] \text{ J}^{-1}$	Ⓢ light use efficiency by photorespiration
$R_{c-CO_2}$	$\frac{K_M}{V_{C\max}} \cdot \frac{\rho_{CO_2T}}{M_{CO_2}}$	$\text{s m}^{-1}$	Ⓢ Ⓢ carboxylation resistance
$R_{CO_2}$	$R_{b-CO_2} + R_{s-CO_2}$	$\text{s m}^{-1}$	stomatal resistance + boundary layer resistance to $\text{CO}_2$ diffusion
$R_{tot-CO_2}$	$R_{CO_2} + R_{c-CO_2}$	$\text{s m}^{-1}$	Ⓢ total resistance to $\text{CO}_2$ diffusion
$P_{mm}$	$\frac{M_{CO_2}}{4} \cdot J_{\max}$	$\text{mg}[\text{CO}_2] \text{ m}^{-2}[\text{leaf}] \text{ s}^{-1}$	maximum endogenous photosynthetic capacity
$P_{nc}$	$\frac{\rho_{CO_2T}}{R_{tot-CO_2}} \cdot (\max(\text{CO}_{2a}, \Gamma) - \Gamma)$	$\text{mg}[\text{CO}_2] \text{ m}^{-2}[\text{leaf}] \text{ s}^{-1}$	Ⓢ Ⓢ $\text{CO}_2$ limited rate of net photosynthesis
$P_{n\max}$	$\left(P_{mm} + P_{nc} - \left((P_{mm} + P_{nc})^2 - 4 \Theta \cdot P_{mm} \cdot P_{nc}\right)^{\frac{1}{2}}\right) / (2 \Theta)$	$\text{mg}[\text{CO}_2] \text{ m}^{-2}[\text{leaf}] \text{ s}^{-1}$	Ⓢ Ⓢ maximum net assimilation rate
$P_{g\max}$	$P_{n\max} + r_{D-uL} \cdot M_{CO_2}$	$\text{mg}[\text{CO}_2] \text{ m}^{-2}[\text{leaf}] \text{ s}^{-1}$	maximum gross assimilation rate leaves (light saturation)

Ⓢ Gijzen (1994); Ⓢ Farquhar and von Caemmerer (1982); Ⓢ Farquhar et al. (1980); Ⓢ Goudriaan and van Laar (1994); Ⓢ Farquhar (1988)

Table 2.7: Model *CG4* (continued)

b: gross assimilation and dark respiration

name	value	unit	contents
Three layer Gaussian integration			
$X_g$	{0.1127, 0.5, 0.8873}	—	Ⓓ relative depth canopy
$W_g$	{0.2778, 0.4444, 0.2778}	—	Ⓓ weight factor
$l_1$	{1, 2, 3}	—	Ⓓ first counter
$l_2$	{1, 2, 3}	—	Ⓓ second counter
$LAI_l(l_1)$	$LAI \cdot X_g(l_1)$	$m^2[leaf] m^{-2}[soil]$	Ⓓ leaf area index, layer $l_1$
Absorbed radiation			
$I_{A\_dif}(l_1)$	$(1 - \beta_{dif}) \cdot I_{P\_dif} \cdot k_{dif} \cdot \tau_{dif}(l_1)$	$W m^{-2}[leaf]$	Ⓓ Ⓓ diffuse flux
$I_{A\_tdir}(l_1)$	$(1 - \beta_{dir}) \cdot I_{P\_dir} \cdot k_{dir} \cdot \tau_{dir}(l_1)$	$W m^{-2}[leaf]$	Ⓓ Ⓓ total direct flux
$I_{A\_dir}(l_1)$	$(1 - \delta) \cdot I_{P\_dir} \cdot k_{dirBL} \cdot \tau_{dirBL}(l_1)$	$W m^{-2}[leaf]$	Ⓓ Ⓓ direct flux
$I_{A\_ppd}(l_1)$	$\frac{1 - \delta}{\sin \beta} \cdot I_{P\_dir}$	$W m^{-2}[leaf]$	Ⓓ Ⓓ direct flux leaves perpendicular on direct beam
$I_{A\_shd}(l_1)$	$I_{A\_dif}(l_1) + I_{A\_tdir}(l_1) - I_{A\_dir}(l_1)$	$W m^{-2}[leaf]$	Ⓓ Ⓓ flux shaded part of canopy
$I_{A\_sun}(l_1, l_2)$	$I_{A\_shd}(l_1) + I_{A\_ppd}(l_1) \cdot X_g(l_2)$	$W m^{-2}[leaf]$	Ⓓ Ⓓ flux sunlit part of canopy
$P_{g\_sun}(l_1)$	$P_{g\ max} \cdot \sum_{l_2=1}^3 W_g(l_2) \cdot \left(1 - e^{-\frac{\varepsilon \cdot I_{A\_sun}(l_1, l_2)}{P_{g\ max}}}\right)$	$mg[CO_2] m^{-2}[leaf] s^{-1}$	Ⓓ gross assimilation rate leaves sunlit part
$P_{g\_shd}(l_1)$	$P_{g\ max} \cdot \left(1 - e^{-\frac{\varepsilon \cdot I_{A\_shd}(l_1)}{P_{g\ max}}}\right)$	$mg[CO_2] m^{-2}[leaf] s^{-1}$	Ⓓ gross assimilation rate leaves shaded part
$P_{g\_L}$	$\sum_{l_1=1}^3 W_g(l_1) \cdot \left(f_{SLA} \cdot P_{g\_sun}(l_1) + (1 - f_{SLA}) \cdot P_{g\_shd}(l_1)\right)$	$mg[CO_2] m^{-2}[leaf] s^{-1}$	Ⓓ gross assimilation rate leaves
$P_g$	$P_{g\_L} \cdot LAI$	$mg[CO_2] m^{-2}[soil] s^{-1}$	gross assimilation rate canopy
$r_D$	$M_{CO_2} \cdot r_{D\_uL} \cdot LAI$	$mg[CO_2] m^{-2}[soil] s^{-1}$	dark respiration rate canopy

Ⓓ Goudriaan and van Laar (1994); Ⓓ Spitters (1986)

The elevation of sun  $\beta_{sun}$  is the angle between the direction of the sun and the horizon described by

$$\beta_{sun} = \arcsin(\sin \beta) \quad \{\text{rad}\} \quad (2.49)$$

in which the sine of solar elevation  $\sin \beta$  is given by

$$\sin \beta = \sin(\lambda_{gh}) \cdot \sin(\delta_{sun}) + \cos(\lambda_{gh}) \cdot \cos(\delta_{sun}) \cdot \cos\left(2\pi \cdot \frac{SOL_{hr} - 12}{24}\right) \quad \{-\} \quad (2.50)$$

the time of day (solar time)  $SOL_{hr}$  with time correction for Middle European Time (M.E.T.) is

$$SOL_{hr} = hour - \left(1 - \frac{\varphi_{gh}}{15}\right) \quad \{\text{h}\} \quad (2.51)$$

and  $hour$  is the hour of the day  $[0,23]$ . The earth rotates  $360^\circ$  every 24 hours, which gives the term  $15^\circ \text{ h}^{-1}$ .

The azimuth of the sun  $\alpha_{sun}$  is the angle between the direction of the sun and the south (in which east is negative and west is positive) described by

$$\alpha_{sun} = \begin{cases} \arccos(\cos\alpha) & \text{if } SOL_{hr} > 12 \\ -\arccos(\cos\alpha) & \text{if } SOL_{hr} \leq 12 \end{cases} \quad \{\text{rad}\} \quad (2.52)$$

in which the cosine of the azimuth  $\cos\alpha$  is given by

$$\cos\alpha = \frac{\sin(\lambda_{gh}) \cdot \sin\beta - \sin(\delta_{sun})}{\cos(\lambda_{gh}) \cdot \cos(\beta_{sun})} \quad -1 \leq \cos\alpha \leq 1 \quad \{-\} \quad (2.53)$$

The solar constant  $solar_C$  is the solar radiation received at the outer layer of the earth's atmosphere. It is described by

$$solar_C = 1367 \left(1 + 0.033 \cos\left(2\pi \cdot \frac{day_{NR}}{365}\right)\right) \quad \{\text{W m}^{-2}\} \quad (2.54)$$

which gives the atmospheric transmission  $\tau_{atm}$

$$\tau_{atm} = \frac{I_o}{solar_C \cdot \sin\beta} \quad \{-\} \quad (2.55)$$

A parameter  $sun_{up}$  is defined, to verify if the sun is up or down, where '1' denotes true and '0' denotes false. The sine of solar elevation  $\sin\beta$  is used to indicate if the sun is up: if  $\sin\beta > 0$ , then the sun is up. A small margin ( $10^{-3}$ ) is used to prevent numerical problems in the computation.

$$sun_{up} = \begin{cases} 1 & \text{if } \sin\beta > 10^{-3} \\ 0 & \text{if } \sin\beta \leq 10^{-3} \end{cases} \quad \{0,1\} \quad (2.56)$$

With the solar parameters azimuth  $\alpha_{sun}$ , elevation  $\beta_{sun}$ , sine of elevation  $\sin\beta$  and atmospheric transmission  $\tau_{atm}$ , the following parameters can be computed: the fraction diffuse radiation  $f_{dif}$  in the outdoor shortwave solar radiation, the fraction PAR radiation  $f_{par}$  in the outdoor shortwave solar radiation, the fraction diffuse radiation  $f_{difpar}$  in the PAR radiation and the transmittances  $\tau_{difR}$  and  $\tau_{dirR}$  of the roof for diffuse and direct PAR radiation.

### 2.B.2 Radiation parameters

The solar radiation parameters  $f_{dif}$ ,  $f_{difpar}$  and  $f_{par}$  are determined according to Gijzen (1994).

The fraction diffuse radiation  $f_{dif}$  in outdoor shortwave solar radiation is given by

$$f_{dif} = \begin{cases} \max(f_{dif1}, f_{dif2}) & \text{if } sun_{up} = 1 \\ 1 & \text{if } sun_{up} = 0 \end{cases} \quad \{-\} \quad (2.57)$$

in which

$$f_{dif1} = \begin{cases} 1 & \text{if } \tau_{atm} \leq p_{db} \\ 1 - p_{da} \cdot (\tau_{atm} - p_{db})^2 & \text{if } p_{db} < \tau_{atm} \leq p_{dc} \\ 1 - p_{da} \cdot ((\tau_{atm} - p_{db})^2 - (\tau_{atm} - p_{dc})^2) & \text{if } \tau_{atm} > p_{dc} \end{cases} \quad \{-\} \quad (2.58)$$

$$f_{dif2} = p_{dd} + (1 - p_{dd}) \cdot \left(1 - e^{-\frac{0.1}{\sin\beta}}\right) \quad \{-\} \quad (2.59)$$

in which the parameter values are:  $p_{da} = 6.4$ ,  $p_{db} = 0.22$ ,  $p_{dc} = 0.35$  and  $p_{dd} = 0.15$  (parameters for De Bilt, The Netherlands).

The fraction diffuse  $f_{difpar}$  in PAR radiation is given by

$$f_{difpar} = \begin{cases} \min(f_{dif} \cdot (1 + 0.35 f_{clear}), 1) & \text{if } sun_{up} = 1 \\ 1 & \text{if } sun_{up} = 0 \end{cases} \quad \{-\} \quad (2.60)$$

in which the apparent fraction clear  $f_{clear}$  is given by

$$f_{clear} = \begin{cases} 0 & \text{if } \tau_{atm} < 0.3 \\ 2(\tau_{atm} - 0.3) & \text{if } 0.3 \leq \tau_{atm} \leq 0.8 \\ 1 & \text{if } \tau_{atm} > 0.8 \end{cases} \quad \{-\} \quad (2.61)$$

The fraction PAR  $f_{par}$  in outdoor shortwave solar radiation is given by

$$f_{par} = \begin{cases} \max\left(\frac{p_{pa} - p_{pe} \cdot e^{\frac{p_{pf}}{\sin\beta}} \cdot (1 - e^{-p_{pb} \cdot \tau_{atm}^{p_{pc}}})}{\zeta}, 0\right) & \text{if } sun_{up} = 1 \\ 0 & \text{if } sun_{up} = 0 \end{cases} \quad \{-\} \quad (2.62)$$

in which the parameter values are:  $p_{pa} = 2.9$ ,  $p_{pb} = 4.9$ ,  $p_{pc} = 0.51$ ,  $p_{pe} = 0.84$  and  $p_{pf} = 0.033$  (parameters for Wageningen and Assen, The Netherlands) and the conversion factor  $\zeta = 4.59 \mu\text{mol}[\text{photons}] \text{J}^{-1}$ .

The transmittance  $\tau_{difR}$  of the roof for diffuse PAR radiation is equal to

$$\tau_{difR} = \begin{cases} 0.78 & \text{solar gh. (de Zwart, 1996)} \\ 0.55 & \text{conv. gh. (parameter estimation §3.9.3)} \end{cases} \quad \{-\} \quad (2.63)$$

The transmittance  $\tau_{dirR}$  of the roof for direct PAR radiation is determined from transmissivity tables by De Zwart (1996) for single glass, double glass and hortiplus glass. The tables contain values for the transmittance depending on the azimuth  $\alpha_{sun}$  and the elevation  $\beta_{sun}$  of the sun. The azimuth and elevation both range from 0 to  $\frac{\pi}{2}$  (0° to 90°).

Since interpolation in these tables — depending on the current position of the sun — is time consuming, in this research the values from the tables have been approximated by functions. They have been determined by fitting an equation for  $\tau_{dirR}$  as a function of  $\alpha_{sun}$  and  $\beta_{sun}$  on the values from the table. In the functions found, the azimuth was found to have little influence on the correctness of the fit. The transmittance  $\tau_{dirR}$  of the roof for direct PAR radiation is then given by

$$\tau_{dirR} = \begin{cases} 0.85 (1 - e^{-0.083 \cdot \frac{360}{2\pi} \cdot \beta_{sun}}) & \text{single glass} \\ 0.82 (1 - e^{-0.066 \cdot \frac{360}{2\pi} \cdot \beta_{sun}}) & \text{double glass} \\ 0.76 (1 - e^{-0.083 \cdot \frac{360}{2\pi} \cdot \beta_{sun}}) & \text{hortiplus glass} \\ 0 & \text{if } sun_{up} = 0 \end{cases} \quad \{-\} \quad (2.64)$$

For the zigzag roof used in this research, it is assumed that the transmittance of the roof for direct PAR radiation  $\tau_{dirR}$  is as high as with a single glass roof.

## 2.C Humidity parameters

The humidity of the air is related to the saturation water vapour pressure, which depends on temperature. The relations between humidity, saturation deficit and relative humidity and temperature are given in the next paragraphs.

### 2.C.1 Saturation pressure and concentration

The saturation deficit between object  $x$  and air is computed by

$$\Delta p_{x\_H_2O} = p_{x\_H_2O_s} - p_{a\_H_2O} \quad \{\text{N m}^{-2}\} \quad (2.65)$$

where  $p_{x\_H_2O_s}$   $\{\text{N m}^{-2}\}$  is the saturation water vapour pressure at object temperature  $T_x$  and  $p_{a\_H_2O}$   $\{\text{N m}^{-2}\}$  is the water vapour pressure at the temperature  $T_a$  of the indoor air.

The saturation vapour pressure  $p_{x\_H_2O_s}$   $\{\text{N m}^{-2}\}$  at a specific temperature  $T_x$   $\{\text{K}\}$  is computed with the Magnus-Tetens equation (Defant and Defant, 1958)

$$p_{x\_H_2O_s} = c_{s1} \cdot e^{\frac{c_{s2} \cdot (T_x - T_0)}{c_{s3} + (T_x - T_0)}} \quad \{\text{N m}^{-2}\} \quad (2.66)$$

in which the correction factor from temperature in Kelvin  $\{\text{K}\}$  to Celsius  $\{\text{°C}\}$   $T_0 = 273.15$  K, where  $c_{s1}$ ,  $c_{s2}$  and  $c_{s3}$  are the saturation pressure coefficients. For the pressure in  $\{\text{mbar}\}$ , divide the pressure in  $\{\text{N m}^{-2}\}$  by 100.

The values of the saturation pressure coefficients (Smithsonian Meteorological Tables, 1966) depend on the temperature  $T_x$  of object  $x$ , which determines the phase condition of the water vapour (water ( $T_x \geq T_0$ ) or ice ( $T_x < T_0$ ))

$$\forall T_x \geq T_0 = \begin{cases} c_{s1} = 610.780 \\ c_{s2} = 17.08085 \\ c_{s3} = 234.175 \end{cases} \quad \forall T_x < T_0 = \begin{cases} c_{s1} = 610.714 \\ c_{s2} = 22.44294 \\ c_{s3} = 272.440 \end{cases} \quad (2.67)$$

The saturation concentration of water vapour  $C_{x\_H_2O_s}$  at a specific temperature  $T_x$   $\{\text{K}\}$  is computed from the saturation vapour pressure  $p_{x\_H_2O_s}$  at temperature  $T_x$  using the law for ideal gas

$$C_{x\_H_2O_s} = \frac{p_{x\_H_2O_s} \cdot M_{H_2O}}{R_g \cdot T_x} \quad \{\text{kg}[\text{H}_2\text{O}] \text{ m}^{-3}\} \quad (2.68)$$

in which  $M_{H_2O} = 18 \cdot 10^{-3} \text{ kg mol}^{-1}$  is the molar mass of water and  $R_g = 8.314 \text{ J mol}^{-1} \text{ K}^{-1}$  is the gas constant.

The water vapour pressure  $p_{x\_H_2O}$  at temperature  $T_x$  is computed by

$$p_{x\_H_2O} = p_{x\_H_2O_s} \cdot \frac{C_{x\_H_2O}}{C_{x\_H_2O_s}} \quad \{\text{N m}^{-2}\} \quad (2.69)$$

where  $p_{x\_H_2O_s}$   $\{\text{N m}^{-2}\}$  is the saturation water vapour pressure at temperature  $T_x$ ,  $C_{x\_H_2O_s}$   $\{\text{kg}[\text{H}_2\text{O}] \text{ m}^{-3}\}$  is the saturation concentration water vapour at temperature  $T_x$  and  $C_{x\_H_2O}$   $\{\text{kg}[\text{H}_2\text{O}] \text{ m}^{-3}\}$  is the water concentration of object  $x$ .

### 2.C.2 Relative humidity

If the dry bulb temperature  $T_x$  and the wet bulb temperature  $T_{x.w}$  are known, the relative humidity  $RH_x$  can be computed from these temperatures

$$RH_x = \begin{cases} 100 \cdot \frac{p_{x.H2O}}{p_{x.H2Os}} & \text{if } p_{x.H2O} > 0 \text{ and } p_{x.H2Os} > 0 \\ 0 & \text{if } p_{x.H2O} \leq 0 \text{ or } p_{x.H2Os} \leq 0 \end{cases} \quad \{\%\} \quad (2.70)$$

where  $p_{x.H2O}$   $\{\text{N m}^{-2}\}$  is the water vapour pressure at dry bulb temperature  $T_x$  and  $p_{x.H2Os}$   $\{\text{N m}^{-2}\}$  is the saturation water vapour pressure at dry bulb temperature  $T_x$ .

The water vapour pressure  $p_{x.H2O}$  at dry bulb temperature  $T_x$  is given by the psychrometric equation

$$p_{x.H2O} = p_{x.w.H2Os} - p_{bar} \cdot A_{psy} \cdot (T_x - T_{x.w}) \quad \{\text{N m}^{-2}\} \quad (2.71)$$

in which the atmospheric pressure  $p_{bar} = 101325 \text{ N m}^{-2}$ , where  $p_{x.w.H2Os}$   $\{\text{N m}^{-2}\}$  is the saturation water vapour pressure at wet bulb temperature  $T_{x.w}$ . The psychrometric coefficient  $A_{psy}$  (Ferrel, 1885) is given by

$$A_{psy} = 0.00066 (1 + 0.00115 (T_{x.w} - T_0)) \quad \{\text{K}^{-1}\} \quad (2.72)$$

in which the correction factor from temperature in Kelvin  $\{\text{K}\}$  to Celsius  $\{\text{°C}\}$   $T_0 = 273.15 \text{ K}$ .

### 2.C.3 Dewpoint temperature

The dewpoint temperature indicates the crop temperature at which water would condensate on the crop surface. The difference between the crop temperature  $T_c$  and the dewpoint temperature  $T_d$  can therefore be used to indicate crop wetness. The dewpoint temperature is given by

$$T_d = T_0 + \frac{c_{s3} \cdot \log\left(\frac{p_{a.H2O}}{c_{s1}}\right)}{c_{s2} - \log\left(\frac{p_{a.H2O}}{c_{s1}}\right)} \quad \{\text{K}\} \quad (2.73)$$

where  $p_{a.H2O}$   $\{\text{N m}^{-2}\}$  is the water vapour pressure at indoor air temperature  $T_a$  and the saturation pressure coefficients are given in eqn. 2.67.



## Chapter 3

# Solar greenhouse model

### 3.1 Introduction

An accurate model of the controlled system is necessary for the successful application of optimal control. Based on this model and a mathematical description of the control objectives, the optimal controller finds the best solution. In practice, the successful application of optimal control depends critically on the quality of the model. Van Henten (1994) and Tap (2000) found that parts of the greenhouse behaviour were not well described by their models. This negatively affects the performance of the optimal control.

For the receding horizon optimal control concept used in chapter 4 a state space description of the system is needed. The model should be sufficiently small with respect to the number of differential equations, controls and external inputs to limit the on-line computational load. On the other hand, it should be sufficiently accurate.

In this chapter a dynamic model<sup>Ⓢ</sup> for the solar greenhouse is developed. With a few small modifications this model can be turned into a model for the conventional greenhouse.

A conventional greenhouse is heated by a boiler, which in the Netherlands is also used to provide CO<sub>2</sub> for crop growth. The roof has a high transmission of solar radiation, but poor heat insulating properties. The greenhouse can be cooled by opening the windows, which also provides a means to decrease humidity.

---

<sup>Ⓢ</sup> All non-smooth equations are smoothed according to the smoothing functions described in appendix 1.A.

In the solar greenhouse design the heat insulation and the transmission of solar radiation are maximized. A warm- and a cold-water aquifer<sup>®</sup> layer are used to store and retrieve the surplus solar energy. At times of heat demand, the greenhouse can be heated with little energy input with a heat pump and warm aquifer water. At times of heat surplus, the greenhouse can be cooled with a heat exchanger and cold aquifer water, while energy is harvested for use at times of heat demand. In contrast to common greenhouses, the CO<sub>2</sub> supply in the solar greenhouse concept is detached from the boiler, thus avoiding the need to use the boiler at times of CO<sub>2</sub> demand. It is assumed that the CO<sub>2</sub> can be acquired from a power plant<sup>®</sup>. Ventilation with heat recovery is used to dehumidify the greenhouse at times of heat demand.

The solar greenhouse has the following changes compared to a conventional greenhouse:

***Improved insulation value and improved light transmission cover:***

to minimize heat loss to outdoor air and maximize the input of solar radiation. This will result in a higher crop yield and lower energy consumption.

***Ventilation with heat recovery:*** if ventilation is needed for high humidity but not for cooling, the sensible heat loss can be partially recovered by exchanging the air through a heat exchanger. The outdoor air is preheated by the indoor greenhouse air, while the humidity content is decreased. Latent heat that is vented out is lost. If ventilation is needed to prevent high humidity and high temperature, the windows are used — as in normal greenhouse practice.

***Aquifer:*** a long-term storage of water in the lower soil layers. The aquifer has a cold ( $T_{aq-c} = 10^{\circ}\text{C}$ ) and a warm ( $T_{aq-h} = 16^{\circ}\text{C}$ ) part. When the greenhouse is cooled, cold water is taken from the cold aquifer part, heat is extracted from the greenhouse with the heat exchanger, and the resulting warm water is stored in the warm aquifer part. When the greenhouse is heated, warm water is taken from the warm aquifer part, heat is supplied to the greenhouse with the heat pump, and the resulting cold water is stored in the cold aquifer part.

***Heat extraction:*** heat can be extracted from the greenhouse by a heat exchanger. The heat exchanger is used to cool water in the finned upper cooling net pipes with water from the cold aquifer part. The cooling net extracts energy from the greenhouse. Water from the cold aquifer part

---

<sup>®</sup> An aquifer is a formation of water-bearing sand material in the soil that can contain and transmit water. Wells can be drilled into the aquifers and water can be pumped into and out of the water layers.

<sup>®</sup> It is possible in the Netherlands to retrieve pure CO<sub>2</sub>. Shell Pernis/OCAP currently supplies about 200 growers with CO<sub>2</sub>, thus reducing the CO<sub>2</sub> emission by 170 kiloton CO<sub>2</sub> per year. This saves the growers 95 million m<sup>3</sup> gas.

is heated to a temperature above  $T_{aq,h}$ . Water with a temperature  $T_{aq,h}$  is stored in the warm aquifer part.

**Heat pump:** heat can be supplied to the greenhouse by a heat pump. The heat pump is used to heat water in the lower heating net with water from the warm aquifer part. The heat pump can attain a heating temperature of about 33°C. The lower heating net supplies energy to the greenhouse. Water from the warm aquifer part is cooled to a temperature below  $T_{aq,c}$ . Water with a temperature  $T_{aq,c}$  is stored in the cold aquifer part.

**Boiler:** used for additional heating if the heat pump cannot supply enough heat.

**Carbondioxide supply:** separate CO<sub>2</sub> supply, since CO<sub>2</sub> is no longer supplied by the boiler.

**Gas motor or electric drive:** used to run the heat pump; the exhaust gas can be used to give additional heat.

The gas motor might be replaced by a windmill that supplies electricity (sustainable instead of fossil energy). In the ideal set-up, the boiler is only needed as a backup. The heating and storage devices have to be controlled to optimize the heat use. This will ensure appropriate production and quality and low energy consumption.

The model of the conventional greenhouse used in this research is developed based on the model by Heesen (1997), who exploited the research by Van Henten (1994), De Zwart (1996), De Jong (1990) and Bot (1983). This conventional greenhouse model has been modified to include a thermal screen and a double glass cover. For the solar greenhouse it has been extended with the solar greenhouse elements described above, which give new possibilities for heating, cooling and dehumidification. The greenhouse model uses the crop model described in chapter 2 for the exchange of heat, CO<sub>2</sub> and water with the crop. This chapter gives a complete and detailed description of the greenhouse model.

The outline of this chapter is as follows. The system is described in §3.2. An overview is given of the system with its states, control inputs and external inputs. The state equations mainly contain terms that describe the exchange of heat, water and CO<sub>2</sub>. In §3.3–3.8 these exchange terms are worked out. Finally in §3.9 the model is calibrated and validated to investigate its accuracy and suitability for optimal control purposes. In appendix B a list of variables and parameters used in the solar greenhouse model is given for easy reference.

## 3.2 System description

The greenhouse configuration is described in §3.2.1. In §3.2.2 all assumptions made in this model are described. Next in §3.2.3 the states, control inputs and external inputs and the state equations that govern the system behaviour are given. All computations are done in Fortran 77.

### 3.2.1 Greenhouse configuration

The greenhouse configuration is given in figure §3.1. The greenhouse is a Venlo greenhouse with a North-South orientation. A Venlo greenhouse is a multi span greenhouse. It is assumed that each span has the same layout with respect to the configuration of the heating and the cooling net, the thermal screen and its size.

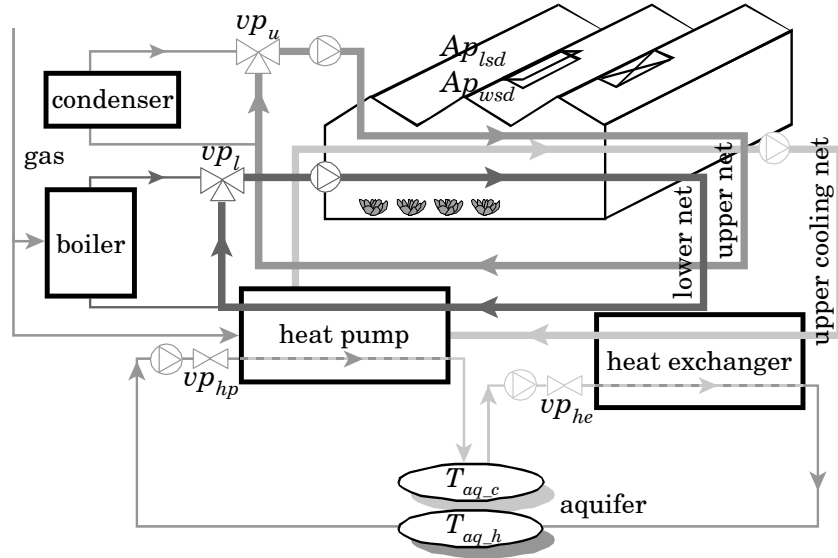


Figure 3.1: Greenhouse configuration

A heating system consisting of a boiler, a condenser and a heat pump can be used to heat the greenhouse. The lower heating net can be heated with the boiler to a temperature of 90°C and with the heat pump to a temperature of about 33°C. The upper heating net is heated by the condenser to a temperature of 45°C. The condenser is heated by the flue gas of the boiler. The heating system is described in §3.8.1 and §3.8.3.

A cooling system consisting of a heat exchanger can be used to cool the greenhouse. The upper cooling net can be cooled with the heat exchanger to a temperature of about 10°C. The cooling system is described in §3.8.4.

The heat pump and the heat exchanger operate in conjunction with an aquifer. A warm- and a cold-water aquifer layer are used to store and retrieve the surplus solar energy. The warm-water layer has a temperature of  $T_{aq,h} = 16^\circ\text{C}$  and the cold-water layer has a temperature of  $T_{aq,c} = 10^\circ\text{C}$ . The warm water is used by the heat pump to heat the greenhouse. The cold water is used by the heat exchanger to cool the greenhouse.

A thermal screen can be closed during the night to reduce the heat loss to the environment if the temperature of the outdoor air is low. The thermal screen is operated based on rules used in common practice, which are described in §3.6.

Ventilation by opening windows can be used to cool the greenhouse and to lower the humidity. At times of heat demand, the humidity can be lowered by using ventilation with heat recovery. The sensible heat that is normally lost during ventilation through windows is partially recovered by exchanging the air through a heat exchanger. The ventilation model is described in §3.7.

The roof has is a double layer zigzag cover, which has a high insulation value and light transmission. This decreases heat loss to the environment and increases radiation in the greenhouse.

To minimize fossil energy consumption, no lighting is used.

The control input trajectories consist of actuator settings, such as window apertures and valve positions of, for instance, the boiler.

For the heat and mass transport the following elements are taken into account: air (above and below the screen), crop, heating and cooling net pipes, roof, screen and soil. These elements are modelled as lumped parameter models, which are assumed internally homogeneous. The soil and the roof are divided into two layers/parts.

### 3.2.2 Assumptions

The following assumptions are made:

- The greenhouse has a North-South orientation.

- Each span in the multi span greenhouse has the same layout with respect to the configuration of the heating and the cooling net, the thermal screen and its size.
- The lower heating net is below the canopy and the upper heating and cooling net are above the canopy, but below the screen.
- All outdoor weather conditions are not influenced by the greenhouse climate conditions.
- All compounds (crop, roof glass, upper soil layer, lower and upper heating net, upper cooling net, screen, aquifer, etc.) and gasses (greenhouse air above and below the screen) are homogeneous: they have a uniform temperature. The air in the greenhouse above and below the screen is perfectly mixed (with respect to  $\text{CO}_2$  and  $\text{H}_2\text{O}$  concentration).
- When the screen is fully opened ( $Cl_{sc} = 0$ ), the temperature and concentration  $\text{CO}_2$  and  $\text{H}_2\text{O}$  can be averaged (proportional with the heat capacity and volume of the air above and below the screen). This is necessary to avoid numerical problems in the integration (see §3.6.3). The screen is impermeable for all gasses ( $\text{H}_2\text{O}$ ,  $\text{CO}_2$  and air). The screen transmits part of the solar radiation. The exchange of heat,  $\text{CO}_2$  and  $\text{H}_2\text{O}$  through the screen opening can be described by a simple air exchange rate.
- The heating nets and the cooling net can be described as a number of loops of pipes with a specific length and diameter. The temperature of the water in the lower and upper heating net and the cooling net can be described by simplified equations. In these equations it is assumed that one temperature can be used to describe the energy content of the net. This temperature depends on the ingoing temperature, from which the outgoing temperature can be directly computed with the heat exchange terms (see §3.B).
- One soil layer can be used to approximate the temperature of the upper soil layer  $T_s$  (see §3.C).
- The double glass zigzag roof cover consists of two layers of glass with air in between. The temperature of the outdoor side of the roof  $T_{ro}$  can be directly computed from the temperature of the indoor side of the roof  $T_{ri}$  and their heat exchange terms (see §3.D).
- The heat pump is a compression heat pump. It is assumed that the heat transfer between the heat pump and the lower net has no dynamics (direct transfer of heat).
- The heat exchanger is a countercurrent heat exchanger. It is assumed that the heat transfer between the heat exchanger and the upper cooling net has no dynamics (direct transfer of heat).

- The aquifer has an infinite amount of warm and cold water available. The loading and unloading of the aquifer buffers is limited by government demands, which indirectly corrects for the fact that the buffers are not infinite.
- Water that condensates on the indoor side of the roof, on the screen and on the upper cooling net pipes is directly removed and therefore not available for evaporation.
- When ventilation with heat recovery is used, a fixed fraction  $\eta_{vhr}$  of the sensible heat is recovered.
- The CO<sub>2</sub> assimilation by the crop is instantaneously converted to biomass.
- The boiler runs on (natural) gas.
- The CO<sub>2</sub> supply in the solar greenhouse is assumed to be detached from the boiler. It is assumed that the CO<sub>2</sub> can be acquired from a power plant.

### 3.2.3 States, control inputs and external inputs

The greenhouse model is written in state space form

$$\dot{x} = f(t, x, u, v)$$

where  $t$  is time,  $x$  are the states,  $u$  are the control inputs,  $v$  are the external inputs and  $f$  is a non-linear function. This function is integrated by using a Runge-Kutta fourth order integration algorithm (Press et al., 1986) to obtain the states.

The model description given here is based on the model described by Heesen (1997), which in turn is based on the research by Van Henten (1994), De Zwart (1996), De Jong (1990) and Bot (1983). This model has been extended with a thermal screen, a double glass cover and the so-called solar greenhouse elements: heat pump, heat exchanger, ventilation with heat recovery and a cooling net to describe the solar greenhouse behaviour. The main external input is the weather.

The state equations have been formed based on the laws of conservation of enthalpy and matter. The dynamic behaviour of the states is described using first order differential equations, which match the state space description of the systems. The notational conventions for the model used in this chapter are given in table 3.1.

A description of the states  $x$ , the control inputs  $u$  and the external inputs  $v$  is given in table 3.2.

The state variables  $x$ , the external inputs  $v$  and the control inputs  $u$  are shown in figure 3.2. In this figure, the frames for the state variables  $x$  are bold, for

Table 3.1: Notational conventions

symbol	description	unit	symbol	description	unit
Variables					
$\Phi_m$	mass flow rate	$\text{kg s}^{-1}$	$T$	temperature	K
$\Phi$	volume rate	$\text{m}^3 \text{s}^{-1}$	$V$	volume	$\text{m}^3$
$A$	surface area	$\text{m}^2$	$\rho \cdot c_p \cdot V$	heat capacity	$\text{J K}^{-1}$
$Q$	heat exchange	W			
Subscripts					
$a$	greenhouse air below screen		$out$	going out of the system	
$as$	greenhouse air above screen		$rd$	shortwave radiation	
$c$	crop		$ri$	roof indoor side	
$CO2$	carbondioxide		$ro(L)$	roof outdoor side (longwave)	
$he$	heat exchanger		$s$	upper soil layer	
$hp$	heat pump		$s2$	lower soil layer	
$H2O$	water		$sc$	screen	
$in$	going into the system		$sk$	sky	
$l$	lower heating net		$u$	upper heating net	
$o$	outdoor		$uc$	upper cooling net	

the external inputs  $v$  are dashed and for the control inputs  $u$  are dotted or dash-dotted. The dotted and the dash-dotted frames are used to distinguish between the control inputs that are set by the optimal control and the control inputs that are directly derived from external inputs or from other control inputs.

The screen condition  $c_{sc}$  is either 0 or 1, where  $c_{sc} = 0$  indicates that the screen is fully opened and  $c_{sc} = 1$  indicates that the screen is (possibly partly) closed. The screen condition is a discrete switch that can be interpreted as an external input  $v$ , since it only depends on the outdoor shortwave solar radiation  $I_o$  and the temperature  $T_o$  of the outdoor air (see §3.6.1).

The state equations are:

Carbondioxide concentration indoor air below the screen

$$\frac{dC_{a\_CO2}}{dt} = \begin{cases} \frac{\Phi_{m\_in\_a\_CO2} - \Phi_{m\_a\_c\_CO2} - \Phi_{m\_a\_as\_CO2}}{V_a} & \text{if } c_{sc} = 1 \\ \frac{\Phi_{m\_in\_a\_CO2} - \Phi_{m\_a\_c\_CO2} - \Phi_{m\_as\_o\_CO2}}{V_a + V_{as}} & \text{if } c_{sc} = 0 \end{cases} \quad \{\text{kg}[\text{CO}_2] \text{ m}^{-3} \text{ s}^{-1}\} \quad (3.1)$$

Table 3.2: States, control inputs and external inputs

symbol	description	unit
States $x$		
$C_{a\_CO2}, C_{as\_CO2}$	CO <sub>2</sub> concentration indoor air below/above screen	kg[CO <sub>2</sub> ] m <sup>-3</sup>
$C_{a\_H2O}, C_{as\_H2O}$	H <sub>2</sub> O concentration indoor air below/above screen	kg[H <sub>2</sub> O] m <sup>-3</sup>
$T_a, T_{as}$	temperature indoor air below/above screen	K
$T_c$	temperature crop	K
$T_{ri}$	temperature roof indoor side	K
$T_s$	temperature soil (upper layer)	K
$T_l, T_u$	temperature lower/upper heating net	K
$T_{uc}$	temperature upper cooling net	K
$T_{sc}$	temperature thermal screen	K
$S_T$	temperature integral	K day
$W$	total biomass	kg[b.m.] m <sup>-2</sup> [soil]
$E_{aq}$	aquifer energy content	J m <sup>-2</sup> [soil]
Control inputs $u$		
$vp_{CO2}$	valve position CO <sub>2</sub> supply	[0,1]
$Ap_{l_{sd}}, Ap_{w_{sd}}$	window aperture lee-side/windward-side	[0,1]
$Cl_{sc}$	thermal screen closure	[0,1]
$op_{vhr}$	option ventilation heat recovery	{0,1}
$vp_l, vp_u$	valve position lower/upper net	[0,1]
$vp_{he}$	valve position heat exchanger	[0,1]
$vp_{hp}$	valve position heat pump	[0,1]
External inputs $v$		
$I_o$	outdoor shortwave solar radiation	W m <sup>-2</sup>
$v_o$	outdoor wind speed	m s <sup>-1</sup>
$T_o$	temperature outdoor air	K
$T_{o-w}^\dagger$	temperature wet bulb	K
$T_{sk}$	temperature sky	K
$C_{o\_CO2}$	CO <sub>2</sub> concentration outdoor air	kg[CO <sub>2</sub> ] m <sup>-3</sup>

<sup>†</sup> the H<sub>2</sub>O concentration outdoor air  $C_{o\_H2O}$  can be computed from the temperatures  $T_o$  and  $T_{o-w}$  (see §2.C)

Carbondioxide concentration indoor air above the screen

$$\frac{dC_{as\_CO2}}{dt} = \begin{cases} \frac{\Phi_{m\_a\_as\_CO2} - \Phi_{m\_as\_o\_CO2}}{V_{as}} & \text{if } c_{sc} = 1 \\ \frac{dC_{a\_CO2}}{dt} & \text{if } c_{sc} = 0 \end{cases} \quad \{\text{kg[CO}_2\text{]} \text{ m}^{-3} \text{ s}^{-1}\} \quad (3.2)$$

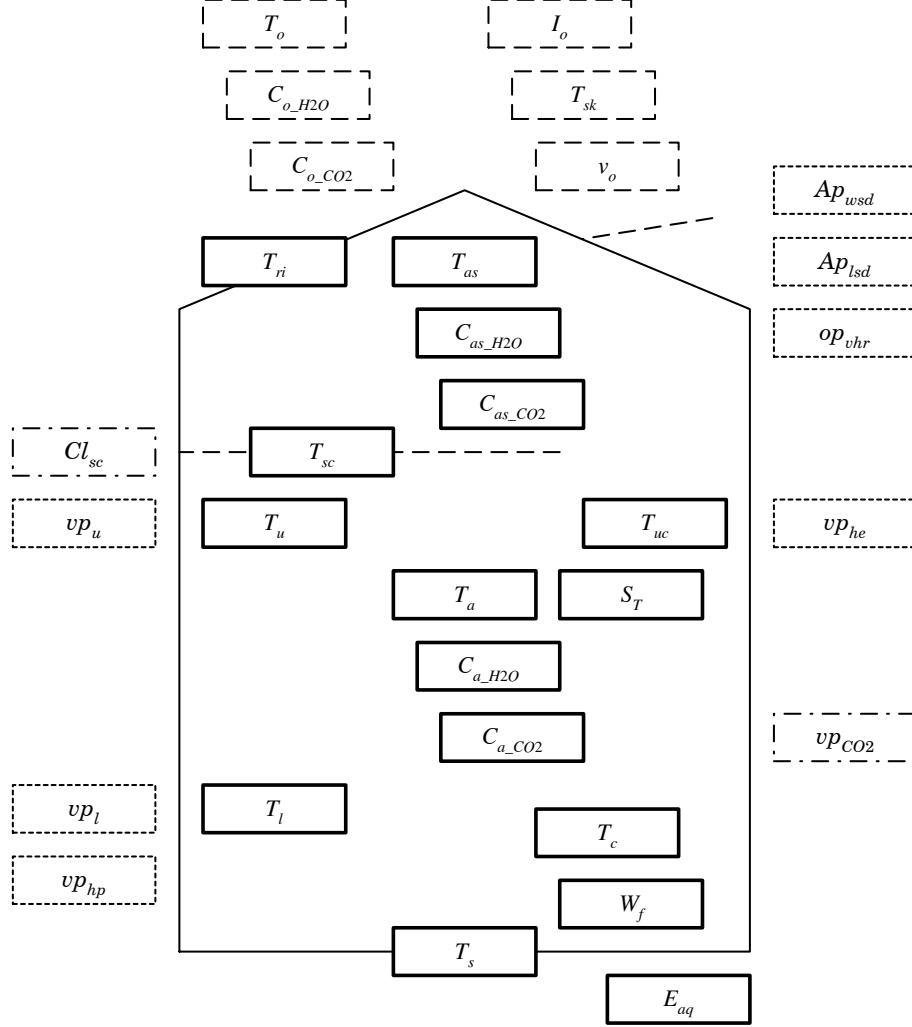


Figure 3.2: States  $x$  (bold), external inputs  $v$  (dashed) and control inputs  $u$  (dotted and dash-dotted) in the solar greenhouse

Water concentration indoor air below the screen

$$\frac{dC_{a,H2O}}{dt} = \begin{cases} \frac{\Phi_{m,c,a,H2O} - \Phi_{m,a,uc,H2O} - \Phi_{m,a,sc,H2O} - \Phi_{m,a,as,H2O}}{V_a} & \text{if } c_{sc} = 1 \\ \frac{\Phi_{m,c,a,H2O} - \Phi_{m,a,uc,H2O} - \Phi_{m,a,sc,H2O} - \Phi_{m,as,ri,H2O} - \Phi_{m,as,o,H2O} - \Phi_{m,as,sc,H2O}}{V_a + V_{as}} & \text{if } c_{sc} = 0 \end{cases} \quad \{\text{kg}[\text{H}_2\text{O}] \text{ m}^{-3} \text{ s}^{-1}\} \quad (3.3)$$

Water concentration indoor air above the screen

$$\frac{dC_{as-H2O}}{dt} = \begin{cases} \frac{\Phi_{m_{a-as-H2O}} - \Phi_{m_{as-ri-H2O}} - \Phi_{m_{as-o-H2O}} - \Phi_{m_{as-sc-H2O}}}{V_{as}} & \text{if } c_{sc} = 1 \\ \frac{dC_{a-H2O}}{dt} & \text{if } c_{sc} = 0 \end{cases} \quad \{\text{kg}[\text{H}_2\text{O}] \text{ m}^{-3} \text{ s}^{-1}\} \quad (3.4)$$

Temperature indoor air below the screen

$$\frac{dT_a}{dt} = \begin{cases} \frac{Q_{l-a} + Q_{u-a} + Q_{uc-a} + Q_{sc-a} - Q_{a-c} - Q_{a-s} - Q_{a-as}}{\rho_a \cdot c_{p-a} \cdot V_a} & \text{if } c_{sc} = 1 \\ \frac{Q_{l-a} + Q_{u-a} + Q_{uc-a} + Q_{sc-a} - Q_{a-c} - Q_{a-s} - Q_{as-o} - Q_{as-ri} + Q_{sc-as}}{\rho_a \cdot c_{p-a} \cdot V_a + \rho_{as} \cdot c_{p-a} \cdot V_{as}} & \text{if } c_{sc} = 0 \end{cases} \quad \{\text{K s}^{-1}\} \quad (3.5)$$

Temperature indoor air above the screen

$$\frac{dT_{as}}{dt} = \begin{cases} \frac{Q_{a-as} + Q_{sc-as} - Q_{as-ri} - Q_{as-o}}{\rho_{as} \cdot c_{p-a} \cdot V_{as}} & \text{if } c_{sc} = 1 \\ \frac{dT_a}{dt} & \text{if } c_{sc} = 0 \end{cases} \quad \{\text{K s}^{-1}\} \quad (3.6)$$

Temperature crop

$$\frac{dT_c}{dt} = \frac{Q_{rd-c} + Q_{a-c} + Q_{l-c} + Q_{ri-c} + Q_{s-c} + Q_{u-c} + Q_{uc-c} - Q_{c-a-H2O} - Q_{c-sc}}{\rho_c \cdot c_{p-c} \cdot V_c} \quad \{\text{K s}^{-1}\} \quad (3.7)$$

Temperature soil

$$\frac{dT_s}{dt} = \frac{Q_{rd-s} + Q_{a-s} + Q_{l-s} + Q_{uc-s} + Q_{u-s} - Q_{s-c} - Q_{s-ri} - Q_{s-s2} - Q_{s-sc}}{(0.7 \rho_s \cdot c_{p-s} + 0.2 \rho_{H2O} \cdot c_{p-H2O} + 0.1 \rho_a \cdot c_{p-a}) \cdot V_s} \quad \{\text{K s}^{-1}\} \quad (3.8)$$

Temperature lower net

$$\frac{dT_l}{dt} = \frac{Q_{in-l} - Q_{out-l} + Q_{rd-l} - Q_{l-a} - Q_{l-c} - Q_{l-ri} - Q_{l-s} - Q_{l-sc}}{\rho_{H2O} \cdot c_{p-H2O} \cdot V_l} \quad \{\text{K s}^{-1}\} \quad (3.9)$$

Temperature upper net

$$\frac{dT_u}{dt} = \frac{Q_{in\_u} - Q_{out\_u} + Q_{rd\_u} - Q_{u\_a} - Q_{u\_c} - Q_{u\_ri} - Q_{u\_s} - Q_{u\_sc}}{\rho_{H2O} \cdot c_{p\_H2O} \cdot V_u} \quad \{\text{K s}^{-1}\} \quad (3.10)$$

Temperature upper cooling net

$$\frac{dT_{uc}}{dt} = \frac{Q_{in\_uc} - Q_{out\_uc} + Q_{rd\_uc} + Q_{a\_uc\_H2O} - Q_{uc\_a} - Q_{uc\_c} - Q_{uc\_ri} - Q_{uc\_s} - Q_{uc\_sc}}{\rho_{H2O} \cdot c_{p\_H2O} \cdot V_{uc}} \quad \{\text{K s}^{-1}\} \quad (3.11)$$

Temperature indoor side of the roof (double or single glass cover)

$$\frac{dT_{ri}}{dt} = \begin{cases} \frac{Q_{rd\_ri} + Q_{as\_ri} + Q_{as\_ri\_H2O} + Q_{l\_ri} + Q_{s\_ri} + Q_{sc\_ri} + Q_{u\_ri} + Q_{uc\_ri} - Q_{ri\_c} - Q_{ri\_ro} - Q_{ri\_roL}}{\rho_r \cdot c_{p\_r} \cdot V_r} & \text{double} \\ \frac{Q_{rd\_ri} + Q_{as\_ri} + Q_{as\_ri\_H2O} + Q_{l\_ri} + Q_{s\_ri} + Q_{sc\_ri} + Q_{u\_ri} + Q_{uc\_ri} - Q_{ri\_c} - Q_{ro\_o} - Q_{ro\_sk}}{\rho_r \cdot c_{p\_r} \cdot V_r} & \text{single} \end{cases} \quad \{\text{K s}^{-1}\} \quad (3.12)$$

Temperature screen

$$\frac{dT_{sc}}{dt} = \frac{Q_{rd\_sc} + Q_{c\_sc} + Q_{l\_sc} + Q_{s\_sc} + Q_{u\_sc} + Q_{uc\_sc} + Q_{a\_sc\_H2O} + Q_{as\_sc\_H2O} - Q_{sc\_a} - Q_{sc\_as} - Q_{sc\_ri}}{\rho_{sc} \cdot c_{p\_sc} \cdot V_{sc}} \quad \{\text{K s}^{-1}\} \quad (3.13)$$

Temperature integral temperature indoor air below the screen (more details in §2.4)

$$\frac{dS_T}{dt} = \frac{T_a - T_{aref}}{n_{secs}} \quad \{\text{K day s}^{-1}\} \quad (3.14)$$

Total biomass

$$\frac{dW}{dt} = \frac{f_{w\_CO2} \cdot \Phi_{m\_a\_c\_CO2}}{A_s} \quad \{\text{kg[b.m.] m}^{-2}[\text{soil}] \text{s}^{-1}\} \quad (3.15)$$

Aquifer energy content

$$\frac{dE_{aq}}{dt} = \frac{Q_{he} - Q_c}{A_s} \quad \{\text{J m}^{-2}[\text{soil}] \text{s}^{-1}\} \quad (3.16)$$

In the subsequent paragraphs, the carbondioxide, water and heat exchanges in the greenhouse are described.

### 3.3 Carbondioxide model

The differential equations for the carbondioxide concentrations of the indoor air below and above the screen ( $C_{a\_CO2}$ ,  $C_{as\_CO2}$  {kg[CO<sub>2</sub>] m<sup>-3</sup>}) and the total biomass ( $W$  {kg[b.m.] m<sup>-2</sup>[soil]}) are given in §3.2.3. The carbondioxide mass flow rates are described in the subsequent paragraphs. The carbondioxide concentrations, the biomass and the carbondioxide mass flows are shown in figure 3.3.

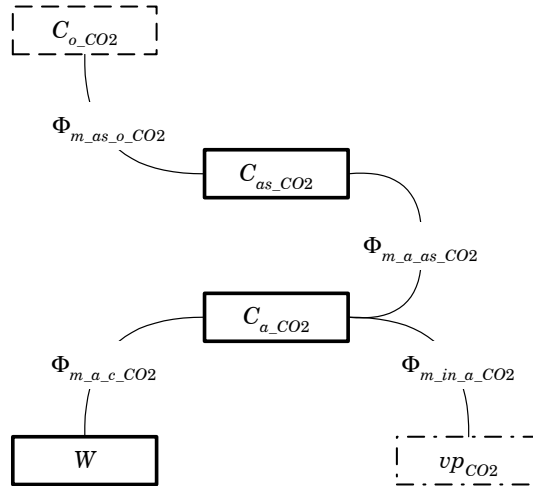


Figure 3.3: States  $x$  (bold), external input  $v$  (dashed) and control input  $u$  (dash-dotted) in the carbondioxide model

All carbondioxide concentrations  $C_{x\_CO2}$  are here expressed in the SI-unit {kg[CO<sub>2</sub>] m<sup>-3</sup>[air]}. In the other chapters the carbondioxide concentrations  $CO_{2x}$  are used, which are expressed in {μmol[CO<sub>2</sub>] mol<sup>-1</sup>[air]}, since this is the unit used in practice. This concentration can be computed with:  $CO_{2x} = \frac{C_{x\_CO2}}{1.8310^{-6}}$ .

#### 3.3.1 Carbondioxide supply

In the solar greenhouse case, the carbondioxide supply is independent of boiler operation, which means that the maximum CO<sub>2</sub> supply  $\Phi_{m\_CO2}$  is a design

parameter. The mass flow rate of carbondioxide  $\Phi_{m_{in.a.CO2}}$  supplied to the indoor air is described by

$$\Phi_{m_{in.a.CO2}} = vp_{CO2} \cdot \Phi_{m.CO2} \quad \{\text{kg}[\text{CO}_2] \text{ s}^{-1}\} \quad (3.17)$$

in which  $\Phi_{m.CO2} = 5 \cdot 10^{-5} A_s \text{ kg}[\text{CO}_2] \text{ s}^{-1}$  is the maximum mass flow rate  $\text{CO}_2$  supply, where  $vp_{CO2} \in [0, 1]$  is the valve position carbondioxide supply (control input).

In a conventional greenhouse in The Netherlands, carbondioxide is a side product of energy supply by the boiler. The carbondioxide supply by the boiler is therefore limited by the amount of carbondioxide  $\Phi_{m_{in.a.CO2} \max}$  produced by the boiler, so

$$\Phi_{m_{in.a.CO2}} = \min(vp_{CO2} \cdot \Phi_{m.CO2}, \Phi_{m_{in.a.CO2} \max}) \quad \{\text{kg}[\text{CO}_2] \text{ s}^{-1}\} \quad (3.18)$$

in which

$$\Phi_{m_{in.a.CO2} \max} = \Phi_{gas} \cdot f_{CO2.gas} \quad \{\text{kg}[\text{CO}_2] \text{ s}^{-1}\} \quad (3.19)$$

in which the conversion factor  $f_{CO2.gas} = 1.78 \text{ kg}[\text{CO}_2] \text{ m}^{-3}[\text{gas}]$ , where  $\Phi_{gas} \{\text{m}^3[\text{gas}] \text{ s}^{-1}\}$  is the gas flow needed by the boiler.

The gas flow  $\Phi_{gas}$  needed by the boiler is defined by

$$\Phi_{gas} = \frac{Q_{boil}}{\eta_{boil} \cdot H_u} \quad \{\text{m}^3[\text{gas}] \text{ s}^{-1}\} \quad (3.20)$$

in which the efficiency of the boiler  $\eta_{boil} = 0.95$  and the (high) combustion value of gas  $H_u = 35.17 \cdot 10^6 \text{ J m}^{-3}[\text{gas}]$ , where  $Q_{boil} \{\text{W}\}$  (eqn. 3.172) is the energy supply by the boiler for heat supply. The high combustion value of gas is the amount of energy available from its complete combustion, including condensation of water vapour that results from the combustion.

### 3.3.2 Photosynthesis and respiration

The mass flow rate of carbondioxide  $\Phi_{m_{a.c.CO2}}$  from the indoor air to the canopy (the net photosynthesis rate of the canopy) is described by

$$\Phi_{m_{a.c.CO2}} = P_{cg} - r_c \quad \{\text{kg}[\text{CO}_2] \text{ m}^{-2}[\text{soil}] \text{ s}^{-1}\} \quad (3.21)$$

in which the gross assimilation rate of the canopy  $P_{cg}$  is given by

$$P_{cg} = 10^{-6} \cdot A_s \cdot P_g \quad \{\text{kg}[\text{CO}_2] \text{ m}^{-2}[\text{soil}] \text{ s}^{-1}\} \quad (3.22)$$

and the dark respiration rate of the canopy  $r_c$  is given by

$$r_c = 10^{-6} \cdot A_s \cdot r_D \quad \{\text{kg}[\text{CO}_2] \text{ m}^{-2}[\text{soil}] \text{ s}^{-1}\} \quad (3.23)$$

where  $P_g$   $\{\text{mg}[\text{CO}_2] \text{ m}^{-2}[\text{soil}] \text{ s}^{-1}\}$  is the gross assimilation rate of the canopy,  $r_D$   $\{\text{mg}[\text{CO}_2] \text{ m}^{-2}[\text{soil}] \text{ s}^{-1}\}$  is the dark respiration rate of the canopy and  $A_s$   $\{\text{m}^2[\text{soil}]\}$  is the surface area of the soil. Several different models can be used to compute these rates (see §2.3). The model used is the new photosynthesis model *CG4* (see §2.3.1).

This carbondioxide is used to produce biomass. It is assumed that the  $\text{CO}_2$  assimilation by the crop is instantaneously converted to biomass. For the conversion from the consumed  $\text{CO}_2$  to the biomass increase rate, the conversion factor  $f_{w\_CO2}$  is used

$$f_{w\_CO2} = \frac{1}{1 - \frac{p_w}{100}} \cdot \frac{c_f \cdot c_{cs}}{ASRQ} \quad \{\text{kg}[\text{b.m.}] \text{ kg}^{-1}[\text{CO}_2]\} \quad (3.24)$$

in which the percentage water in total biomass  $p_w = 94\%$ , the fraction of produced biomass material for dry weight  $c_f = 1$ , the conversion factor from  $\text{CO}_2$  to  $\text{CH}_2\text{O}$  (fraction of molar masses)  $c_{cs} = \frac{30}{44} \text{ kg}[\text{CH}_2\text{O}] \text{ kg}[\text{CO}_2]^{-1}$  and the conversion factor from dry weight to  $\text{CH}_2\text{O}$  (glucose requirement)  $ASRQ = 1.2 \text{ kg}[\text{CH}_2\text{O}] \text{ kg}[\text{d.w.}]^{-1}$ .

### 3.3.3 Carbondioxide transport due to ventilation

The mass flow rate of carbondioxide  $\Phi_{m\_as\_o\_CO2}$  from the indoor to the outdoor air is described by

$$\Phi_{m\_as\_o\_CO2} = \Phi_{as\_o} \cdot (C_{as\_CO2} - C_{o\_CO2}) \quad \{\text{kg}[\text{CO}_2] \text{ s}^{-1}\} \quad (3.25)$$

where  $\Phi_{as\_o}$   $\{\text{m}^3 \text{ s}^{-1}\}$  is the ventilation flow (eqn. 3.150),  $C_{as\_CO2}$   $\{\text{kg m}^{-3}\}$  is the carbondioxide concentration of indoor air above the screen and  $C_{o\_CO2}$   $\{\text{kg m}^{-3}\}$  is the carbondioxide concentration of outdoor air.

### 3.3.4 Carbondioxide transport past the screen

The mass flow rate of carbondioxide  $\Phi_{m\_a\_as\_CO2}$  from the indoor air below the screen to the indoor air above the screen is described by

$$\Phi_{m\_a\_as\_CO2} = \Phi_{a\_as} \cdot (C_{a\_CO2} - C_{as\_CO2}) \quad \{\text{kg}[\text{CO}_2] \text{ s}^{-1}\} \quad (3.26)$$

where  $\Phi_{a\_as}$   $\{\text{m}^3 \text{ s}^{-1}\}$  is the volume flow of air from below the screen to above the screen (eqn. 3.145),  $C_{a\_CO2}$   $\{\text{kg m}^{-3}\}$  is the carbondioxide concentration of indoor air below the screen and  $C_{as\_CO2}$   $\{\text{kg m}^{-3}\}$  is the carbondioxide concentration of indoor air above the screen.

### 3.4 Water vapour model

The differential equations for the water vapour concentrations of the indoor air below and above the screen ( $C_{a\_H2O}$ ,  $C_{as\_H2O}$  {kg[H<sub>2</sub>O] m<sup>-3</sup>}) are given in §3.2.3. The water vapour mass flow rates are described in the subsequent paragraphs. The water vapour concentrations and the water vapour mass flows are shown in figure 3.4.

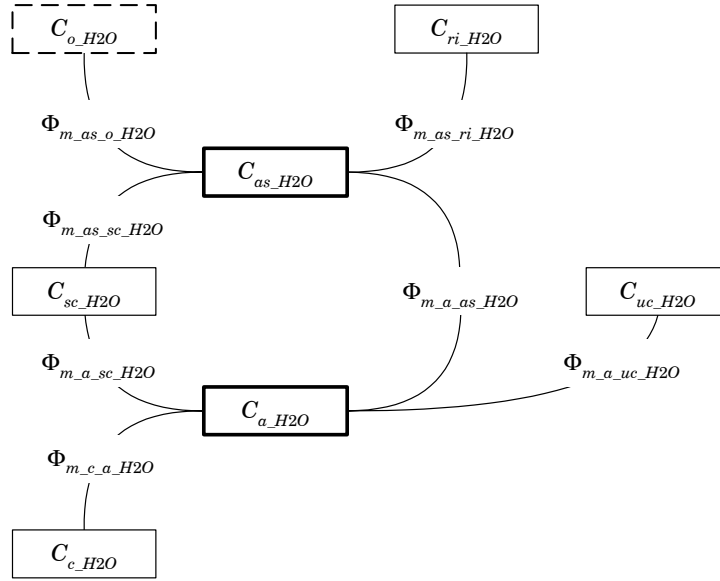


Figure 3.4: States  $x$  (bold) and external input  $v$  (dashed) in the water vapour model

#### 3.4.1 Canopy transpiration

The canopy transpiration is determined based on the thesis of Stanghellini (1987). The mass flow rate of water vapour  $\Phi_{m\_c\_a\_H2O}$  from the canopy to the indoor air due to transpiration {kg[H<sub>2</sub>O] s<sup>-1</sup>} is given in §2.2.

#### 3.4.2 Condensation of water

Water will condensate on a surface when the concentration of water vapour in the air is higher than the saturation concentration of water vapour of the surface. The saturation concentration of water vapour of the surface depends on the surface temperature and the humidity of the air. It is assumed that

water that condensates is directly removed, and is therefore not available for evaporation.

#### 3.4.2.1 Condensation of water on roof indoor side

The mass flow rate of water vapour  $\Phi_{m_{as}ri\_H2O}$  from the indoor air above the screen to the indoor side of the roof due to condensation is

$$\Phi_{m_{as}ri\_H2O} = \max(A_r \cdot k_{as\_ri\_H2O} \cdot (C_{as\_H2O} - C_{ri\_H2Os}), 0) \quad \{\text{kg}[\text{H}_2\text{O}] \text{ s}^{-1}\} \quad (3.27)$$

where  $A_r$   $\{\text{m}^2\}$  is the surface area of the roof,  $k_{as\_ri\_H2O}$   $\{\text{m s}^{-1}\}$  is the mass transfer coefficient of water vapour from the indoor air above the screen to the indoor side of the roof,  $C_{ri\_H2Os}$   $\{\text{kg}[\text{H}_2\text{O}] \text{ m}^{-3}[\text{air}]\}$  is the saturation concentration of water vapour at the temperature of the indoor side of the roof (see §2.C.1) and  $C_{as\_H2O}$   $\{\text{kg}[\text{H}_2\text{O}] \text{ m}^{-3}[\text{air}]\}$  is the concentration of water vapour at the temperature of the indoor air above the screen. If  $C_{as\_H2O} \leq C_{ri\_H2Os}$ , then  $\Phi_{m_{as}ri\_H2O} = 0$  (no condensation).

The mass transfer coefficient of water vapour  $k_{as\_ri\_H2O}$  from the indoor air above the screen to the indoor side of the roof is defined by Bot (1983)

$$k_{as\_ri\_H2O} = \frac{\alpha_{as\_ri}}{\rho_{as} \cdot c_{p,a} \cdot Le^{\frac{2}{3}}} \quad \{\text{m s}^{-1}\} \quad (3.28)$$

where  $\alpha_{as\_ri}$   $\{\text{W m}^{-2} \text{ K}^{-1}\}$  is the heat transfer coefficient from the indoor air above the screen to the indoor side of the roof (eqn. 3.55),  $\rho_{as}$   $\{\text{kg m}^{-3}\}$  is the density of air above the screen,  $c_{p,a}$   $\{\text{J kg}^{-1} \text{ K}^{-1}\}$  is the specific heat capacity of air and  $Le = 0.89$   $\{-\}$  is the Lewis number for water vapour in air.

#### 3.4.2.2 Condensation of water on upper cooling net

The mass flow rate of water vapour  $\Phi_{m_{a\_uc\_H2O}}$  from the indoor air below the screen to the upper cooling net due to condensation is

$$\Phi_{m_{a\_uc\_H2O}} = \max(A_{uc} \cdot k_{a\_uc\_H2O} \cdot (C_{a\_H2O} - C_{uc\_H2Os}), 0) \quad \{\text{kg}[\text{H}_2\text{O}] \text{ s}^{-1}\} \quad (3.29)$$

where  $A_{uc}$   $\{\text{m}^2\}$  is the surface area of the upper cooling net,  $k_{a\_uc\_H2O}$   $\{\text{m s}^{-1}\}$  is the mass transfer coefficient of water vapour from the indoor air to the upper cooling net,  $C_{uc\_H2Os}$   $\{\text{kg}[\text{H}_2\text{O}] \text{m}^{-3}[\text{air}]\}$  is the saturation concentration of water vapour at the temperature of the upper cooling net (see §2.C.1) and  $C_{a\_H2O}$   $\{\text{kg}[\text{H}_2\text{O}] \text{m}^{-3}[\text{air}]\}$  is the concentration of water vapour at the temperature of the indoor air below the screen. If  $C_{a\_H2O} \leq C_{uc\_H2Os}$ , then  $\Phi_{m\_a\_uc\_H2O} = 0$  (no condensation).

The mass transfer coefficient of water vapour  $k_{a\_uc\_H2O}$  from the indoor air below the screen to the upper cooling net is defined by Bot (1983)

$$k_{a\_sc\_H2O} = \frac{\alpha_{uc\_a}}{\rho_a \cdot c_{p\_a} \cdot Le^{\frac{2}{3}}} \quad \{\text{m s}^{-1}\} \quad (3.30)$$

where  $\alpha_{uc\_a}$   $\{\text{W m}^{-2} \text{K}^{-1}\}$  is the heat transfer coefficient from the indoor air below the screen to the upper cooling net (eqn. 3.49),  $\rho_a$   $\{\text{kg m}^{-3}\}$  is the density of air below the screen,  $c_{p\_a}$   $\{\text{J kg}^{-1} \text{K}^{-1}\}$  is the specific heat capacity of air and  $Le = 0.89$   $\{-\}$  is the Lewis number for water vapour in air.

### 3.4.2.3 Condensation of water on screen

The mass flow rates of water vapour  $\Phi_{m\_a\_sc\_H2O}$  and  $\Phi_{m\_as\_sc\_H2O}$  from the indoor air below and above the screen to the screen due to condensation are

$$\Phi_{m\_a\_sc\_H2O} = \max(A_{sc} \cdot k_{a\_sc\_H2O} \cdot (C_{a\_H2O} - C_{sc\_H2Os}), 0) \quad \{\text{kg}[\text{H}_2\text{O}] \text{s}^{-1}\} \quad (3.31)$$

$$\Phi_{m\_as\_sc\_H2O} = \max(A_{sc} \cdot k_{as\_sc\_H2O} \cdot (C_{as\_H2O} - C_{sc\_H2Os}), 0) \quad \{\text{kg}[\text{H}_2\text{O}] \text{s}^{-1}\} \quad (3.32)$$

where  $A_{sc}$   $\{\text{m}^2\}$  is the surface area of the screen,  $k_{a\_sc\_H2O}$  and  $k_{as\_sc\_H2O}$   $\{\text{m s}^{-1}\}$  are the mass transfer coefficients of water vapour from the indoor air below and above the screen to the screen,  $C_{sc\_H2Os}$   $\{\text{kg}[\text{H}_2\text{O}] \text{m}^{-3}[\text{air}]\}$  is the saturation concentration of water vapour at the temperature of the screen (see §2.C.1) and  $C_{a\_H2O}$  and  $C_{as\_H2O}$   $\{\text{kg}[\text{H}_2\text{O}] \text{m}^{-3}[\text{air}]\}$  are the concentrations of water vapour at the temperature of the indoor air below and above the screen. If  $C_{a\_H2O} \leq C_{sc\_H2Os}$ , then  $\Phi_{m\_a\_sc\_H2O} = 0$  (no condensation). If  $C_{as\_H2O} \leq C_{sc\_H2Os}$ , then  $\Phi_{m\_as\_sc\_H2O} = 0$  (no condensation).

The mass transfer coefficients of water vapour  $k_{a\_sc\_H2O}$  and  $k_{as\_sc\_H2O}$  from the indoor air below and above the screen to the screen are defined by Bot (1983)

$$k_{a\_sc\_H2O} = \frac{\alpha_{a\_sc}}{\rho_a \cdot c_{p,a} \cdot Le^{\frac{2}{3}}} \quad \{\text{m s}^{-1}\} \quad (3.33)$$

$$k_{as\_sc\_H2O} = \frac{\alpha_{as\_sc}}{\rho_{as} \cdot c_{p,a} \cdot Le^{\frac{2}{3}}} \quad \{\text{m s}^{-1}\} \quad (3.34)$$

where  $\alpha_{a\_sc}$  and  $\alpha_{as\_sc}$   $\{\text{W m}^{-2} \text{K}^{-1}\}$  are the heat transfer coefficients from the indoor air below and above the screen to the screen (eqns. 3.60 and 3.62),  $\rho_a$  and  $\rho_{as}$   $\{\text{kg m}^{-3}\}$  are the densities of air below and above the screen,  $c_{p,a}$   $\{\text{J kg}^{-1} \text{K}^{-1}\}$  is the specific heat capacity of air and  $Le = 0.89$   $\{-\}$  is the Lewis number for water vapour in air.

### 3.4.3 Water vapour transport due to ventilation

The mass flow rate of water vapour  $\Phi_{m\_as\_o\_H2O}$  from the indoor air above the screen to the outdoor air is described by

$$\Phi_{m\_as\_o\_H2O} = \Phi_{as,o} \cdot (C_{as\_H2O} - C_{o\_H2O}) \quad \{\text{kg}[\text{H}_2\text{O}] \text{s}^{-1}\} \quad (3.35)$$

where  $\Phi_{as,o}$   $\{\text{m}^3 \text{s}^{-1}\}$  is the ventilation flow (eqn. 3.150),  $C_{as\_H2O}$   $\{\text{kg m}^{-3}\}$  is the water concentration of indoor air above the screen and  $C_{o\_H2O}$   $\{\text{kg m}^{-3}\}$  is the water concentration of outdoor air.

### 3.4.4 Water vapour transport past the screen

The mass flow rate of water vapour  $\Phi_{m\_a\_as\_H2O}$  from the indoor air below the screen to the indoor air above the screen is described by

$$\Phi_{m\_a\_as\_H2O} = \Phi_{a,as} \cdot (C_{a\_H2O} - C_{as\_H2O}) \quad \{\text{kg}[\text{H}_2\text{O}] \text{s}^{-1}\} \quad (3.36)$$

where  $\Phi_{a,as}$   $\{\text{m}^3 \text{s}^{-1}\}$  is the volume flow of air from below the screen to above the screen (eqn. 3.145),  $C_{a\_H2O}$   $\{\text{kg m}^{-3}\}$  is the water concentration of indoor air below the screen and  $C_{as\_H2O}$   $\{\text{kg m}^{-3}\}$  is the water concentration of indoor air above the screen.

### 3.5 Thermal model

The differential equations for the temperatures of the roof, the indoor air below and above the screen, the crop, the soil (upper layer), the lower and the upper heating net, the upper cooling net and the thermal screen ( $T_{ri}$ ,  $T_a$ ,  $T_{as}$ ,  $T_c$ ,  $T_s$ ,  $T_l$ ,  $T_u$ ,  $T_{uc}$ ,  $T_{sc}$  {K}) are given in §3.2.3. The heat transfer terms are described in the subsequent paragraphs. The temperatures and the heat transfer terms are shown in figure 3.5. The control inputs  $vp_l$ ,  $vp_u$ ,  $vp_{hp}$ ,  $vp_{he}$  in the thermal model and the heat transfer terms corresponding to these control inputs  $Q_{in,l}$ ,  $Q_{out,l}$ ,  $Q_{in,u}$ ,  $Q_{out,u}$ ,  $Q_{in,uc}$ ,  $Q_{out,uc}$ ,  $Q_{he}$  and  $Q_{hp}$  are not incorporated in this figure.

#### 3.5.1 Convection

Convection is the heat transfer between solid and a gas or fluid material. Convection is also part of the ventilation process and the heat exchange past the screen. The heat transfer  $Q_{A,B}$  from  $A$  to  $B$  is described by the equation (Newton's law of cooling)

$$Q_{A,B} = A_{A,B} \cdot \alpha_{A,B} \cdot (T_A - T_B) \quad \{\text{W}\} \quad (3.37)$$

where  $A_{A,B}$  {m<sup>2</sup>} is the surface area for heat transfer,  $\alpha_{A,B}$  {W m<sup>-2</sup> K<sup>-1</sup>} is the heat transfer coefficient between  $A$  and  $B$  and  $T_A$  and  $T_B$  {K} are the temperatures of  $A$  and  $B$ .

##### 3.5.1.1 Convection from indoor air to canopy

The convective heat transfer  $Q_{a,c}$  from the indoor air to the canopy is defined by

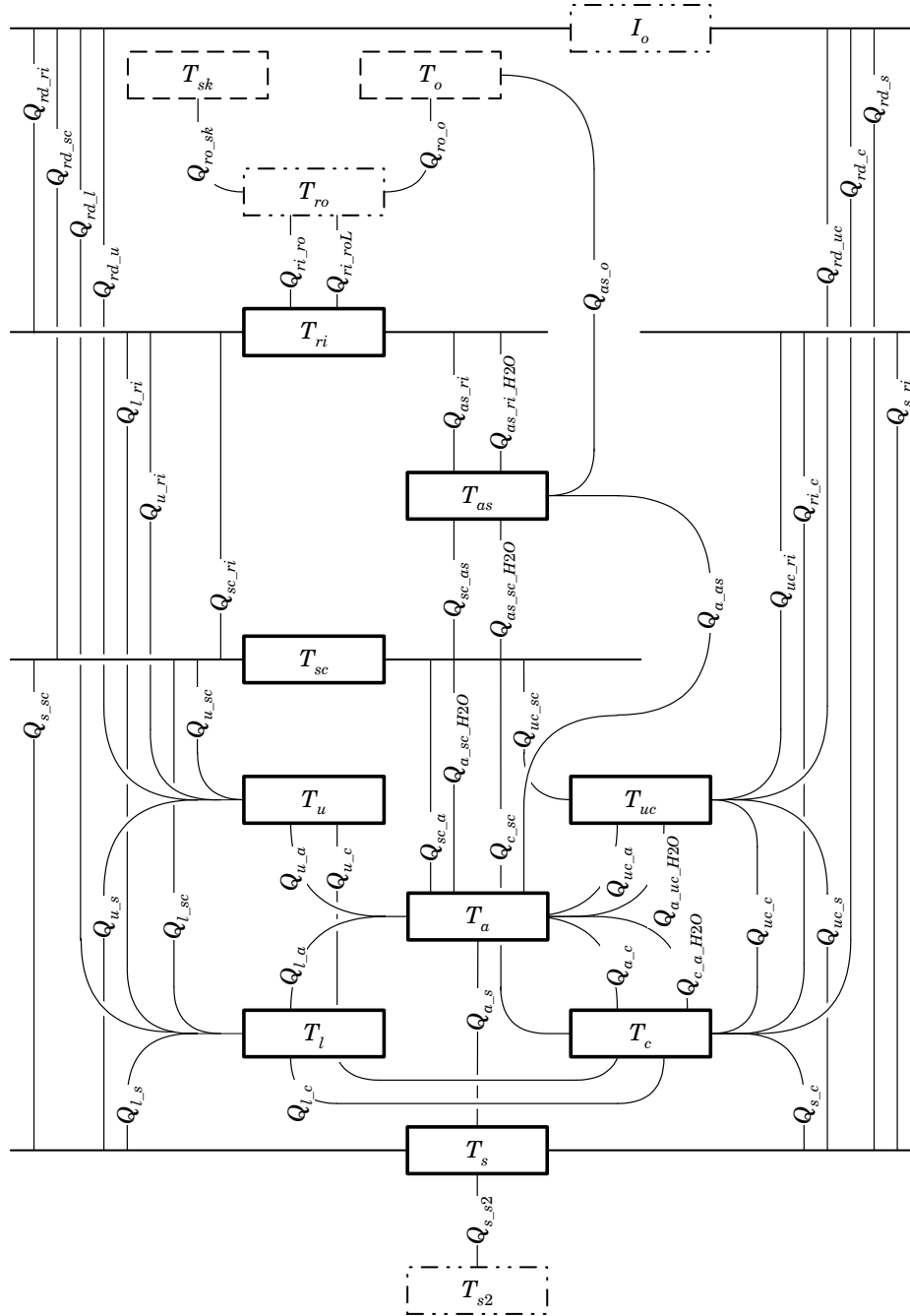
$$Q_{a,c} = A_c \cdot \alpha_{a,c} \cdot (T_a - T_c) \quad \{\text{W}\} \quad (3.38)$$

where  $T_a$  and  $T_c$  {K} are the temperatures of indoor air below the screen and the canopy.

The surface area  $A_c$  of the canopy is computed based on the leaf area index  $LAI$  {m<sup>2</sup>[leaf] m<sup>-2</sup>[soil]}

$$A_c = 2 LAI \cdot A_s \quad \{\text{m}^2\} \quad (3.39)$$

where 2 accounts for two sides of the leaf, while  $LAI$  refers to only one side of the leaf.

Figure 3.5: States  $x$  (bold) and external inputs  $v$  (--) in the thermal model

The heat transfer coefficient  $\alpha_{a-c}$  from the indoor air to the canopy is related to the leaf boundary layer resistance to heat transport  $R_{b,heat}$   $\{\text{s m}^{-1}\}$  (eqn. 2.9) by (de Zwart, 1996)

$$\alpha_{a-c} = \frac{\rho_a \cdot c_{p,a}}{R_{b,heat}} \quad \{\text{W m}^{-2} [\text{leaf}] \text{K}^{-1}\} \quad (3.40)$$

where  $\rho_a$   $\{\text{kg m}^{-3}\}$  is the density of air and  $c_{p,a}$   $\{\text{J kg}^{-1} \text{K}^{-1}\}$  is the specific heat capacity of air.

### 3.5.1.2 Convection from lower net to indoor air

The convective heat transfer  $Q_{l-a}$  from the lower net to the indoor air is defined by

$$Q_{l-a} = A_l \cdot \alpha_{l-a} \cdot (T_l - T_a) \quad \{\text{W}\} \quad (3.41)$$

where  $T_l$  and  $T_a$   $\{\text{K}\}$  are the temperatures of the lower net and the indoor air below the screen.

The surface area  $A_l$  of the lower net is computed by

$$A_l = n_s \cdot n_l \cdot \pi \cdot d_l \cdot l_l \quad \{\text{m}^2\} \quad (3.42)$$

where  $n_s$  is the number of greenhouse spans,  $n_l$  is the number of pipes of the lower net per span,  $d_l$   $\{\text{m}\}$  is the outer diameter of the lower net pipe and  $l_l$   $\{\text{m}\}$  is the length of one loop of the lower net.

The heat transfer coefficient  $\alpha_{l-a}$  from the lower net to the indoor air is described by (de Zwart, 1996)

$$\alpha_{l-a} = \frac{1.28}{d_l^{0.25}} \cdot |T_l - T_a|^{0.25} \quad \{\text{W m}^{-2} \text{K}^{-1}\} \quad (3.43)$$

### 3.5.1.3 Convection from upper net to indoor air

The convective heat transfer  $Q_{u-a}$  from the upper net to the indoor air is defined by

$$Q_{u-a} = A_u \cdot \alpha_{u-a} \cdot (T_u - T_a) \quad \{\text{W}\} \quad (3.44)$$

where  $T_u$  and  $T_a$   $\{\text{K}\}$  are the temperatures of the upper net and the indoor air below the screen.

The surface area  $A_u$  of the upper net is computed by

$$A_u = n_s \cdot n_u \cdot \pi \cdot d_u \cdot l_u \quad \{\text{m}^2\} \quad (3.45)$$

where  $n_s$  is the number of greenhouse spans,  $n_u$  is the number of pipes of the upper net per span,  $d_u$  {m} is the outer diameter of the upper net pipe and  $l_u$  {m} is the length of one loop of the upper net.

The heat transfer coefficient  $\alpha_{u.a}$  from the upper net to the indoor air is described by (de Zwart, 1996)

$$\alpha_{u.a} = \frac{1.28}{d_u^{0.25}} \cdot |T_u - T_a|^{0.25} \quad \{\text{W m}^{-2} \text{K}^{-1}\} \quad (3.46)$$

#### 3.5.1.4 Convection from upper cooling net to indoor air

The convective heat transfer  $Q_{uc.a}$  from the cooling net to the indoor air below the screen is defined by

$$Q_{uc.a} = A_{uc} \cdot \alpha_{uc.a} \cdot (T_{uc} - T_a) \quad \{\text{W}\} \quad (3.47)$$

where  $T_{uc}$  and  $T_a$  {K} are the temperatures of the upper cooling net and the indoor air below the screen.

The surface area  $A_{uc}$  of the upper cooling net is computed by

$$A_{uc} = 4 n_s \cdot n_{uc} \cdot \pi \cdot d_{uc} \cdot l_{uc} \quad \{\text{m}^2\} \quad (3.48)$$

where  $n_s$  is the number of greenhouse spans,  $n_{uc}$  is the number of pipes of the upper cooling net per span,  $d_{uc}$  {m} is the outer diameter of the upper cooling net pipe and  $l_{uc}$  {m} is the length of one loop of the upper cooling net. The number 4 indicates the surface area amplification for the finned pipe compared to a normal pipe.

The heat transfer coefficient  $\alpha_{uc.a}$  from the upper cooling net to the indoor air is described by (de Zwart, 1996)

$$\alpha_{uc.a} = \frac{1.28}{d_{uc}^{0.25}} \cdot |T_{uc} - T_a|^{0.25} \quad \{\text{W m}^{-2} \text{K}^{-1}\} \quad (3.49)$$

#### 3.5.1.5 Convection from indoor air to soil

The convective heat transfer  $Q_{a.s}$  from the indoor air to the soil is defined by

$$Q_{a.s} = A_s \cdot \alpha_{a.s} \cdot (T_a - T_s) \quad \{\text{W}\} \quad (3.50)$$

where  $T_a$  and  $T_s$  {K} are the temperatures of the indoor air below the screen and the soil.

The surface area  $A_s$  of the soil is computed by

$$A_s = n_s \cdot l_s \cdot w_s \quad \{\text{m}^2\} \quad (3.51)$$

where  $n_s$  is the number of greenhouse spans,  $l_s$  {m} is the length of the span and  $w_s$  {m} is the width of the span.

The heat transfer coefficient  $\alpha_{a-s}$  from the indoor air to the soil is described by (de Zwart, 1996)

$$\alpha_{a-s} = \begin{cases} 1.7 |T_a - T_s|^{\frac{1}{3}} & \forall T_a < T_s \\ 1.3 |T_a - T_s|^{0.25} & \forall T_a \geq T_s \end{cases} \quad \{\text{W m}^{-2} \text{K}^{-1}\} \quad (3.52)$$

#### 3.5.1.6 Convection from indoor air to roof indoor side

The convective heat transfer  $Q_{as-ri}$  from the indoor air above the screen to the indoor side of the roof is defined by

$$Q_{as-ri} = A_r \cdot \alpha_{as-ri} \cdot (T_{as} - T_{ri}) \quad \{\text{W}\} \quad (3.53)$$

where  $T_{as}$  and  $T_{ri}$  {K} are the temperatures of the indoor air above the screen and the indoor side of the roof.

The surface area  $A_r$  of the roof is computed based on the angle  $\gamma$  {rad} of the roof with horizontal plane

$$A_r = \frac{1}{\cos(\gamma)} \cdot A_s \quad \{\text{m}^2\} \quad (3.54)$$

The heat transfer coefficient  $\alpha_{as-ri}$  from the indoor air above the screen to the indoor side of the roof is described by (Stoffers, 1989)

$$\alpha_{as-ri} = 3 |T_{as} - T_{ri}|^{\frac{1}{3}} \quad \{\text{W m}^{-2} \text{K}^{-1}\} \quad (3.55)$$

#### 3.5.1.7 Convection from roof outdoor side to outdoor air

The convective heat transfer  $Q_{ro-o}$  from the roof to the outdoor air is defined by

$$Q_{ro-o} = A_r \cdot \alpha_{ro-o} \cdot (T_{ro} - T_o) \quad \{\text{W}\} \quad (3.56)$$

where  $T_{ro}$  and  $T_o$  {K} are the temperatures of the outdoor side of the roof and the outdoor air.

The heat transfer coefficient  $\alpha_{ro-o}$  from the roof to the outdoor air depends on the outdoor wind speed  $v_o$   $\{\text{m s}^{-1}\}$  (Bot, 1983)

$$\alpha_{ro-o} = \begin{cases} 2.8 + 1.2 v_o & \forall v_o < 4 \\ 2.5 v_o^{0.8} & \forall v_o \geq 4 \end{cases} \quad \{\text{W m}^{-2} \text{K}^{-1}\} \quad (3.57)$$

### 3.5.1.8 Convection from screen to indoor air below screen

The convective heat transfer  $Q_{sc-a}$  from the screen to the indoor air below the screen is defined by

$$Q_{sc-a} = A_{sc} \cdot \alpha_{a-sc} \cdot (T_{sc} - T_a) \quad \{\text{W}\} \quad (3.58)$$

where  $T_{sc}$  and  $T_a$   $\{\text{K}\}$  are the temperatures of the screen and the indoor air below the screen.

The surface area  $A_{sc}$  of the screen is equal to the surface area  $A_s$  of the soil

$$A_{sc} = A_s \quad \{\text{m}^2\} \quad (3.59)$$

The heat transfer coefficient  $\alpha_{a-sc}$  from the indoor air below the screen to the screen is described by (Stoffers, 1989)

$$\alpha_{a-sc} = Cl_{sc} \cdot 3 |T_a - T_{sc}|^{\frac{1}{3}} \quad \{\text{W m}^{-2} \text{K}^{-1}\} \quad (3.60)$$

where  $Cl_{sc} \in [0, 1]$  is the thermal screen closure.

### 3.5.1.9 Convection from screen to indoor air above screen

The convective heat transfer  $Q_{sc-as}$  from the screen to the indoor air above the screen is defined by

$$Q_{sc-as} = A_{sc} \cdot \alpha_{as-sc} \cdot (T_{sc} - T_{as}) \quad \{\text{W}\} \quad (3.61)$$

where  $A_{sc}$   $\{\text{m}^2\}$  is the surface area of the screen (eqn. 3.59) and  $T_{sc}$  and  $T_{as}$   $\{\text{K}\}$  are the temperatures of the screen and the indoor air above the screen.

The heat transfer coefficient  $\alpha_{as-sc}$  from the indoor air above the screen to the screen is described by (Stoffers, 1989)

$$\alpha_{as-sc} = Cl_{sc} \cdot 3 |T_{as} - T_{sc}|^{\frac{1}{3}} \quad \{\text{W m}^{-2} \text{K}^{-1}\} \quad (3.62)$$

where  $Cl_{sc} \in [0, 1]$  is the thermal screen closure.

### 3.5.1.10 Convection, heat exchange past the screen

The heat exchange  $Q_{a-as}$  between indoor air below the screen and indoor air above the screen is defined by

$$Q_{a-as} = \bar{\rho}_a \cdot c_{p-a} \cdot \Phi_{a-as} \cdot (T_a - T_{as}) \quad \{\text{W}\} \quad (3.63)$$

where  $\bar{\rho}_a$   $\{\text{kg m}^{-3}\}$  is the average density of air below and above the screen,  $c_{p-a}$   $\{\text{J kg}^{-1} \text{K}^{-1}\}$  is the specific heat capacity of air,  $\Phi_{a-as}$   $\{\text{m}^3 \text{s}^{-1}\}$  is the volume flow of air from below the screen to above the screen (eqn. 3.145) and  $T_a$  and  $T_{as}$   $\{\text{K}\}$  are the temperatures of the air below and above the screen.

### 3.5.1.11 Convection, heat exchange through ventilation

The heat exchange  $Q_{as-o}$  between indoor and outdoor air by natural ventilation is defined by

$$Q_{as-o} = (1 - op_{vhr} \cdot \eta_{vhr}) \cdot \rho_{as} \cdot c_{p-a} \cdot \Phi_{as-o} \cdot (T_{as} - T_o) \quad \{\text{W}\} \quad (3.64)$$

where  $\rho_{as}$   $\{\text{kg m}^{-3}\}$  is the density of air above the screen,  $c_{p-a}$   $\{\text{J kg}^{-1} \text{K}^{-1}\}$  is the specific heat capacity of air,  $\Phi_{as-o}$   $\{\text{m}^3 \text{s}^{-1}\}$  is the ventilation flow (eqn. 3.150) and  $T_{as}$  and  $T_o$   $\{\text{K}\}$  are the temperatures of the air above the screen and the outdoor air.

The option ventilation heat recovery  $op_{vhr} = 1$  indicates that ventilation with heat recovery is used. The option  $op_{vhr} = 0$  applies to normal ventilation. When ventilation with heat recovery is used, the outdoor air is preheated by the indoor greenhouse air with a heat exchanger. It is assumed that a fixed fraction of the sensible heat is recovered. The efficiency factor for the ventilation with heat recovery  $\eta_{vhr} = 0.9$ , which means that 90% of the sensible heat is recovered. Latent heat that is vented out is lost. Ventilation with heat recovery is used when the greenhouse is heated, otherwise normal ventilation is used

$$\begin{aligned} op_{vhr} &= 0 & \forall \quad vp_{hp} = 0 \ \& \ vp_l = 0 \\ op_{vhr} &= 1 & \forall \quad vp_{hp} > 0 \ \mid \ vp_l > 0 \end{aligned} \quad \{-\} \quad (3.65)$$

where  $vp_{hp} \in [0, 1]$  and  $vp_l \in [0, 1]$   $\{-\}$  are the valve positions of the heat pump and the lower net (boiler) (both control inputs).

### 3.5.2 Longwave radiation absorption

Radiation absorption is the heat transfer due to radiation between two materials. For longwave radiation absorption, the heat transfer  $Q_{A-B}$  from object  $A$  to object  $B$  is described by the equation (Stefan-Boltzmann)

$$Q_{A-B} = A_{A-B} \cdot E_A \cdot E_B \cdot F_{A-B} \cdot \sigma \cdot (T_A^4 - T_B^4) \quad \{W\} \quad (3.66)$$

where  $A_{A-B}$   $\{m^2\}$  is the surface area for heat transfer,  $E_A$  and  $E_B$   $\{-\}$  are the emission coefficients for  $A$  and  $B$ ,  $F_{A-B}$   $\{-\}$  is the view factor from  $A$  to  $B$ ,  $\sigma$   $\{W m^{-2} K^{-4}\}$  is the Stefan-Boltzmann constant and  $T_A$  and  $T_B$   $\{K\}$  are the temperatures of  $A$  and  $B$ . The view factors are derived in §3.A. The values of the emission coefficients can be found in appendix B.

#### 3.5.2.1 Longwave radiation absorption from lower net to canopy

The longwave radiation  $Q_{l-c}$  coming from the lower net and absorbed by the canopy is defined by

$$Q_{l-c} = A_l \cdot E_l \cdot E_c \cdot F_{l-c} \cdot \sigma \cdot (T_l^4 - T_c^4) \quad \{W\} \quad (3.67)$$

where  $A_l$   $\{m^2\}$  is the surface area of the lower net,  $E_l$  and  $E_c$   $\{-\}$  are the emission coefficients for the lower net and the canopy and  $T_l$  and  $T_c$   $\{K\}$  are the temperatures of the lower net and the canopy.

The view factor  $F_{l-c}$  from the lower net to the canopy is described by

$$F_{l-c} = 1 - F_{l-s} - F_{l-ri} - F_{l-sc} \quad \{-\} \quad (3.68)$$

where  $F_{l-s}$ ,  $F_{l-ri}$  and  $F_{l-sc}$   $\{-\}$  are the view factors from the lower net to the soil, the roof and the screen.

#### 3.5.2.2 Longwave radiation absorption from lower net to soil

The longwave radiation  $Q_{l-s}$  coming from the lower net and absorbed by the soil is defined by

$$Q_{l-s} = A_l \cdot E_l \cdot E_s \cdot F_{l-s} \cdot \sigma \cdot (T_l^4 - T_s^4) \quad \{W\} \quad (3.69)$$

where  $A_l$   $\{m^2\}$  is the surface area of the lower net,  $E_l$  and  $E_s$   $\{-\}$  are the emission coefficients for the lower net and the soil and  $T_l$  and  $T_s$   $\{K\}$  are the temperatures of the lower net and the soil.

The view factor  $F_{l-s}$  from the lower net to the soil is described by

$$F_{l-s} = 0.5 \quad \{-\} \quad (3.70)$$

### 3.5.2.3 Longwave radiation absorption from lower net to roof indoor side

The longwave radiation  $Q_{l_{ri}}$  coming from the lower net and absorbed by the roof is defined by

$$Q_{l_{ri}} = A_l \cdot E_l \cdot E_{ri} \cdot F_{l_{ri}} \cdot \sigma \cdot (T_l^4 - T_{ri}^4) \quad \{W\} \quad (3.71)$$

where  $A_l$   $\{m^2\}$  is the surface area of the lower net,  $E_l$  and  $E_{ri}$   $\{-\}$  are the emission coefficients for the lower net and the roof and  $T_l$  and  $T_{ri}$   $\{K\}$  are the temperatures of the lower net and the indoor side of the roof.

The view factor  $F_{l_{ri}}$  from the lower net to the indoor side of the roof is described by

$$F_{l_{ri}} = 0.5 (1 - Cl_{sc}) \cdot \tau_{c_{Il}} \quad \{-\} \quad (3.72)$$

where  $Cl_{sc} \in [0, 1]$  is the thermal screen closure and  $\tau_{c_{Il}}$   $\{-\}$  is the transmittance of longwave radiation by the canopy.

The transmittance of longwave radiation  $\tau_{c_{Il}}$  by the canopy is computed based on the extinction coefficient for longwave radiation by the canopy  $k_{c_{Il}}$   $\{-\}$  and the leaf area index  $LAI$   $\{m^2[leaf] m^{-2}[soil]\}$

$$\tau_{c_{Il}} = e^{-k_{c_{Il}} \cdot LAI} \quad \{-\} \quad (3.73)$$

### 3.5.2.4 Longwave radiation absorption from lower net to screen

The longwave radiation  $Q_{l_{sc}}$  coming from the lower net and absorbed by the screen is defined by

$$Q_{l_{sc}} = A_l \cdot E_l \cdot E_{sc} \cdot F_{l_{sc}} \cdot \sigma \cdot (T_l^4 - T_{sc}^4) \quad \{W\} \quad (3.74)$$

where  $A_l$   $\{m^2\}$  is the surface area of the lower net,  $E_l$  and  $E_{sc}$   $\{-\}$  are the emission coefficients for the lower net and the screen and  $T_l$  and  $T_{sc}$   $\{K\}$  are the temperatures of the lower net and the screen.

The view factor  $F_{l_{sc}}$  from the lower net to the screen is described by

$$F_{l_{sc}} = 0.5 Cl_{sc} \cdot \tau_{c_{Il}} \quad \{-\} \quad (3.75)$$

where  $Cl_{sc} \in [0, 1]$  is the thermal screen closure and  $\tau_{c_{Il}}$   $\{-\}$  (eqn. 3.73) is the transmittance of longwave radiation by the canopy.

### 3.5.2.5 Longwave radiation absorption from upper net to canopy

The longwave radiation  $Q_{u.c}$  coming from the upper net and absorbed by the canopy is defined by

$$Q_{u.c} = A_u \cdot E_u \cdot E_c \cdot F_{u.c} \cdot \sigma \cdot (T_u^4 - T_c^4) \quad \{W\} \quad (3.76)$$

where  $A_u$   $\{m^2\}$  is the surface area of the upper net,  $E_u$  and  $E_c$   $\{-\}$  are the emission coefficients for the upper net and the canopy and  $T_u$  and  $T_c$   $\{K\}$  are the temperatures of the upper net and the canopy.

The view factor  $F_{u.c}$  from the upper net to the canopy is described by

$$F_{u.c} = 1 - F_{u.ri} - F_{u.sc} - F_{u.s} \quad \{-\} \quad (3.77)$$

where  $F_{u.ri}$ ,  $F_{u.s}$  and  $F_{u.sc}$   $\{-\}$  are the view factors from the upper net to the roof, the screen and the soil.

### 3.5.2.6 Longwave radiation absorption from upper net to soil

The longwave radiation  $Q_{u.s}$  coming from the upper net and absorbed by the soil is defined by

$$Q_{u.s} = A_u \cdot E_u \cdot E_s \cdot F_{u.s} \cdot \sigma \cdot (T_u^4 - T_s^4) \quad \{W\} \quad (3.78)$$

where  $A_u$   $\{m^2\}$  is the surface area of the upper net,  $E_u$  and  $E_s$   $\{-\}$  are the emission coefficients for the upper net and the soil and  $T_u$  and  $T_s$   $\{K\}$  are the temperatures of the upper net and the soil.

The view factor  $F_{u.s}$  from the upper net to the soil is described by

$$F_{u.s} = 0.5 \tau_{c.ll} \quad \{-\} \quad (3.79)$$

where  $\tau_{c.ll}$   $\{-\}$  (eqn. 3.73) is the transmittance of longwave radiation by the canopy.

### 3.5.2.7 Longwave radiation absorption from upper net to roof indoor side

The longwave radiation  $Q_{u.ri}$  coming from the upper net and absorbed by the roof is defined by

$$Q_{u.ri} = A_u \cdot E_u \cdot E_{ri} \cdot F_{u.ri} \cdot \sigma \cdot (T_u^4 - T_{ri}^4) \quad \{W\} \quad (3.80)$$

where  $A_u$   $\{\text{m}^2\}$  is the surface area of the upper net,  $E_u$  and  $E_{ri}$   $\{-\}$  are the emission coefficients for the upper net and the roof and  $T_u$  and  $T_{ri}$   $\{\text{K}\}$  are the temperatures of the upper net and the indoor side of the roof.

The view factor  $F_{u,ri}$  from the upper net to the indoor side of the roof is described by

$$F_{u,ri} = 0.5 (1 - Cl_{sc}) \quad \{-\} \quad (3.81)$$

where  $Cl_{sc} \in [0, 1]$  is the thermal screen closure.

### 3.5.2.8 Longwave radiation absorption from upper net to screen

The longwave radiation  $Q_{u,sc}$  coming from the upper net and absorbed by the screen is defined by

$$Q_{u,sc} = A_u \cdot E_u \cdot E_{sc} \cdot F_{u,sc} \cdot \sigma \cdot (T_u^4 - T_{sc}^4) \quad \{\text{W}\} \quad (3.82)$$

where  $A_u$   $\{\text{m}^2\}$  is the surface area of the upper net,  $E_u$  and  $E_{sc}$   $\{-\}$  are the emission coefficients for the upper net and the screen and  $T_u$  and  $T_{sc}$   $\{\text{K}\}$  are the temperatures of the upper net and the screen.

The view factor  $F_{u,sc}$  from the upper net to the screen is described by

$$F_{u,sc} = 0.5 Cl_{sc} \quad \{-\} \quad (3.83)$$

where  $Cl_{sc} \in [0, 1]$  is the thermal screen closure.

### 3.5.2.9 Longwave radiation absorption from upper cooling net to canopy

The longwave radiation  $Q_{uc,c}$  coming from the upper cooling net and absorbed by the canopy is defined by

$$Q_{uc,c} = A_{uc} \cdot E_{uc} \cdot E_c \cdot F_{uc,c} \cdot \sigma \cdot (T_{uc}^4 - T_c^4) \quad \{\text{W}\} \quad (3.84)$$

where  $A_{uc}$   $\{\text{m}^2\}$  is the surface area of the upper cooling net,  $E_{uc}$  and  $E_c$   $\{-\}$  are the emission coefficients for the upper cooling net and the canopy and  $T_{uc}$  and  $T_c$   $\{\text{K}\}$  are the temperatures of the upper cooling net and the canopy.

The view factor  $F_{uc,c}$  from the upper cooling net to the canopy is described by

$$F_{uc,c} = 1 - F_{uc,ri} - F_{uc,sc} - F_{uc,s} \quad \{-\} \quad (3.85)$$

where  $F_{uc,ri}$ ,  $F_{uc,s}$  and  $F_{uc,sc}$   $\{-\}$  are the view factors from the upper cooling net to the roof, the soil and the screen.

### 3.5.2.10 Longwave radiation absorption from upper cooling net to soil

The longwave radiation  $Q_{uc.s}$  coming from the upper cooling net and absorbed by the soil is defined by

$$Q_{uc.s} = A_{uc} \cdot E_{uc} \cdot E_s \cdot F_{uc.s} \cdot \sigma \cdot (T_{uc}^4 - T_s^4) \quad \{W\} \quad (3.86)$$

where  $A_{uc}$   $\{m^2\}$  is the surface area of the upper cooling net,  $E_{uc}$  and  $E_s$   $\{-\}$  are the emission coefficients for the upper cooling net and the soil and  $T_{uc}$  and  $T_s$   $\{K\}$  are the temperatures of the upper cooling net and the soil.

The view factor  $F_{uc.s}$  from the upper cooling net to the soil is described by

$$F_{uc.s} = 0.5 \tau_{c.II} \quad \{-\} \quad (3.87)$$

### 3.5.2.11 Longwave radiation absorption from upper cooling net to roof indoor side

The longwave radiation  $Q_{uc.ri}$  coming from the upper cooling net and absorbed by the indoor side of the roof is defined by

$$Q_{uc.ri} = A_{uc} \cdot E_{uc} \cdot E_{ri} \cdot F_{uc.ri} \cdot \sigma \cdot (T_{uc}^4 - T_{ri}^4) \quad \{W\} \quad (3.88)$$

where  $A_{uc}$   $\{m^2\}$  is the surface area of the upper cooling net,  $E_{uc}$  and  $E_{ri}$   $\{-\}$  are the emission coefficients for the upper cooling net and the indoor side of the roof and  $T_{uc}$  and  $T_{ri}$   $\{K\}$  are the temperatures of the upper cooling net and the indoor side of the roof.

The view factor  $F_{uc.ri}$  from the upper cooling net to the indoor side of the roof is described by

$$F_{uc.ri} = 0.5 (1 - Cl_{sc}) \quad \{-\} \quad (3.89)$$

where  $Cl_{sc} \in [0, 1]$  is the thermal screen closure and  $\tau_{c.II}$   $\{-\}$  (eqn. 3.73) is the transmittance of longwave radiation by the canopy.

### 3.5.2.12 Longwave radiation absorption from upper cooling net to screen

The longwave radiation  $Q_{uc.sc}$  coming from the upper cooling net and absorbed by the screen is defined by

$$Q_{uc.sc} = A_{uc} \cdot E_{uc} \cdot E_{sc} \cdot F_{uc.sc} \cdot \sigma \cdot (T_{uc}^4 - T_{sc}^4) \quad \{W\} \quad (3.90)$$

where  $A_{uc}$   $\{\text{m}^2\}$  is the surface area of the upper cooling net,  $E_{uc}$  and  $E_{sc}$   $\{-\}$  are the emission coefficients for the upper cooling net and the screen and  $T_{uc}$  and  $T_{sc}$   $\{\text{K}\}$  are the temperatures of the upper cooling net and the screen.

The view factor  $F_{uc-sc}$  from the upper cooling net to the screen is described by

$$F_{uc-sc} = 0.5 Cl_{sc} \quad \{-\} \quad (3.91)$$

where  $Cl_{sc} \in [0, 1]$  is the thermal screen closure and  $\tau_{c-ll}$   $\{-\}$  (eqn. 3.73) is the transmittance of longwave radiation by the canopy.

### 3.5.2.13 Longwave radiation absorption from soil to canopy

The longwave radiation  $Q_{s-c}$  coming from the soil and absorbed by the canopy is defined by

$$Q_{s-c} = A_s \cdot E_s \cdot E_c \cdot F_{s-c} \cdot \sigma \cdot (T_s^4 - T_c^4) \quad \{\text{W}\} \quad (3.92)$$

where  $A_s$   $\{\text{m}^2\}$  is the surface area of the soil,  $E_s$  and  $E_c$   $\{-\}$  are the emission coefficients for the soil and the canopy and  $T_s$  and  $T_c$   $\{\text{K}\}$  are the temperatures of the soil and the canopy.

The view factor  $F_{s-c}$  from the soil to the canopy is described by

$$F_{s-c} = (1 - \tau_{c-ll}) \cdot (1 - F_{s-l}) \quad \{-\} \quad (3.93)$$

where  $\tau_{c-ll}$   $\{-\}$  (eqn. 3.73) is the transmittance of longwave radiation by the canopy and  $F_{s-l}$   $\{-\}$  is the view factors from the soil to the lower net.

### 3.5.2.14 Longwave radiation absorption from soil to roof indoor side

The longwave radiation  $Q_{s-ri}$  coming from the soil and absorbed by the roof is defined by

$$Q_{s-ri} = A_s \cdot E_s \cdot E_{ri} \cdot F_{s-ri} \cdot \sigma \cdot (T_s^4 - T_{ri}^4) \quad \{\text{W}\} \quad (3.94)$$

where  $A_s$   $\{\text{m}^2\}$  is the surface area of the soil,  $E_s$  and  $E_{ri}$   $\{-\}$  are the emission coefficients for the soil and the roof and  $T_s$  and  $T_{ri}$   $\{\text{K}\}$  are the temperatures of the soil and the indoor side of the roof.

The view factor  $F_{s-ri}$  from the soil to the indoor side of the roof is described by

$$F_{s-ri} = (1 - Cl_{sc}) \cdot (1 - F_{s-c} - F_{s-l} - F_{s-u} - F_{s-uc}) \quad \{-\} \quad (3.95)$$

where  $Cl_{sc} \in [0, 1]$  is the thermal screen closure and  $F_{s-c}$ ,  $F_{s-l}$ ,  $F_{s-u}$  and  $F_{s-uc}$   $\{-\}$  are the view factors from the soil to the canopy, the lower net, the upper net and the upper cooling net.

### 3.5.2.15 Longwave radiation absorption from soil to screen

The longwave radiation  $Q_{s-sc}$  coming from the soil and absorbed by the screen is defined by

$$Q_{s-sc} = A_s \cdot E_s \cdot E_{sc} \cdot F_{s-sc} \cdot \sigma \cdot (T_s^4 - T_{sc}^4) \quad \{W\} \quad (3.96)$$

where  $A_s$   $\{m^2\}$  is the surface area of the soil,  $E_s$  and  $E_{sc}$   $\{-\}$  are the emission coefficients for the soil and the screen and  $T_s$  and  $T_{sc}$   $\{K\}$  are the temperatures of the soil and the screen.

The view factor  $F_{s-sc}$  from the soil to the screen is described by

$$F_{s-sc} = Cl_{sc} \cdot (1 - F_{s-c} - F_{s-l} - F_{s-u} - F_{s-uc}) \quad \{-\} \quad (3.97)$$

where  $Cl_{sc} \in [0, 1]$  is the thermal screen closure and  $F_{s-c}$ ,  $F_{s-l}$ ,  $F_{s-u}$  and  $F_{s-uc}$   $\{-\}$  are the view factors from the soil to the canopy, the lower net, the upper net and the upper cooling net.

### 3.5.2.16 Longwave radiation absorption from roof indoor side to canopy

The longwave radiation  $Q_{ri-c}$  coming from the roof and absorbed by the canopy is defined by

$$Q_{ri-c} = A_r \cdot E_{ri} \cdot E_c \cdot F_{ri-c} \cdot \sigma \cdot (T_{ri}^4 - T_c^4) \quad \{W\} \quad (3.98)$$

where  $A_r$   $\{m^2\}$  is the surface area of the roof,  $E_{ri}$  and  $E_c$   $\{-\}$  are the emission coefficients for the roof and the canopy and  $T_{ri}$  and  $T_c$   $\{K\}$  are the temperatures of the indoor side of the roof and the canopy.

The view factor  $F_{ri-c}$  from the roof to the canopy is described by

$$F_{ri-c} = (1 - Cl_{sc}) \cdot (1 - \tau_{c-l}) \cdot \left( F_{ro-sk} - 0.5 \frac{A_u}{A_r} - 0.5 \frac{A_{uc}}{A_r} \right) \quad \{-\} \quad (3.99)$$

where  $Cl_{sc} \in [0, 1]$  is the thermal screen closure,  $\tau_{c-l}$   $\{-\}$  (eqn. 3.73) is the transmittance of longwave radiation by the canopy and  $F_{ro-sk}$ ,  $0.5 \frac{A_u}{A_r}$  and  $0.5 \frac{A_{uc}}{A_r}$   $\{-\}$  are the view factors from the roof to the sky, the upper net and the upper cooling net (without the correction for the screen).

### 3.5.2.17 Longwave radiation absorption from roof indoor side to roof outdoor side

The longwave radiation  $Q_{ri.roL}$  (for a double glass cover) coming from the indoor side of the roof and absorbed by the outdoor side of the roof is defined by

$$Q_{ri.roL} = A_r \cdot E_{ri} \cdot E_{ro} \cdot F_{ri.ro} \cdot \sigma \cdot (T_{ri}^4 - T_{ro}^4) \quad \{W\} \quad (3.100)$$

where  $A_r$   $\{m^2\}$  is the surface area of the roof,  $E_{ri}$  and  $E_{ro}$   $\{-\}$  are the emission coefficients for the indoor and the outdoor side of the roof and  $T_{ri}$  and  $T_{ro}$   $\{K\}$  are the temperatures of the indoor and the outdoor side of the roof.

The view factor  $F_{ri.ro}$  from the roof indoor to the outdoor side of the roof is described by

$$F_{ri.ro} = 1 \quad \{-\} \quad (3.101)$$

since the indoor and the outdoor side of the roof are parallel glass panes.

### 3.5.2.18 Longwave radiation absorption from roof outdoor side to sky

The longwave radiation  $Q_{ro.sk}$  coming from the outdoor side of the roof and absorbed by the sky is defined by

$$Q_{ro.sk} = A_r \cdot E_{ro} \cdot E_{sk} \cdot F_{ro.sk} \cdot \sigma \cdot (T_{ro}^4 - T_{sk}^4) \quad \{W\} \quad (3.102)$$

where  $A_r$   $\{m^2\}$  is the surface area of the roof,  $E_{ro}$  and  $E_{sk}$   $\{-\}$  are the emission coefficients for the roof and the sky and  $T_{ro}$  and  $T_{sk}$   $\{K\}$  are the temperatures of the outdoor side of the roof and the sky.

The view factor  $F_{ro.sk}$  from the outdoor side of the roof to the sky is described by

$$F_{ro.sk} = 1 \cdot \frac{A_s}{A_r} = \cos(\gamma) \quad \{-\} \quad (3.103)$$

where  $\gamma$   $\{rad\}$  is the angle of the roof with the horizontal plane.

### 3.5.2.19 Longwave radiation absorption from canopy to screen

The longwave radiation  $Q_{c.sc}$  coming from the canopy and absorbed by the screen is defined by

$$Q_{c.sc} = A_s \cdot E_c \cdot E_{sc} \cdot F_{c.sc} \cdot \sigma \cdot (T_c^4 - T_{sc}^4) \quad \{W\} \quad (3.104)$$

where  $A_s$   $\{\text{m}^2\}$  is the surface area of the soil,  $E_c$  and  $E_{sc}$   $\{-\}$  are the emission coefficients for the canopy and the screen and  $T_c$  and  $T_{sc}$   $\{\text{K}\}$  are the temperatures of the canopy and the screen.

The view factor  $F_{c-sc}$  from the canopy to the screen is described by

$$F_{c-sc} = Cl_{sc} \cdot (1 - \tau_{c-ll}) \cdot \left(1 - 0.5 \frac{A_u}{A_{sc}} - 0.5 \frac{A_{uc}}{A_{sc}}\right) \quad \{-\} \quad (3.105)$$

where  $Cl_{sc} \in [0, 1]$  is the thermal screen closure,  $\tau_{c-ll}$   $\{-\}$  (eqn. 3.73) is the transmittance of longwave radiation by the canopy and  $0.5 \frac{A_u}{A_{sc}}$  and  $0.5 \frac{A_{uc}}{A_{sc}}$   $\{-\}$  are the view factors from the screen to the upper net and the upper cooling net (without the correction for the screen).

### 3.5.2.20 Longwave radiation absorption from screen to roof indoor side

The longwave radiation  $Q_{sc-ri}$  coming from the screen and absorbed by the indoor side of the roof is defined by

$$Q_{sc-ri} = A_{sc} \cdot E_{sc} \cdot E_{ri} \cdot F_{sc-ri} \cdot \sigma \cdot (T_{sc}^4 - T_{ri}^4) \quad \{\text{W}\} \quad (3.106)$$

where  $A_{sc}$   $\{\text{m}^2\}$  is the surface area of the screen,  $E_{sc}$  and  $E_{ri}$   $\{-\}$  are the emission coefficients for the screen and the indoor side of the roof and  $T_{sc}$  and  $T_{ri}$   $\{\text{K}\}$  are the temperatures of the screen and the indoor side of the roof.

The view factor  $F_{sc-ri}$  from the screen to the indoor side of the roof is described by

$$F_{sc-ri} = Cl_{sc} \quad \{-\} \quad (3.107)$$

where  $Cl_{sc} \in [0, 1]$  is the thermal screen closure.

### 3.5.3 Shortwave radiation absorption

For shortwave radiation absorption, the heat  $Q_{rd-A}$  absorbed by object  $A$  is described by the equation

$$Q_{rd-A} = A_A \cdot \eta_{A-Is} \cdot I_o \quad \{\text{W}\} \quad (3.108)$$

where  $A_A$   $\{\text{m}^2\}$  is the surface area for heat transfer,  $\eta_{A-Is}$   $\{-\}$  is the shortwave radiation absorption coefficient for  $A$  and  $I_o$   $\{\text{W m}^{-2}\}$  is the outdoor shortwave solar radiation. The transmitted shortwave solar radiation depends on the position of the object  $A$  in the greenhouse. Also corrections are made for the transmittance of shortwave radiation by the roof  $\tau_{r-Is}$  and by the screen  $\tau_{sc-Is}$   $\{-\}$ .

The transmittance  $\tau_{r\_Is}$  of shortwave radiation by the roof  $\{-\}$  is given by

$$\tau_{r\_Is} = f_{dif} \cdot \tau_{difR} + (1 - f_{dif}) \cdot \tau_{dirR} \quad \{-\} \quad (3.109)$$

with transmittance of diffuse radiation by the roof  $\tau_{difR} = 0.78$ , where  $\tau_{dirR}$   $\{-\}$  is the transmittance of direct radiation by the roof and  $f_{dif}$   $\{-\}$  is the fraction diffuse radiation in shortwave radiation (see §2.B).

The transmittance  $\tau_{sc\_Is}$  of shortwave radiation by the screen  $\{-\}$  is given by

$$\tau_{sc\_Is} = (1 - Cl_{sc}) + \tau_{sc\_Is0} \cdot Cl_{sc} \quad \{-\} \quad (3.110)$$

in which the transmittance of the fully closed screen  $\tau_{sc\_Is0} = 0.8$ . This gives the transmittance  $\tau_{sc\_Is} = 0.8$  if the screen is fully closed ( $Cl_{sc} = 1$ ) and  $\tau_{sc\_Is} = 1$  if the screen is fully opened ( $Cl_{sc} = 0$ ).

The shortwave radiation absorption coefficient  $\eta_{A\_Is}$  for  $A$  describes the part of the shortwave radiation that is absorbed by object  $A$ . In general there is a term for the fraction going past the screen and a term correcting for reflection

$$\eta_{A\_Is} = 1 - \beta_{A\_Is} - \tau_{A\_Is} \quad \{-\} \quad (3.111)$$

where  $\beta_{A\_Is}$   $\{-\}$  is the shortwave radiation coefficient for reflection by the object  $A$ . It is assumed that all shortwave radiation not reflected or transmitted by the object  $A$  is absorbed.

### 3.5.3.1 Shortwave radiation absorption by roof indoor and outdoor side

The shortwave radiation  $Q_{rd\_ri}$  and  $Q_{rd\_ro}$  absorbed by the indoor side and the outdoor side of the roof are defined by

$$Q_{rd\_ri} = A_r \cdot \eta_{ri\_Is} \cdot I_o \quad \{W\} \quad (3.112)$$

$$Q_{rd\_ro} = A_r \cdot \eta_{ro\_Is} \cdot I_o \quad \{W\} \quad (3.113)$$

where  $A_r$   $\{m^2\}$  is the surface area of the roof,  $\eta_{ri\_Is}$  and  $\eta_{ro\_Is}$   $\{-\}$  are the absorption coefficients for shortwave radiation by the roof indoor and outdoor side and  $I_o$   $\{W m^{-2}\}$  is the outdoor shortwave solar radiation.

The absorption coefficients  $\eta_{ri\_Is}$  and  $\eta_{ro\_Is}$  for shortwave radiation by the roof indoor and outdoor side are defined by

$$\eta_{ri\_Is} = 0.02 \sqrt{\tau_{r\_Is}} \quad \{-\} \quad (3.114)$$

$$\eta_{ro\_Is} = 0.02 \quad \{-\} \quad (3.115)$$

The transmittance  $\sqrt{\tau_{r\_Is}}$  is used since it is a single layer of glass, while  $\tau_{r\_Is}$  holds for a double glass cover. If the roof has a single glass cover,  $\eta_{ro\_Is} = 0$ .

### 3.5.3.2 Shortwave radiation absorption by screen

The shortwave radiation  $Q_{rd.sc}$  absorbed by the screen is defined by

$$Q_{rd.sc} = A_{sc} \cdot \eta_{sc.Is} \cdot I_o \quad \{W\} \quad (3.116)$$

where  $A_{sc} \{m^2\}$  is the surface area of the screen and  $\eta_{sc.Is} \{-\}$  is the absorption coefficient for shortwave radiation by the screen.

The absorption coefficient  $\eta_{sc.Is}$  for shortwave radiation by the screen is defined by

$$\eta_{sc.Is} = \tau_{r.Is} \cdot Cl_{sc} \cdot (1 - \beta_{sc.Is} - \tau_{sc.Is0}) \quad \{-\} \quad (3.117)$$

where  $Cl_{sc} \in [0, 1]$  is the thermal screen closure and  $\beta_{sc.Is} \{-\}$  is the shortwave radiation coefficient for reflection by the screen.

### 3.5.3.3 Shortwave radiation absorption by upper net

The shortwave radiation  $Q_{rd.u}$  absorbed by the upper net is defined by

$$Q_{rd.u} = A_u \cdot \eta_{u.Is} \cdot I_o \quad \{W\} \quad (3.118)$$

where  $A_u \{m^2\}$  is the surface area of the upper net and  $\eta_{u.Is} \{-\}$  is the absorption coefficient for shortwave radiation by the upper net.

The absorption coefficient  $\eta_{u.Is}$  for shortwave radiation by the upper net is defined by

$$\eta_{u.Is} = \tau_{r.Is} \cdot \tau_{sc.Is} \cdot 0.5 (1 - \beta_{u.Is}) \quad \{-\} \quad (3.119)$$

where  $\beta_{u.Is} \{-\}$  is the shortwave radiation coefficient for reflection by the upper net and 0.5 indicates that only half the pipe surface is seen by the shortwave radiation.

### 3.5.3.4 Shortwave radiation absorption by upper cooling net

The shortwave radiation  $Q_{rd.uc}$  absorbed by the upper cooling net is defined by

$$Q_{rd.uc} = A_{uc} \cdot \eta_{uc.Is} \cdot I_o \quad \{W\} \quad (3.120)$$

where  $A_{uc} \{m^2\}$  is the surface area of the upper cooling net and  $\eta_{uc.Is} \{-\}$  is the absorption coefficient for shortwave radiation by the upper cooling net.

The absorption coefficient  $\eta_{uc.Is}$  for shortwave radiation by the upper cooling net is equal to absorption coefficient for shortwave radiation by the upper net

$$\eta_{uc.Is} = \eta_{u.Is} \quad \{-\} \quad (3.121)$$

### 3.5.3.5 Shortwave radiation absorption by lower net

The shortwave radiation  $Q_{rd,l}$  absorbed by the lower net is defined by

$$Q_{rd,l} = A_l \cdot \eta_{l,Is} \cdot I_o \quad \{W\} \quad (3.122)$$

where  $A_l \{m^2\}$  is the surface area of the lower net and  $\eta_{l,Is} \{-\}$  is the absorption coefficient for shortwave radiation by the lower net.

The absorption coefficient  $\eta_{l,Is}$  for shortwave radiation by the lower net is defined by

$$\eta_{l,Is} = \tau_{r,Is} \cdot \tau_{sc,Is} \cdot (\tau_{c,Il} + (1 - \tau_{c,Il}) \cdot \tau_{c,Is}) \cdot 0.5 (1 - \beta_{l,Is}) \quad \{-\} \quad (3.123)$$

where  $\beta_{l,Is} \{-\}$  is the shortwave radiation coefficient for reflection by the lower net,  $\tau_{c,Is} \{-\}$  is the transmittance of shortwave radiation by the canopy,  $\tau_{c,Il} \{-\}$  (eqn. 3.73) is the transmittance of longwave radiation by the canopy and 0.5 indicates that only half the pipe surface is seen by the shortwave radiation. The term  $\tau_{c,Il} + (1 - \tau_{c,Il})$  is used for the total transmittance of the canopy for radiation.

### 3.5.3.6 Shortwave radiation absorption by canopy

The shortwave radiation  $Q_{rd,c}$  absorbed by the canopy is defined by (Stanghellini, 1987)

$$Q_{rd,c} = A_s \cdot \eta_{c,Is} \cdot I_o \quad \{W\} \quad (3.124)$$

where  $A_s \{m^2\}$  is the surface area of the soil and  $\eta_{c,Is} \{-\}$  is the absorption coefficient for shortwave radiation by the canopy. *Note:* the surface area  $A_s$  of the soil is used, not the surface area  $A_c$  of the crop. This is due to the definition of the absorption coefficient  $\eta_{c,Is}$  by Stanghellini.

The absorption coefficient  $\eta_{c,Is}$  for shortwave radiation by the canopy is given by Stanghellini (1987) as

$$\eta_{c,Is} = \tau_{r,Is} \cdot \tau_{sc,Is} \cdot (1 + \tau_{c,Is} \cdot \beta_{s,Is}) \cdot (1 - \tau_{c,Is} - \beta_{c,Is}) \quad \{-\} \quad (3.125)$$

where  $\beta_{c,Is} \{-\}$  is the shortwave radiation coefficient for reflection by the canopy,  $\tau_{c,Is} \{-\}$  is the transmittance of shortwave radiation by the canopy and  $\beta_{s,Is} \{-\}$  is the shortwave radiation coefficient for reflection by the soil. The term  $\tau_{c,Is} \cdot \beta_{s,Is}$  corrects for the reflection by the soil.

The reflection coefficient  $\beta_{c,Is}$  for shortwave radiation by the canopy is given by Stanghellini (1987) as

$$\beta_{c,Is} = (1 - \tau_{c,Il}) \cdot \beta_{c,Is\infty} \quad \{-\} \quad (3.126)$$

where  $\beta_{c-Is\infty} \{-\}$  is the shortwave radiation coefficient for reflection by the canopy for a dense stand and  $\tau_{c-Il} \{-\}$  (eqn. 3.73) is the transmittance of longwave radiation by the canopy, which is used here as a measure for the permeability of the canopy.

The transmittance  $\tau_{c-Is}$  of shortwave radiation by the canopy is computed based on the extinction coefficient  $k_{c-Is} \{-\}$  for shortwave radiation by the canopy and the leaf area index  $LAI \{m^2[leaf] m^{-2}[soil]\}$

$$\tau_{c-Is} = e^{-k_{c-Is} \cdot LAI} \quad \{-\} \quad (3.127)$$

### 3.5.3.7 Shortwave radiation absorption by soil

The shortwave radiation  $Q_{rd-s}$  absorbed by the soil is defined by

$$Q_{rd-s} = A_s \cdot \eta_{s-Is} \cdot I_o \quad \{W\} \quad (3.128)$$

where  $A_s \{m^2\}$  is the surface area of the soil and  $\eta_{s-Is} \{-\}$  is the absorption coefficient for shortwave radiation by the soil.

The absorption coefficient  $\eta_{s-Is}$  for shortwave radiation by the soil is defined by

$$\eta_{s-Is} = \tau_{r-Is} \cdot \tau_{sc-Is} \cdot (\tau_{c-Il} + (1 - \tau_{c-Il}) \cdot \tau_{c-Is}) \cdot (1 - \beta_{s-Is}) \quad \{-\} \quad (3.129)$$

where  $\beta_{s-Is} \{-\}$  is the shortwave radiation coefficient for reflection by the soil (white foil),  $\tau_{c-Is} \{-\}$  is the transmittance of shortwave radiation by the canopy and  $\tau_{c-Il} \{-\}$  (eqn. 3.73) is the transmittance of longwave radiation by the canopy. The term  $\tau_{c-Il} + (1 - \tau_{c-Il})$  is used for the total transmittance of the canopy for radiation.

### 3.5.4 Conduction

For conduction, the heat transfer  $Q_{A-B}$  between the locations  $A$  and  $B$  in a homogeneous medium is described by the equation

$$Q_{A-B} = A_{A-B} \cdot \frac{\lambda}{d} \cdot (T_A - T_B) \quad \{W\} \quad (3.130)$$

where  $A_{A-B} \{m^2\}$  is the surface area for heat transfer,  $\lambda \{W m^{-1} K^{-1}\}$  is the thermal conductivity of the homogeneous medium,  $d \{m\}$  is the distance between the locations  $A$  and  $B$  and  $T_A$  and  $T_B \{K\}$  are the temperatures of  $A$  and  $B$ .

#### 3.5.4.1 Conduction from upper to lower soil layer

The conductive heat transfer  $Q_{s-s2}$  from the upper to the lower soil layer is given by

$$Q_{s-s2} = A_s \cdot \frac{\lambda_s}{dx_s} \cdot (T_s - T_{s2}) \quad \{\text{W}\} \quad (3.131)$$

where  $A_s$   $\{\text{m}^2\}$  is the surface area of the soil,  $\lambda_s$   $\{\text{W m}^{-1} \text{K}^{-1}\}$  is the thermal conductivity of the soil,  $dx_s$   $\{\text{m}\}$  is the distance between the centers of the upper soil layer and the subsoil layer and  $T_s$  and  $T_{s2}$   $\{\text{K}\}$  are the temperatures of the soil and the subsoil layer.

The temperature  $T_{s2}$  of the subsoil layer is a function of the day number  $day_{NR}$  [1,365].

$$T_{s2} = T_0 + 15 + 2.5 \sin(1.72 \cdot 10^{-2} (day_{NR} - 140)) \quad \{\text{K}\} \quad (3.132)$$

Instead of 6 soil layers (de Zwart, 1996), only one layer is used. This defines the values for the distance  $dx_s$  in eqn. 3.131, and the distance  $d_s$  that defines the volume  $V_s$  in eqn. 3.8. These values are derived in §3.C from the model by De Zwart (1996).

#### 3.5.4.2 Conduction from indoor to outdoor side roof

The conductive heat transfer  $Q_{ri-ro}$  (for a double glass cover) from the roof indoor to the outdoor side of the roof is given by

$$Q_{ri-ro} = A_r \cdot \frac{\lambda_a}{d_{ra}} \cdot (T_{ri} - T_{ro}) \quad \{\text{W}\} \quad (3.133)$$

where  $A_r$   $\{\text{m}^2\}$  is the surface area of the roof,  $\lambda_a$   $\{\text{W m}^{-1} \text{K}^{-1}\}$  is the thermal conductivity of the air,  $d_{ra}$   $\{\text{m}\}$  is the distance between the inner and outer roof cover and  $T_{ri}$  and  $T_{ro}$   $\{\text{K}\}$  are the temperatures of the roof indoor and outdoor side.

#### 3.5.5 Latent heat exchange

Latent heat exchange is due to a change in the level of ‘free’ energy of water. It is not directly sensed as an increase or decrease in temperature. As the surrounding environment loses heat, water condensates, and it changes from a higher to a lower state of ‘free’ energy, whereby latent heat is released to the environment. As the surrounding environment is heated, water evaporates,

and it changes from a lower to a higher state of ‘free’ energy, whereby latent heat is absorbed from the environment.

#### 3.5.5.1 Latent heat exchange through condensation of water on roof

The latent heat transfer  $Q_{as\_ri\_H2O}$  from indoor air above the screen to the indoor side of the roof due to condensation of water on the roof is defined by

$$Q_{as\_ri\_H2O} = r_w \cdot \Phi_{m\_as\_ri\_H2O} \quad \{W\} \quad (3.134)$$

where  $r_w \{J\,kg^{-1}\}$  is the heat of evaporation of water and  $\Phi_{m\_as\_ri\_H2O} \{kg\,s^{-1}\}$  (eqn. 3.27) is the mass flow rate of water vapour from the indoor air above the screen to the indoor side of the roof due to condensation.

#### 3.5.5.2 Latent heat exchange through condensation of water on upper cooling net

The latent heat transfer  $Q_{a\_uc\_H2O}$  from indoor air below the screen to the upper cooling net due to condensation of water on the upper cooling net pipes is defined by

$$Q_{a\_uc\_H2O} = r_w \cdot \Phi_{m\_a\_uc\_H2O} \quad \{W\} \quad (3.135)$$

where  $r_w \{J\,kg^{-1}\}$  is the heat of evaporation of water and  $\Phi_{m\_a\_uc\_H2O} \{kg\,s^{-1}\}$  is the mass flow rate of water vapour from the indoor air below the screen to the upper cooling net due to condensation (eqn. 3.29).

#### 3.5.5.3 Latent heat exchange through condensation of water on screen

The latent heat transfers  $Q_{a\_sc\_H2O}$  and  $Q_{as\_sc\_H2O}$  from the indoor air below and above the screen to the screen due to condensation of water on the screen material are defined by

$$Q_{a\_sc\_H2O} = r_w \cdot \Phi_{m\_a\_sc\_H2O} \quad \{W\} \quad (3.136)$$

$$Q_{as\_sc\_H2O} = r_w \cdot \Phi_{m\_as\_sc\_H2O} \quad \{W\} \quad (3.137)$$

where  $r_w \{J\,kg^{-1}\}$  is the heat of evaporation of water and  $\Phi_{m\_a\_sc\_H2O}$  and  $\Phi_{m\_as\_sc\_H2O} \{kg\,s^{-1}\}$  are the mass flow rates of water vapour from the indoor air below and above the screen to the screen due to condensation (eqns. 3.31 and 3.32).

#### 3.5.5.4 Latent heat exchange through canopy transpiration

The latent heat transfer  $Q_{c.a.H_2O}$  from the canopy to the indoor air due to canopy transpiration is defined by

$$Q_{c.a.H_2O} = r_w \cdot \Phi_{m.c.a.H_2O} \quad \{\text{W}\} \quad (3.138)$$

where  $r_w$   $\{\text{J kg}^{-1}\}$  is the heat of evaporation of water and  $\Phi_{m.c.a.H_2O}$   $\{\text{kg}[\text{H}_2\text{O}]\text{s}^{-1}\}$  is the mass flow rate of water vapour from the canopy to the indoor air due to transpiration (see §2.2).

### 3.6 Modelling the screen

A thermal screen is used to decrease heat loss during cold periods with little solar radiation. Screen operation should therefore depend on the outdoor shortwave solar radiation  $I_o$  and the temperature of the outdoor air  $T_o$ . The screen closure  $Cl_{sc} \in [0, 1]$  is a control variable. It is however not optimized in the optimal control since the ‘rules’ for the control are quite straightforward, and the screen is opened and closed in about 3 min, which is much smaller than the time interval  $t_{s.u}$  for the computed control inputs of 30 min. The rules used here are similar to those used in commercial greenhouse horticulture. The screen is either open or closed. Furthermore the optimal control of the screen might lead to strange behaviour, e.g., the screen could be closed for 30 min during daytime to increase temperature and then cooled with the heat exchanger to retrieve heat. This is not the way the screen should be operated (or at least current screens are not designed to be opened and closed 20 times a day). The rules for the screen closure are described in §3.6.1.

It is assumed that the screen is impermeable for all gasses ( $\text{H}_2\text{O}$ ,  $\text{CO}_2$  and air). The exchange of heat,  $\text{CO}_2$  and  $\text{H}_2\text{O}$  through the screen opening can be described by a simple air exchange rate. This is described in §3.6.2. This air exchange causes the exchange of carbondioxide, water vapour and heat. These are described in §3.3.4, §3.4.4 and §3.5.1.10.

It is assumed that the screen can be opened or closed within a time interval of 10 min. If the screen is closed, the temperature,  $\text{CO}_2$  and  $\text{H}_2\text{O}$  concentration are not the same above and below the screen. Therefore separate state variables are used to describe these temperatures and concentrations above and below the screen (see §3.2.3). When the screen is open, it is assumed that the temperature and concentration  $\text{CO}_2$  and  $\text{H}_2\text{O}$  can be averaged (proportional to the heat capacity and volume of the air above and below the screen). This

is necessary to avoid numerical problems in the integration. The equations for the averaging of these states are given in §3.6.3.

If the screen is closed, only part of the solar radiation is transmitted through the screen. The transmittance  $\tau_{sc,Is}$   $\{-\}$  of shortwave radiation by the screen is given in eqn. 3.110.

### 3.6.1 Screen closure

The screen closure  $Cl_{sc}$   $\{0,1\}$  is defined by

$$Cl_{sc} = 0.97 c_{sc} \quad \{-\} \quad (3.139)$$

where  $c_{sc} \in \{0,1\}$  is the screen condition. When the screen is closed, a 3% crack opening is kept to carry off moisture, which gives a value of  $Cl_{sc} = 0.97$ . This is the equation used in the optimal control. Since the screen condition  $c_{sc} \in \{0,1\}$  is either 0 or 1, it means that the screen closure is either 0 or 0.97. In the simulation with data (e.g., model validation) the screen closure  $Cl_{sc}$  is an input, so it can take any value.

The screen is either opened or closed. This is indicated by the screen condition  $c_{sc} \in \{0,1\}$ . The screen is opened if  $c_{sc} = 0$  and closed if  $c_{sc} = 1$ . The screen condition depends only on the external inputs  $v$ . It is determined based on the outdoor shortwave solar radiation  $I_o$  and the temperature of the outdoor air  $T_o$ . The screen condition  $c_{sc}$  is a logical (boolean) combination of the screen conditions for radiation  $c_{sc,I}$  and for temperature  $c_{sc,T}$ .

$$c_{sc} = c_{sc,I} \ \& \ c_{sc,T} \quad \{-\} \quad (3.140)$$

which means that both conditions must be 1 for the screen to close.

The screen condition  $c_{sc,I}$  for radiation is switched if the outdoor shortwave solar radiation  $I_o$   $\{\text{W m}^{-2}[\text{soil}]\}$  is between  $I_{o,low}$  and  $I_{o,high}$

$$c_{sc,I} = \begin{cases} 0 & \text{if } c_{sc,I0} = 1 \ \& \ I_o \geq I_{o,high} \\ 1 & \text{if } c_{sc,I0} = 0 \ \& \ I_o \leq I_{o,low} \\ c_{sc,I0} & \text{if } (c_{sc,I0} = 0 \ \& \ I_o > I_{o,low}) \mid (c_{sc,I0} = 1 \ \& \ I_o < I_{o,high}) \end{cases} \quad \{-\} \quad (3.141)$$

in which  $I_{o,low} = I_{o,scr} - \Delta I_{o,scr}$  and  $I_{o,high} = I_{o,scr} + \Delta I_{o,scr}$   $\{\text{W m}^{-2}[\text{soil}]\}$ , where  $c_{sc,I0}$  is the previous screen condition for radiation. The screen condition parameters for radiation are given by:  $I_{o,scr} = 40 \text{ W m}^{-2}[\text{soil}]$ ,  $\Delta I_{o,scr} = 20 \text{ W m}^{-2}[\text{soil}]$ .

The term  $\Delta I_{o\_scr}$  is used to create a zone where the screen condition  $c_{sc\_I}$  does not change. This is done to prevent the screen from opening and closing more than once, reacting to small variations in the radiation.

Eqn. 3.141 indicates that the screen condition for radiation is switched:

- from closed to open if the radiation rises above the high level
- from open to closed if the radiation drops below the low level

The previous screen condition  $c_{sc\_I0}$  for radiation is initialized at  $t = 0$  with

$$c_{sc\_I0} = \begin{cases} 0 & \text{if } I_o > I_{o\_low} \\ 1 & \text{if } I_o \leq I_{o\_low} \end{cases} \quad \{-\} \quad (3.142)$$

The screen condition  $c_{sc\_T}$  for temperature is switched if the temperature of the outdoor air  $T_o$  {K} is between  $T_{o\_low}$  and  $T_{o\_high}$

$$c_{sc\_T} = \begin{cases} 0 & \text{if } c_{sc\_T0} = 1 \text{ \& } T_o \geq T_{o\_high} \\ 1 & \text{if } c_{sc\_T0} = 0 \text{ \& } T_o \leq T_{o\_low} \\ c_{sc\_T0} & \text{if } (c_{sc\_T0} = 0 \text{ \& } T_o > T_{o\_low}) \mid (c_{sc\_T0} = 1 \text{ \& } T_o < T_{o\_high}) \end{cases} \quad \{-\} \quad (3.143)$$

in which  $T_{o\_low} = T_{o\_scr} - \Delta T_{o\_scr}$  and  $T_{o\_high} = T_{o\_scr} + \Delta T_{o\_scr}$  {K}, where  $c_{sc\_T0}$  is the previous screen condition for temperature and  $T_0 = 273.15$  K. The screen condition parameters for temperature are given by:  $T_{o\_scr} = T_0 + 10$  K and  $\Delta T_{o\_scr} = 2$  K.

The term  $\Delta T_{o\_scr}$  is used to create a zone where the screen condition  $c_{sc\_T}$  does not change. This is done to prevent the screen from opening and closing more than once, reacting to small variations in the temperature.

Eqn. 3.143 indicates that the screen condition for temperature is switched:

- from closed to open if the temperature rises above the high level
- from open to closed if the temperature drops below the low level

The previous screen condition  $c_{sc\_T0}$  for temperature is initialized at  $t = 0$  with

$$c_{sc\_T0} = \begin{cases} 0 & \text{if } T_o > T_{o\_low} \\ 1 & \text{if } T_o \leq T_{o\_low} \end{cases} \quad \{-\} \quad (3.144)$$

### 3.6.2 Volume flow air past the screen

The convective air exchange through the screen material and along the crack opening is caused by the temperature difference and the pressure difference above and below the screen. A physical model of the air exchange exists (de Zwart, 1996) that describes the air exchange rate past the screen as a function of the temperature difference and the pressure difference below and above the screen.

In the simulation these equations give numerical problems due to the fast dynamics of this air exchange. It is therefore described by a simplified equation, in which it is assumed that the air exchange speed between the air below and above the screen (past the screen) is constant. It is assumed that the screen is impermeable for all gasses ( $\text{H}_2\text{O}$ ,  $\text{CO}_2$  and air), so there is no exchange through the screen material.

The volume flow  $\Phi_{a.as}$  of air from below the screen to above the screen is given by

$$\Phi_{a.as} = v_{a.as} \cdot A_{sc} \cdot (1 - Cl_{sc}) \quad \{\text{m}^3 \text{s}^{-1}\} \quad (3.145)$$

in which the air exchange rate  $v_{a.as}$  between the air below and above the screen is given by

$$v_{a.as} = 0.05 \quad \{\text{m s}^{-1}\} \quad (3.146)$$

where  $A_{sc} \{\text{m}^2\}$  is the surface area of the screen and  $Cl_{sc} \in [0, 1]$  is the thermal screen closure.

### 3.6.3 Temperatures and concentration $\text{CO}_2$ and $\text{H}_2\text{O}$ when the screen is open

The differential equations for temperature and concentration  $\text{CO}_2$  and  $\text{H}_2\text{O}$  are different if the screen is opened or closed (see §3.2.3). It is assumed in the control that the screen can be opened or closed within a time interval of 10 min. In the control it is changed from open to closed within one sampling interval of the controller  $t_s = 30$  min. This means that if the screen is opened, a very rapid exchange of heat,  $\text{CO}_2$  and  $\text{H}_2\text{O}$  occurs. These exchanges cause the system to become very stiff, which leads to numerical integration problems (large derivatives, small step size for integration). This is avoided by averaging the temperatures and concentrations above and below the screen when the screen is opened. To average, in the temperature the heat capacity  $\rho \cdot c_p \cdot V$  is

used, and in the concentrations the volume  $V$  is used. This gives, if  $c_{sc} = 0$  (screen is opened)

$$\left. \begin{matrix} T_a^+ \\ T_{as}^+ \end{matrix} \right\} = \frac{T_a^- \cdot \rho_a \cdot c_{p,a} \cdot V_a + T_{as}^- \cdot \rho_{as} \cdot c_{p,a} \cdot V_{as}}{\rho_a \cdot c_{p,a} \cdot V_a + \rho_{as} \cdot c_{p,a} \cdot V_{as}} \quad \{\text{K}\} \quad (3.147)$$

$$\left. \begin{matrix} C_{a,CO_2}^+ \\ C_{as,CO_2}^+ \end{matrix} \right\} = \frac{C_{a,CO_2}^- \cdot V_a + C_{as,CO_2}^- \cdot V_{as}}{V_a + V_{as}} \quad \{\text{kg}[\text{CO}_2] \text{ m}^{-3}\} \quad (3.148)$$

$$\left. \begin{matrix} C_{a,H_2O}^+ \\ C_{as,H_2O}^+ \end{matrix} \right\} = \frac{C_{a,H_2O}^- \cdot V_a + C_{as,H_2O}^- \cdot V_{as}}{V_a + V_{as}} \quad \{\text{kg}[\text{H}_2\text{O}] \text{ m}^{-3}\} \quad (3.149)$$

where the terms with superscript ‘ $-$ ’ denote the previous values, before the screen was opened and the terms with superscript ‘ $+$ ’ denote the new values, after the screen has opened. These computations are based on steady state assumptions: before the screen is opened, the temperatures,  $\text{CO}_2$  and  $\text{H}_2\text{O}$  concentrations above and below the screen are different, after the screen is opened they are equal.

### 3.7 Modelling ventilation

Greenhouse ventilation is performed through the opening of windows. Furthermore there is always a certain amount of ventilation due to leakage. The air exchange through the windows is caused by the temperature difference between the indoor and outdoor air and by the outdoor wind speed. The equations given in this paragraph are taken from the thesis of De Jong (1990).

Ventilation causes the exchange of carbondioxide, water vapour exchange and heat. These are described in §3.3.3, §3.4.3 and §3.5.1.11.

#### 3.7.1 Volume flow air through windows and leak

The ventilation flow  $\Phi_{as,o}$  is the sum of the ventilation through the windows and the ventilation due to leakage

$$\Phi_{as,o} = \Phi_{leak} + \Phi_{win} \quad \{\text{m}^3 \text{ s}^{-1}\} \quad (3.150)$$

where  $\Phi_{leak} \{\text{m}^3 \text{ s}^{-1}\}$  is the ventilation due to leakage of the greenhouse construction and  $\Phi_{win} \{\text{m}^3 \text{ s}^{-1}\}$  is the ventilation through the windows.

The ventilation flow  $\Phi_{leak}$  due to leakage of the greenhouse construction is described by

$$\Phi_{leak} = A_s \cdot (8.3 \cdot 10^{-5} + 3.5 \cdot 10^{-5} v_o \cdot f_a) \quad \{\text{m}^3 \text{ s}^{-1}\} \quad (3.151)$$

where  $A_s$   $\{\text{m}^2\}$  is the surface area of the soil,  $v_o$   $\{\text{m s}^{-1}\}$  is the outdoor wind speed and  $f_a$   $\{-\}$  is the infiltration factor.

The ventilation flow  $\Phi_{win}$  through the windows is described by

$$\Phi_{win} = \sqrt{\Phi_{wind}^2 + (\Phi_{\Delta T_{lsd}} + \Phi_{\Delta T_{wsd}})^2} \quad \{\text{m}^3 \text{s}^{-1}\} \quad (3.152)$$

where  $\Phi_{wind}$   $\{\text{m}^3 \text{s}^{-1}\}$  is the wind induced component, and  $\Phi_{\Delta T_{lsd}}$   $\{\text{m}^3 \text{s}^{-1}\}$  and  $\Phi_{\Delta T_{wsd}}$   $\{\text{m}^3 \text{s}^{-1}\}$  are the components determined by the temperature difference between indoor and outdoor air, subdivided into lee- and windward-side.

The wind-induced component  $\Phi_{wind}$  is described by

$$\Phi_{wind} = n_{win} \cdot (f_{lsd} + f_{wsd}) \cdot v_o \cdot L_1 \cdot L_2 \quad \{\text{m}^3 \text{s}^{-1}\} \quad (3.153)$$

where  $f_{lsd}$  and  $f_{wsd}$   $\{-\}$  are the ventilation functions for the lee- and the windward-side,  $L_1$  and  $L_2$   $\{\text{m}\}$  are the length and the width of the window and  $n_{win}$   $\{-\}$  is the total number of windows per side of the greenhouse span.

The ventilation functions  $f_{lsd}$  and  $f_{wsd}$  for the lee- and the windward-side are defined by

$$f_{lsd} = c_{lsd3} \cdot Ap_{lsd}^3 - c_{lsd2} \cdot Ap_{lsd}^2 + c_{lsd1} \cdot Ap_{lsd} + c_{lsd0} \quad \{-\} \quad (3.154)$$

$$f_{wsd} = c_{wsd3} \cdot Ap_{wsd}^3 - c_{wsd2} \cdot Ap_{wsd}^2 + c_{wsd1} \cdot Ap_{wsd} + c_{wsd0} \quad \{-\} \quad (3.155)$$

where  $c_{lsd0}$  to  $c_{lsd3}$  and  $c_{wsd0}$  to  $c_{wsd3}$   $\{-\}$  are ventilation function coefficients for the lee- and the windward-side and  $Ap_{lsd} \in [0, 1]$  and  $Ap_{wsd} \in [0, 1]$  are the window aperture of the lee- and the windward-side (control inputs).

The components  $\Phi_{\Delta T_{lsd}}$  and  $\Phi_{\Delta T_{wsd}}$  determined by the temperature difference between indoor and outdoor air for lee- and windward-side are defined by

$$\Phi_{\Delta T_{lsd}} = n_{win} \cdot \frac{1}{3} c_w \cdot L_1 \cdot \sqrt{\left| g \cdot \frac{T_o - T_{as}}{T_o} \right|} \cdot L_{win_{lsd}}^{1.5} \quad \{\text{m}^3 \text{s}^{-1}\} \quad (3.156)$$

$$\Phi_{\Delta T_{wsd}} = n_{win} \cdot \frac{1}{3} c_w \cdot L_1 \cdot \sqrt{\left| g \cdot \frac{T_o - T_{as}}{T_o} \right|} \cdot L_{win_{wsd}}^{1.5} \quad \{\text{m}^3 \text{s}^{-1}\} \quad (3.157)$$

where  $L_1$   $\{\text{m}\}$  is the window length,  $c_w$   $\{-\}$  is the discharge coefficient through the windows,  $g$   $\{\text{m s}^{-2}\}$  is gravity,  $L_{win_{lsd}}$  and  $L_{win_{wsd}}$   $\{\text{m}\}$  are the lengths of the vertical projection of the windows opening on the lee- and the windward-side and  $T_{as}$  and  $T_o$   $\{\text{K}\}$  are the temperatures of the air above the screen and the outdoor air.

The lengths  $L_{win\_lsd}$  and  $L_{win\_wsd}$  of the vertical projection of the windows opening on the lee- and the windward-side are computed by

$$L_{win\_lsd} = 2 L_2 \cdot \cos(\gamma - 0.5 A_{plsd} \cdot \Theta_{\max}) \cdot \sin(0.5 A_{plsd} \cdot \Theta_{\max}) \quad \{\text{m}\} \quad (3.158)$$

$$L_{win\_wsd} = 2 L_2 \cdot \cos(\gamma - 0.5 A_{pwsd} \cdot \Theta_{\max}) \cdot \sin(0.5 A_{pwsd} \cdot \Theta_{\max}) \quad \{\text{m}\} \quad (3.159)$$

where  $L_2$  {m} is the window height,  $\gamma$  {rad} is the angle of the roof with the horizontal plane and  $\Theta_{\max}$  {rad} is the maximum angle of the window aperture.

### 3.8 Modelling the heating and the cooling system

The heating system consists of a boiler, a condenser and a heat pump (see figure 3.6). The boiler can be used to heat the lower net to a temperature of about 90°C. The condenser is heated by the flue gas of the boiler. It can be used to heat the upper net to a temperature of about 45°C. The heat pump can be used to heat the lower net to a temperature of about 33°C. The heating system with the boiler, the condenser and the heat pump is described in §3.8.1 and §3.8.3.

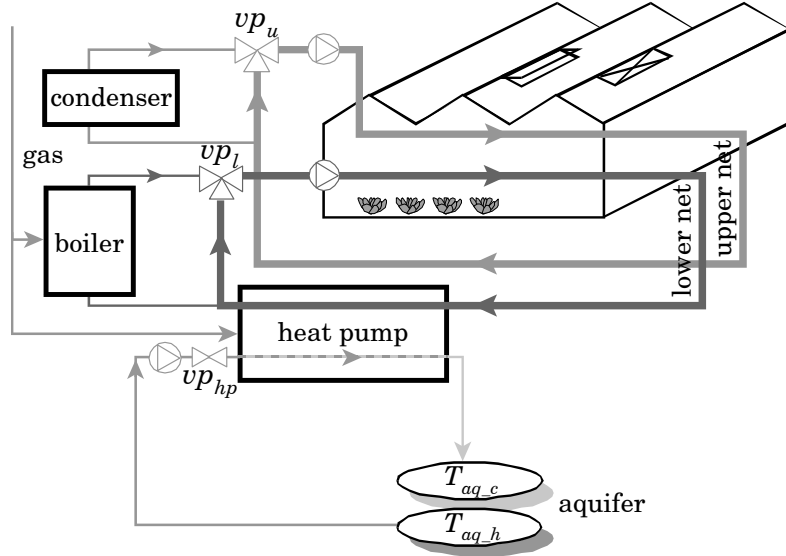


Figure 3.6: Heating with boiler, condenser and heat pump

The cooling system consists of a heat exchanger (see figure 3.7). The heat exchanger can be used to cool the upper cooling net to a temperature of about 10°C. The cooling system is described in §3.8.4.

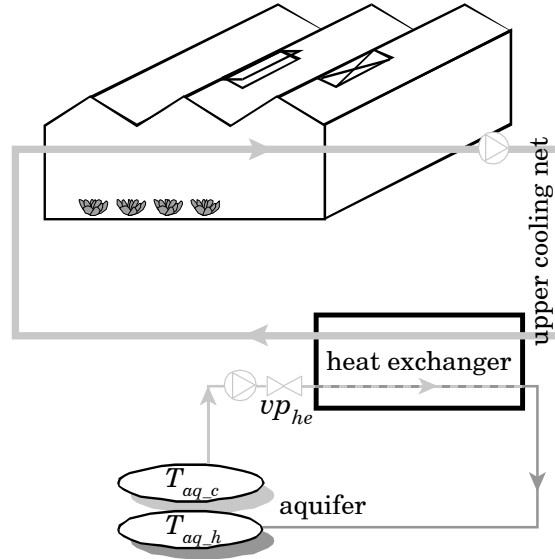


Figure 3.7: Cooling with heat exchanger

The heat pump and the heat exchanger operate in conjunction with an aquifer. The aquifer has a warm ( $T_{aq,h} = 16^\circ\text{C}$ ) and a cold ( $T_{aq,c} = 10^\circ\text{C}$ ) side. The warm water is used by the heat pump to heat the greenhouse. The cold water is used by the heat exchanger to cool the greenhouse.

In the dimensions (length of pipes, number of loops) of the lower and upper heating net and the cooling net it is assumed that the layout is the same in every greenhouse span. The net can then be described by a number of loops of pipes with a specific length and diameter. The flow entering a net is equal to the flow leaving the net, and for each net there is one water temperature entering the net and one water temperature leaving the net.

### 3.8.1 Heating system boiler and condenser

The boiler is used to heat the lower net to a temperature of about  $90^\circ\text{C}$ . The flue gas of the boiler is used to heat a condenser, which heats the upper net to a temperature of about  $45^\circ\text{C}$ . The heating system is shown in figure 3.6. The input of the lower net is taken from the boiler. The output of the lower net is the input of the heat pump. The output of the heat pump can be partly led through the boiler and partly through the lower net bypass. If the valve position of the lower net  $vp_l = 0$ , then no water is led to the boiler and if the valve position of the lower net  $vp_l = 1$ , then no water is led through the lower

net bypass. The input of the upper net is taken from the condenser. The output of the upper net can be partly led through the condenser and partly through the upper net bypass. If the valve position of the upper net  $vp_u = 0$ , then no water is led to the condenser and if the valve position of the upper net  $vp_u = 1$ , then no water is led through the upper net bypass.

### 3.8.1.1 Lower net

The input of the lower net (where it enters the greenhouse) is taken from the boiler and the lower net bypass. The output of the lower net (where it leaves the greenhouse) is the input of the heat pump. The energy transport terms  $Q_{in,l}$  and  $Q_{out,l}$  due to the water flow into and out of the lower net are defined by

$$Q_{in,l} = \rho_{H_2O} \cdot c_{p,H_2O} \cdot \Phi_{in,l} \cdot T_{in,l} \quad \{\text{W}\} \quad (3.160)$$

$$Q_{out,l} = \rho_{H_2O} \cdot c_{p,H_2O} \cdot \Phi_{in,l} \cdot T_{out,l} \quad \{\text{W}\} \quad (3.161)$$

where  $\rho_{H_2O}$   $\{\text{kg m}^{-3}\}$  is the density of water,  $c_{p,H_2O}$   $\{\text{J kg}^{-1} \text{K}^{-1}\}$  is the specific heat capacity of water,  $\Phi_{in,l}$   $\{\text{m}^3 \text{s}^{-1}\}$  is the flow rate of water into the lower net and  $T_{in,l}$  and  $T_{out,l}$   $\{\text{K}\}$  are the water temperatures entering and leaving the lower net.

The flow rate of water  $\Phi_{in,l}$  into the lower net is equal to the pump flow rate

$$\Phi_{in,l} = \Phi_{pump,l} \quad \{\text{m}^3 [\text{H}_2\text{O}] \text{s}^{-1}\} \quad (3.162)$$

where  $\Phi_{pump,l}$   $\{\text{m}^3 \text{s}^{-1}\}$  is the maximum flow rate from the pump into the lower net.

The water temperature  $T_{in,l}$  entering the lower net is defined by

$$T_{in,l} = vp_l \cdot T_{boil} + (1 - vp_l) \cdot T_{l,bypass} \quad \{\text{K}\} \quad (3.163)$$

in which the boiler water temperature  $T_{boil} = T_0 + 90 \text{ K}$ , where  $vp_l \in [0, 1]$  is the valve position of the lower net (control input). The water temperature  $T_{l,bypass}$  through the lower net bypass is equal to the water temperature  $T_{out,hp}$  leaving the heat pump

$$T_{l,bypass} = T_{out,hp} \quad \{\text{K}\} \quad (3.164)$$

The water temperature  $T_{out,l}$  leaving the lower net is given by (see §3.B)

$$T_{out,l} = T_l + \frac{Q_{rd,l} - Q_{l,a} - Q_{l,c} - Q_{l,ri} - Q_{l,s} - Q_{l,sc}}{\rho_{H_2O} \cdot c_{p,H_2O} \cdot \Phi_{in,l}} \quad \{\text{K}\} \quad (3.165)$$

where  $T_l$   $\{\text{K}\}$  is the lower net water temperature,  $\rho_{H_2O}$   $\{\text{kg m}^{-3}\}$  is the density of water and  $c_{p,H_2O}$   $\{\text{J kg}^{-1} \text{K}^{-1}\}$  is the specific heat capacity of water.

### 3.8.1.2 Upper net

The input of the upper net (where it enters the greenhouse) is taken from the condenser and the upper net bypass. The output of the upper net (where it leaves the greenhouse) can be partly led through the condenser and partly through the upper net bypass. The energy transport terms  $Q_{in,u}$  and  $Q_{out,u}$  due to the water flow into and out of the upper net are defined by

$$Q_{in,u} = \rho_{H_2O} \cdot c_{p,H_2O} \cdot \Phi_{in,u} \cdot T_{in,u} \quad \{\text{W}\} \quad (3.166)$$

$$Q_{out,u} = \rho_{H_2O} \cdot c_{p,H_2O} \cdot \Phi_{in,u} \cdot T_{out,u} \quad \{\text{W}\} \quad (3.167)$$

where  $\rho_{H_2O}$   $\{\text{kg m}^{-3}\}$  is the density of water,  $c_{p,H_2O}$   $\{\text{J kg}^{-1} \text{K}^{-1}\}$  is the specific heat capacity of water,  $\Phi_{in,u}$   $\{\text{m}^3 \text{s}^{-1}\}$  is the flow rate of water into the upper net and  $T_{in,u}$  and  $T_{out,u}$   $\{\text{K}\}$  are the water temperatures entering and leaving the upper net.

The flow rate of water  $\Phi_{in,u}$  into the upper net is equal to the pump flow rate

$$\Phi_{in,u} = \Phi_{pump,u} \quad \{\text{m}^3[\text{H}_2\text{O}] \text{s}^{-1}\} \quad (3.168)$$

where  $\Phi_{pump,u}$   $\{\text{m}^3 \text{s}^{-1}\}$  is the maximum flow rate from the pump into the upper net.

The water temperature  $T_{in,u}$  entering the upper net is defined by

$$T_{in,u} = v_{p_u} \cdot T_{cond} + (1 - v_{p_u}) \cdot T_{u,bypass} \quad \{\text{K}\} \quad (3.169)$$

in which the condenser water temperature  $T_{cond} = T_0 + 45 \text{ K}$ , where  $v_{p_u} \in [0, 1]$  is the valve position of the upper net (control input). The water temperature  $T_{u,bypass}$  through the upper net bypass is equal to the water temperature  $T_{out,u}$  leaving the upper net

$$T_{u,bypass} = T_{out,u} \quad \{\text{K}\} \quad (3.170)$$

The water temperature  $T_{out,u}$  leaving the upper net is given by (see §3.B)

$$T_{out,u} = T_u + \frac{Q_{rd,u} - Q_{u,a} - Q_{u,c} - Q_{u,ri} - Q_{u,s} - Q_{u,sc}}{\rho_{H_2O} \cdot c_{p,H_2O} \cdot \Phi_{in,u}} \quad \{\text{K}\} \quad (3.171)$$

where  $T_u$   $\{\text{K}\}$  is the upper net water temperature,  $\rho_{H_2O}$   $\{\text{kg m}^{-3}\}$  is the density of upper net water and  $c_{p,H_2O}$   $\{\text{J kg}^{-1} \text{K}^{-1}\}$  is the specific heat capacity of water.

### 3.8.1.3 Boiler

The energy supply  $Q_{boil}$  by the boiler is defined by

$$Q_{boil} = \rho_{H_2O} \cdot c_{p-H_2O} \cdot \Phi_{boil} \cdot (T_{boil} - T_{in\_boil}) \quad \{\text{W}\} \quad (3.172)$$

where  $\rho_{H_2O}$   $\{\text{kg m}^{-3}\}$  is the density of water,  $c_{p-H_2O}$   $\{\text{J kg}^{-1} \text{K}^{-1}\}$  is the specific heat capacity of water,  $\Phi_{boil}$   $\{\text{m}^3 \text{s}^{-1}\}$  is the flow rate of water leaving the boiler and  $T_{boil}$  and  $T_{in\_boil}$   $\{\text{K}\}$  are the water temperatures in the boiler and entering the boiler. The water temperature  $T_{boil}$  is either set to a fixed value ( $T_{boil} = T_0 + 90 \text{ K}$ ), or follows from data.

The flow rate of water  $\Phi_{boil}$  leaving the boiler is determined by

$$\Phi_{boil} = v_{pl} \cdot \Phi_{pump\_l} \quad \{\text{m}^3[\text{H}_2\text{O}] \text{s}^{-1}\} \quad (3.173)$$

where  $\Phi_{pump\_l}$   $\{\text{m}^3[\text{H}_2\text{O}] \text{s}^{-1}\}$  is the maximum flow rate from the pump into the lower net and  $v_{pl} \in [0, 1]$  is the valve position of the lower net (control input).

The water temperature  $T_{in\_boil}$  entering the boiler is equal to the water temperature in the lower net bypass  $T_{l\_bypass}$

$$T_{in\_boil} = T_{l\_bypass} \quad \{\text{K}\} \quad (3.174)$$

### 3.8.2 The aquifer

An aquifer is a formation of water-bearing sand material in the soil that can contain and transmit water. Wells can be drilled into the aquifers and water can be pumped into and out of the water layers.

The heat pump and the heat exchanger operate in conjunction with an aquifer. The aquifer has a warm ( $T_{aq\_h} = 16^\circ\text{C}$ ) and a cold ( $T_{aq\_c} = 10^\circ\text{C}$ ) side. The warm water is used by the heat pump to heat the greenhouse and the cold water is used by the heat exchanger to cool the greenhouse.

It is assumed that the aquifer has an infinite amount of warm and cold water available. The loading and unloading of the aquifer buffers is limited by government demands, since the aquifer has to be energy neutral year-round. This indirectly corrects for the fact that the buffers are not infinite. These issues are worked out in the optimal control in §4.3.5.

### 3.8.3 Heating system heat pump

A gasfired heat pump is used to heat the lower net to a temperature of about 33°C. The heat pump heats the water in the lower net with water from the warm side of the aquifer. The cold water obtained in this process is led to the cold side of the aquifer. The heating system is shown in figure 3.6. It is assumed that the heat transfer between the heat pump and the lower net has no dynamics (direct transfer of heat).

The lower net equations are given in §3.8.1.1. The heat pump equations are derived in §3.E. The configuration and the energy transport of the heat pump is given in figure 3.8. In this figure the following water temperatures {K} are shown:  $T_{in\_hp}$  and  $T_{out\_hp}$  flowing into and out of the heat pump (greenhouse side),  $T_{aq\_h}$  and  $T_{aq\_c\_hp}$  of the warm and the cold side of the aquifer (aquifer side) and  $T_{hs}$  and  $T_{cs}$  of the warm and the cold side of the heat pump (inside the heat pump). Water temperature  $T_{aq\_c\_hp}$  should be lower than the desired water temperature  $T_{aq\_c}$ , so that the water temperature  $T_{aq\_c}$  can be achieved by mixing with water with temperature  $T_{aq\_h}$ . This has to be solved locally (outside the system boundary considered here).

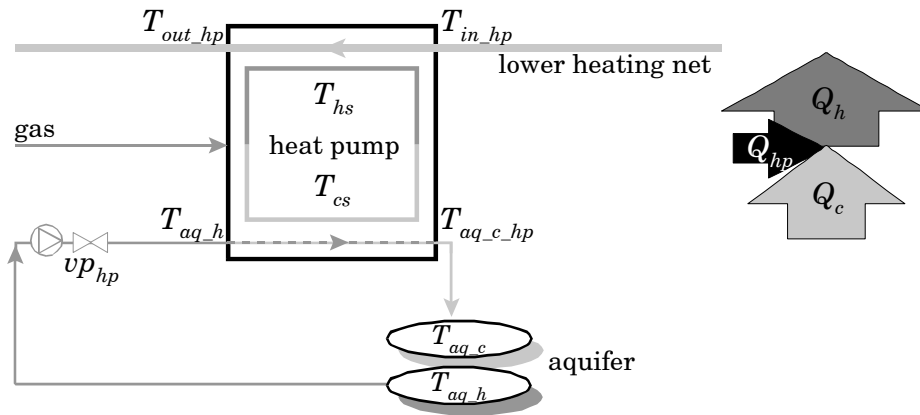


Figure 3.8: Configuration and energy transport heat pump

The water temperature  $T_{aq\_h}$  of the warm side of the aquifer (aquifer side) is known, as well as the water temperature  $T_{in\_hp}$  flowing into the heat pump (greenhouse side). With the valve position  $vp_{hp}$  of the heat pump (control input), the water temperature  $T_{out\_hp}$  flowing out of the heat pump (greenhouse side), the water temperatures  $T_{hs}$  and  $T_{cs}$  (inside the heat pump), the water temperature  $T_{aq\_c\_hp}$  (aquifer side), the energy transport terms  $Q_h$  and  $Q_c$  and the energy used by the heat pump  $Q_{hp}$  can be computed.

### 3.8.3.1 Heat pump

The water temperature  $T_{in\_hp}$  entering the heat pump is equal to the water temperature  $T_{out\_l}$  leaving the lower net

$$T_{in\_hp} = T_{out\_l} \quad \{K\} \quad (3.175)$$

The water temperature  $T_{out\_hp}$   $\{K\}$  leaving the heat pump can be partly led through the boiler and partly through the lower net bypass. If the valve position of the heat pump  $vp_{hp} = 0$ , then no water is led through the heat pump (the heat pump is off).

It is assumed here that a compression heat pump is used. The operation of a compression heat pump is based on the compression and evaporation of a fluid. The fluid evaporates when thermal energy  $Q_c$  is added from the warm side of the aquifer. The fluid condensates when thermal energy  $Q_h$  is subtracted by the lower net. The energy used by the heat pump to drive this process  $Q_{hp}$  is given by

$$Q_{hp} = Q_h - Q_c \quad \{W\} \quad (3.176)$$

This amount of energy determines the coefficient of performance  $COP$  of the heat pump

$$COP = \frac{Q_h}{Q_h - Q_c} \quad \{-\} \quad (3.177)$$

The energy transport  $Q_h$  due to the water flow on the lower net side and the energy transport  $Q_c$  due to the water flow on the aquifer side are given by (see figure 3.8)

$$Q_h = \rho_{H2O} \cdot c_{p-H2O} \cdot \Phi_{pump\_l} \cdot (T_{out\_hp} - T_{in\_hp}) \quad \{W\} \quad (3.178)$$

$$Q_c = \rho_{H2O} \cdot c_{p-H2O} \cdot vp_{hp} \cdot \Phi_{pump\_hp} \cdot (T_{aq\_h} - T_{aq\_c\_hp}) \quad \{W\} \quad (3.179)$$

where  $\rho_{H2O}$   $\{kg\ m^{-3}\}$  is the density of water,  $c_{p-H2O}$   $\{J\ kg^{-1}\ K^{-1}\}$  is the specific heat capacity of water,  $\Phi_{pump\_l}$  and  $\Phi_{pump\_hp}$   $\{m^3\ s^{-1}\}$  are the maximum flow rates of water into the lower net and through the heat pump and  $vp_{hp} \in [0, 1]$  is the valve position of the heat pump (control input).

The resulting temperature  $T_{aq\_c\_hp}$  of the aquifer water cooled by the heat pump (derived in §3.E) is given by

$$T_{aq\_c\_hp} = \frac{\eta_{hp} \cdot (c_1 - 1) \cdot (h_1 \cdot T_{out\_hp} - T_{in\_hp}) \cdot v_{p_{hp}} \cdot \Phi_{pump\_hp} \cdot T_{aq\_h} + \Phi_{pump\_L} \cdot (T_{out\_hp} - T_{in\_hp}) \cdot ((1 - \eta_{hp}) \cdot (c_1 - 1) \cdot (h_1 \cdot T_{out\_hp} - T_{in\_hp}) + T_{aq\_h} \cdot (h_1 - 1))}{\eta_{hp} \cdot (c_1 - 1) \cdot (h_1 \cdot T_{out\_hp} - T_{in\_hp}) \cdot v_{p_{hp}} \cdot \Phi_{pump\_hp} + \Phi_{pump\_L} \cdot (T_{out\_hp} - T_{in\_hp}) \cdot c_1 \cdot (h_1 - 1)} \quad \{K\} \quad (3.180)$$

in which  $h_1 = e^{\frac{k_{hp} \cdot A_{hp}}{\rho_{H2O} \cdot c_{p\_H2O} \cdot \Phi_{pump\_L}}}$  and  $c_1 = e^{\frac{k_{hp} \cdot A_{hp}}{\rho_{H2O} \cdot c_{p\_H2O} \cdot v_{p_{hp}} \cdot \Phi_{pump\_hp}}}$ , where  $k_{hp}$   $\{W\ m^{-2}\ K^{-1}\}$  is the heat pump heat transfer coefficient,  $A_{hp}$   $\{m^2\}$  is the heat pump surface for heat transfer and  $\eta_{hp}$   $\{-\}$  is the efficiency of the heat pump.

The water temperature  $T_{out\_hp}$  leaving the heat pump (derived in §3.E) is given by

$$T_{out\_hp} = \frac{1}{12 \cdot a_T} \cdot \left( -3 b_T - \sqrt{3} p_{T7} + \left( \frac{3}{p_{T6} \cdot p_{T7}} \cdot \left( 2 \cdot (3 b_T^2 - 8 a_T \cdot c_T - a_T \cdot p_{T6}) \cdot p_{T6} \cdot p_{T7} + 8 a_T \cdot (3 b_T \cdot d_T - 12 a_T \cdot e_T - c_T^2) \cdot p_{T7} + 6 \sqrt{3} \cdot (8 a_T^2 \cdot d_T + b_T^3 - 4 a_T \cdot b_T \cdot c_T) \cdot p_{T6} \right) \right)^{\frac{1}{2}} \right) \quad \{K\} \quad (3.181)$$

where  $a_T$ ,  $b_T$ ,  $c_T$ ,  $d_T$  and  $e_T$  are parameters of a fourth order equation and  $p_{T1}$ ,  $p_{T2}$ ,  $p_{T3}$ ,  $p_{T4}$ ,  $p_{T5}$  and  $p_{T6}$  are parameter combinations (see §3.E).

The minimum valve position  $v_{p_{hp}}$  — determined by the heat pump characteristics — is  $v_{p_{hp}\min} = 0.57$ . Below this value the temperature  $T_{aq\_c\_hp} \leq T_0$  ( $T_0 = 273.15\ K$ ). Since the optimal control will compute the value for the valve position  $v_{p_{hp}}^*$  between 0 and 1, the valve position is scaled between the minimum valve position  $v_{p_{hp}\min}$  and the maximum value of 1

$$v_{p_{hp}} = \begin{cases} (1 - v_{p_{hp}\min}) \cdot v_{p_{hp}}^* + v_{p_{hp}\min} & \text{if } v_{p_{hp}}^* > 0 \\ 0 & \text{if } v_{p_{hp}}^* = 0 \end{cases} \quad \{-\} \quad (3.182)$$

where  $v_{p_{hp}}^*$  is the valve position computed by the optimal control.

There are some restrictions as to the operation of the heat pump. The heat pump cannot be operated:

- If the temperature  $T_{in\_hp}$  is too high ( $T_{in\_hp} > T_{in\_hp\max}$ ), the heat pump cannot increase this temperature any further. With the chosen heat pump characteristics this temperature  $T_{in\_hp\max} = T_0 + 30.1$  K.
- If the valve position  $vp_{hp}^*$  of the heat pump is so low that the temperature  $T_{aq\_c\_hp} \leq T_0$  ( $vp_{hp}^* < vp_{hp\min}$ ), which would mean that the aquifer water would freeze. This is avoided by using eqn. 3.182.
- If the resulting water temperature  $T_{aq\_c\_hp}$  for the cold side of the aquifer is higher than the desired temperature  $T_{aq\_c}$ , since the desired temperature cannot be reached by mixing with water with temperature  $T_{aq\_h}$ . If this occurs, the valve position  $vp_{hp}^*$  is decreased by 0.1, such that the water runs slower, decreasing the temperature  $T_{aq\_c\_hp}$ . The valve position is decreased further until  $T_{aq\_c\_hp} < T_{aq\_c}$ .
- The heat pump is turned off ( $vp_{hp} = 0$ ) if any of the temperature differences in eqns. 3.251, 3.252, 3.253 and 3.254 is lower than or equal to zero, which would mean that the heat transfer would take place in the opposite direction. It is also turned off if  $T_{aq\_c\_hp} \leq T_0$ , since then the aquifer water would freeze.

### 3.8.4 Cooling system heat exchanger

The heat exchanger is used to cool the upper cooling net to a temperature of about 10°C. The heat exchanger cools the water in the upper cooling net with water from the cold side of the aquifer. The warm water obtained in this process is led to the warm side of the aquifer. The cooling system is shown in figure 3.7. It is assumed that the heat transfer between the heat exchanger and the upper cooling net has no dynamics (direct transfer of heat).

The upper cooling net equations are given in §3.8.4.1. The heat exchanger equations are derived in §3.F. The configuration and the energy transport of the heat exchanger is given in figure 3.9. In this figure the following water temperatures {K} are shown:  $T_{in\_he}$  and  $T_{out\_he}$  flowing into and out of the heat exchanger (greenhouse side) and  $T_{aq\_c}$  and  $T_{aq\_h\_he}$  of the cold and the warm side of the aquifer (aquifer side). Water temperature  $T_{aq\_h\_he}$  should be higher than the desired water temperature  $T_{aq\_h}$ , so that the water temperature  $T_{aq\_h}$  can be achieved by mixing with water with temperature  $T_{aq\_c}$ . This has to be solved locally (outside the system boundary considered here).

The water temperature  $T_{aq\_c}$  of the cold side of the aquifer (aquifer side) is known, as well as the water temperature  $T_{in\_he}$  flowing into the heat exchanger (greenhouse side). With the valve position  $vp_{he}$  of the heat exchanger (con-

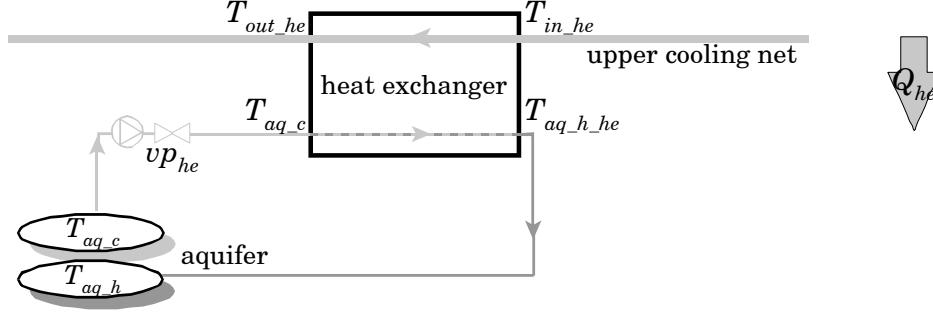


Figure 3.9: Configuration and energy transport heat exchanger

trol input), the water temperature  $T_{out\_he}$  flowing out of the heat exchanger (greenhouse side), the water temperature  $T_{aq\_h\_he}$  (aquifer side) and the energy transport term  $Q_{he}$  can be computed.

#### 3.8.4.1 Upper cooling net

The input of the upper cooling net is taken from the heat exchanger. The output of the upper cooling net is the input of the heat exchanger. The energy transport terms  $Q_{in\_uc}$  and  $Q_{out\_uc}$  due to the water flow into and out of the upper cooling net are defined by

$$Q_{in\_uc} = \rho_{H2O} \cdot c_{p\_H2O} \cdot \Phi_{in\_uc} \cdot T_{in\_uc} \quad \{W\} \quad (3.183)$$

$$Q_{out\_uc} = \rho_{H2O} \cdot c_{p\_H2O} \cdot \Phi_{in\_uc} \cdot T_{out\_uc} \quad \{W\} \quad (3.184)$$

where  $\rho_{H2O}$   $\{kg\ m^{-3}\}$  is the density of water,  $c_{p\_H2O}$   $\{J\ kg^{-1}\ K^{-1}\}$  is the specific heat capacity of water,  $\Phi_{in\_uc}$   $\{m^3\ s^{-1}\}$  is the flow rate of water into the upper cooling net and  $T_{in\_uc}$  and  $T_{out\_uc}$   $\{K\}$  are the water temperatures entering and leaving the upper cooling net.

The flow rate of water  $\Phi_{in\_uc}$  into the upper cooling net is equal to the pump flow rate

$$\Phi_{in\_uc} = \Phi_{pump\_uc} \quad \{m^3[H_2O]\ s^{-1}\} \quad (3.185)$$

where  $\Phi_{pump\_uc}$   $\{m^3\ s^{-1}\}$  is the maximum flow rate from the pump into the upper cooling net.

The water temperature  $T_{in\_uc}$  entering the upper cooling net is equal to the water temperature leaving the heat exchanger

$$T_{in\_uc} = T_{out\_he} \quad \{K\} \quad (3.186)$$

The water temperature  $T_{out\_uc}$  leaving the upper cooling net is given by (see §3.B)

$$T_{out\_uc} = T_{uc} + \frac{Q_{rd\_uc} + Q_{a\_uc\_H2O} - Q_{uc\_a} - Q_{uc\_c} - Q_{uc\_ri} - Q_{uc\_s} - Q_{uc\_sc}}{\rho_{H2O} \cdot c_{p\_H2O} \cdot \Phi_{in\_uc}} \quad \{K\} \quad (3.187)$$

where  $T_{uc}$  {K} is the upper cooling net temperature,  $\rho_{H2O}$  {kg m<sup>-3</sup>} is the density of water and  $c_{p\_H2O}$  {J kg<sup>-1</sup> K<sup>-1</sup>} is the specific heat capacity of water.

### 3.8.4.2 Heat exchanger

The water temperature  $T_{in\_he}$  entering the heat exchanger is equal to the water temperature  $T_{out\_uc}$  leaving the upper cooling net

$$T_{in\_he} = T_{out\_uc} \quad \{K\} \quad (3.188)$$

The water temperature  $T_{out\_he}$  {K} leaving the heat exchanger is the input of the upper cooling net (eqn. 3.186). If the valve position of the heat exchanger  $vp_{he} = 0$ , then no water is led through the heat exchanger (the heat exchanger is off).

It is assumed here that a countercurrent heat exchanger is used. The energy transfer  $Q_{he}$  by the heat exchanger is defined by the energy transport due to the water flow on the aquifer side, given by

$$Q_{he} = \rho_{H2O} \cdot c_{p\_H2O} \cdot vp_{he} \cdot \Phi_{pump\_he} \cdot (T_{aq\_h\_he} - T_{aq\_c}) \quad \{W\} \quad (3.189)$$

where  $\rho_{H2O}$  {kg m<sup>-3</sup>} is the density of water,  $c_{p\_H2O}$  {J kg<sup>-1</sup> K<sup>-1</sup>} is the specific heat capacity of water,  $\Phi_{pump\_he}$  {m<sup>3</sup> s<sup>-1</sup>} is the maximum flow rate of water through the heat exchanger and  $vp_{he} \in [0, 1]$  is the valve position of the heat exchanger (control input).

The resulting temperature  $T_{aq\_h\_he}$  of the aquifer water heated by the heat exchanger (derived in §3.F) is given by

$$T_{aq\_h\_he} = \begin{cases} \frac{c_{he} \cdot T_{aq\_c} \cdot (vp_{he} \cdot \Phi_{pump\_he} - \Phi_{pump\_uc}) + T_{in\_he} \cdot \Phi_{pump\_uc} \cdot (c_{he} - 1)}{c_{he} \cdot vp_{he} \cdot \Phi_{pump\_he} - \Phi_{pump\_uc}} & \text{if } c_{he} > 1 \\ T_{aq\_c} & \text{if } c_{he} = 1 \end{cases} \quad \{K\} \quad (3.190)$$

in which  $c_{he} = e^{\frac{k_{he} \cdot A_{he}}{\rho_{H2O} \cdot c_{p-H2O}} \cdot (\frac{1}{\Phi_{pump-uc}} - \frac{1}{vp_{he} \cdot \Phi_{pump-he}})}$ , where  $k_{he}$   $\{\text{W m}^{-2} \text{K}^{-1}\}$  is the heat exchanger heat transfer coefficient,  $A_{he}$   $\{\text{m}^2\}$  is the heat exchanger surface for heat transfer and  $\Phi_{pump-uc}$   $\{\text{m}^3 \text{s}^{-1}\}$  is the maximum flow rate of water into the upper cooling net.

The water temperature  $T_{out\_he}$  leaving the heat exchanger (derived in §3.F) is given by

$$T_{out\_he} = T_{in\_he} - \frac{vp_{he} \cdot \Phi_{pump\_he} \cdot (T_{aq\_h\_he} - T_{aq\_c})}{\Phi_{pump\_uc}} \quad \{\text{K}\} \quad (3.191)$$

The minimum valve position  $vp_{he}$  — determined by the heat exchanger characteristics — is  $vp_{he \min} = 0.43$ . Below this value the temperature difference  $\Delta T_{m\_he} < 0$  (eqn. 3.268). Since the optimal control will compute the value for the valve position  $vp_{he}^*$  between 0 and 1, the valve position is scaled between the minimum valve position  $vp_{he \min}$  and the maximum value of 1

$$vp_{he} = \begin{cases} (1 - vp_{he \min}) \cdot vp_{he}^* + vp_{he \min} & \text{if } vp_{he}^* > 0 \\ 0 & \text{if } vp_{he}^* = 0 \end{cases} \quad \{-\} \quad (3.192)$$

where  $vp_{he}^*$  is the valve position computed by the optimal control.

There are some restrictions as to the operation of the heat exchanger. The heat exchanger cannot be operated:

- If the temperature  $T_{in\_he}$  is too low ( $T_{in\_he} < T_{in\_he \min}$ ), the heat exchanger cannot decrease this temperature any further. The minimum temperature is equal to the temperature of the warm aquifer side  $T_{in\_he \min} = T_{aq\_h}$ .
- If the valve position of the heat pump  $vp_{he}^*$  is so low that the temperature difference  $\Delta T_{m\_he} < 0$  ( $vp_{he}^* < vp_{he \min}$ ), which would mean that heat transfer would take place in the opposite direction.
- If the resulting temperature for the warm side of the aquifer  $T_{aq\_h\_he}$  is lower than the desired temperature  $T_{aq\_h}$ , since the desired temperature cannot be reached by mixing with water with temperature  $T_{aq\_c}$ . If this occurs, the valve position  $vp_{he}^*$  is decreased by 0.1, such that the water runs slower, increasing temperature  $T_{aq\_h\_he}$ . The valve position is decreased further until  $T_{aq\_h\_he} > T_{aq\_h}$ .
- The heat exchanger is turned off ( $vp_{he} = 0$ ) if any of the temperature differences in eqns. 3.269 and 3.270 is lower than or equal to zero, which would mean that the heat transfer would take place in the opposite direction.

### 3.9 Validation conventional greenhouse model

The greenhouse model described in this chapter and the crop model described in chapter 2 are developed for the use in a receding horizon optimal control context.

The control horizon  $t_f$  of the receding horizon optimal controller is one day, which means that the model should approximate the measured data over a time span of one day. The dynamic behaviour of the temperatures  $T_a$  and  $T_c$ , the humidity  $C_{a\_H2O}$  and the CO<sub>2</sub> concentration  $C_{a\_CO2}$  should be described well.

To validate the greenhouse with crop model, data is used from a conventional greenhouse. The differences between the solar greenhouse model and the conventional greenhouse model used for the validation are specified in §3.9.1.

The model is validated by simulating the greenhouse with crop model with known control inputs  $u$  and known external inputs  $v$ . The resulting simulated data are compared with the measured data. It was found that the model results agreed quite well with the measured data on some days, and less well on other days. To improve the model, parameter estimation was performed (§3.9.3). The parameters likely to improve the model were found by performing sensitivity analysis (§3.9.2).

#### 3.9.1 Conventional versus solar greenhouse model

The data from the conventional greenhouse are from a greenhouse in Olsthoorn, The Netherlands. The greenhouse dimensions are given in appendix B. This greenhouse has a single glass cover and a thermal screen. The differences between the conventional greenhouse model and the solar greenhouse model described are given in the next paragraphs. The names of the data sets like *040323* indicate the measurement date (*yymmdd*). The sampling time  $\Delta t$  of the data is 1 min.

##### 3.9.1.1 Control inputs

Some control inputs  $u$  are different from those defined in table 3.2. These differences are described here.

**Heating temperatures instead of valve positions:** Instead of the valve positions  $vp_l \in [0, 1]$  and  $vp_u \in [0, 1]$  of the lower and the upper net, the water temperatures  $T_{in\_l}$  and  $T_{in\_u}$  {K} entering the lower and upper net are measured. The flow rates of water into the lower and upper net are no longer equal to the pump flow rate, they now depend on the pump state. The pump is either off or on, which means that the valve position of the lower and the upper net is either 0 or 1 {0,1}. The flow rates into the lower and upper net are

$$\Phi_{in\_l} = vp_l \cdot \Phi_{pump\_l} \quad \{\text{m}^3[\text{H}_2\text{O}] \text{ s}^{-1}\} \quad (3.193)$$

$$\Phi_{in\_u} = vp_u \cdot \Phi_{pump\_u} \quad \{\text{m}^3[\text{H}_2\text{O}] \text{ s}^{-1}\} \quad (3.194)$$

*Note:* from the data analysis it was found that the upper net was not used in this greenhouse, so ( $vp_u = 0$ ).

**No solar greenhouse elements:** The conventional greenhouse has no heat pump, heat exchanger, ventilation with heat recovery and cooling net. To describe this, the valve positions  $vp_{hp}$  and  $vp_{he}$  of the heat pump and the heat exchanger, the option  $op_{vhr}$  for ventilation with heat recovery and all terms for the upper cooling net are set to zero. This ensures that all associated exchange terms are zero. There is no aquifer. This means that there are two states less ( $T_{uc}$  and  $E_{aq}$ ).

**Thermal screen closure:** The thermal screen closure  $Cl_{sc} \in [0, 1]$  is measured. In eqn. 3.139 thermal screen closure is computed from the screen condition. Now the screen condition has to be derived from the thermal screen closure

$$c_{sc} = \begin{cases} 0 & \text{if } Cl_{sc} < 0.95 \\ 1 & \text{if } Cl_{sc} \geq 0.95 \end{cases} \quad \{-\} \quad (3.195)$$

The value 0.95 is derived from the data sets, where during the night the screen closure varies between 0.95 and 1 when the screen is closed.

**Boiler:** The boiler temperature  $T_{boil}$  {K} is measured, whereas in the solar greenhouse model it is constant ( $T_{boil} = T_0 + 90$  K). The heat and CO<sub>2</sub> supply by the boiler depend on the flow rate of water  $\Phi_{boil}$  leaving the boiler. This flow rate defines the maximum carbondioxide supply by the boiler  $\Phi_{m\_in\_a\_CO2\max}$  (via  $Q_{boil}$  and  $\Phi_{gas}$ ). This limits the mass flow rate  $\Phi_{m\_in\_a\_CO2}$  of carbondioxide to indoor air. This flow rate is now defined differently from in eqn. 3.173

$$\Phi_{boil} = vp_{boil} \cdot \Phi_{pump\_boil} \quad \{\text{m}^3 \text{ s}^{-1}\} \quad (3.196)$$

where the valve position  $vp_{boil} \in [0, 1]$  of the boiler is a control input.

### 3.9.1.2 External inputs

All external inputs  $v$  used in the model are measured. From the first evaluation of the simulation results it was found that the sky temperature  $T_{sk}$  is not a measured but a computed value. It was computed with the equations given below, with a clouded fraction of the sky  $c_{Tsk} = 1$ . This means that it was assumed that the sky was 100% clouded (overcast sky). If this fraction is changed to 0.5 (partly cloudy sky), the computed sky temperature is 10°C lower than the ‘measured’ sky temperature. This difference for the sky temperature was found to give a large difference in the simulation results. To correct for this, the sky temperature is computed. Since the clouded fraction of the sky  $c_{Tsk}$  is unknown, it is a parameter in the parameter estimation (§3.9.3).

The sky temperature  $T_{sk}$  can be computed from the temperature and the humidity of the outdoor air (Monteith and Unsworth, 1990).

$$T_{sk} = \sqrt[4]{(1 - c_{Tsk}) \cdot E_{sky\_clear} \cdot T_o^4 + c_{Tsk} \cdot \left(T_o^4 - \frac{9}{\sigma}\right)} \quad \{\text{K}\} \quad (3.197)$$

in which the fictive emission coefficient  $E_{sky\_clear}$  of the clear sky is given by

$$E_{sky\_clear} = 0.53 + 6 \cdot 10^{-3} \sqrt{p_{o\_H2O}} \quad \{-\} \quad (3.198)$$

where  $T_o$  {K} is the outdoor air temperature,  $c_{Tsk} \in [0, 1]$  {-} is the clouded fraction of the sky,  $\sigma$  {W m<sup>-2</sup> K<sup>-4</sup>} is the Stefan-Boltzmann constant and  $p_{o\_H2O}$  {N m<sup>-2</sup>} is the vapour pressure of the outdoor air.

### 3.9.1.3 States

The following states are measured, and can be compared with simulated results: temperatures of the indoor air below and above the screen, crop, and indoor side of the roof ( $T_a$ ,  $T_{as}$ ,  $T_c$ ,  $T_{ri}$  {K}) and concentrations of CO<sub>2</sub> and H<sub>2</sub>O below the screen ( $C_{a\_CO2}$ ,  $C_{a\_H2O}$  {kg m<sup>-3</sup>}).

## 3.9.2 Sensitivity analysis

Sensitivity analysis is used to find model terms and parameters for which the model is most sensitive. This is used to find suitable model parameters to calibrate the model. It is also used to analyze sensitivity to the inputs. Parameters that are suitable for calibration are both sensitive and not well established. No adjustments are made to the well established physical and

physiological equations. The theory on sensitivity analysis as used here is given in §3.G.

Two data sets were selected (040323, 040925). These data sets were expected to give good results for the sensitivity analysis, since they both show excitation of all the control and external inputs  $u$  and  $v$ . The sensitivity analysis is performed over a period of two days (040322–040323), where only the result of the second day is used for the analysis. This is done to make sure that the initial states have little influence on the result.

Instead of changing the actual model terms and parameters themselves, they are multiplied by the parameters  $\theta$ , which have a nominal value of 1. This introduces scaling of the model parameters, which is necessary since they are not in the same range (e.g.,  $c_{Tsk}$  and  $\Phi_{m\_CO2}$ ). Then the sensitivity to these parameters  $\theta$  is investigated. The results are called relative sensitivities (Bernaerts and van Impe, 2004).

The model holds a large number of equations and adjustable parameters. First the sensitivity to the exchange terms  $E$  for heat, water and carbondioxide ( $Q_{A\_B}$ ,  $\Phi_{m\_A\_B\_H2O}$ ,  $\Phi_{m\_A\_B\_CO2}$ ) in the state equations (eqns. 3.1–3.16) is investigated.

$$\frac{dx}{dt} = \frac{\theta_1 \cdot E_1 + \theta_2 \cdot E_2 + \theta_3 \cdot E_3 + \dots + \theta_n \cdot E_n}{\tau} \quad (3.199)$$

Each exchange term  $E_i$  is multiplied by an associated scalar parameter  $\theta_i$  with a nominal value of 1. Next the sensitivity to the parameters  $\theta_i$  is investigated. In this way scaling is achieved and the sensitivity to the parameters  $\theta_i$  indicates the sensitivity to the exchange terms  $E_i$ . If, for instance, the parameter  $\theta_2$  is found to be sensitive, the underlying equation for  $E_2$  is further examined. The sensitive parameters are selected based on the Fisher information matrix  $\tilde{F}$  of the relative sensitivities (see eqn. 3.281). It is assumed here that the capacities ( $\rho \cdot c_p \cdot V$  or  $V$ ), which determine the time constant  $\tau$  of the state, are well established parameters. For the weighing matrix  $Q_F$  for the Fisher information matrix, the identity matrix is used. Numerical integration is used in the sensitivity analysis instead of an analytical solution.

The following 46 exchange terms are examined, where the terms in square brackets use the same parameter:  $Q_{a\_as}$ ,  $Q_{a\_c}$ ,  $Q_{a\_s}$ ,  $Q_{as\_o}$ ,  $Q_{as\_ri}$ ,  $Q_{c\_sc}$ ,  $Q_{in\_l}$ ,  $Q_{out\_l}$ ,  $Q_{l\_a}$ ,  $Q_{l\_c}$ ,  $Q_{l\_ri}$ ,  $Q_{l\_s}$ ,  $Q_{l\_sc}$ ,  $Q_{in\_u}$ ,  $Q_{out\_u}$ ,  $Q_{u\_a}$ ,  $Q_{u\_c}$ ,  $Q_{u\_ri}$ ,  $Q_{u\_s}$ ,  $Q_{u\_sc}$ ,  $Q_{rd\_c}$ ,  $Q_{rd\_l}$ ,  $Q_{rd\_ri}$ ,  $Q_{rd\_s}$ ,  $Q_{rd\_sc}$ ,  $Q_{rd\_u}$ ,  $Q_{ri\_c}$ ,  $Q_{ro\_o}$ ,  $Q_{ro\_sk}$ ,  $Q_{s\_c}$ ,  $Q_{s\_ri}$ ,  $Q_{s\_s2}$ ,  $Q_{s\_sc}$ ,  $Q_{sc\_a}$ ,  $Q_{sc\_as}$ ,  $Q_{sc\_ri}$ ,  $\Phi_{m\_a\_as\_CO2}$ ,  $\Phi_{m\_a\_as\_H2O}$ ,  $\Phi_{m\_a\_c\_CO2}$ ,  $\Phi_{m\_as\_o\_CO2}$ ,  $\Phi_{m\_as\_o\_H2O}$ ,  $\Phi_{m\_in\_a\_CO2}$ ,  $[Q_{a\_sc\_H2O}, \Phi_{m\_a\_sc\_H2O}]$ ,  $[Q_{as\_ri\_H2O}, \Phi_{m\_as\_ri\_H2O}]$ ,  $[Q_{as\_sc\_H2O}, \Phi_{m\_as\_sc\_H2O}]$ ,  $[Q_{c\_a\_H2O}, \Phi_{m\_c\_a\_H2O}]$ .

See appendix B for a description of the variables.

The most important exchange terms are:

**exchange terms ( $Q, \Phi$ ):**  $Q_{in,l}, Q_{out,l}, Q_{rd,c}, Q_{ro,o}, Q_{ro,sk}, \Phi_{m,a,c}CO_2, \Phi_{m,as,o}CO_2, \Phi_{m,as,o}H_2O, \Phi_{m,in,a}CO_2, [Q_{as,ri}H_2O, \Phi_{m,as,ri}H_2O], [Q_{c,a}H_2O, \Phi_{m,c,a}H_2O]$ .

The same procedure is used to determine the sensitivity to the control inputs ( $vp_{CO_2}, Ap_{l,sd}, Ap_{w,sd}, Cl_{sc}, vp_{boil}, T_{boil}, T_{in,l}, T_{in,u}$ ) and the external inputs ( $I_o, v_o, T_o, T_{o,w}, T_{sk}, C_{o,CO_2}$ ).

The most important inputs are:

**control inputs  $u$ :**  $Ap_{l,sd}, vp_{CO_2}, Cl_{sc}, T_{boil}, T_{in,l}$ , which means that  $Ap_{w,sd}, vp_{boil}$  and  $T_{in,u}$  are less important. For  $T_{in,u}$  it is obvious that it has no influence, since the upper net is not used.

**external inputs  $v$ :**  $I_o, v_o, T_o, T_{o,w}, T_{sk}, C_{o,CO_2}$ , which means that they are all important.

For model validation and calibration it is important to have data of the sensitive control inputs  $u$  and the external inputs  $v$ . There are in general no parameters to adjust. The only exception in this case is the sky temperature  $T_{sk}$ , which is not measured but computed from measurements.

From the remaining 11 sensitive terms the underlying equations are studied in more detail:  $Q_{in,l}, Q_{out,l}, Q_{rd,c}, Q_{ro,o}, Q_{ro,sk}, \Phi_{m,a,c}CO_2, \Phi_{m,as,o}CO_2, \Phi_{m,as,o}H_2O, \Phi_{m,in,a}CO_2, [Q_{as,ri}H_2O, \Phi_{m,as,ri}H_2O], [Q_{c,a}H_2O, \Phi_{m,c,a}H_2O], T_{sk}$ .

The goal is to locate model parameters within these terms that are not well known. This gives the following candidates for parameters estimation:

$Q_{in,l}, Q_{out,l}$	$\rightarrow \Phi_{pump,l}$
$Q_{rd,c}$	$\rightarrow \tau_{difR}$
$Q_{ro,o}$	$\rightarrow$ no parameter found (all parameters known)
$Q_{ro,sk}, T_{sk}$	$\rightarrow c_{Tsk}$
$\Phi_{m,a,c}CO_2$	$\rightarrow P_g, r_D$
$\Phi_{m,as,o}CO_2, \Phi_{m,as,o}H_2O$	$\rightarrow L_1, L_2$
$\Phi_{m,in,a}CO_2$	$\rightarrow \Phi_{pump,boil}, \Phi_{m,CO_2}$
$Q_{as,ri}H_2O, \Phi_{m,as,ri}H_2O$	$\rightarrow$ no parameter found (all parameters known)
$Q_{c,a}H_2O, \Phi_{m,c,a}H_2O$	$\rightarrow k_{c,a}H_2O$

No parameters of the crop model are estimated, since it is based on already validated models. This means that no adjustments are made to  $P_g, r_D$  and  $k_{c,a}H_2O$ . This leaves the following 7 parameters as candidates for calibration:  $c_{Tsk}, \tau_{difR}, L_1, L_2, \Phi_{pump,boil}, \Phi_{pump,l}$  and  $\Phi_{m,CO_2}$ .

The following 7 terms are set in the model:  $c_{Tsk} = 1 \theta_1$ ,  $\tau_{difR} = 1 \theta_2$ ,  $L_1 = 2.25 \theta_3$ ,  $L_2 = 1 \theta_4$ ,  $\Phi_{pump\_boil} = 1.62 \cdot 10^{-3} \theta_5$ ,  $\Phi_{pump\_l} = 1.62 \cdot 10^{-3} \theta_6$ ,  $\Phi_{m\_CO2} = 1 \cdot 10^{-5} A_s \cdot \theta_7$ . Remember:  $\theta$  is changed instead of the actual model parameter to prevent scaling problems.

From the sensitivity analysis it was found that data set 040323 was better suited for parameter estimation than 040925, since the modified E-criterion  $\varphi_E(\tilde{F})$  of the Fisher information matrix (eqn. 3.280) was lower ( $2.7 \cdot 10^4$  compared to  $5.2 \cdot 10^5$ ).

The Fisher information matrix  $\tilde{F}$  of the relative sensitivities is determined for these 7 parameters (the lower triangular part is omitted since it is identical to the upper triangular part).

$\tilde{F} = 10^4$	<b>0.39</b>	0.24	-0.34	-0.34	-0.00	0.02	0.02	$c_{Tsk}$
		<b>1.51</b>	0.12	0.13	-0.04	-0.04	-1.09	$\tau_{difR}$
			<b>4.87</b>	4.97	-0.11	0.06	-3.53	$L_1$
				<b>5.08</b>	-0.11	0.06	-3.62	$L_2$
					<b>0.07</b>	-0.03	0.23	$\Phi_{pump\_boil}$
						<b>0.04</b>	-0.08	$\Phi_{pump\_l}$
							<b>6.40</b>	$\Phi_{m\_CO2}$
	$c_{Tsk}$	$\tau_{difR}$	$L_1$	$L_2$	$\Phi_{pump\_boil}$	$\Phi_{pump\_l}$	$\Phi_{m\_CO2}$	

From the values on the diagonal it can be seen that the model is not equally sensitive to all parameters.

For this  $\tilde{F}$ -matrix the D-criterion (information content, eqn. 3.279) and the modified E-criterion (parameter identification, eqn. 3.280) are determined:  $\varphi_D(\tilde{F}) = 8.6 \cdot 10^{22}$ ,  $\varphi_E(\tilde{F}) = 2.7 \cdot 10^4$ . The high value for  $\varphi_D(\tilde{F})$  indicates that the experiment data has a high information content. The high value for  $\varphi_E(\tilde{F})$  indicates that some parameters are correlated.

To minimize  $\varphi_E$ , the parameter  $L_1$  (window length) is removed from the set, since it is highly correlated to  $L_2$  (window height). This gives a D-criterion  $\varphi_D(\tilde{F}) = 8.5 \cdot 10^{21}$  and a modified E-criterion  $\varphi_E(\tilde{F}) = 4.9 \cdot 10^2$ , which is a significant improvement. This finally leaves 6 parameters to calibrate:  $c_{Tsk}$ ,  $\tau_{difR}$ ,  $L_2$ ,  $\Phi_{pump\_boil}$ ,  $\Phi_{pump\_l}$  and  $\Phi_{m\_CO2}$ .

The Fisher information matrix gives an indication of the parameters that are most important. The relative sensitivity trajectories  $\tilde{x}_\theta(t)$  (eqn. 3.277) as a function of time  $t$  indicate the sensitivity of the different state variables to the calibration parameters at each time  $t$ .

These relations are given here (more pluses indicate stronger influence)

	$T_a$	$T_{as}$	$T_c$	$T_{ri}$	$T_s$	$T_l$	$T_u$	$T_{sc}$	$C_{a\_CO2}$	$C_{as\_CO2}$	$C_{a\_H2O}$	$C_{as\_H2O}$	$W$
$c_{Tsk}$		+		+			+	+	+	+	++	++	+
$\tau_{difR}$	+	+	+	+			+		++	++	++	++	++
$L_2$	+	+	+	+			+		++	++	++	++	+
$\Phi_{pump\_boil}$									++	++			
$\Phi_{pump\_l}$						+			++	++	+	+	+
$\Phi_{m\_CO2}$									++	++	+	+	++

This shows that:

- Temperature  $T_s$  cannot be corrected with any of the parameters.
- Temperatures  $T_a$  and  $T_c$  can be corrected with the parameters  $\tau_{difR}$  and  $L_2$ .
- Temperatures  $T_{as}$ ,  $T_{ri}$  and  $T_u$  can be corrected with the parameters  $c_{Tsk}$ ,  $\tau_{difR}$  and  $L_2$ .
- Temperature  $T_l$  can be corrected with the parameter  $\Phi_{pump\_l}$ .
- Temperature  $T_{sc}$  can be corrected with the parameter  $c_{Tsk}$ .
- CO<sub>2</sub> concentrations  $C_{a\_CO2}$  and  $C_{as\_CO2}$  can be corrected with all parameters.
- H<sub>2</sub>O concentrations  $C_{a\_H2O}$  and  $C_{as\_H2O}$  and total biomass  $W$  can be corrected with all parameters except  $\Phi_{pump\_boil}$ .

### 3.9.3 Parameter estimation

To calibrate the 6 parameters, the measured states ( $T_a$ ,  $T_{as}$ ,  $T_c$ ,  $T_{ri}$ ,  $C_{a\_CO2}$ ,  $C_{a\_H2O}$ ) have to be compared to the simulated states. The parameters are fitted on one day of data (040323). The initial state values are based on the measured values when they are available. Otherwise an estimate is made from the known values. These estimates are specified in table 3.3. It is assumed that the time constants are smaller than  $\frac{1}{3}$  of a day.

The Matlab® procedure *lsqnonlin* is used for the parameter fit. The differences between the simulation and the measurement ( $T_a$ ,  $T_{as}$ ,  $T_c$ ,  $T_{ri}$ ,  $C_{a\_CO2}$ ,  $C_{a\_H2O}$ ) are scaled with a factor  $c_m = \{3, 1, 1, 1, 5000, 4000\}$  to get about the same amplitude range. The temperatures  $T_{as}$ ,  $T_c$  and  $T_{ri}$  are weighed less strong, since they are less important than  $T_a$ ,  $C_{a\_CO2}$  and  $C_{a\_H2O}$ . The sampling time  $\Delta t$  of the data is 1 min, which gives a time vector of  $\frac{t_f}{\Delta t} = 1440$  discrete time steps. This gives  $n_m = 6$  vectors of 1440 data points.

Table 3.3: Initial values states

symbol	initial value	symbol	initial value
$C_{a\_CO2}$	measured	$T_a$	measured
$C_{a\_H2O}$	measured	$T_{as}$	measured
$S_T$	0	$T_c$	measured
$W$	0*	$T_{ri}$	measured
$C_{as\_CO2}$	$\begin{cases} \frac{1}{2} C_{a\_CO2} + \frac{1}{2} C_{o\_CO2} & \text{if } c_{sc} = 1 \\ C_{a\_CO2} & \text{if } c_{sc} = 0 \end{cases}$	$T_l$	$\begin{cases} \frac{1}{3} T_a + \frac{2}{3} T_{in\_l} & \text{if } vp_l = 1 \\ T_a & \text{if } vp_l = 0 \end{cases}$
$C_{as\_H2O}$	$\begin{cases} \frac{1}{2} C_{a\_H2O} + \frac{1}{2} C_{o\_H2O} & \text{if } c_{sc} = 1 \\ C_{a\_H2O} & \text{if } c_{sc} = 0 \end{cases}$	$T_u$	$\begin{cases} \frac{1}{3} T_a + \frac{2}{3} T_{in\_u} & \text{if } vp_u = 1 \\ T_a & \text{if } vp_u = 0 \end{cases}$
$T_{sc}$	$\frac{1}{2} T_a + \frac{1}{2} T_{as}$	$T_s$	$\frac{1}{2} T_{sub\_slab}^{**} + \frac{1}{2} (T_0 + 15)$

\*It is assumed that the crop is fully grown ( $LAI = 3$ ). There is no measurement of  $W$  to compare with, and since the biomass increase is a function of the  $LAI$  (not of the biomass  $W$ ) the initial value does not matter.

\*\* $T_{sub\_slab}$  is the measured temperature substrate slab. The average temperature of the subsoil is 15°C (see eqn. 3.132).

The error  $\epsilon$  to minimize (weighed least squares) is defined as

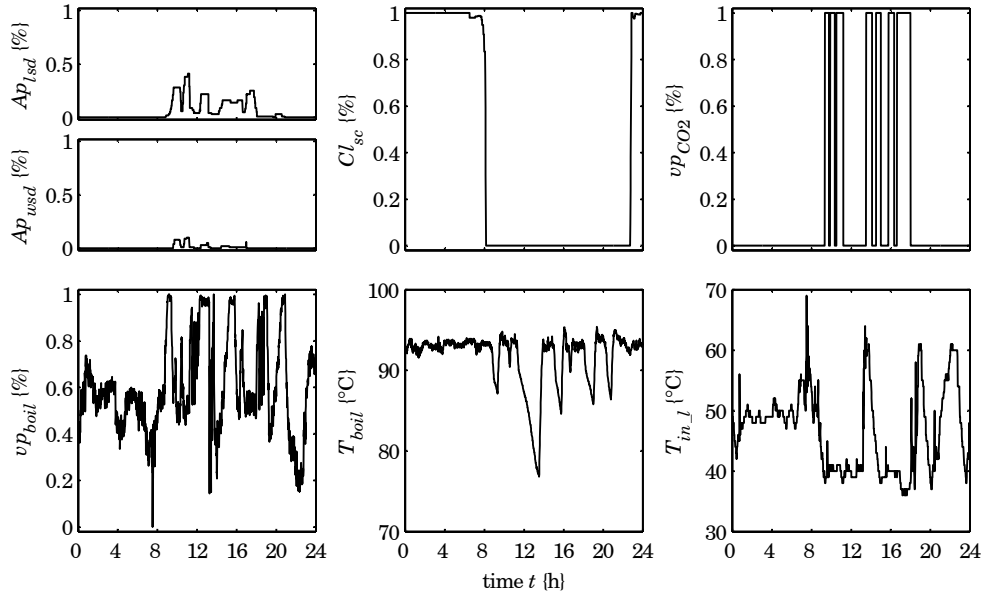
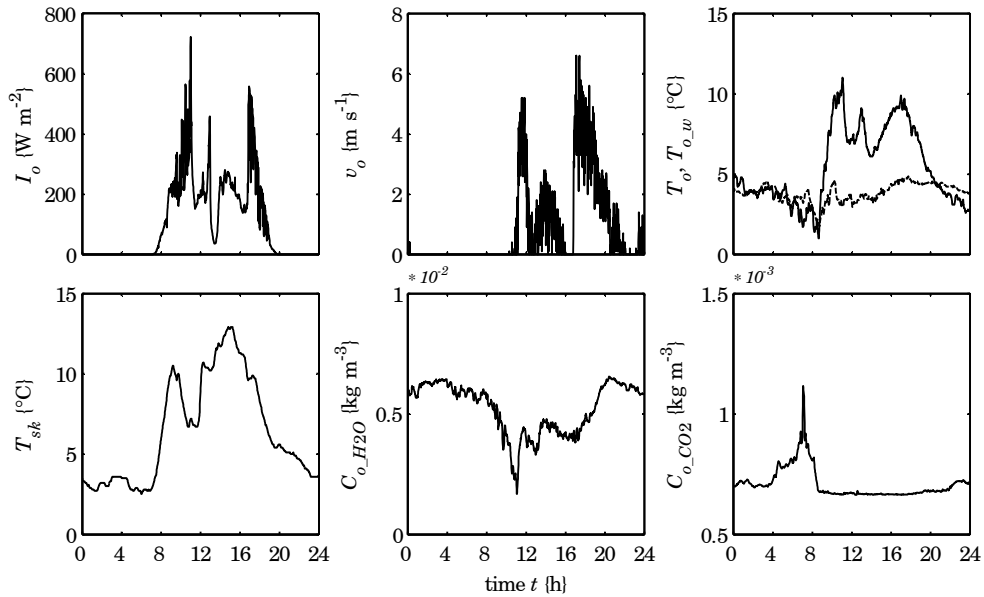
$$\epsilon(\theta) = \sum_{i_m=1}^{n_m} c_m(i_m) \cdot \sqrt{\sum_{k_\nu=1}^{\frac{t_f}{\Delta t}} (x_{meas}(k_\nu, i_m) - x_{sim}(k_\nu, i_m, \theta))^2} \quad \{-\} \quad (3.200)$$

where  $x_{meas}$  and  $x_{sim}$  are the measured and the simulated state values at discrete time step  $k_\nu$   $\{-\}$ .

The following 6 parameter values are found from the parameter calibration:  $\theta = [0.6, 0.55, 1, 1, 1, 0.4]$ , which gives:  $c_{Tsk} = 0.6$ ,  $\tau_{difR} = 0.55$ ,  $L_2 = 1$ ,  $\Phi_{pump\_boil} = 1.62 \cdot 10^{-3}$ ,  $\Phi_{pump\_l} = 1.62 \cdot 10^{-3}$  and  $\Phi_{m\_CO2} = 0.4 \cdot 10^{-5} A_s$ .

The control inputs, the external inputs and the measured and simulated states are given in figures 3.10, 3.11 and 3.12. The lower net heating pump is on ( $vp_l = 1$ ).

From these results it can be seen that after calibration the greenhouse with crop model gives a good description of the dynamic behaviour. The temperatures  $T_a$  and  $T_c$  of the indoor air and the crop and the humidity  $C_{a\_H2O}$  are well described. The  $CO_2$  concentration  $C_{a\_CO2}$  fits less good. Although the dynamics seem quite good, there is a static deviation during nighttime. Since the deviation is during the night, the problem is not that bad. The  $CO_2$  concentration influences the total biomass  $W$  mainly through the photosynthesis rate  $P_g$  during daytime. These terms are important in the optimal control concept, so they should match well.

Figure 3.10: Estimation: control inputs  $u$ , data set 040323Figure 3.11: Estimation: external inputs  $v$ , data set 040323

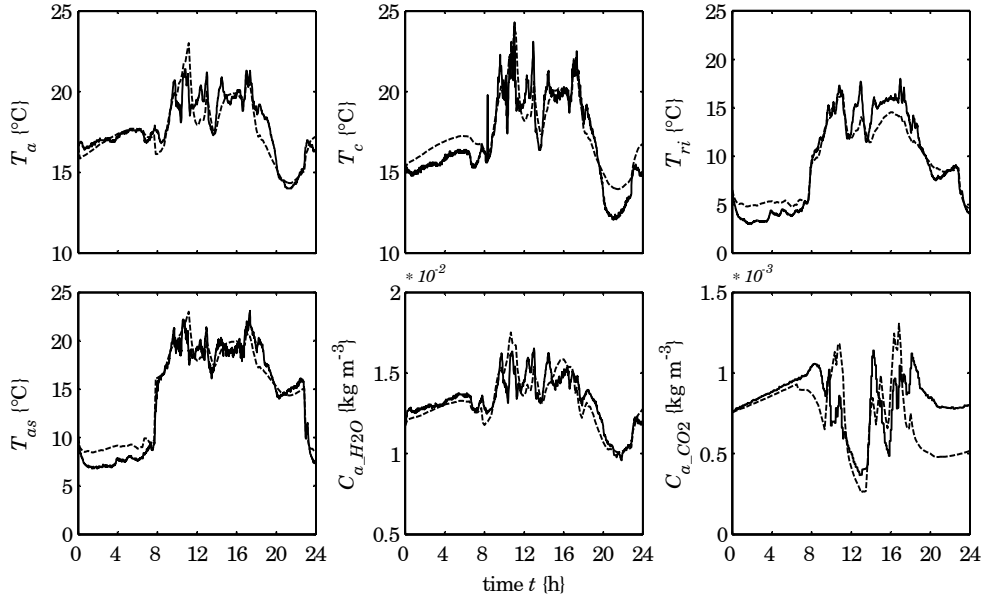


Figure 3.12: Estimation: measured (—) and simulated (---) states  $x$ , data set 040323

The average deviation and the standard deviation between the simulated and the measured states are given in table 3.4.

Table 3.4: Average deviation and standard deviation between simulation and measurement

data set		$\Delta T_a$	$\Delta T_{as}$	$\Delta T_c$	$\Delta T_{ri}$	$\Delta C_{a\_H2O}$ $\cdot 10^{-3}$	$\Delta C_{a\_CO2}$ $\cdot 10^{-4}$
040323	total	0.2 (0.8)	0.3 (1.2)	0.5 (1.0)	0.1 (1.4)	0.2 (0.8)	1.8 (4.0)
	day	0.4 (1.1)	0.1 (1.3)	0.1 (1.1)	1.1 (1.1)	0.1 (1.0)	1.1 (4.8)
	night	0.0 (0.3)	0.8 (1.0)	1.1 (0.4)	0.9 (0.6)	0.2 (0.3)	2.7 (2.7)
040617	total	0.4 (1.1)	0.6 (1.0)	0.1 (1.1)	2.1 (1.3)	0.2 (0.8)	2.4 (1.6)
	day	0.3 (1.3)	0.6 (1.2)	0.1 (1.2)	2.5 (1.2)	0.1 (0.9)	1.9 (1.6)
	night	0.5 (0.4)	0.6 (0.4)	0.5 (0.4)	1.0 (0.7)	0.3 (0.5)	3.6 (0.5)
040910	total	0.6 (1.8)	0.2 (1.5)	1.3 (2.5)	0.9 (2.4)	1.5 (2.6)	3.7 (1.5)
	day	1.0 (2.2)	0.2 (1.8)	1.3 (3.1)	2.0 (2.6)	1.9 (3.4)	4.5 (1.1)
	night	0.2 (1.2)	0.1 (1.0)	1.3 (1.5)	0.5 (1.1)	1.1 (0.8)	2.7 (1.3)

Furthermore the following is observed from the measured data:

- The temperature  $T_{ri}$  of the roof indoor side is closely related to the temperatures  $T_{as}$  and  $T_o$  of the indoor air above the screen and the outdoor air. During the night (without ventilation) it is closer to  $T_o$ , while during daytime (with ventilation) it is about the average of  $T_{as}$  and  $T_o$ .

- The difference between the temperatures  $T_a$  and  $T_c$  of the indoor air below the screen and the crop is smaller than  $2^\circ\text{C}$ .
- The difference between the temperatures  $T_a$  and  $T_{as}$  of the indoor air below and above the screen is smaller than  $1.5^\circ\text{C}$  when the screen is open ( $Cl_{sc} = 0$ ). The model assumes this difference to be  $0^\circ\text{C}$  (perfectly mixed).
- The time between a change in the outdoor shortwave solar radiation  $I_o$  and the temperature  $T_a$  of the indoor air below the screen is about 5 min.
- The time between  $\text{CO}_2$  supply with valve  $vp_{\text{CO}_2}$  and the change in  $\text{CO}_2$  concentration  $C_{a,\text{CO}_2}$  of the indoor air is about 18 min.
- The time between the aperture  $Ap_{l\text{sd}}$  and  $Ap_{w\text{sd}}$  of the windows and the change in humidity  $C_{a,\text{H}_2\text{O}}$  is about 40 min.

The latter three observations indicate that the assumption that the time constants are smaller than  $\frac{1}{3}$  of a day is valid.

To verify the overall validity of the parameter values, they are subsequently used on other data sets in other seasons (040617 and 040910). These results are given in figures 3.13 and 3.14. The average deviation and the standard deviation between the simulated and the measured states are given in table 3.4. From these results, it can be seen that the simulations give a fair fit of the measurements. The deviation in the  $\text{CO}_2$  concentration is again seen.

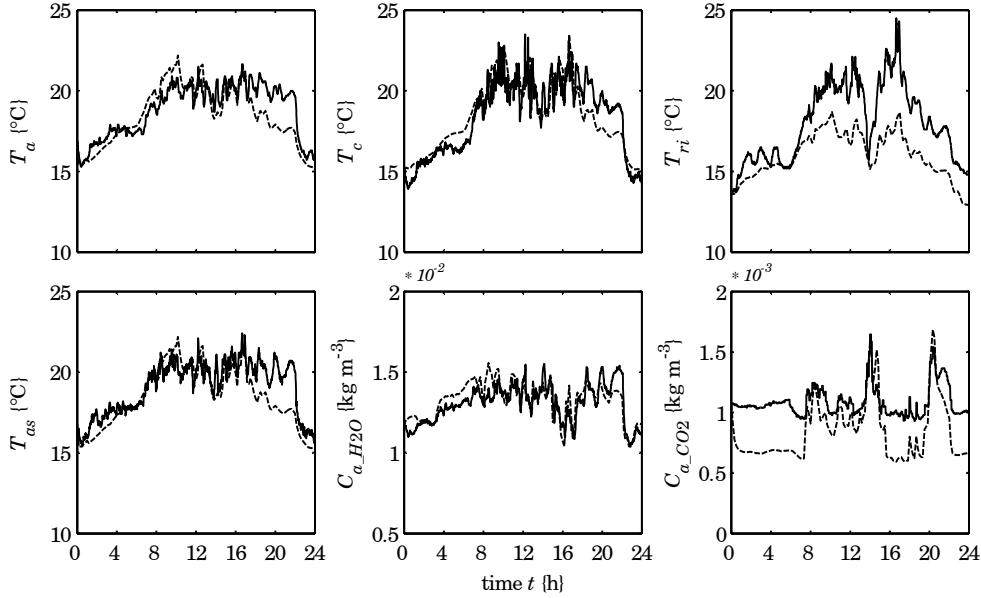


Figure 3.13: Validation: measured (—) and simulated (---) states  $x$ , data set 040617

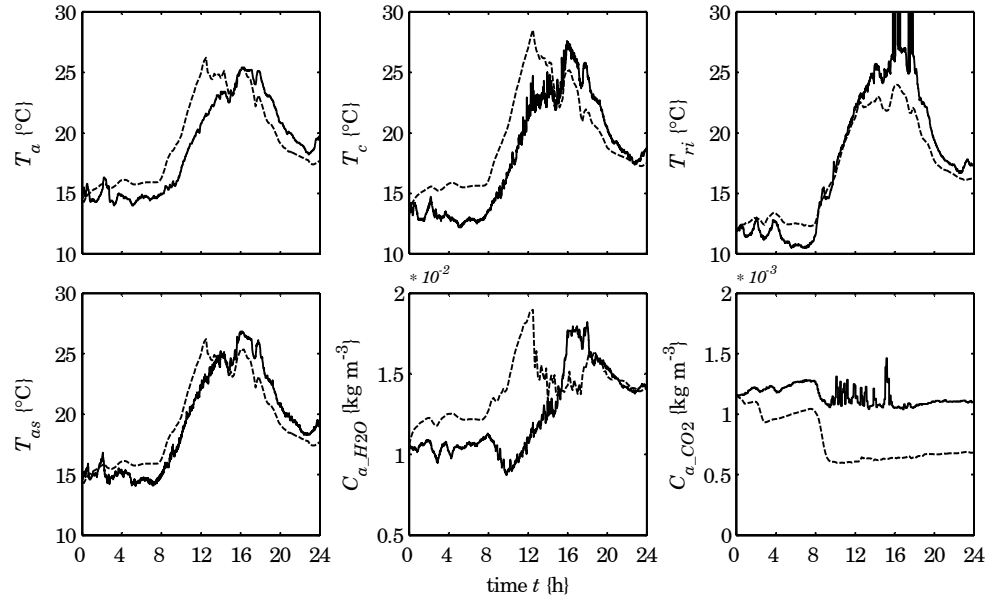


Figure 3.14: Validation: measured (—) and simulated (---) states  $x$ , data set 040910

All calibrated parameters are assumed to have a fixed value during the day. The parameter  $c_{T_{sk}}$  describes the fraction of clouded sky, which is unlikely to stay the same all day. It is therefore strongly recommended to measure the sky temperature  $T_{sk}$ , instead of computing it. This is expected to further enhance the accuracy of the calibrated model. For 040323 the value  $c_{T_{sk}} = 0.6$  was found in the parameter estimation. If this parameter is estimated for 040617 and 040910 (keeping all other parameters as found for 040323), the fraction of the clouded sky is 0.77 and 0.24 respectively.

## References

- K. Bernaerts and J.F. van Impe (2004). Data-driven approaches to the modelling of bioprocesses. *Transactions of the institute of measurement and control*, 26(5), pp. 349–372.
- G.P.A. Bot (1983). *Greenhouse climate: from physical processes to a dynamic model*. Ph.D. thesis, Wageningen Agricultural University, Wageningen, The Netherlands. 240 p.
- J.J.G. Breuer, H.F. de Zwart, and G.P.A. Bot (1999). Aspecten warmtepompen. IMAG-DLO, nota 99–130, Wageningen, The Netherlands. (in Dutch).
- T. de Jong (1990). *Natural ventilation of large multi-span greenhouses*. Ph.D. thesis, Wageningen Agricultural University, Wageningen, The Netherlands.

- H.F. de Zwart (1996). *Analyzing energy-saving options in greenhouse cultivation using a simulation model*. Ph.D. thesis, Wageningen Agricultural University, Wageningen, The Netherlands. 236 p.
- J. Goudriaan (1987). *Simulatie van gewasgroei*. Wageningen Agricultural University, the Netherlands. (in Dutch).
- L. Heesen (1997). *Definitie, gevoeligheidsanalyse en evaluatie van een dynamisch model van het kas-gewasproductieproces*. M.Sc. thesis, Wageningen Agricultural University, Wageningen, The Netherlands. (in Dutch).
- J.L. Monteith and M.H. Unsworth (1990). *Principles of environmental physics*. Edward Arnold, London, United Kingdom, 2<sup>nd</sup> edition. 291 p.
- A. Munack (1991). *Biotechnology, a multi-volume comprehensive treatise, Measuring, modelling and control*, vol. 4, chapter 8: Optimization of sampling, pp. 252–264. VCH, Weinheim, Germany. Editors: H.-J. Rehm, G. Reed, A. Pühler, and P. Stadler.
- W.H. Press, B.P. Flannery, S.A. Teukolsky, and W.T. Vetterling (1986). *Numerical recipes*. Cambridge University Press, Cambridge, United Kingdom, 2<sup>nd</sup> edition. 291 p.
- E.M. Sparrow and R.D. Cess (1970). *Radiation heat transfer*. Brooks/Cole Publishers, Belmont, U.S.A., rev. ed. edition. 340 p.
- C. Stanghellini (1987). *Transpiration of greenhouse crops — an aid to climate management*. Ph.D. thesis, Wageningen Agricultural University, Wageningen, The Netherlands. 150 p.
- J.A. Stoffers (1989). *Tuinbouwtechnische aspecten van de druppelprofieling bij kasverwarmingsbuis*. Intern rapport, IMAG-DLO, Wageningen, The Netherlands. (in Dutch), 24 p.
- R.F. Tap (2000). *Economics-based optimal control of greenhouse tomato crop production*. Ph.D. thesis, Wageningen Agricultural University, Wageningen, The Netherlands.
- E.J. van Henten (1994). *Greenhouse climate management: an optimal control approach*. Ph.D. thesis, Wageningen Agricultural University, Wageningen, The Netherlands. 329 p.
- A.J.M. van Kimmenade (1986). *Warmteleer voor technici*. Educaboek B.V., Culemborg, the Netherlands. 576 p.
- R.J.C. van Ooteghem (2002). *New heating model*. Internal report, Wageningen University, Wageningen, The Netherlands.
- A. van Strien (1988). *Klimaat in een enkel- en dubbeldekskas — metingen en simulaties*. M.Sc. thesis, Wageningen Agricultural University, Wageningen, The Netherlands. (in Dutch), 2 dl.
- E. Walter and L. Pronzato (1997). *Identification of parametric models*. Springer, Masson, Great Britain. 159 p.

## Appendices chapter 3

### 3.A View factors

View factors are basic functions used to compute how much radiation energy two generic surfaces exchange. The view factor  $F_{A-B}$  between two generic surfaces  $A$  and  $B$  is a geometric function depending on their size, separation distance and orientation, defined as  $\frac{W_{A-B}}{W_A}$ , namely the fraction of the power emerging from  $A$  directly intercepted by  $B$ .

It is assumed that the upper net pipes are above the canopy and the lower net and upper cooling net pipes are below the canopy. There is a thermal screen with thermal screen closure  $Cl_{sc} \in [0, 1]$ , where 0 indicates ‘screen fully opened’ and 1 indicates ‘screen fully closed’. The screen is placed above the canopy and the upper net. A summary of the view factor equations developed in §3.A.1–3.A.5 is given in §3.A.6.

#### 3.A.1 Lower net

In the computation the view factor between the lower net pipes themselves is neglected. It is assumed that half of the pipe ‘sees’ the roof, and the other half ‘sees’ the soil (van Strien, 1988).

The view factor  $F_{l-s}$  from the lower net to the soil is

$$F_{l-s} = 0.5 \quad \{-\} \quad (3.201)$$

The view factors  $F_{l-ri}$  and  $F_{l-sc}$  from the lower net to the indoor side of the roof and the screen are

$$F_{l-ri} = 0.5 (1 - Cl_{sc}) \cdot \tau_{c-ll} \quad \{-\} \quad (3.202)$$

$$F_{l-sc} = 0.5 Cl_{sc} \cdot \tau_{c-ll} \quad \{-\} \quad (3.203)$$

where  $Cl_{sc} \in [0, 1]$  is the thermal screen closure and  $\tau_{c-ll} \{-\}$  (eqn. 3.73) is the transmittance of longwave radiation by the canopy.

The sum of the view factors of a body has to equal 1, which gives the view factor  $F_{l-c}$  from the lower net to the canopy

$$F_{l-c} = 1 - F_{l-s} - F_{l-ri} - F_{l-sc} \quad \{-\} \quad (3.204)$$

### 3.A.2 Upper net and upper cooling net

In the computation the view factor between the upper net pipes themselves is neglected. It is assumed that half of the pipe ‘sees’ the roof (van Strien, 1988). The equations for the view factors for the upper net ( $u$ ) and the upper cooling net ( $uc$ ) are the same.

The view factors  $F_{u,ri}$  and  $F_{u,sc}$  from the upper net to the indoor side of the roof and the screen are

$$F_{u,ri} = 0.5 (1 - Cl_{sc}) \quad \{-\} \quad (3.205)$$

$$F_{u,sc} = 0.5 Cl_{sc} \quad \{-\} \quad (3.206)$$

where  $Cl_{sc} \in [0, 1]$  is the thermal screen closure.

If the canopy is uniform (no rows) with a uniform overcast sky, a spherical leaf angle distribution and black leaves, the longwave radiation shows an exponential extinction of the transmittance  $\tau_{c,II} = e^{-k_{c,II} \cdot LAI}$  (eqn. 3.73) (Goudriaan, 1987).

The view factor  $F_{u,s}$  from the upper net to the soil is then described by

$$F_{u,s} = 0.5 \tau_{c,II} \quad \{-\} \quad (3.207)$$

The sum of the view factors of a body has to equal 1, which gives the view factor  $F_{u,c}$  from the upper net to the canopy

$$F_{u,c} = 1 - F_{u,ri} - F_{u,sc} - F_{u,s} \quad \{-\} \quad (3.208)$$

where  $F_{u,ri}$ ,  $F_{u,sc}$  and  $F_{u,s} \{-\}$  are the view factors from the upper net to the indoor side of the roof, the screen and the soil.

### 3.A.3 Soil

Most of the view factors can be computed from the reverse view factor by multiplying by the ratio of the surface areas.

The view factor  $F_{s,l}$  from the soil to the lower net is

$$F_{s,l} = \frac{A_l}{A_s} \cdot F_{l,s} \quad \{-\} \quad (3.209)$$

The view factor  $F_{s,u}$  from the soil to the upper net is

$$F_{s,u} = \frac{A_u}{A_s} \cdot F_{u,s} \quad \{-\} \quad (3.210)$$

The view factor  $F_{s_{uc}}$  from the soil to the upper cooling net is

$$F_{s_{uc}} = \frac{A_{uc}}{A_s} \cdot F_{uc_s} \quad \{-\} \quad (3.211)$$

where  $A_s$ ,  $A_l$ ,  $A_u$  and  $A_{uc}$   $\{\text{m}^2\}$  are surface areas of the soil, lower net, upper net and upper cooling net.

The part the canopy ‘sees’ from the part going beyond the lower net  $1 - F_{s_l}$ , is  $1 - \tau_{c_{ll}}$ , so the view factor  $F_{s_c}$  from the soil to the canopy is

$$F_{s_c} = (1 - \tau_{c_{ll}}) \cdot (1 - F_{s_l}) \quad \{-\} \quad (3.212)$$

where  $\tau_{c_{ll}}$   $\{-\}$  is the transmittance of longwave radiation by the canopy.

The sum of the view factors of a body has to equal 1, which gives the view factors  $F_{s_{ri}}$  and  $F_{s_{sc}}$  from the soil to the indoor side of the roof and the screen

$$F_{s_{ri}} = (1 - Cl_{sc}) \cdot (1 - F_{s_c} - F_{s_l} - F_{s_u} - F_{s_{uc}}) \quad \{-\} \quad (3.213)$$

$$F_{s_{sc}} = Cl_{sc} \cdot (1 - F_{s_c} - F_{s_l} - F_{s_u} - F_{s_{uc}}) \quad \{-\} \quad (3.214)$$

where  $Cl_{sc} \in [0, 1]$  is the thermal screen closure.

### 3.A.4 Roof

The view factor  $F_{ri_{ro}}$  from the roof indoor to the outdoor side of the roof is

$$F_{ri_{ro}} = 1 \quad \{-\} \quad (3.215)$$

since the indoor and the outdoor side of the roof are parallel glass panes.

The view factors of objects under an angle is found in Sparrow and Cess (1970). The view factor  $F_{ro_{sk}}$  from the outdoor side of the roof to the sky is

$$F_{ro_{sk}} = 1 \cdot \frac{A_s}{A_r} = \cos(\gamma) \quad \{-\} \quad (3.216)$$

where  $\gamma$   $\{\text{rad}\}$  is the angle of the roof with the horizontal plane.

The part the canopy ‘sees’ from the part going beyond the upper heating and cooling net  $F_{ro_{sk}} - 0.5 \frac{A_u}{A_r} - 0.5 \frac{A_{uc}}{A_r}$ , is  $1 - \tau_{c_{ll}}$ , so the view factor  $F_{ri_c}$  from the indoor side of the roof to the canopy is

$$F_{ri_c} = (1 - Cl_{sc}) \cdot (1 - \tau_{c_{ll}}) \cdot \left( F_{ro_{sk}} - 0.5 \frac{A_u}{A_r} - 0.5 \frac{A_{uc}}{A_r} \right) \quad \{-\} \quad (3.217)$$

where  $0.5 \frac{A_u}{A_r}$  and  $0.5 \frac{A_{uc}}{A_r}$   $\{-\}$  are the view factors from the roof to the upper net and the upper cooling net (without the correction for the screen) and  $\tau_{c_{ll}}$   $\{-\}$  is the transmittance of longwave radiation by the canopy.

### 3.A.5 Screen

The view factor  $F_{sc,ri}$  from the screen to the indoor side of the roof is

$$F_{sc,ri} = Cl_{sc} \quad \{-\} \quad (3.218)$$

where  $Cl_{sc} \in [0, 1]$  is the thermal screen closure.

The part the canopy ‘sees’ from the part going beyond the upper heating and cooling net  $1 - 0.5 \frac{A_u}{A_{sc}} - 0.5 \frac{A_{uc}}{A_{sc}}$ , is  $1 - \tau_{c,Il}$ , so the view factor  $F_{c,sc}$  from the canopy to the screen is

$$F_{c,sc} = Cl_{sc} \cdot (1 - \tau_{c,Il}) \cdot \left(1 - 0.5 \frac{A_u}{A_{sc}} - 0.5 \frac{A_{uc}}{A_{sc}}\right) \quad \{-\} \quad (3.219)$$

where  $A_u$  and  $A_{uc}$   $\{m^2\}$  are surface areas of the upper net and upper cooling net,  $0.5 \frac{A_u}{A_{sc}}$  and  $0.5 \frac{A_{uc}}{A_{sc}}$   $\{-\}$  are the view factors from the screen to the upper net and the upper cooling net (without the correction for the screen) and  $\tau_{c,Il}$   $\{-\}$  is the transmittance of longwave radiation by the canopy.

### 3.A.6 Summary

In table 3.5 a summary is given of the view factors derived in the previous paragraphs. The values of the view factors, for the values used in the solar greenhouse model, are given in table 3.6.

Table 3.5: View factors  $\{-\}$

$F_{l,ri} = 0.5(1 - Cl_{sc}) \cdot \tau_{c,Il}$	$F_{uc,ri} = 0.5(1 - Cl_{sc})$
$F_{l,sc} = 0.5 Cl_{sc} \cdot \tau_{c,Il}$	$F_{uc,sc} = 0.5 Cl_{sc}$
$F_{l,s} = 0.5$	$F_{uc,s} = 0.5 \tau_{c,Il}$
$F_{l,c} = 1 - F_{l,s} - F_{l,ri} - F_{l,sc}$	$F_{uc,c} = 1 - F_{uc,ri} - F_{uc,sc} - F_{uc,s}$
$F_{u,ri} = 0.5(1 - Cl_{sc})$	$F_{s,l}^* = \frac{A_l}{A_s} \cdot F_{l,s}$
$F_{u,sc} = 0.5 Cl_{sc}$	$F_{s,uc}^* = \frac{A_{uc}}{A_s} \cdot F_{uc,s}$
$F_{u,s} = 0.5 \tau_{c,Il}$	$F_{s,u}^* = \frac{A_u}{A_s} \cdot F_{u,s}$
$F_{u,c} = 1 - F_{u,ri} - F_{u,sc} - F_{u,s}$	$F_{s,c} = (1 - \tau_{c,Il}) \cdot (1 - F_{s,l})$
$F_{ro,sk} = 1 \cdot \frac{A_s}{A_r} = \cos(\gamma)$	$F_{s,ri} = (1 - Cl_{sc}) \cdot (1 - F_{s,c} - F_{s,l} - F_{s,u} - F_{s,uc})$
$F_{ri,ro} = 1$	$F_{s,sc} = Cl_{sc} \cdot (1 - F_{s,c} - F_{s,l} - F_{s,u} - F_{s,uc})$
$F_{ri,c} = (1 - Cl_{sc}) \cdot (1 - \tau_{c,Il}) \cdot$ $\left(F_{ro,sk} - 0.5 \frac{A_u}{A_r} - 0.5 \frac{A_{uc}}{A_r}\right)$	$F_{c,sc} = Cl_{sc} \cdot (1 - \tau_{c,Il}) \cdot \left(1 - 0.5 \frac{A_u}{A_{sc}} - 0.5 \frac{A_{uc}}{A_{sc}}\right)$
$F_{sc,ri} = Cl_{sc}$	

\*Intermediate variables.

Table 3.6: View factor values with screen open ( $Cl_{sc} = 0$ ) and closed ( $Cl_{sc} = 1$ )

view factor	screen open ( $Cl_{sc} = 0$ )	screen closed ( $Cl_{sc} = 1$ )	view factor	screen open ( $Cl_{sc} = 0$ )	screen closed ( $Cl_{sc} = 1$ )
$F_{l_{ri}}$	0.0733	0	$F_{uc_{ri}}$	0.5000	0
$F_{l_{sc}}$	0	0.0733	$F_{uc_{sc}}$	0	0.5000
$F_{l_{s}}$	0.5000	0.5000	$F_{uc_{s}}$	0.0733	0.0733
$F_{l_{c}}$	0.4267	0.4267	$F_{uc_{c}}$	0.4267	0.4267
$F_{u_{ri}}$	0.5000	0	$F_{s_{l}}^*$	0.0979	0.0979
$F_{u_{sc}}$	0	0.5000	$F_{s_{uc}}^*$	0.0574	0.0574
$F_{u_{s}}$	0.0733	0.0733	$F_{s_{u}}^*$	0.0079	0.0079
$F_{u_{c}}$	0.4267	0.4267	$F_{s_{c}}$	0.7698	0.7698
$F_{ro_{sk}}$	0.9272	0.9272	$F_{s_{ri}}$	0.0670	0
$F_{ri_{ro}}$	1	1	$F_{s_{sc}}$	0	0.0670
$F_{ri_{c}}$	0.4389	0	$F_{c_{sc}}$	0	0.4733
$F_{sc_{ri}}$	0	1			

\*Intermediate variables.

Computation with (rounded values):  $\tau_{c_{ll}} = 0.1466$ ,  $\gamma = 22^\circ$  and surface areas  $\{m^2\}$   $A_l = 614.05$ ,  $A_u = 337.12$ ,  $A_{uc} = 2456.19$ ,  $A_s = 3136$ ,  $A_r = 3382.28$  and  $A_{sc} = 3136$ .

## 3.B Derivation temperature leaving heating or cooling net

### 3.B.1 Original heating net model

The best way to get an accurate description of the ingoing and outgoing temperature is to describe them with partial differential equations over small segments of pipe (de Zwart, 1996). This gives a large number of differential equations (distributed parameter system) to describe these temperatures, which is not wanted for optimal control, since it increases computation time exponentially.

An approximation has been derived for the energy content of the heating or cooling net and the ingoing and outgoing temperatures with only one differential equation (van Ooteghem, 2002).

The derivation of the temperature leaving the heating or cooling net is described here for the lower net. The same equations also apply for the upper heating net and the upper cooling net. The temperature of the net is described by three temperatures: the temperature entering the net  $T_{in,l}$ , the temperature leaving the net  $T_{out,l}$  and the temperature of the net  $T_l$ . The latter temperature is the result of numerical integration of a differential equation. It is not an actual temperature but a measure for the energy content

of the heating net. The ingoing and outgoing temperature describe actual temperatures.

Given the differential equation

$$\frac{dT_l}{dt} = \frac{Q_{in,l} - Q_{out,l} + Q_{\Sigma l}}{\rho_{H_2O} \cdot c_{p,H_2O} \cdot V_l} \quad \{\text{K s}^{-1}\} \text{ (eqn. 3.9)}$$

in which the energy transport and transfer terms are given by

$$\begin{aligned} Q_{in,l} &= \rho_{H_2O} \cdot c_{p,H_2O} \cdot \Phi_{in,l} \cdot T_{in,l} & \{\text{W}\} \\ Q_{out,l} &= \rho_{H_2O} \cdot c_{p,H_2O} \cdot \Phi_{in,l} \cdot T_{out,l} & \{\text{W}\} \\ Q_{\Sigma l} &= Q_{rd,l} - Q_{l,a} - Q_{l,c} - Q_{l,ri} - Q_{l,s} - Q_{l,sc} & \{\text{W}\} \end{aligned}$$

This gives

$$\begin{aligned} \frac{dT_l}{dt} &= \frac{\rho_{H_2O} \cdot c_{p,H_2O} \cdot \Phi_{in,l} \cdot (T_{in,l} - T_{out,l}) + Q_{\Sigma l}}{\rho_{H_2O} \cdot c_{p,H_2O} \cdot V_l} & \{\text{K s}^{-1}\} \\ \frac{dT_l}{dt} &= \frac{\Phi_{in,l} \cdot (T_{in,l} - T_{out,l})}{V_l} + \frac{Q_{\Sigma l}}{\rho_{H_2O} \cdot c_{p,H_2O} \cdot V_l} & \{\text{K s}^{-1}\} \\ \frac{dT_l}{dt} &= \frac{\Phi_{in,l} \cdot (T_{in,l} - T_l)}{V_l} + \frac{\Phi_{in,l} \cdot (T_l - T_{out,l})}{V_l} + \frac{Q_{\Sigma l}}{\rho_{H_2O} \cdot c_{p,H_2O} \cdot V_l} & \{\text{K s}^{-1}\} \end{aligned}$$

Now it is assumed that

- the dynamics of the (virtual) temperature  $T_l$  in response to the changes in  $T_{in,l}$  can be approximated by a first order process;
- the energy transfer  $Q_{\Sigma l}$  at temperature  $T_l$  determines the temperature difference between  $T_l$  and  $T_{out,l}$ .

which gives

$$\frac{dT_l}{dt} = \frac{\Phi_{in,l} \cdot (T_{in,l} - T_l)}{V_l} \quad \{\text{K s}^{-1}\}$$

and

$$0 = \frac{\Phi_{in,l} \cdot (T_l - T_{out,l})}{V_l} + \frac{Q_{\Sigma l}}{\rho_{H_2O} \cdot c_{p,H_2O} \cdot V_l} \quad \{\text{K s}^{-1}\}$$

This leads to

$$T_{out,l} = T_l + \frac{Q_{\Sigma l}}{\rho_{H_2O} \cdot c_{p,H_2O} \cdot \Phi_{in,l}} \quad \{\text{K}\}$$

### 3.C Derivation temperature soil

#### 3.C.1 Original soil model

The soil temperature  $T_s$  {K} is described by De Zwart (1996) by a soil model consisting of 6 layers. The thickness {m} of the subsequent layers from the top to the bottom is:  $d_{s0} = 0.01$ ,  $d_{s1} = 0.02$ ,  $d_{s2} = 0.04$ ,  $d_{s3} = 0.08$ ,  $d_{s4} = 0.16$ ,  $d_{s5} = 0.32$  and  $d_{s6} = 0.64$ .

The conductive heat transfer  $Q_{s\{i,i+1\}}$  between two layers  $i$  and  $i + 1$  is

$$Q_{s\{i,i+1\}} = A_s \cdot \frac{\lambda_{s\{i,i+1\}}}{dx_{s\{i,i+1\}}} \cdot (T_{s\{i\}} - T_{s\{i+1\}}) \quad \{\text{W}\} \quad (3.220)$$

where  $A_s$  {m<sup>2</sup>} is the surface area of the soil,  $\lambda_s$  {W m<sup>-1</sup> K<sup>-1</sup>} is thermal conductivity,  $dx_s$  {m} is the distance between the centers of the layers and  $T_s$  {K} is the temperature of the soil layer.

The distances  $dx_{s\{i,i+1\}}$  {m} are:  $dx_{s\{0,1\}} = 0.015$ ,  $dx_{s\{1,2\}} = 0.03$ ,  $dx_{s\{2,3\}} = 0.06$ ,  $dx_{s\{3,4\}} = 0.12$ ,  $dx_{s\{4,5\}} = 0.24$ ,  $dx_{s\{5,6\}} = 0.48$  and  $dx_{s\{6,7\}} = 0.32$ .

The thermal conductivity  $\lambda_{s\{i,i+1\}}$  {W m<sup>-1</sup> K<sup>-1</sup>} is determined from the reciprocal of the weighed mean of the separate reciprocal conductivities. The first 0.03 m are concrete, the next 1.24 m are soil. Using  $\lambda_{concrete} = 1.7$  and  $\lambda_{soil} = 0.85$ , this gives:  $\lambda_{s\{0,1\}} = 1.7$ ,  $\lambda_{s\{1,2\}} = 1.02$ ,  $\lambda_{s\{2,3\}} = \lambda_{s\{3,4\}} = \lambda_{s\{4,5\}} = \lambda_{s\{5,6\}} = \lambda_{s\{6,7\}} = 0.85$ .

The temperature derivatives for the upper ( $s\{0\}$ ) and the lower ( $s\{i\}$ ) soil layers are

$$\frac{dT_{s\{0\}}}{dt} = \frac{Q_{rd,s} - Q_{s\{0,1\}} + Q_{\Sigma s}}{\rho_s \cdot c_{p,s} \cdot A_s \cdot d_{s0}} \quad \{\text{K s}^{-1}\} \quad (3.221)$$

$$\frac{dT_{s\{i\}}}{dt} = \frac{Q_{s\{i-1,i\}} - Q_{s\{i,i+1\}}}{\rho_s \cdot c_{p,s} \cdot A_s \cdot d_{si}} \quad \forall i = 1, 2, \dots, 6 \quad \{\text{K s}^{-1}\} \quad (3.222)$$

in which the energy loss term  $Q_{\Sigma s}$  due to the absorption of longwave radiation by the greenhouse components is given by

$$Q_{\Sigma s} = Q_{a,s} + Q_{l,s} + Q_{uc,s} + Q_{u,s} - Q_{s,c} - Q_{s,ri} - Q_{s,sc} \quad \{\text{W}\}$$

where  $Q_{rd,s}$  {W} (eqn. 3.128) is shortwave radiation absorbed by the soil.

For the volumetric heat capacity of the soil it is assumed that the soil consists of 70% sand, 20% water and 10% air

$$\rho_s \cdot c_{p-s} = 0.7 \rho_{sand} \cdot c_{p-sand} + 0.2 \rho_{H2O} \cdot c_{p-H2O} + 0.1 \rho_a \cdot c_{p-a} \quad \{\text{J m}^{-3} \text{K}^{-1}\} \quad (3.223)$$

where  $\rho$   $\{\text{kg m}^{-3}\}$  are densities and  $c_p$   $\{\text{J kg}^{-1} \text{K}^{-1}\}$  are specific heat capacities, in which:  $\rho_{sand} = 1600$ ,  $c_{p-sand} = 800$ ,  $\rho_{H2O} = 998$ ,  $c_{p-H2O} = 4186$ ,  $\rho_a = 1.29 \frac{T_0}{T_a}$  and  $c_{p-a} = 1000$ .

The temperature of the lowest soil layer is

$$T_{s\{7\}} = T_0 + 15 + 2.5 \sin(1.72 \cdot 10^{-2} (day_{NR} - 140)) \quad \{\text{K}\} \quad (3.224)$$

where  $day_{NR}$  [1,365] is the day number.

### 3.C.2 Simplified soil model

Since we want to use the soil model in an optimal control context, it is favourable to have a small number of differential equations with regard to computation time. The soil model by De Zwart (1996) uses 7 differential equations to describe the soil temperature. This is reduced to one differential equation (one-layer) in the simplified soil model derived here.

The conductive heat transfer  $Q_{s-s2}$  between the upper and the lower soil layer is (as in eqn. 3.220)

$$Q_{s-s2} = A_s \cdot \frac{\lambda_s}{dx_s} \cdot (T_s - T_{s2}) \quad \{\text{W}\} \quad (3.225)$$

where  $A_s$   $\{\text{m}^2\}$  is the surface area of the soil,  $\lambda_s$   $\{\text{W m}^{-1} \text{K}^{-1}\}$  is thermal conductivity,  $T_s$   $\{\text{K}\}$  and  $T_{s2}$  is temperature of soil and subsoil and  $dx_s$   $\{\text{m}\}$  is the distance between the centers of the layers.

The thermal conductivity  $\lambda_s$   $\{\text{W m}^{-1} \text{K}^{-1}\}$  is determined from the reciprocal of the weighed mean of the separate reciprocal conductivities. The first 0.03 m are concrete, the next 1.24 m are soil. This gives the thermal conductivity  $\lambda_s = 0.86 \text{ W m}^{-1} \text{K}^{-1}$ .

The temperature derivative for the single soil layer is (as in eqn. 3.221)

$$\frac{dT_s}{dt} = \frac{Q_{rd-s} - Q_{s-s2} - Q_{\Sigma s}}{\rho_s \cdot c_{p-s} \cdot A_s \cdot d_s} \quad \{\text{K s}^{-1}\} \quad (3.226)$$

where  $Q_{rd,s}$  {W} (eqn. 3.128) is shortwave radiation absorbed by the soil,  $Q_{\Sigma s}$  is the heat loss to the environment and  $\rho_s \cdot c_{p,s}$  {J m<sup>-3</sup> K<sup>-1</sup>} (eqn. 3.223) is the volumetric heat capacity of the soil. The subsoil temperature  $T_{s2} = T_{s\{7\}}$  {K} is given in eqn. 3.224.

The thickness of the layer  $d_s$  {m} and the distance between the centers of the layers  $dx_{s\{0,7\}}$  {m} have to be estimated.

From year-round data it is found that the energy loss  $Q_{\Sigma s}$  varies from about  $-100$  to  $100$  W m<sup>-2</sup>, which is about  $-300000$  to  $300000$  W with a soil surface  $A_s = 3136$  m<sup>2</sup>. No difference is seen between the upward and the downward response with respect to the time constant. In the same year-round data the outdoor shortwave solar radiation  $I_o$  varies from 0 to about  $1000$  W m<sup>-2</sup>. The energy loss to the soil is correlated with the solar radiation, since more heat input from the sun leads to warmer materials and thus more energy loss to the colder surfaces (i.e., the soil). For the estimation it is therefore assumed that  $Q_{\Sigma s} = 300 I_o$ .

For the estimation 6 values are used for the outdoor shortwave solar radiation, which are kept constant year-round:  $I_o = 0, 200, 400, 600, 800$  and  $1000$  W m<sup>-2</sup>. It is assumed that the fraction diffuse radiation in outdoor shortwave solar radiation  $f_{dif} = 1$  (only diffuse radiation),  $Cl_{sc} = 0$  (screen is fully opened) and the temperature of the indoor air above the screen  $T_a = T_0 + 20$  K (the latter is only needed for  $\rho_a$  in eqn. 3.223). The soil temperature of the upper layer (eqn. 3.226) has to comply with the results of the original soil model (eqn. 3.221).

The estimated values are:  $d_s = 0.65$  m and  $dx_{s\{0,7\}} = 1.247$  m. The results are shown in figure 3.15a, where the dash-dotted line represents the temperature of the subsoil  $T_{s2}$ . Although the model is very simple, the estimation is quite good. The estimation error (difference between the original and the simplified soil model) is smaller than  $0.057^\circ\text{C}$  (see figure 3.15b).

### 3.D Derivation temperature roof outdoor side

For the use of the roof model in an optimal control context, a small number of differential equations is desirable with regard to computation time. A roof model of a double layer roof would normally take two differential equations: one for the roof temperature indoor side  $T_{ri}$  and one for the roof temperature outdoor side  $T_{ro}$ . This is reduced to one differential equation in the roof model derived here.

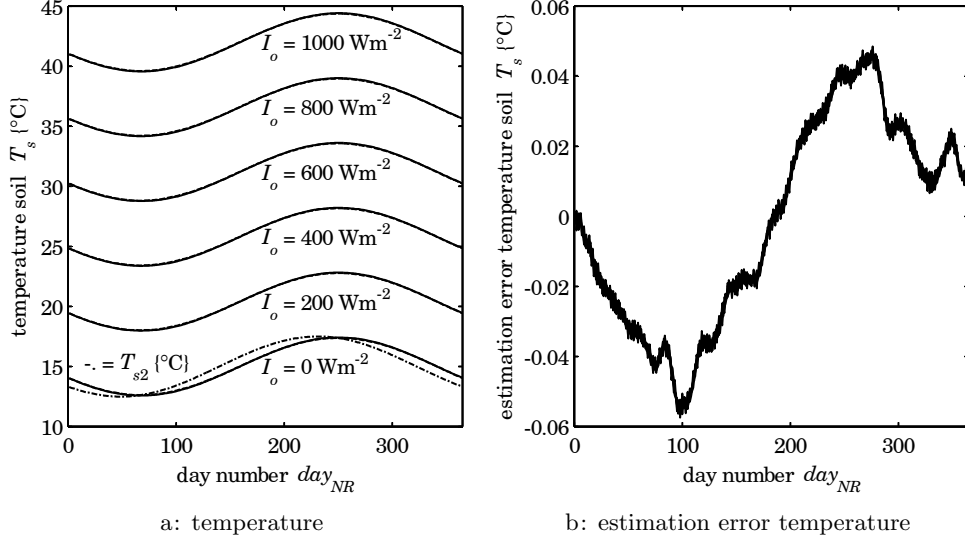


Figure 3.15: Soil temperature  $T_s$  original (—) and simplified (---) model, subsoil temperature  $T_{s2}$  (-·-) and estimation error

The derivatives for the temperatures  $T_{ri}$  {K} (eqn. 3.12) and  $T_{ro}$  {K} of the indoor and the outdoor side of the roof are

$$\begin{aligned} \frac{dT_{ri}}{dt} &= \frac{Q_{rd,ri} + Q_{as,ri} + Q_{as,ri,H2O} + Q_{l,ri} + Q_{s,ri} + Q_{sc,ri} + Q_{u,ri} + Q_{uc,ri} - Q_{ri,c} - Q_{ri,ro} - Q_{ri,roL}}{\rho_r \cdot c_{p,r} \cdot V_r} \quad \{K s^{-1}\} \\ \frac{dT_{ro}}{dt} &= \frac{Q_{rd,ro} - Q_{ro,o} - Q_{ro,sk} + Q_{ri,ro} + Q_{ri,roL}}{\rho_r \cdot c_{p,r} \cdot V_r} \quad \{K s^{-1}\} \quad (3.227) \end{aligned}$$

where  $Q$  {W} are the heat exchange terms between the indoor side of the roof ( $ri$ ), the outdoor side of the roof ( $ro$ ) and the greenhouse components (respectively eqns. 3.53, 3.134, 3.71, 3.88, 3.94, 3.106, 3.80, 3.112, 3.98, 3.133, 3.100, 3.113, 3.56, 3.102). The heat capacity is  $\rho_r \cdot c_{p,r} \cdot V_r$ , where  $\rho_r$  {kg m<sup>-3</sup>} is the density of the roof glass,  $c_{p,r}$  {J kg<sup>-1</sup> K<sup>-1</sup>} is the specific heat capacity of the roof glass and  $V_r$  is the volume of the roof glass.

The indoor roof temperature  $T_{ri}$  is the most interesting, since it is the main term in the energy exchange with the indoor greenhouse environment. To get to a one state model it is assumed that the outdoor roof temperature  $T_{ro}$  {K} is static (does not change in time) and the indoor roof temperature  $T_{ri}$  is the state variable. Now the temperature  $T_{ro}$  can be computed directly from the temperature  $T_{ri}$ .

This gives the differential equations

$$\frac{dT_{ri}}{dt} = \frac{\Sigma Q_{i\_ri} - \Sigma Q_{ri\_ro}}{\rho_r \cdot c_{p,r} \cdot V_r} \quad \{\text{K s}^{-1}\} \quad (3.228)$$

$$\frac{dT_{ro}}{dt} = \frac{\Sigma Q_{o\_ro} + \Sigma Q_{ri\_ro}}{\rho_r \cdot c_{p,r} \cdot V_r} \quad \{\text{K s}^{-1}\} \quad (3.229)$$

in which

$$\begin{aligned} \Sigma Q_{i\_ri} = & Q_{rd\_ri} + Q_{as\_ri} + Q_{as\_ri\_H2O} + Q_{l\_ri} + Q_{s\_ri} \\ & + Q_{sc\_ri} + Q_{u\_ri} + Q_{uc\_ri} - Q_{ri\_c} \end{aligned} \quad \{\text{W}\} \quad (3.230)$$

$$\Sigma Q_{o\_ro} = Q_{rd\_ro} - Q_{ro\_o} - Q_{ro\_sk} \quad \{\text{W}\} \quad (3.231)$$

$$\Sigma Q_{ri\_ro} = Q_{ri\_ro} + Q_{ri\_roL} \quad \{\text{W}\} \quad (3.232)$$

where  $\Sigma Q_{i\_ri} \{\text{W}\}$  is the heat exchange between the indoor side of the roof and the indoor greenhouse environment,  $\Sigma Q_{o\_ro} \{\text{W}\}$  is the heat exchange between the outdoor side of the roof and the outdoor environment and  $\Sigma Q_{ri\_ro} \{\text{W}\}$  is the heat transfer between the roof indoor and outdoor side (conduction ( $ri\_ro$ ) and longwave radiation ( $ri\_roL$ )).

Now assume that temperature  $T_{ro}$  is static in eqn. 3.227

$$\frac{dT_{ro}}{dt} = 0 \quad \rightarrow \quad Q_{rd\_ro} - Q_{ro\_o} - Q_{ro\_sk} + Q_{ri\_ro} + Q_{ri\_roL} = 0 \quad (3.233)$$

and solve  $T_{ro}$  by filling in the heat exchange terms  $Q$

$$\begin{aligned} & A_r \cdot \eta_{ro\_Is} \cdot I_o \\ & - A_r \cdot \alpha_{ro\_o} \cdot (T_{ro} - T_o) \\ & - A_r \cdot E_{ro} \cdot E_{sk} \cdot F_{ro\_sk} \cdot \sigma \cdot (T_{ro}^4 - T_{sk}^4) \\ & + A_r \cdot \frac{\lambda_a}{d_{ra}} \cdot (T_{ri} - T_{ro}) \\ & + A_r \cdot E_{ri} \cdot E_{ro} \cdot F_{ri\_ro} \cdot \sigma \cdot (T_{ri}^4 - T_{ro}^4) = 0 \end{aligned} \quad \{\text{W}\} \quad (3.234)$$

This equation can be rewritten to

$$c_{Tr1} \cdot T_{ro}^4 + c_{Tr2} \cdot T_{ro} + c_{Tr3} = 0 \quad (3.235)$$

in which

$$c_{Tr1} = -E_{ro} \cdot \sigma \cdot (E_{ri} \cdot F_{ri.ro} + E_{sk} \cdot F_{ro.sk}) \quad (3.236)$$

$$c_{Tr2} = - \left( \alpha_{ro.o} + \frac{\lambda_a}{d_{ra}} \right) \quad (3.237)$$

$$c_{Tr3} = \eta_{ro.Is} \cdot I_o + \alpha_{ro.o} \cdot T_o + \frac{\lambda_a}{d_{ra}} \cdot T_{ri} + E_{ro} \cdot \sigma \cdot (E_{sk} \cdot F_{ro.sk} \cdot T_{sk}^4 + E_{ri} \cdot F_{ri.ro} \cdot T_{ri}^4) \quad (3.238)$$

Equation 3.235 has four analytical solutions for  $T_{ro}$

$$T_{ro} = \pm \frac{1}{12} \sqrt{6} \left( \sqrt{c_{Tr5}} \pm \sqrt{-c_{Tr5} - \frac{12\sqrt{6} c_{Tr2}}{c_{Tr1} \cdot \sqrt{c_{Tr5}}}} \right) \quad \{K\} \quad (3.239)$$

in which

$$c_{Tr4} = \sqrt[3]{12 c_{Tr1} \cdot (9 c_{Tr2}^2 + \sqrt{81 c_{Tr2}^4 - 768 c_{Tr1} \cdot c_{Tr3}^3})} \quad (3.240)$$

$$c_{Tr5} = \frac{c_{Tr4}}{c_{Tr1}} + \frac{48 c_{Tr3}}{c_{Tr4}} \quad (3.241)$$

Note: the terms  $c_{Tr4}$  and  $c_{Tr5}$  are complex numbers since  $c_{Tr1}$  and  $c_{Tr2}$  are negative, but the resulting temperature  $T_{ro}$  will be real.

Only one of the four analytical solutions gives a correct representation of the roof temperature outdoor side

$$T_{ro} = \frac{1}{12} \sqrt{6} \left( \sqrt{c_{Tr5}} + \sqrt{-c_{Tr5} - \frac{12\sqrt{6} c_{Tr2}}{c_{Tr1} \cdot \sqrt{c_{Tr5}}}} \right) \quad \{K\} \quad (3.242)$$

The following differential equations are derived for a double (eqn. 3.228) and a single glass cover

$$\begin{aligned} \frac{dT_{ri}}{dt} &= \frac{\Sigma Q_{i.ri} - \Sigma Q_{ri.ro}}{\rho_r \cdot c_{p.r} \cdot V_r} & \text{if double glass cover} & \quad \{K s^{-1}\} \\ \frac{dT_{ri}}{dt} &= \frac{\Sigma Q_{i.ri} + \Sigma Q_{ro.o}}{\rho_r \cdot c_{p.r} \cdot V_r} & \text{if single glass cover} & \quad \{K s^{-1}\} \end{aligned} \quad (3.243)$$

where, in the single glass cover model  $T_{ro} = T_{ri}$  and  $\eta_{ro.Is} = 0$ .

This simplified (one state) roof model (eqns. 3.12 and 3.242) is tested against the original (two state) roof model (eqns. 3.12 and 3.227). To verify the correctness of the model, the indoor and the outdoor roof temperatures  $T_{ri}$  and  $T_{ro}$  and the energy absorbed by the indoor side of the roof  $\Sigma Q_{i.ri}$  are compared.

Ten step responses are simulated, where the indoor air temperature below the screen  $T_a$  is increased from 18°C to 40°C with steps of 2°C (18 → 20, 20 → 22, etc.). The responses of the roof temperatures to these stepwise changes in the air temperature are simulated with the simplified and with the two state roof model. The following conditions are used: outdoor shortwave solar radiation  $I_o = 500 \text{ W m}^{-2}$  [soil], thermal screen closure  $Cl_{sc} = 0$  (screen is fully opened), relative humidity indoor air  $RH_a = 95\%$  (high humidity, so condensation on indoor roof cover), relative humidity indoor air above the screen  $RH_{as} = RH_a$  and outdoor wind speed  $v_o = 3 \text{ m s}^{-1}$ . The temperatures are: outdoor air  $T_o = 18^\circ\text{C}$ , sky  $T_{sk} = 13^\circ\text{C}$ , lower net  $T_l = 60^\circ\text{C}$ , upper net  $T_l = 40^\circ\text{C}$  and soil  $T_s = 15^\circ\text{C}$ . The temperatures of the indoor air above the screen  $T_{as}$ , the crop  $T_c$ , the upper cooling net  $T_{uc}$  and the screen  $T_{sc}$  are equal to the indoor air temperature below the screen  $T_a$ .

The results are shown in figure 3.16. The estimation is quite good. The maximum deviation of the roof temperature indoor side  $T_{ri}$  is 0.070°C, of the roof temperature outdoor side  $T_{ro}$  is 0.42°C and of the energy absorbed by the indoor side of the roof  $\Sigma Q_{i,ri}$  is  $7.8 \cdot 10^3 \text{ W}$ . The difference between the roof temperature on the indoor and the outdoor side varies from 2°C to 10.5°C for the indoor air temperatures  $T_a$  selected.

### 3.E Derivation heat pump equations

Since the derivation of the equations for the temperatures  $T_{out, hp}$  and  $T_{aq, c, hp}$  is quite elaborate, it is given here.

The coefficient of performance  $COP$  of an ideal compression heat pump (assuming a Carnot cycle) is computed from the condensation and the evaporation temperatures  $T_{hs}$  and  $T_{cs}$  {K}

$$COP = \frac{T_{hs}}{T_{hs} - T_{cs}} \quad \{-\} \quad (3.244)$$

If the heat pump does not operate according to the Carnot cycle, we correct for that with an efficiency of the heat pump  $\eta_{hp}$

$$COP = \eta_{hp} \cdot \frac{T_{hs}}{T_{hs} - T_{cs}} \quad \{-\} \quad (3.245)$$

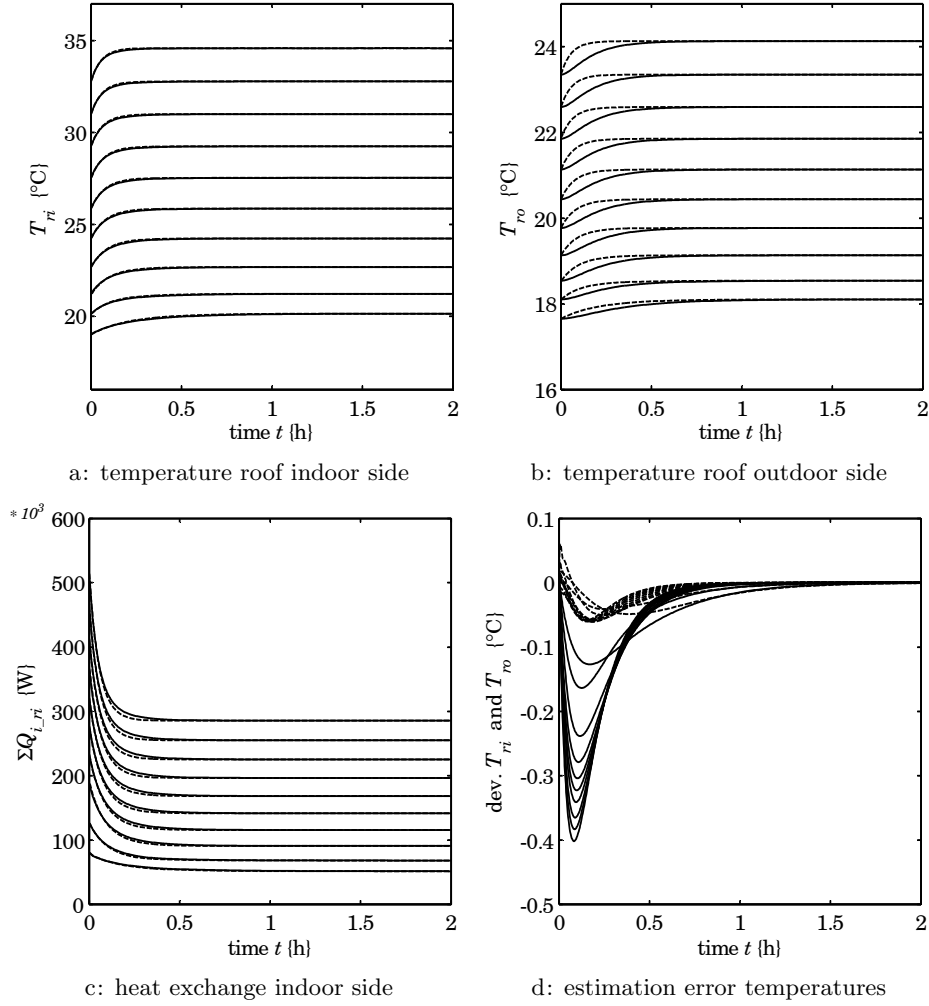


Figure 3.16: Roof temperatures  $T_{ri}$  and  $T_{ro}$  original (—) and simplified (---) model, energy absorbed by indoor side of the roof  $\Sigma Q_{i,ri}$  and temperature deviation  $T_{ri}$  (---) and  $T_{ro}$  (—)

Another equation for the  $COP$  is found from values in practice (Breuer et al., 1999)

$$COP = \frac{1}{(p_{C1} \cdot (T_{cs} - T_0) + p_{C2}) \cdot (T_{hs} - T_0) + p_{C3} \cdot (T_{cs} - T_0) + p_{C4}} \quad \{-\} \quad (3.246)$$

in which the parameter values are:  $p_{C1} = -7.2956 \cdot 10^{-5}$ ,  $p_{C2} = 6.9194 \cdot 10^{-3}$ ,  $p_{C3} = -3.1741 \cdot 10^{-3}$ ,  $p_{C4} = 1.7438 \cdot 10^{-2}$ , and  $T_0 = 273.15$  K is the correction factor from temperature in Kelvin {K} to Celsius {°C}.

The thermal energies  $Q_h$  and  $Q_c$  defined in eqns. 3.178 and 3.179 can also be written in terms of the internal heat pump conditions

$$Q_h = k_{hp} \cdot A_{hp} \cdot \Delta T_{mh.hp} \quad \{W\} \quad (3.247)$$

$$Q_c = k_{hp} \cdot A_{hp} \cdot \Delta T_{mc.hp} \quad \{W\} \quad (3.248)$$

where  $k_{hp}$  {W m<sup>-2</sup> K<sup>-1</sup>} is the heat pump heat transfer coefficient,  $A_{hp}$  {m<sup>2</sup>} is the heat pump surface for heat transfer and  $\Delta T_{mh.hp}$  and  $\Delta T_{mc.hp}$  {K} are the mean temperature differences for heat transfer.

The mean temperature differences for heat transfer are given by Van Kimmenade (1986) as

$$\Delta T_{mh.hp} = \frac{\Delta T_{\max.hp.h} - \Delta T_{\min.hp.h}}{\ln \left( \frac{\Delta T_{\max.hp.h}}{\Delta T_{\min.hp.h}} \right)} \quad \{K\} \quad (3.249)$$

$$\Delta T_{mc.hp} = \frac{\Delta T_{\max.hp.c} - \Delta T_{\min.hp.c}}{\ln \left( \frac{\Delta T_{\max.hp.c}}{\Delta T_{\min.hp.c}} \right)} \quad \{K\} \quad (3.250)$$

in which the temperature differences are given by

$$\Delta T_{\max.hp.h} = T_{hs} - T_{in.hp} \quad \{K\} \quad (3.251)$$

$$\Delta T_{\min.hp.h} = T_{hs} - T_{out.hp} \quad \{K\} \quad (3.252)$$

$$\Delta T_{\max.hp.c} = T_{aq.h} - T_{cs} \quad \{K\} \quad (3.253)$$

$$\Delta T_{\min.hp.c} = T_{aq.c.hp} - T_{cs} \quad \{K\} \quad (3.254)$$

The temperatures  $T_{hs}$  and  $T_{cs}$  of the warm and the cold side of the heat pump can be found by equating the energy transport terms in eqns. 3.178 with 3.247 and 3.179 with 3.248

$$T_{hs} = \frac{h_1 \cdot T_{out.hp} - T_{in.hp}}{h_1 - 1} \quad \{K\} \quad (3.255)$$

$$T_{cs} = \frac{c_1 \cdot T_{aq.c.hp} - T_{aq.h}}{c_1 - 1} \quad \{K\} \quad (3.256)$$

in which  $h_1 = e^{\frac{k_{hp} \cdot A_{hp}}{\rho_{H2O} \cdot c_{p.H2O} \cdot \Phi_{pump.l}}}$  and  $c_1 = e^{\frac{k_{hp} \cdot A_{hp}}{\rho_{H2O} \cdot c_{p.H2O} \cdot v_{p.hp} \cdot \Phi_{pump.hp}}}$ , where  $k_{hp}$  {W m<sup>-2</sup> K<sup>-1</sup>} is the heat pump heat transfer coefficient and  $A_{hp}$  {m<sup>2</sup>} is the heat pump surface for heat transfer.

Combining eqns. 3.177 with 3.178 and 3.179 gives

$$COP = \frac{\Phi_{pump,l} \cdot (T_{out,hp} - T_{in,hp})}{\Phi_{pump,l} \cdot (T_{out,hp} - T_{in,hp}) - (vp_{hp} \cdot \Phi_{pump,hp} \cdot (T_{aq,h} - T_{aq,c,hp}))} \quad \{-\} \quad (3.257)$$

and combining eqns. 3.245 with 3.255 and 3.256 gives

$$COP = \frac{\eta_{hp} \cdot (c_1 - 1) \cdot (h_1 \cdot T_{out,hp} - T_{in,hp})}{(c_1 - 1) \cdot (h_1 \cdot T_{out,hp} - T_{in,hp}) + (h_1 - 1) \cdot (-c_1 \cdot T_{aq,c,hp} + T_{aq,h})} \quad \{-\} \quad (3.258)$$

The temperature  $T_{aq,c,hp}$  of the cooled aquifer water resulting from the heat pump can be found by equating the coefficients of performance in eqns. 3.257 and 3.258, which gives

$$T_{aq,c,hp} = \frac{\eta_{hp} \cdot (c_1 - 1) \cdot (h_1 \cdot T_{out,hp} - T_{in,hp}) \cdot vp_{hp} \cdot \Phi_{pump,hp} \cdot T_{aq,h} + \Phi_{pump,l} \cdot (T_{out,hp} - T_{in,hp}) \cdot ((1 - \eta_{hp}) \cdot (c_1 - 1) \cdot (h_1 \cdot T_{out,hp} - T_{in,hp}) + T_{aq,h} \cdot (h_1 - 1))}{\eta_{hp} \cdot (c_1 - 1) \cdot (h_1 \cdot T_{out,hp} - T_{in,hp}) \cdot vp_{hp} \cdot \Phi_{pump,hp} + \Phi_{pump,l} \cdot (T_{out,hp} - T_{in,hp}) \cdot c_1 \cdot (h_1 - 1)} \quad \{K\} \quad (3.259)$$

The temperature leaving the heat pump  $T_{out,hp}$  {K} can be found by equating the coefficients of performance in eqns. 3.246 and 3.258 and substituting  $T_{aq,c,hp}$  by eqn. 3.259, which gives a fourth order equation. Solving  $T_{out,hp}$  gives

$$T_{out,hp} = \frac{1}{12 \cdot a_T} \cdot \left( -3 b_T - \sqrt{3} p_{T7} + \left( \frac{3}{p_{T6} \cdot p_{T7}} \cdot \left( 2 \cdot (3 b_T^2 - 8 a_T \cdot c_T - a_T \cdot p_{T6}) \cdot p_{T6} \cdot p_{T7} + 8 a_T \cdot (3 b_T \cdot d_T - 12 a_T \cdot e_T - c_T^2) \cdot p_{T7} + 6 \sqrt{3} \cdot (8 a_T^2 \cdot d_T + b_T^3 - 4 a_T \cdot b_T \cdot c_T) \cdot p_{T6} \right) \right)^{\frac{1}{2}} \right) \quad \{K\} \quad (3.260)$$

in which the parameters are given by

$$a_T = -p_{c1} \cdot c_1 \cdot h_1^3 \cdot (\eta_{hp} - 1) \cdot \Phi_{pump,l} \quad (3.261)$$

$$b_T = \eta_{hp} \cdot h_1^3 \cdot (c_1 - 1) \cdot p_{T4} \cdot v_{p_{hp}} \cdot \Phi_{pump,hp} \\ + c_1 \cdot h_1^2 \cdot (p_{c1} \cdot (\eta_{hp} - 1) \cdot (h_1 + 3) \cdot T_{in,hp} \\ + (h_1 - 1) \cdot p_{T2}) \cdot \Phi_{pump,l} \quad (3.262)$$

$$c_T = -h_1^2 \cdot (c_1 - 1) \cdot (3 \eta_{hp} \cdot p_{T4} \cdot T_{in,hp} + (h_1 - 1) \cdot p_{T5}) \\ \cdot v_{p_{hp}} \cdot \Phi_{pump,hp} \\ - c_1 \cdot h_1 \cdot (3 p_{c1} \cdot (\eta_{hp} - 1) \cdot (h_1 + 1) \cdot T_{in,hp}^2 \\ + (h_1 + 2) \cdot (h_1 - 1) \cdot p_{T2} \cdot T_{in,hp} \\ + (h_1 - 1)^2 \cdot (p_{T3} + 1)) \cdot \Phi_{pump,l} \quad (3.263)$$

$$d_T = h_1 \cdot (c_1 - 1) \cdot (3 \eta_{hp} \cdot p_{T4} \cdot T_{in,hp}^2 + 2 (h_1 - 1) \cdot p_{T5} \cdot T_{in,hp} \\ + T_{aq,h} \cdot (h_1 - 1)^2) \cdot v_{p_{hp}} \cdot \Phi_{pump,hp} \\ + c_1 \cdot T_{in,hp} \cdot (p_{c1} \cdot (\eta_{hp} - 1) \cdot (3 h_1 + 1) \cdot T_{in,hp}^2 \\ + (2 h_1 + 1) \cdot (h_1 - 1) \cdot p_{T2} \cdot T_{in,hp} \\ + (h_1 + 1) \cdot (h_1 - 1)^2 \cdot (p_{T3} + 1)) \cdot \Phi_{pump,l} \quad (3.264)$$

$$e_T = -T_{in,hp} \cdot (c_1 - 1) \cdot (\eta_{hp} \cdot p_{T4} \cdot T_{in,hp}^2 \\ + (h_1 - 1) \cdot p_{T5} \cdot T_{in,hp} + T_{aq,h} \cdot (h_1 - 1)^2) \cdot v_{p_{hp}} \cdot \Phi_{pump,hp} \\ - c_1 \cdot T_{in,hp}^2 \cdot (p_{c1} \cdot (\eta_{hp} - 1) \cdot T_{in,hp}^2 + (h_1 - 1) \cdot p_{T2} \cdot T_{in,hp} \\ + (h_1 - 1)^2 \cdot (p_{T3} + 1)) \cdot \Phi_{pump,l} \quad (3.265)$$

and parameters (defined for shorter writing):

$$p_{T1} = p_{c1} \cdot T_0 - p_{C3} \\ p_{T2} = p_{T1} \cdot \eta_{hp} - 2 p_{c1} \cdot T_0 + p_{C2} + p_{C3} \\ p_{T3} = (-p_{T1} + p_{C2}) \cdot T_0 - p_4 \\ p_{T4} = p_{c1} \cdot (T_{aq,h} - T_0) + p_{C2} \\ p_{T5} = \eta_{hp} \cdot (p_{T1} \cdot T_{aq,h} + p_{T3}) + 1$$

$$\begin{aligned}
p_{T6} = & \left( -288 a_T \cdot c_T \cdot e_T + 108 a_T \cdot d_T^2 \right. \\
& + 108 b_T^2 \cdot e_T - 36 b_T \cdot c_T \cdot d_T + 8 c_T^3 \\
& + 12\sqrt{3} \cdot (-256 a_T^3 \cdot e_T^3 + 192 a_T^2 \cdot b_T \cdot d_T \cdot e_T^2 \\
& - 144 a_T \cdot b_T^2 \cdot c_T \cdot e_T^2 - 144 a_T^2 \cdot c_T \cdot d_T^2 \cdot e_T \\
& + 128 a_T^2 \cdot c_T^2 \cdot e_T^2 + 80 a_T \cdot b_T \cdot c_T^2 \cdot d_T \cdot e_T \\
& + 27 a_T^2 \cdot d_T^4 + 27 b_T^4 \cdot e_T^2 \\
& - 18 b_T^3 \cdot c_T \cdot d_T \cdot e_T - 18 a_T \cdot b_T \cdot c_T \cdot d_T^3 \\
& - 16 a_T \cdot c_T^4 \cdot e_T + 6 a_T \cdot b_T^2 \cdot d_T^2 \cdot e_T \\
& + 4 b_T^3 \cdot d_T^3 + 4 b_T^2 \cdot c_T^3 \cdot e_T \\
& \left. + 4 a_T \cdot c_T^3 \cdot d_T^2 - b_T^2 \cdot c_T^2 \cdot d_T^2 \right)^{\frac{1}{3}} \\
p_{T7} = & \left( \frac{1}{p_{T6}} \cdot (2 a_T \cdot p_{T6}^2 + (3 b_T^2 - 8 a_T \cdot c_T) \cdot p_{T6} \right. \\
& \left. + 8 a_T \cdot (c_T^2 - 3 b_T \cdot d_T + 12 a_T \cdot e_T) \right)^{\frac{1}{2}}
\end{aligned}$$

### 3.F Derivation heat exchanger equations

Since the derivation of the equations for the temperatures  $T_{out,he}$  and  $T_{aq,h,he}$  is a bit elaborate, it is given here.

It is assumed here that a countercurrent heat exchanger is used. The energy transfer by the heat exchanger  $Q_{he}$  defined in eqn. 3.189 can also be defined by the energy transport due to the water flow on the upper cooling net side (see figure 3.9)

$$Q_{he} = \rho_{H2O} \cdot c_{p,H2O} \cdot \Phi_{pump,uc} \cdot (T_{in,he} - T_{out,he}) \quad \{\text{W}\} \quad (3.266)$$

where  $\rho_{H2O}$   $\{\text{kg m}^{-3}\}$  is the density of water,  $c_{p,H2O}$   $\{\text{J kg}^{-1} \text{K}^{-1}\}$  is the specific heat capacity of water and  $\Phi_{pump,uc}$   $\{\text{m}^3 \text{s}^{-1}\}$  is the maximum flow rate of water into the upper cooling net.

The thermal energy  $Q_{he}$  as defined in eqns. 3.189 and 3.266 can also be written in terms of the internal heat exchanger conditions

$$Q_{he} = k_{he} \cdot A_{he} \cdot \Delta T_{m,he} \quad \{\text{W}\} \quad (3.267)$$

where  $k_{he}$   $\{\text{W m}^{-2} \text{K}^{-1}\}$  is the heat exchanger heat transfer coefficient,  $A_{he}$   $\{\text{m}^2\}$  is the heat exchanger surface for heat transfer and  $\Delta T_{m,he}$   $\{\text{K}\}$  is the mean temperature difference for heat transfer.

The mean temperature difference  $\Delta T_{m\_he}$  for heat transfer is given by Van Kimmenade (1986) as

$$\Delta T_{m\_he} = \frac{\Delta T_{\max\_he} - \Delta T_{\min\_he}}{\ln \left( \frac{\Delta T_{\max\_he}}{\Delta T_{\min\_he}} \right)} \quad \{K\} \quad (3.268)$$

in which the temperature differences are given by

$$\Delta T_{\max\_he} = T_{in\_he} - T_{aq\_h\_he} \quad \{K\} \quad (3.269)$$

$$\Delta T_{\min\_he} = T_{out\_he} - T_{aq\_c} \quad \{K\} \quad (3.270)$$

The temperature leaving the heat exchanger  $T_{out\_he}$  {K} can be found by equating the energies in eqns. 3.266 and 3.189, which gives

$$T_{out\_he} = T_{in\_he} - \frac{vp_{he} \cdot \Phi_{pump\_he} \cdot (T_{aq\_h\_he} - T_{aq\_c})}{\Phi_{pump\_uc}} \quad \{K\} \quad (3.271)$$

The temperature  $T_{aq\_h\_he}$  of the heated aquifer water resulting from the heat exchanger can be found by equating the energies in eqns. 3.189 and 3.267, which gives

$$T_{aq\_h\_he} = \begin{cases} \frac{c_{he} \cdot T_{aq\_c} \cdot (vp_{he} \cdot \Phi_{pump\_he} - \Phi_{pump\_uc}) + T_{in\_he} \cdot \Phi_{pump\_uc} \cdot (c_{he} - 1)}{c_{he} \cdot vp_{he} \cdot \Phi_{pump\_he} - \Phi_{pump\_uc}} & \text{if } c_{he} > 1 \\ T_{aq\_c} & \text{if } c_{he} = 1 \end{cases} \quad \{K\} \quad (3.272)$$

in which  $c_{he} = e^{\frac{k_{he} \cdot A_{he}}{\rho_{H2O} \cdot c_{p\_H2O}} \cdot \left( \frac{1}{\Phi_{pump\_uc}} - \frac{1}{vp_{he} \cdot \Phi_{pump\_he}} \right)}$ , where  $k_{he}$  {W m<sup>-2</sup> K<sup>-1</sup>} is the heat exchanger heat transfer coefficient and  $A_{he}$  {m<sup>2</sup>} is the heat exchanger surface for heat transfer.

### 3.G Sensitivity analysis and Fisher information matrix

The use of sensitivity analysis as a basis for the selection of parameters for parameter estimation has been extensively studied and described in the literature (Munack, 1991; Walter and Pronzato, 1997). Bernaerts and van Impe (2004) give a good overview of criteria that can be used, and the use of the Fisher information matrix in conjunction with relative sensitivities.

The model is described by the differential equations

$$\dot{x} = f(t, x, u, v, \theta) \quad (3.273)$$

where  $t \in \mathbb{R}^l$  is time,  $x = x(t) \in \mathbb{R}^n$  is the state vector,  $u = u(t) \in \mathbb{R}^m$  is the control input vector,  $v = v(t) \in \mathbb{R}^w$  is the external input vector,  $\theta \in \mathbb{R}^p$  is the parameter vector and  $f$  is a non-linear function. The description of these variables is given in table 3.2.

The local sensitivities of the states  $x$  for the parameters  $\theta$  are given by

$$\dot{x}_\theta = \frac{\partial f(t, x, u, v, \theta)}{\partial x} \cdot x_\theta + \frac{\partial f(t, x, u, v, \theta)}{\partial \theta} \quad (3.274)$$

where  $x_\theta = \frac{\partial x}{\partial \theta}$  are the sensitivities of the states  $x$  for changes in the parameters  $\theta$ .

The function given in eqn. 3.273 is integrated numerically from the initial time  $t_0$  to the final time  $t_f$  by using a Runge-Kutta fourth order integration algorithm (Press et al., 1986). This integration is performed with the nominal parameter values  $\bar{\theta}$ .

$$x(t, x, u, v, \bar{\theta}) = \int_{t_0}^{t_f} f(t, x, u, v, \bar{\theta}) dt \quad x \in \mathbb{R}^n \quad (3.275)$$

The trajectories of the sensitivities  $S = x_\theta$  are determined by integration of eqn. 3.274, since the derivatives are not analytically known. This integration is done by the Euler forward integration method.

$$x_\theta(t) = \int_{t_0}^{t_f} \left\{ \frac{\partial f(t, x, u, v, \theta)}{\partial x} \cdot x_\theta + \frac{\partial f(t, x, u, v, \theta)}{\partial \theta} \right\} dt \quad x_\theta \in \mathbb{R}^{l \cdot n \cdot p} \quad (3.276)$$

in which  $x_\theta(t = t_0) = 0$ . Here  $\frac{\partial f}{\partial x}$  and  $\frac{\partial f}{\partial \theta}$  are computed through numerical differentiation using finite differences<sup>⊙</sup>. To get a fair comparison of the sensitivity trajectories the relative sensitivity  $\tilde{x}_\theta$  is used instead of the sensitivity  $x_\theta$ . This weighing is used since the states are not in the same order of magnitude.

$$\tilde{x}_\theta(i_l, i_p, i_n) = x_\theta(i_l, i_p, i_n) \cdot \frac{\theta(i_p)}{x(i_l, i_n)} \quad \begin{matrix} i_l = 1, \dots, l \\ i_p = 1, \dots, p \\ i_n = 1, \dots, n \end{matrix} \quad \tilde{x}_\theta \in \mathbb{R}^{l \cdot n \cdot p} \quad (3.277)$$

<sup>⊙</sup> A first order approach is used for the finite differences computation. Small perturbations are applied to the states  $x$  and the parameters  $\theta$  to numerically determine the derivatives. The perturbations used in the finite differences computation are, for the parameters  $\theta$ : 0.001; and for the states  $x$ : 0.1 for temperature, 0.001 for CO<sub>2</sub> concentration and 0.0001 for H<sub>2</sub>O concentration.

With the states  $x = x(t) \in \mathbb{R}^n$  and the parameters  $\theta \in \mathbb{R}^p$ , this gives  $n \cdot p$  trajectories to examine. This number can become quite large if many states and parameters are used. Since the nominal parameter values are equal to one in our case,  $\tilde{x}_\theta$  is called the semi-relative sensitivity function (Bernaerts and van Impe, 2004).

To arrive at some indicator of the information content of the experiment with respect to the parameter uncertainties, the Fisher information matrix  $F$  can be used.

$$F = \int_{t_0}^{t_f} x_\theta(t)^T \cdot Q_F^{-1} \cdot x_\theta(t) dt \quad F \in \mathbb{R}^{p \times p} \quad (3.278)$$

where  $Q_F$  is a weighing matrix. The values of the weights on the diagonal of  $Q_F$  can be one (identity matrix) or  $\frac{1}{\sigma^2}$  (where  $\sigma^2$  is the measurement error variance). The matrix  $F$  is symmetric. The higher the value of the diagonal elements of matrix  $F$ , the higher the sensitivity (and thus the better the identifiability) of the corresponding parameter  $\theta$ . The off-diagonal elements provide information on the covariance of the parameter estimates for the given experiment (correlation), which can be characterized by the modified E-criterion explained below.

Norms of the Fisher information matrix  $F$  can be used to determine information content, reliability and correlation of the data. The D- and the modified E-criterion are used here.

$$\varphi_D(F) = \det(F) \quad (3.279)$$

$$\varphi_E(F) = \frac{\lambda_{\max}(F)}{\lambda_{\min}(F)} \quad (3.280)$$

- It is beneficial to maximize the D-criterion. This criterion deals with the volume of the confidence region ( $\frac{1}{\det(F)}$  is proportional to this volume). It is an indicator for the information content of the experiment data, and it is used to minimize the uncertainty of the individual parameter values and for decorrelation.
- It is beneficial to minimize the modified E-criterion. This criterion deals with the shape of the confidence region. It is an indicator for the identifiability of the parameters, and it is used for decorrelation only. The minimum value of the modified E-criterion is one: then the length of the axes of the asymptotic confidence ellipsoids are equal. A high value indicates that parameters are correlated ( $\varphi_E(F) \gg 1$ ).

If the relative sensitivities  $\tilde{x}_\theta$  are used instead of the sensitivities  $x_\theta$ , the Fisher information matrix  $\tilde{F}$  is used to describe the Fisher information matrix of the relative sensitivities.

$$\tilde{F} = \int_{t_0}^{t_f} \tilde{x}_\theta(t)^T \cdot Q_F^{-1} \cdot \tilde{x}_\theta(t) dt \quad F \in \mathbb{R}^{p \times p} \quad (3.281)$$

Bernaerts and van Impe (2004) state that — if the nominal parameter values are equal to one — the interpretation of the D- and the modified E-criterion still hold.

## Chapter 4

# Optimal control of a solar greenhouse

### 4.1 Introduction

The advantages of using optimal control instead of conventional greenhouse climate control can be summarized as follows. Explicit quantitative scientific knowledge concerning greenhouses and crops can be incorporated in a dynamic model as shown in the chapters 2 and 3. Optimal control uses this model and furthermore requires that the control objectives — such as maximizing crop growth and minimizing gas use — are quantified and made explicit in the cost function. For maximizing crop growth the biomass increase must be maximized, while the temperature, the temperature integral and the relative humidity are kept within bounds to obtain good development conditions and to decrease the risk for diseases and fungi. These bounds are translated to penalties, which are used as soft constraints. All the terms used in the cost function should be quantitative and made explicit.

By making everything explicit and quantitative the design becomes highly transparent and can therefore be easily modified. Also the designer is forced to carefully think about what he actually wants. Moreover the optimal control concept guarantees that the best possible solution is obtained. Please note that this does not guarantee that the results will be satisfactory in practice. But if the results are not satisfactory this can only be due to errors in modeling and in the definition of the cost function. If the model has a clear physical and physiological interpretation, as the models in the previous chapters have, then such errors are easily detected. A similar argumentation holds for the

cost function. Compared to conventional greenhouse climate control, these are huge advantages. In conventional control many settings are incorporated, the meaning of which is not always transparent and certainly not quantified. Explicit quantitative knowledge of greenhouses and crops is not easily integrated in these settings.

To demonstrate the principle advantages outlined above, a feasibility study of the optimal control of the solar greenhouse is performed in this chapter. The algorithms and software to put the optimal control into practice are now readily available, but unfortunately the solar greenhouse only exists on paper. Using the algorithms described in this chapter, the results of this feasibility study presented here are entirely based on simulations. In these simulations we tried to mimic reality as closely as possible. Specifically in the major long-term year-round simulation, which uses a receding horizon optimal controller to control the greenhouse, the actual weather is different from the forecasted weather that is used for the on-line optimal control computations (as in reality).

The year-round simulation of the receding horizon optimal control — as is done in this feasibility study — presents a serious computational problem. A receding horizon optimal controller is a computationally ‘expensive’ controller. When implemented it therefore uses a significant part of the real-time that is available for computation. Not too long ago (Tap, 2000) a simulation over one year with the receding horizon optimal control system lasted a significant part of that year. In our case the year-round computation with the gradient search method took about 8 days. In the testing of the concepts and different scenarios this is still quite a long time. To significantly reduce the computation time, a grid search method was introduced to use instead of the gradient search method. This highly simplified method uses only a few discrete control input values and a priori knowledge of the optimal control problem. It enables the simulation to finish within a reasonable amount of time (in our case about 8 hours), and it can also be used to initialize the receding horizon optimal controller itself. Because our optimal control problem is nonlinear, it is important to start the optimal control search with an initial guess for the control input values that is already more or less close to the solution. This initial guess for the control input values is computed by our grid search method.

The implementation of the aquifer turned out to be a brain teaser. The RHOC control horizon was set to one day, which means that we are only looking one day ahead. The government demands that an aquifer runs approximately energy neutral year-round. To incorporate this demand in the RHOC cost function, some a priori knowledge about the course of the aquifer energy con-

tent has to be used. This a priori knowledge is then translated to bounds on the aquifer energy content, which are used in the cost function.

The outline of this chapter is as follows. First a short comment is given on the greenhouse-with-crop model with respect to control in §4.2. The receding horizon optimal controller is described in §4.3.

The computations are given in §4.4–4.7. The overview below explains the contents of these paragraphs.

	open loop summer and winter day		RHOC year-round
	$\mathcal{PI}$	$TI$	
grid search	§4.4	§4.5	§4.6
gradient search			§4.7

First the optimal control computations are performed over one day in summer and in winter without ( $\mathcal{PI}$ ) and with ( $TI$ ) temperature integration (§4.4 and §4.5). These computations are performed to check whether the greenhouse-with-crop model and the cost function perform satisfactory under different circumstances. They are also used to check the changes between the results of the grid search and the gradient search method. Then year-round simulations of the receding horizon optimal control system are presented. This long period will provide insight concerning the use of the heat pump, boiler and heat exchanger in the different seasons of the year. These computations are first done with the grid search method in §4.6 to check the control of the aquifer energy content. This is an important part of the solar greenhouse and should therefore perform satisfactory. The average energy content of the aquifer over one year should be constant: the aquifer is not allowed to heat up or cool down significantly. In §4.7 the year-round computation is repeated with the gradient search method to check the simulation results and the expected improvement compared to the grid search method. All computations are done in Fortran 77.

In paragraph §4.8 comparisons are made to evaluate the optimal control search method, seasonal influences and the separate solar greenhouse elements. General conclusions with discussion on the optimal control are given in §4.9.

## 4.2 Greenhouse-with-crop model

For the successful application of optimal control an accurate model of the controlled processes is needed. The model needs to be sufficiently complex

to include all processes in a broad working area, the temperature range, for instance, should not be constrained to 0–30°C. Preference is given to a white model, since the internal variables have a physical meaning and can be easily interpreted. To limit computation time, the number of states has to be limited.

The model of the conventional greenhouse used in this research (see chapter 3) is based on the model by Heesen (1997), which was developed based on the research by Van Henten (1994), De Zwart (1996), De Jong (1990) and Bot (1983). A photosynthesis model (Körner et al., 2002; Körner and van Ooteghem, 2003; Heuvelink, 1996; Farquhar et al., 1980) and an evaporation model (Stanghellini, 1987) are used to simulate the crop responses (see chapter 2). The temperature and humidity bounds and the temperature integral have been developed by Körner (Körner, 2003; Körner and Challa, 2003).

The greenhouse-with-crop model — without the solar greenhouse elements — has been validated with greenhouse data, and was found to give an accurate description of the processes (§3.9; van Ooteghem, 2003a,b). The model has been extended with the new solar greenhouse elements (heat pump, heat exchanger, ventilation with heat recovery), a cooling net and a thermal screen. This model (chapters 2 and 3) is used for all computations in this chapter. The main disturbance is the weather, which can be forecasted reasonably well up to three days ahead (Doeswijk and Keesman, 2005; Lukasse et al., 2006).

Very high or low temperatures can cause irreversible damage to the crop. High CO<sub>2</sub> concentrations in the indoor air can also cause crop damage, but exact values are not known. In practice a CO<sub>2</sub> concentration of 1000  $\mu\text{mol}[\text{CO}_2] \text{mol}^{-1}[\text{air}]$  is used. High humidity increases the risk at infection by mould. For the short-term, temperature and humidity should remain within specific bounds (Körner, 2003), which can be set by the horticulturist. For the long-term effects of temperature on crop growth a temperature integral is used (Körner, 2003; Körner and Challa, 2003). By using temperature integration the grower can allow wider temperature bounds.

### 4.3 The receding horizon optimal controller: methodology and implementation

The receding horizon optimal control (RHOC) concept is a special form of model predictive control. With predicted weather and a model describing the dynamic behaviour of greenhouse and crop in time, the influence of control changes on greenhouse climate can be simulated. A cost function is formulated,

in which costs are defined to penalize fossil energy consumption, to reward biomass increase and to keep temperature, humidity, temperature integral and the aquifer energy content within bounds.

With a search routine, the optimal control inputs (actuator trajectories) are determined over the control horizon  $t_f$ , while minimizing the costs defined in the cost function. These optimal control input trajectories result in trajectories for temperature, humidity and CO<sub>2</sub> concentration that optimize this cost function. Only the first value of these optimal control input trajectories is applied to the process. Then measurements are performed to estimate the next state of the greenhouse climate (and ideally the crop). Subsequently the optimal control computation is repeated, starting from the next estimated state over the new time horizon, shifting time by one time interval (hence *receding* horizon). The feedback thus achieved is intended to limit deviations between model predictions and reality.

#### **4.3.1 Conventional versus optimal greenhouse climate control**

In horticulture, climate computers require a very large number of settings and weather dependent corrections. By means of feedback control, it is attempted to track set-point trajectories as good as possible. The influence of these set-points on crop growth and energy use is not taken into account. Moreover, the consequences of set-point changes on crop growth and energy use are not obvious.

The solar greenhouse design with its extra control possibilities is a challenge from the control-engineering point of view. The receding horizon optimal control (RHOC) concept is used in process industry with increasing success. It provides optimal control as well as feedback. The concept has also shown good applicability in greenhouse control as shown by Tap (2000) and Van Henten (1994). Van Henten concluded that using RHOC could in principle give a significant improvement in efficiency of greenhouse climate management. The performance of the optimal control largely depends on the ability of the control system to deal with modelling and weather prediction errors. Tap showed that only short-term weather predictions are needed for optimal greenhouse climate control. Van Henten and Tap both state that improved results can be obtained with optimal control.

### 4.3.2 Control horizon and time intervals

The receding horizon optimal controller uses a number of time intervals, which are defined as

- $t_f$  **control horizon**: the time interval over which the optimal control input trajectories are computed;
- $t_{s-u}$  **time interval  $u^*$** : the time interval over which the computed optimal control inputs  $u^*$  are kept piecewise constant;
- $t_s$  **sampling interval RHOC**: the time interval between the RHOC computations (time shift).

The choice of the control horizon  $t_f$  depends upon the computation time, the time interval for the control inputs  $t_{s-u}$  and the weather prediction time span. Control horizons ranging from one hour to several days are used in research by Shina and Seginer (1989) and Van Henten and Bontsema (1991). These long time intervals are used because crop growth and development respond slowly to greenhouse climate changes. Van Willigenburg et al. (2000) specifically investigated the influence of these different time intervals ( $t_s$ ,  $t_{s-u}$  and  $t_f$ ) on the receding horizon optimal control of a greenhouse.

In the solar greenhouse, the use of solar radiation for heating the greenhouse is essential and may fluctuate rapidly during the day, which calls for time intervals  $t_s$  and  $t_{s-u}$  smaller than one hour. The short-term crop growth is accounted for by the biomass (eqn. 4.4), which is a function of the photosynthesis rate. Photosynthesis is instantaneously influenced by solar radiation.

To include long-term crop growth and development, temperature integration is used over a range of six days (eqn. 4.5), with five days in the past and one day in the future. Furthermore it is assumed that the weather prediction of two days ahead is relatively accurate. This calls for a control horizon  $t_f$  of one day.

The control horizon  $t_f$  selected here is 86400 s (one day), the time interval  $t_{s-u}$  for the control inputs is 1800 s (30 min) and the sampling interval  $t_s$  for the receding horizon controller is 1800 s (30 min). This means that  $\frac{t_f}{t_{s-u}} = 48$  values are determined for each control input at each receding horizon time step. For the sampling interval  $t_s$  a relatively large value is chosen, since the values of the weather conditions in our case are hourly values (*SELyear*). In a set up where the actual weather conditions are measured, the sampling interval  $t_s$  should be as small as the sampling interval of the weather observations (e.g., 2 min; van Willigenburg et al., 2000). The integration time step used in the Runge-Kutta integration is 60 s (1 min), which ensures that faster dynamics

are correctly incorporated in the computed results. Smaller time intervals ( $t_s$ ,  $t_{s-u}$ ) or a longer control horizon ( $t_f$ ) will result in a longer computation time.

### 4.3.3 The receding horizon control principle

The receding horizon control principle is a form of feedback control that uses model predictions to determine the control inputs. The current control inputs are determined by solving on-line an open-loop optimal control problem, for each sampling interval  $t_s$ , over a finite horizon  $t_f$ , using the current state of the system as the initial state. The first control action is applied to the system and the procedure is repeated for future sampling intervals. An example of the receding horizon control principle is given in figure 4.1.

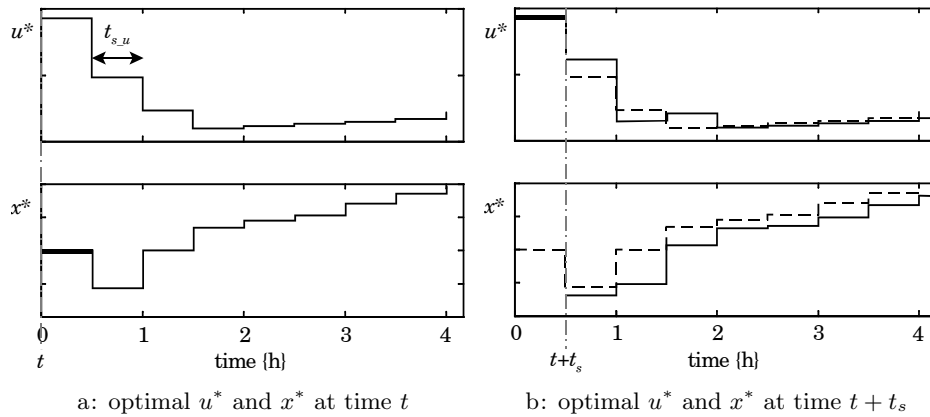


Figure 4.1: Example receding horizon optimal control

At time  $t$  measurements are performed from which the current state  $x_0$  is derived (thick line  $x^*$  in figure 4.1a). Since no measurements are available the initial state values  $x_0$  are determined here with the greenhouse-with-crop model with the actual weather  $v$ . State predictions are computed by simulating the model with the initial state  $x_0$  and the expected external inputs  $\tilde{v}$  (the weather prediction, see §4.3.9) over the control horizon  $t_f$  with different control input trajectories  $u$ . The control input trajectory that yields the lowest cost function value  $J$  is selected. This is the optimal control input trajectory  $u^*$ . The optimal control input trajectory  $u^*$  and the corresponding state trajectory  $x^*$  are given in figure 4.1a, and also as dashed lines in figure 4.1b. From this a priori optimal control trajectory only the first value is applied to the system (thick line  $u^*$  in figure 4.1b).

This procedure is repeated for every sampling interval  $t_s$  for the receding horizon controller. The control horizon  $t_f$  for the optimization is shifted, thus leading to a receding horizon. With this principle feedback is realized; the optimization is started with the actual state of the system — based on measurements or simulations — and the best predictions available at that time for the external inputs  $\tilde{v}$ .

The initial state value  $x_0$  for the next time interval is determined with the greenhouse-with-crop model, where instead of the weather prediction  $\tilde{v}$ , the actual weather  $v$  is used. Then new controls and states are computed, indicated by solid lines figure 4.1b. The dashed lines indicate the expectations from the previous control interval, shown in figure 4.1a. Since the external inputs (weather) are different from the ones on which the computation was first based, this will cause the state values  $x$  (solid line) to deviate from the a priori expected state values (dashed line). The deviation between the predicted and the actual weather is meant to make the simulations more realistic.

#### 4.3.4 Cost function

Optimal control is concerned with the computation of optimal control input trajectories based on a cost function. The control solution consists of actuator trajectories (e.g., window apertures, valve positions) that result in state trajectories (e.g., temperature, humidity and CO<sub>2</sub> concentration) that optimize a cost function. The aim is to minimize fossil energy consumption, while maximizing biomass and keeping temperature and relative humidity within certain bounds. In the cost function, costs are defined to penalize fossil energy consumption, to reward biomass increase and to keep temperature, humidity, temperature integral and the aquifer energy content within bounds.

Using a state space greenhouse-with-crop model describing the dynamic behaviour of the greenhouse (chapter 3) and the crop (chapter 2) in time together with weather predictions (*SELyear*; Breuer and van de Braak, 1989), the influence of control changes on greenhouse climate can be simulated. The state space model has the general form

$$\dot{x} = f(t, x, u, v) \quad (4.1)$$

where  $t$  is time,  $x = x(t) \in \mathbb{R}^n$  is the state vector,  $u = u(t) \in \mathbb{R}^m$  is the control input vector,  $v = v(t) \in \mathbb{R}^w$  is the external input vector and  $f$  is a non-linear vector function. The description of these variables is given in table 3.2.

The goal is to minimize the cost function, which has the general form

$$J(u) = \Phi(x, t_f) + \int_{t_0}^{t_f} L(x, u, t) dt \quad \{\text{cost}\} \quad (4.2)$$

where the terminal cost  $\Phi: \mathbb{R}^{n+1} \rightarrow \mathbb{R}$  and the penalty function  $L: \mathbb{R}^{n+m+w+1} \rightarrow \mathbb{R}$  are differentiable a sufficient number of times with respect to their arguments. The final time  $t_f$  is set to the control horizon, which is equal to one day and therefore will not be subject to optimization.

The values used for the weight factors  $c$  and the bounds (to be defined below) in the cost function are given in table 4.1. Some terms are taken per square meter to enhance the portability of the cost function to other greenhouse dimensions. The weight factors indicate how important specific greenhouse conditions are, they however do not represent euros or dollars. The weight factors have to be balanced such that one penalty does not outweigh another penalty. The weight factors have been tuned based on open loop computations of single days throughout the year to make sure that they hold in different seasons.

Table 4.1: Cost function: weight factors and bounds

symbol	unit	$x_{\min}$	$x_{\max}$	$\frac{\text{cost}}{\text{day} \cdot \text{unit}}$	$J(u)$
$RH_a$	%	–	85	$c_{RH} = 5$	$\int L_{RH_a} dt$
$E_{aq}$	$\text{J m}^{-2}$	$E_{aq \min}^{\dagger}$	$E_{aq \max}^{\dagger}$	$c_{aq} = 10 \cdot 10^6$	$\int L_{aq} dt$
$Q_{used}$	$\text{W m}^{-2}$			$c_Q = 61.44$	$\int L_Q dt$
$W$	$\text{kg m}^{-2}$			$c_W = 76.8$	$\Phi_W$
$CO_{2a}$	$\mu\text{mol}[\text{CO}_2] \text{ mol}^{-1}[\text{air}]$	320	1000	$c_{CO2} = 0$	0
without temperature integration ( $\mathcal{NI}$ )					
$T_a^{\ddagger}$	$^{\circ}\text{C}$	16	24	$c_T = 5$	$\int L_{T_a} dt$
$\Delta T_{a-TI}^{\ddagger}$	$^{\circ}\text{C}$	–	–	$c_{TI} = 0$	
$T_{aref}^{\ddagger}$	$^{\circ}\text{C}$		–		
with temperature integration ( $TI$ )					
$T_a^{\ddagger}$	$^{\circ}\text{C}$	10	34	$c_T = 5$	$\int L_{T_a} dt$
$\Delta T_{a-TI}^{\ddagger}$	$^{\circ}\text{C}$	-6	6	$c_{TI} = 25$	$\int L_{TI} dt$
$T_{aref}^{\ddagger}$	$^{\circ}\text{C}$		19		$\Phi_{TI}$

$^{\dagger}$  the aquifer energy content bounds are derived in §4.3.5

$^{\ddagger}$   $T_a$ ,  $\Delta T_{a-TI}$  and  $T_{aref}$  in  $\{\text{K}\}$  in computations, in  $\{^{\circ}\text{C}\}$  here for readability

The terminal cost  $\Phi$  is determined by the yield in the form of biomass  $W$  (eqn. 3.15) and the temperature integral  $S_T$  (eqn. 3.14) (which gives the average temperature deviation  $\Delta T_{a\_TI}$ ) at the end of the control horizon  $t_f$

$$\Phi(x, t_f) = \Phi_W(x, t_f) + \Phi_{TI}(x, t_f) \quad \{\text{cost}\} \quad (4.3)$$

in which

$$\Phi_W(x, t_f) = -c_W \cdot (W(t_f) - W(t_0)) \quad \{\text{cost}\} \quad (4.4)$$

$$\Phi_{TI}(x, t_f) = c_{TI} \cdot |\Delta T_{a\_TI}(t_f)| \quad \{\text{cost}\} \quad (4.5)$$

where  $c_W$  and  $c_{TI}$  are the weight factors for biomass and temperature integral. Terminal cost  $\Phi_W$  should preferably be large and negative and  $\Phi_{TI}$  should be zero. These terminal costs are used as soft terminal constraints.

The penalty function  $L$  contains penalties for the loss of crop yield due to exceeding temperature, humidity and — if used — temperature integration bounds, exceeding the aquifer energy content bounds and the cost of energy. To this end the penalty function  $L$   $\{\text{cost s}^{-1}\}$  is given by the sum of the penalties for temperature  $T_a$  ( $L_{Ta}$ ), relative humidity  $RH_a$  ( $L_{RH_a}$ ), temperature integral  $\Delta T_{a\_TI}$  ( $L_{TI}$ ), year-round aquifer energy content  $E_{aq}$  ( $L_{aq}$ ) and energy consumption  $Q_{used}$  ( $L_Q$ )

$$\begin{aligned} L(x, u, t) = & L_{Ta}(x, u, t) + L_{RH_a}(x, u, t) + L_{TI}(x, u, t) \\ & + L_{aq}(x, u, t) + L_Q(x, u, t) \end{aligned} \quad \{\text{cost s}^{-1}\} \quad (4.6)$$

The penalties for temperature  $L_{Ta}$ , relative humidity  $L_{RH_a}$ , temperature integral  $L_{TI}$  and aquifer energy content  $L_{aq}$  are given by

$$\begin{aligned} L_x(x, u, t) = & \frac{c_x}{2} \cdot \left( \sqrt{(x_{\min} - x(t))^2 + \beta} \right. \\ & + \sqrt{(x_{\max} - x(t))^2 + \beta} \\ & \left. - (x_{\max} - x_{\min}) \right) \end{aligned} \quad \{\text{cost s}^{-1}\} \quad (4.7)$$

which is the smooth version of

$$L_x(x, u, t) = \begin{cases} c_x \cdot |x_{\min} - x(t)| & x_{\min} > x(t) \\ 0 & x_{\min} \leq x(t) \leq x_{\max} \\ c_x \cdot |x_{\max} - x(t)| & x(t) > x_{\max} \end{cases} \quad \{\text{cost s}^{-1}\}$$

in which  $\beta = 1 \cdot 10^{-3}$ , where  $c_x$  is the weight factor associated with exceeding the boundary values  $x_{\min}$  and  $x_{\max}$  of state  $x$ . This penalty function increases linearly in value with the deviation from the boundary values. In between the boundary values the penalty function is zero. The function given in eqn. 4.7 is the smoothed function, which is smooth around  $x_{\min}$  and  $x_{\max}$  (see also appendix 1.A). These penalties are used as soft constraints.

The total amount of energy used  $Q_{used}$  per square meter greenhouse is defined as

$$Q_{used} = \frac{Q_{boil} + Q_{hp}}{A_s} \quad \{\text{W m}^{-2}\} \quad (4.8)$$

where  $Q_{boil}$  {W} is the energy used by the boiler,  $Q_{hp}$  {W} is the energy used by the heat pump and  $A_s$  {m<sup>2</sup>[soil]} is the surface area of the soil. The energy  $Q_{used}$  is a measure for the total gas use per square meter greenhouse surface.

The penalty for the energy consumption  $L_Q$  is given by

$$L_Q(x, u, t) = c_Q \cdot Q_{used} \quad \{\text{cost s}^{-1}\} \quad (4.9)$$

where  $c_Q$  is the weight factor for energy use.

There is no penalty on the CO<sub>2</sub> concentration ( $c_{CO_2} = 0$ ); the bounds are used for the proportional controller (see eqn. 4.29). The boundary values for temperature and temperature integral are taken from Körner (2003). When temperature integration is used, the temperature bounds can be further expanded, since the temperature integral will keep the average temperature at its reference value  $T_{ref}$ .

From the penalties and terminal costs given here, the penalty  $L_Q$  represents gas use, the penalty  $L_{aq}$  represents aquifer energy content and all other penalties ( $L_{Ta}$ ,  $L_{RHa}$ ,  $L_{TI}$ ) and terminal costs ( $\Phi_W$ ,  $\Phi_{TI}$ ) represent terms that are important for crop growth and development.

The temperature integral is penalized by two terms in the cost function: the terminal cost  $\Phi_{TI}$  penalizes long-term crop processes, and the penalty  $\int L_{TI}$  penalizes short-term crop processes.

The control inputs are constrained by

$$u_{i,\min} \leq u_i(\tau) \leq u_{i,\max} \quad i = 1, \dots, m; \quad t_0 \leq \tau \leq t_f \quad (4.10)$$

A control input trajectory  $u(\tau)$  that satisfies the constraints in eqn. 4.10 is called admissible. For the states there are trajectory constraints (bounds, see eqn. 4.7), which are considered ‘soft’. With these prerequisites the control problem is to find

$$u^*(\tau) = \arg \min_u J(u) \quad (4.11)$$

given the expected external inputs (weather prediction)  $\tilde{v}(\tau)$  for  $\tau \in [t_0, t_f]$ , subject to the differential equations (eqn. 4.1) and the control input constraints (eqn. 4.10). In other words, the objective is to find admissible input trajectories  $u^*(\tau)$  on the time interval  $\tau \in [t_0, t_f]$  such that the process given by eqn. 4.1 has control and state trajectories that minimize the performance criterion (cost function value)  $J$ . The resulting control input and state trajectories are referred to as the optimal trajectories.

#### 4.3.5 Derivation bounds for aquifer energy content

An aquifer is a formation of water-bearing sand material in the soil that can contain and transmit water. The aquifer has a warm and a cold side. The warm water is used by the heat pump to heat the greenhouse and the cold water is used by the heat exchanger to cool the greenhouse.

The aquifer must be approximately energy neutral year-round. This means that the amount of energy put into the aquifer must equal the amount of energy withdrawn from the aquifer. If this demand is not fulfilled the aquifer will warm up or cool down, which is unwanted. Therefore this demand must be incorporated in the cost function of the optimal control.

In the receding horizon control the control horizon is one day. This means that the aquifer energy content cannot be directly computed for a time period of one year in the optimal control procedure. A solution is found in which a year-round reference curve for the accumulated energy content of the aquifer is used. The reference curve is based on a year-round optimal control run with the grid search method. It gives an indication of what the energy content will look like. Relative to this reference curve bounds are defined, which represent the freedom to deviate from this curve. These bounds for the accumulated energy content of the aquifer can then be used as optimal control bounds. The energy accumulated in the aquifer must stay between these bounds. The bounds are time dependent since the reference curve is not a constant.

It is assumed that the aquifer has an infinite amount of warm and cold water available. The aquifer energy content bounds will limit the amount of energy that can be stored or retrieved. This indirectly corrects for the fact that the buffers are not infinite.

#### 4.3.5.1 Government demands

The government demands that the aquifer is energy neutral year-round. At any arbitrary reference date, the aquifer will have a specific initial energy content. Starting from that date the accumulated energy is monitored to make sure that the amount of energy stored in the aquifer is equal to the amount of energy retrieved from the aquifer over a period of one year.

If  $E_{aq}(t)$   $\{\text{J m}^{-2}\}$  describes the accumulated energy content of the aquifer over the time period  $t$ , the government demand is

$$E_{aq}(n_{secs\_yr}) = 0 \quad \{\text{J m}^{-2}\} \quad (4.12)$$

in which  $n_{secs\_yr} = 31536000 \text{ s yr}^{-1}$  is the number of seconds in a year.

The energy content  $E_{aq}$  of the aquifer, accumulated over a time period  $t$  is given by

$$E_{aq}(t) = E_{he}(t) - E_{hp}(t) + E_{aq0} \quad \{\text{J m}^{-2}\} \quad (4.13)$$

in which the amount of energy  $E_{he}$  extracted from the greenhouse by the heat exchanger and stored in the aquifer is given by

$$E_{he}(t) = \frac{1}{A_s} \cdot \int_0^t Q_{he} dt \quad \{\text{J m}^{-2}\} \quad (4.14)$$

and the amount of energy  $E_{hp}$  supplied to the greenhouse by the heat pump and retrieved from the aquifer is given by

$$E_{hp}(t) = \frac{1}{A_s} \cdot \int_0^t Q_c dt \quad \{\text{J m}^{-2}\} \quad (4.15)$$

and  $E_{aq0}$   $\{\text{J m}^{-2}\}$  is the initial value of the accumulated energy content of the aquifer. This is the energy that has been accumulated in the previous period, which should still be corrected for by the optimal control. At the first start of the aquifer use,  $E_{aq0} = 0$  (no energy accumulated yet). The energy transport term  $Q_{he}$   $\{\text{W}\}$  is the heat extracted from the greenhouse and supplied to the aquifer by the heat exchanger. The energy transport term  $Q_c$   $\{\text{W}\}$  is the heat retrieved from the aquifer and supplied to the greenhouse by the heat pump.

In the receding horizon control, the control horizon is one day, which means that a demand for a year cannot be implemented directly. The actual requirement by the government is not quite as strict as defined in eqn. 4.12. A grower should not deplete or warm up the aquifer too much, so the deviation of the energy content year-round should be within limits, such that it can be corrected during the next year. It is necessary to know the shape of the energy content curve to define limits relative to this curve, which can serve as bounds for the optimal control. This is the topic of the next paragraph.

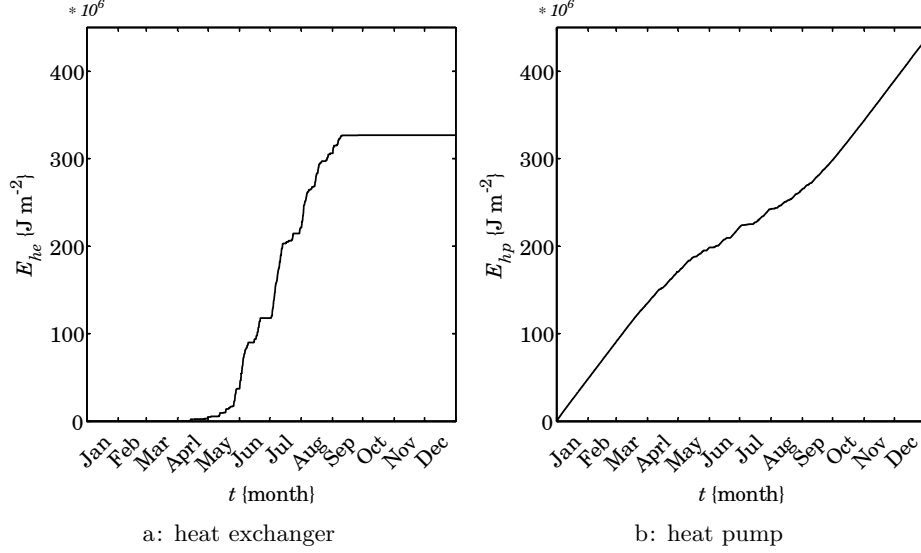
#### 4.3.5.2 The energy content of the aquifer

To achieve that the aquifer is energy neutral year-round, the optimal control needs a function that describes the bounds for the amount of energy stored in the aquifer as a function of time. To obtain a reference curve for the energy content  $E_{aq}^*$  year-round, the energy content is determined with the weather data from the *SEL*year (Breuer and van de Braak, 1989) and the receding horizon optimal control with grid search as described in §4.6. The initial version of this reference curve has been developed by Van Dongen (2004).

The amounts of energy  $E_{he}$  stored in the aquifer and  $E_{hp}$  retrieved by the heat pump are given in figure 4.2. The heat exchanger is used in spring and summer (May through August). This results in the energy curve for  $E_{he}$  stored by the heat exchanger shown in figure 4.2a, which has a clear S-shape. The heat pump is used intensively in fall and winter to heat the greenhouse, and slightly less in spring and summer to reduce the relative humidity in the greenhouse. This results in the energy curve for  $E_{hp}$  retrieved by the heat pump shown in figure 4.2b, which is almost linear with time with a slight S-shape.

It can be seen that more energy is retrieved from the aquifer ( $E_{hp}$ ) than stored in the aquifer ( $E_{he}$ ). The aim is to get an energy content reference curve  $E_{aq}^*$  that is equal to zero at the end of the year. This means that the energy curves  $E_{hp}$  and  $E_{he}$  in figure 4.2 should have the same value at the end of the year. It is assumed that the optimal control can increase the amount of energy  $E_{he}$  supplied to the aquifer by the heat exchanger to match the amount of energy  $E_{hp}$  retrieved from the aquifer by using the heat exchanger more intensively. The energy  $E_{he}$  is therefore scaled to match  $E_{hp}$ .

To find a function for the amount of energy  $E_{aq}$ , functions are estimated for  $E_{he}$  and  $E_{hp}$ . The energy  $E_{he}$  stored by the heat exchanger is approximated by


 Figure 4.2: Energy extraction and supply for the aquifer with *SELyear*

a S-shaped curve. The energy  $E_{hp}$  retrieved by the heat pump is approximated by a linear function in combination with a S-shaped curve. This gives

$$E_{he}^*(t) = \frac{0.5 \max(E_{he})}{1 + e^{-\theta_{hea} \cdot (\frac{t}{n_{secs\_yr}} - \theta_{heb})}} \quad \{\text{J m}^{-2}\} \quad (4.16)$$

$$E_{hp}^*(t) = \frac{\max(E_{he}) - \theta_{hpc}}{1 + e^{-\theta_{hpa} \cdot (\frac{t}{n_{secs\_yr}} - \theta_{hpb})}} + \theta_{hpc} \cdot \frac{t}{n_{secs\_yr}} \quad \{\text{J m}^{-2}\} \quad (4.17)$$

in which  $\max(E_{he}) = 435 \cdot 10^6 \text{ J m}^{-2}$  and the fraction of the year is  $\frac{t}{n_{secs\_yr}}$ , where  $t \{s\}$  is time,  $n_{secs\_yr} \{syr^{-1}\}$  is the number of seconds per year and  $\theta_{he}$  and  $\theta_{hp}$  are the parameters for the heat exchanger and the heat pump curve.

Parameter calibration gives the following values:  $\theta_{hea} = 18$ ,  $\theta_{heb} = 0.52$ ,  $\theta_{hpa} = 9$ ,  $\theta_{hpb} = 0.50$ ,  $\theta_{hpc} = 610 \cdot 10^6$ . The estimated curves are given in figure 4.3.

The estimated function for the amount of energy  $E_{aq}^*$  stored in the aquifer as a function of time is given by

$$E_{aq}^*(t) = E_{he}^*(t) - E_{hp}^*(t) \quad \{\text{J m}^{-2}\} \quad (4.18)$$

The result is shown in figure 4.4, where the dashed line is the aquifer energy content reference curve  $E_{aq}^*$  and the line represents the originally computed values.

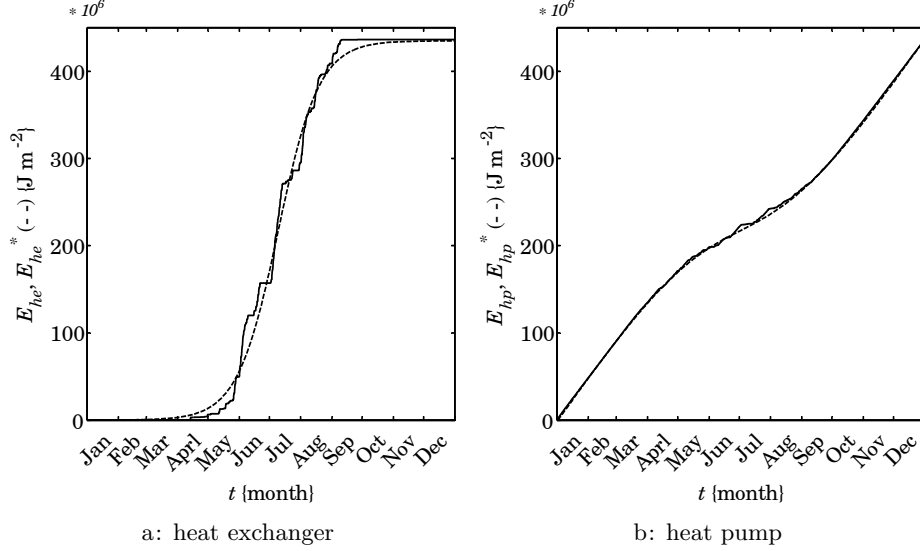


Figure 4.3: Energy extraction and supply for the aquifer with *SELyear*, computed (—) and estimated (---) curves

The aquifer does not have to be exactly energy neutral year-round. Bounds are defined around the aquifer energy content reference curve. These aquifer energy content reference bounds are relative to the aquifer energy content reference curve  $E_{aq}^*$ . The government does not allow nett heat storage in the aquifer year-round. The energy content is thus allowed to deviate more to the negative side, than to the positive side. Furthermore the bounds are wider during summer to allow for more deviation in the period that energy is harvested. The bounds are set to  $E_{aq\min}$  and  $E_{aq\max}$

$$E_{aq\min}(t) = E_{aq}^*(t) - \left( 200 \cdot 10^6 \sin\left(\frac{t}{n_{secs\_yr}} \cdot \pi\right) + 100 \cdot 10^6 \right) \{J m^{-2}\} \quad (4.19)$$

$$E_{aq\max}(t) = E_{aq}^*(t) + \left( 200 \cdot 10^6 \sin\left(\frac{t}{n_{secs\_yr}} \cdot \pi\right) + 75 \cdot 10^6 \right) \{J m^{-2}\} \quad (4.20)$$

where  $\frac{t}{n_{secs\_yr}}$  is the fraction of the year,  $t$  {s} is time and  $n_{secs\_yr}$  {syr<sup>-1</sup>} is the number of seconds per year.

The resulting demand for the optimal control is to keep the aquifer energy content  $E_{aq}$  between these bounds

$$E_{aq\min} \leq E_{aq}(t) \leq E_{aq\max} \quad \{J m^{-2}\} \quad (4.21)$$

These bounds are shown in figure 4.4 as dotted lines.

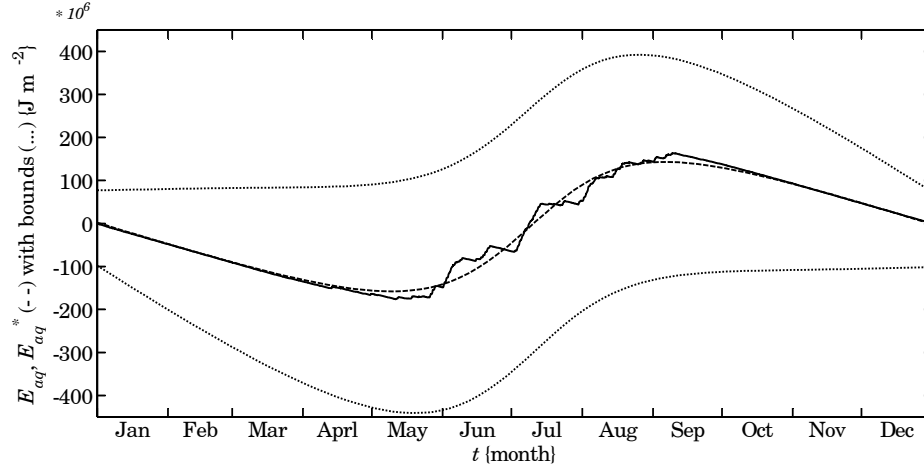


Figure 4.4: Aquifer energy content with  $SEL_{year}$ , computed (—) and estimated (---) curve and bounds (···)

The impact of the penalty  $\int L_{aq}$  for the aquifer energy content has been tested by running the solar greenhouse optimization for a week in summer and winter. In summer the initial aquifer energy content  $E_{aq}$  was set to a value above its upper bound  $E_{aq\max}$ . This prevented the use of the heat exchanger; the greenhouse was cooled by opening the windows. In winter the aquifer energy content  $E_{aq}$  was set to a value below its lower bound  $E_{aq\min}$ . This prevented the use of the heat pump; the greenhouse was heated by the boiler. The difference between the bound and the initial value was chosen small enough to see that when the energy content was between the bounds again, the heat exchanger c.q. heat pump were used again. This indicates that the penalty is working correctly.

#### 4.3.6 Control inputs

In conventional greenhouse control, the greenhouse climate is controlled by heuristic rules and set-points (heating and ventilation temperature). Through local PID controllers these set points result in window apertures and valve positions, which are the actual control inputs. The greenhouse climate model used in this research computes the actual control inputs directly.

In the first tests of the optimal control all control inputs were optimized by the optimal control. In a number of computations the optimal control results would yield control inputs where heating and cooling was used at the same time. In view of the cost function as it has been defined this was unexpected.

Evaluation of these results led to the conclusion that the optimal control got stuck in a local minimum. The same would hold for the window aperture: opening the lee- or windward side windows makes no difference in the results (but it does require extra computations). Therefore these control inputs are coupled into a combined control input, which is optimized by the optimal control.

A number of control inputs are computed by the optimal control, while other control inputs are determined directly from other control inputs, external inputs or states. In figure 3.2 this difference is denoted by dotted (set by optimal control) and dash-dotted frames (directly derived from other inputs).

The following control inputs (see figure 4.5a) are computed by the optimal control: the valve positions for heating and cooling with the boiler ( $vp_l$ ,  $vp_u$ ), heat pump ( $vp_{hp}^*$ ) and heat exchanger ( $vp_{he}^*$ ), the window apertures ( $Ap_{lsc}$ ,  $Ap_{wsd}$ ) and the option ventilation with heat recovery ( $op_{vhr}$ ). This is explained in §4.3.6.1.

The following control inputs (see figure 4.5b) are determined directly from other control inputs, external inputs or states: the valve position for CO<sub>2</sub> supply ( $vp_{CO_2}$ ) and the thermal screen closure ( $Cl_{sc}$ ). These relations are given in §4.3.6.2.

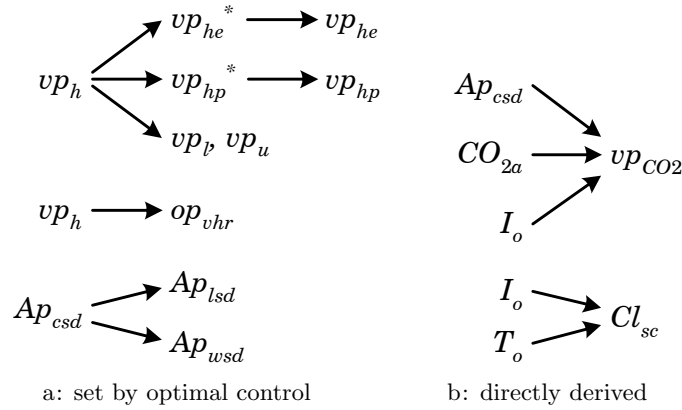


Figure 4.5: Relations control inputs

Here a short argumentation is given for the choice of the control inputs:

- Heating and cooling should not take place at the same time.
- When heating is needed, it should preferably be done with the lowest cost. Therefore the first choice is heating with the heat pump and the second choice is heating with the boiler.

- When ventilation is needed to decrease humidity, but not to decrease temperature, ventilation with heat recovery should be used.
- To prevent the wind from blowing through the greenhouse the lee-side windows are opened before the windward-side windows.
- CO<sub>2</sub> supply is only needed during daytime, when there is radiation, since then it is needed for photosynthesis. CO<sub>2</sub> is ventilated out when the windows are opened, and therefore it would make sense to restrict the CO<sub>2</sub> supply when the windows are opened.
- The thermal screen is used to decrease heat loss during cold periods with little solar radiation. The screen closure therefore fully depends on the outdoor weather condition (radiation and temperature).

#### 4.3.6.1 Control inputs set by optimal control

The control inputs for heating and cooling with the boiler, heat pump and heat exchanger ( $vp_l$ ,  $vp_u$ ,  $vp_{hp}^*$ ,  $vp_{he}^*$ ), the window apertures ( $Ap_{lsd}$ ,  $Ap_{wsd}$ ) and the option ventilation with heat recovery ( $op_{vhr}$ ) are computed by the optimal control.

The control inputs computed by the optimal control are combined into two control inputs:

- The combined heating valve position  $vp_h$   $[-1,2]$ , which determines the valve positions  $vp_l$ ,  $vp_u$ ,  $vp_{hp}^*$  and  $vp_{he}^*$ .
- The combined window aperture  $Ap_{csd}$   $[0,2]$ , which determines the window apertures  $Ap_{lsd}$  and  $Ap_{wsd}$ .

These combined optimal control inputs ( $vp_h$ ,  $Ap_{csd}$ ) are computed by the receding horizon optimal controller.

The relations between the combined control inputs computed by the optimal control and the control inputs used by the model are shown in figure 4.5a. The actual control inputs  $vp_{hp}$  and  $vp_{he}$  used by the model are derived from the computed control inputs  $vp_{hp}^*$  and  $vp_{he}^*$  with eqns. 3.182 and 3.192.

For heating/cooling the combined heating valve position  $vp_h$   $[-1,2]$  is used. It is subdivided into the valve positions for heat exchanger  $vp_{he}^*$ , heat pump  $vp_{hp}^*$ , lower net  $vp_l$  and upper net  $vp_u$  (see figure 4.6). The idea of this subdivision is that heating and cooling at the same time makes no sense, so this should be ruled out. If the greenhouse needs heating, this is preferably done by the heat pump, where the boiler is added if the heat pump cannot supply enough heat.

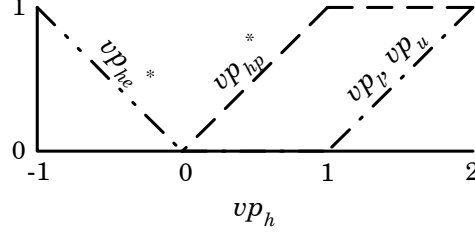


Figure 4.6: Combined heating valve position  $vp_h$ , with  $vp_{he}^*$  ( $- \cdot \cdot -$ ),  $vp_{hp}^*$  ( $- \cdot -$ ) and  $\{vp_l, vp_u\}$  ( $- \cdot \cdot -$ )

The relations for the combined heating valve position  $vp_h$  are given by

$$vp_{he}^*(t) = \begin{cases} -vp_h(t) & -1 \leq vp_h(t) < 0 \\ 0 & 0 \leq vp_h(t) \leq 2 \end{cases} \quad [0,1] \quad (4.22)$$

$$vp_{hp}^*(t) = \begin{cases} 0 & -1 \leq vp_h(t) < 0 \\ vp_h(t) & 0 \leq vp_h(t) < 1 \\ 1 & 1 \leq vp_h(t) \leq 2 \end{cases} \quad [0,1] \quad (4.23)$$

$$vp_l(t) = \begin{cases} 0 & -1 \leq vp_h(t) < 1 \\ vp_h(t) - 1 & 1 \leq vp_h(t) \leq 2 \end{cases} \quad [0,1] \quad (4.24)$$

$$vp_u(t) = \begin{cases} 0 & -1 \leq vp_h(t) < 1 \\ vp_h(t) - 1 & 1 \leq vp_h(t) \leq 2 \end{cases} \quad [0,1] \quad (4.25)$$

Ventilation with heat recovery  $op_{vhr}$  (eqn. 3.65) is used at times of heat demand, which is determined by the use of heat pump or boiler ( $vp_h > 0$ ). When ventilation with heat recovery is used, 90% of the sensible heat is recovered. Its value is either 0 (false) or 1 (true).

For ventilation the combined window aperture  $Ap_{csd}$  [0,2] is used. It is subdivided into the lee-side  $Ap_{lsd}$  and windward-side  $Ap_{wsd}$  window aperture (see figure 4.7). This shows that first the lee-side windows are opened, and if more ventilation is needed, the windward-side windows are opened. This is done to prevent the wind from blowing through the greenhouse.

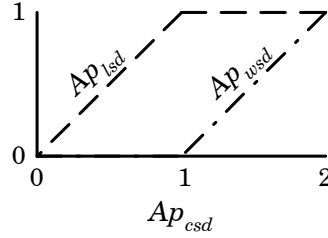


Figure 4.7: Combined window aperture  $Ap_{csd}$ , with  $Ap_{lsd}$  (--) and  $Ap_{wsd}$  (-.-)

The relations for the combined window aperture  $Ap_{csd}$  are given by

$$Ap_{lsd}(t) = \begin{cases} Ap_{csd}(t) & Ap_{csd}(t) \leq 1 \\ 1 & Ap_{csd}(t) > 1 \end{cases} \quad [0,1] \quad (4.26)$$

$$Ap_{wsd}(t) = \begin{cases} 0 & Ap_{csd}(t) \leq 1 \\ Ap_{csd}(t) - 1 & Ap_{csd}(t) > 1 \end{cases} \quad [0,1] \quad (4.27)$$

#### 4.3.6.2 Control inputs directly derived from other inputs

The control inputs for CO<sub>2</sub> supply ( $vp_{CO_2}$ ) and thermal screen closure  $Cl_{sc}$  are determined directly from other control inputs, external inputs or states. The relations are shown in figure 4.5b.

In common greenhouse practice (Nederhoff, 1994) the CO<sub>2</sub> supply is determined based on an instantaneous CO<sub>2</sub> set point that depends on the heat demand and the ventilation rate. A high set point is used when the heating is on, a low set point when there is no heat demand and little or none ventilation, and a minimum set point when the greenhouse is ventilated. The heat demand term is necessary in the conventional greenhouse since CO<sub>2</sub> is only available when the boiler is on. In the solar greenhouse CO<sub>2</sub> supply is independent from boiler operation, so this term can be left out.

The valve position for CO<sub>2</sub> supply  $vp_{CO_2}$  is controlled with a proportional controller. The idea here is that CO<sub>2</sub> supply is only necessary during daytime, when there is photosynthesis. If the windows are opened, CO<sub>2</sub> is ventilated out, so it would make sense to restrict the CO<sub>2</sub> supply depending on the window aperture. CO<sub>2</sub> supply is only needed when the CO<sub>2</sub> concentration in the greenhouse is below its maximum value. The CO<sub>2</sub> set point  $CO_{2a\_sp}$  { $\mu\text{mol}[\text{CO}_2] \text{ mol}^{-1}[\text{air}]$ } is determined directly based on the combined window aperture  $Ap_{csd}$  and the incoming short-wave radiation  $I_o$

$$CO_{2a\_sp}(t) = \begin{cases} CO_{2a\_max} - \frac{Ap_{csd}}{4} \cdot (CO_{2a\_max} - CO_{2a\_min}) & I_o > 0 \\ 0 & I_o = 0 \end{cases} \quad \{\mu\text{mol}[\text{CO}_2] \text{ mol}^{-1}[\text{air}]\} \quad (4.28)$$

$$vp_{CO_2}(t) = 0.01 (CO_{2a\_sp}(t) - CO_{2a}(t)) \quad [0,1] \quad (4.29)$$

in which  $CO_{2a\_min} = 320$  and  $CO_{2a\_max} = 1000$   $\{\mu\text{mol}[\text{CO}_2] \text{ mol}^{-1}[\text{air}]\}$  as given in table 4.1. This valve position is constrained to the range  $[0,1]$ . The valve position for  $\text{CO}_2$  supply  $vp_{CO_2}$  is still partly set by the optimal control, since it depends on  $Ap_{csd}$ .

With this controller a set point  $CO_{2a\_sp}$  of  $1000 \mu\text{mol}[\text{CO}_2] \text{ mol}^{-1}[\text{air}]$  is used when the windows are fully closed ( $Ap_{csd} = 0$ ), and a set point of  $660 \mu\text{mol}[\text{CO}_2] \text{ mol}^{-1}[\text{air}]$  when the windows are fully opened ( $Ap_{csd} = 2$ ). This setting was chosen because according to Nederhoff (1994) a set point of twofold the outdoor concentration (of about  $320 \mu\text{mol}[\text{CO}_2] \text{ mol}^{-1}[\text{air}]$ ) already has a large positive effect on the photosynthesis rate.

The thermal screen closure  $Cl_{sc}$  (eqn. 3.139) is not optimized in the optimal control since the ‘rules’ for the control are quite straightforward, and the screen is opened and closed in about 3 min, which is much smaller than the time interval  $t_{s\_u}$  for the control inputs of 30 min. The rules used (see §3.6.1) are similar to those used in greenhouse horticulture. The thermal screen closure  $Cl_{sc}$  is determined directly from the screen condition  $c_{sc} \in \{0,1\}$ . This screen condition is a discrete switch, which can be seen as an external input  $v$ , since it only depends on the outdoor shortwave solar radiation  $I_o$  and the temperature  $T_o$  of the outdoor air. The value of the screen closure  $Cl_{sc}$  in the optimal control is 0 (open) or 0.97 (closed, with a 3% crack opening to carry off moisture).

#### 4.3.7 Initial guess control inputs

Control input trajectories  $u^*$  (eqn. 4.11) that minimize the cost function value  $J$  have to be found. Only two control inputs are set by the optimal control (§4.3.6.1). Each control input consists of 48 values (§4.3.2), so at each receding horizon time step 96 values have to be computed.

This can be done with several optimization methods. In this research a conjugate gradient algorithm is used. The optimization is repeated with the sampling interval  $t_s$ . The optimization starts with initial values  $u_0$  for the

control input trajectories and changes these values until the minimum cost function value  $J$  is found. By default, the optimization for the next interval is started with the values for the control inputs found in the previous optimization, from which the first value is omitted, and the last value is equal to the last but one.

Since the model used is highly non-linear, the search procedure is likely to find a local minimum instead of the global minimum when the search is started from ill chosen initial values. Therefore a good initial guess for the control input trajectories  $u_0$  is needed. The procedure suggested here is partly based on a priori knowledge of the system, and partly on common sense. The procedure was first described in Van Ooteghem et al. (2003a). An example of the procedure described in this and in the next paragraph is given in §4.4.

At first the initial values for the control input trajectories are kept constant. This means that during the whole control horizon  $t_f$  (one day), the same values are used for each control input. The two optimal control inputs computed by the receding horizon optimal controller are:  $vp_h$  and  $Ap_{csd}$ . The combined valve position  $vp_h$  can take all values between  $-1$  and  $2$ , and the combined window aperture  $Ap_{csd}$  can take all values between  $0$  and  $2$ .

With two (constant) control inputs, it is easy to imagine a grid spanned over all possible control input values. The control space is discretized by restricting the possible values of the control inputs  $vp_h$  and  $Ap_{csd}$  to  $\{-1 -0.5 0 0.5 1 1.5 2\}$  and  $\{0 0.5 1 1.5 2\}$ , respectively. With weather predictions for the next day (external inputs  $v$ ), the influence of the control (control inputs  $u$ ) on the greenhouse climate (states  $x$ ) and the cost function value  $J$  can be simulated. If the cost function values  $J(u)$  are plotted against the control values  $vp_h$  and  $Ap_{csd}$ , a surface is formed. The control input combination  $u_0$  with the lowest cost function value  $J_{\min}$  is chosen. This is a good first guess for the control input values.

Since the control horizon  $t_f$  is one day, it may not always be desirable that the initial guesses for the control values are constant during this whole day. Therefore so called state dependent control input bounds are introduced, to rule out control values that make no sense based on knowledge of the system.

#### 4.3.8 State dependent control input bounds

Based on a priori knowledge of the system, bounds are set on the initial guess for the control inputs to push the optimal control solutions into the correct direction. These bounds are based on the initial states  $x$  for the time interval

$t_{s,u}$  (30 min) for the control inputs. From these states, the values of the indoor air temperature  $T_a$  and the relative humidity of the indoor air  $RH_a$  (based on the  $H_2O$  concentration of the indoor air  $C_{a,H_2O}$ ) are used to determine the input bounds. The minimum and maximum values for  $T_a$  and  $RH_a$  are the boundary values given in table 4.1. For the combined window aperture  $Ap_{csd}$  also the screen condition  $c_{sc}$  is used, which depends solely on the external inputs  $v$  (eqn. 3.140). The rules for the control input bounds are different for control with ( $TI$ ) and without ( $\cancel{TI}$ ) temperature integration.

The control input bounds on the combined heating valve position  $vp_h$   $[-1,2]$  are displayed graphically in figure 4.8.

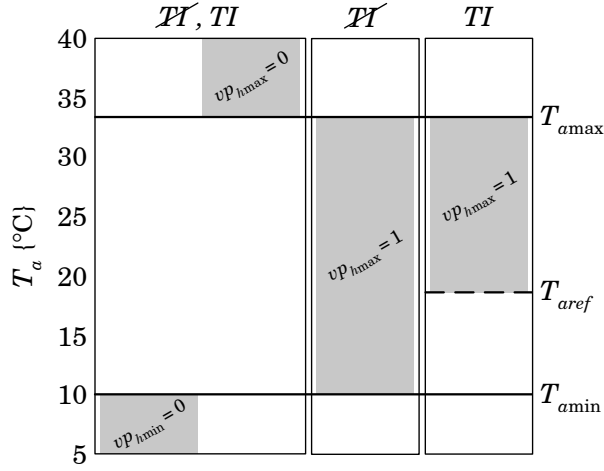


Figure 4.8: Bounds for combined heating valve position  $vp_h$

These bounds are defined by

$$\begin{array}{lll}
 \cancel{TI}, TI & vp_{h\min}(t) = 0 & T_a < T_{a\min} \\
 \cancel{TI} & vp_{h\max}(t) = 1 & T_{a\min} < T_a \leq T_{a\max} \\
 TI & vp_{h\max}(t) = 1 & T_{aref} < T_a \leq T_{a\max} \\
 \cancel{TI}, TI & vp_{h\max}(t) = 0 & T_{a\max} < T_a
 \end{array} \quad (4.30)$$

This can be interpreted as:

- $\cancel{TI}, TI$  No cooling with the heat exchanger if temperature  $T_a$  is below its lower bound  $T_{a\min}$ .
- $\cancel{TI}$  No heating with the boiler if temperature  $T_a$  is above its lower bound  $T_{a\min}$ .
- $TI$  No heating with the boiler if temperature  $T_a$  is above the reference temperature  $T_{aref}$ .

$\cancel{\mathcal{H}}, TI$  No heating with the heat pump or the boiler if temperature  $T_a$  is above its upper bound  $T_{a \max}$ .

The control input bound on the combined window aperture  $Ap_{csd}$   $[0,2]$  is displayed graphically in figure 4.9.

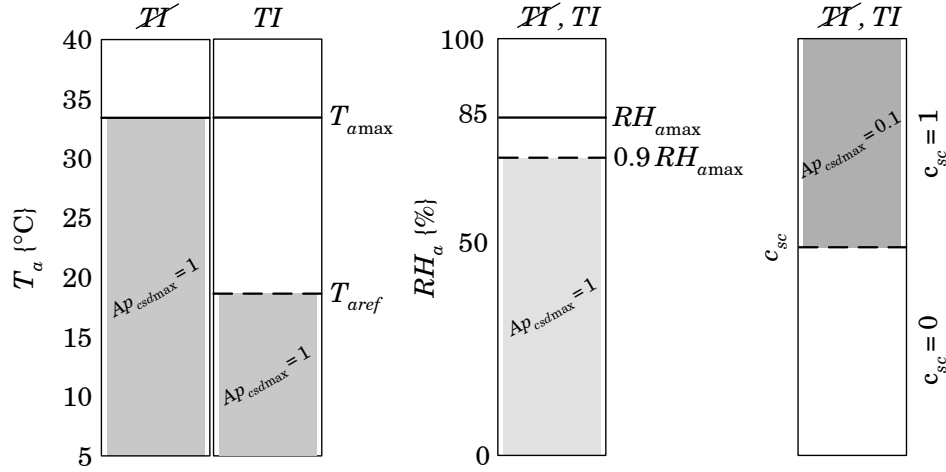


Figure 4.9: Bounds for combined window aperture  $Ap_{csd}$

This bound is defined by

$$\begin{array}{lll}
 \cancel{\mathcal{H}} & Ap_{csd \max}(t) = 1 & T_a < T_{a \max} \quad \text{and} \quad RH_a < 0.9 RH_{a \max} \\
 TI & Ap_{csd \max}(t) = 1 & T_a < T_{aref} \quad \text{and} \quad RH_a < 0.9 RH_{a \max} \\
 \cancel{\mathcal{H}}, TI & Ap_{csd \max}(t) = 0.1 & c_{sc} = 1
 \end{array} \tag{4.31}$$

This can be interpreted as:

- $\cancel{\mathcal{H}}$  Less ventilation if temperature  $T_a$  and relative humidity  $RH_a$  are below their upper bounds.
- $TI$  Less ventilation if temperature  $T_a$  is below the reference temperature  $T_{aref}$  for the temperature integral and relative humidity  $RH_a$  is below its upper bound.
- $\cancel{\mathcal{H}}, TI$  Much less ventilation when the screen is closed (as is done in greenhouse horticulture practice). The influence of the climate above the screen on the climate below the screen is small if the screen is closed (only 3% crack opening, see §3.6.1). Furthermore this prevents a sudden drop in temperature or humidity when the screen is opened.

A 10% safety margin is used for the upper bound of the relative humidity, since it can increase very fast and the time interval  $t_{s,u}$  for the control inputs is relatively large (30 min).

### 4.3.9 Weather prediction

For the current weather conditions and the weather predictions the *SELyear* weather data is used (Breuer and van de Braak, 1989). The *SELyear* data consists of Dutch climate data on selected months (Jan. 1971, Feb. 1973, etc.) that are fairly representative for the Dutch climate. The *SELyear* weather data contains hourly values for  $I_o$ ,  $v_o$ ,  $T_o$ ,  $T_{o,w}$  and  $T_{sk}$ . The relative humidity  $RH_o$  of the outdoor air is determined from the temperatures of the outdoor air  $T_o$  (dry bulb) and  $T_{o,w}$  (wet bulb) (see §2.C). For the  $CO_2$  concentration of the outdoor air no value is given in the *SELyear* data, so it is assumed that  $CO_{2o} = 320 \mu\text{mol}[CO_2] \text{ mol}^{-1}[\text{air}]$  ( $C_{o-CO_2} = 585.6 \cdot 10^{-6} \text{ kg}[CO_2] \text{ m}^{-3}[\text{air}]$ ). This data is shown in figure 4.10.

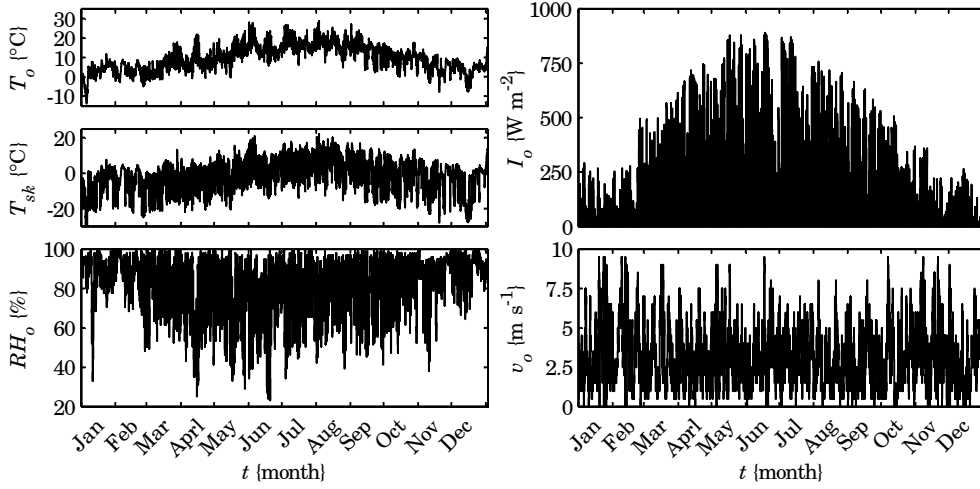


Figure 4.10: *SELyear* weather data  $v$

For the weather prediction a so called ‘lazy man weather prediction’ is used. Tap et al. (1996) used this method to predict the weather conditions during the next hour. They assumed that the weather conditions during the next hour were the same as the weather conditions during the past hour.

Now a weather prediction for one day is needed, since our control horizon  $t_f$  is one day. Assuming that the predicted weather conditions  $\tilde{v}(t, \tau)$  on the current day at time  $t$  are equal to the weather conditions  $v(t, t - t_f + \tau)$  of the previous day would be too crude an assumption, therefore a small correction is made. The weather conditions  $v(t, t - t_f + \tau)$  of the previous day are adjusted to match the current weather conditions  $v(t, t_0)$ , where  $\tau \in [t_0, t_f]$ .

$$\tilde{v}(t, \tau) = v(t, t - t_f + \tau) + (v(t, t_0) - v(t, t - t_f + t_0)) \quad \forall \tau \in [t_0, t_f] \quad (4.32)$$

i.e., if the current outdoor temperature  $T_o(t, t_0) = 15^\circ\text{C}$  and the temperature at the same time one day earlier was  $T_o(t, t - t_f + t_0) = 10^\circ\text{C}$ , then the correction (offset) for the whole temperature trajectory of the previous day  $T_o(t, t - t_f + \tau)$  is  $5^\circ\text{C}$ .

Eqn. 4.32 is used for the weather conditions:  $v_o$ ,  $T_o$ ,  $T_{o,w}$ ,  $T_{sk}$  and  $C_{o,CO2}$ . The wind speed  $v_o$  is set to zero if eqn. 4.32 gives a negative value. For the outdoor shortwave solar radiation  $I_o$  the value of the previous day is used without correction, since the correction would lead to incorrect radiation profiles.

An example of the weather prediction is shown in figure 4.11 for the outdoor temperature  $T_o$ . The actual weather data  $v$  is given for July 31 and August 1 as a solid line. The predicted weather data  $\tilde{v}$  is given for August 1 (dashed line), for the time  $t$  of 0 o'clock and 12 o'clock on August 1. The correction for the outdoor temperature  $T_o$  is  $-0.2^\circ\text{C}$  at 0 o'clock and  $6.9^\circ\text{C}$  at 12 o'clock. It can be seen that the trajectories for July 31 are adjusted with this offset. It is clear that the weather prediction is not accurate at 0 o'clock and quite good at 12 o'clock. This indicates that for the real implementation of the receding horizon optimal control preferably better weather predictions should be used.

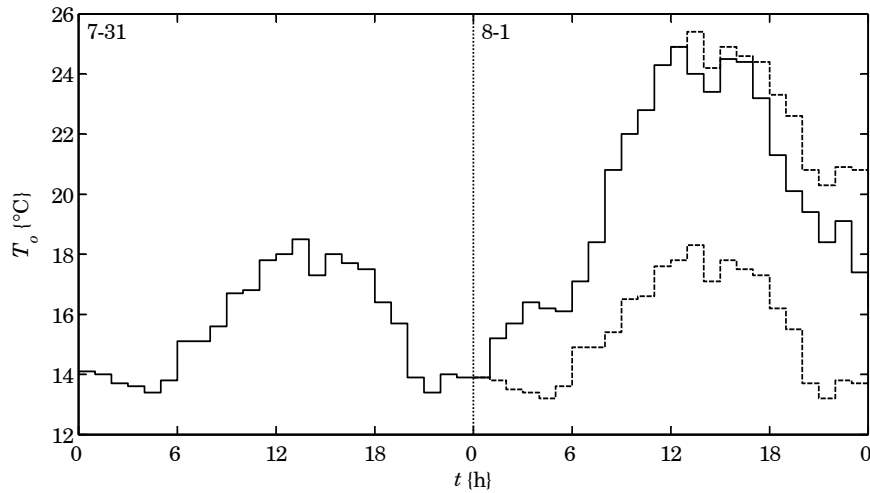


Figure 4.11: Weather data with predictions for August 1,  $v$  (—) and  $\tilde{v}$  (---)

In the receding horizon concept, this adjustment is made at every sampling interval  $t_s$  for the receding horizon controller to obtain a correction for the weather prediction. This sampling interval is 30 min, which means that the weather conditions (hourly values) have to be interpolated. This is done by linear interpolation.

#### 4.3.10 Open and closed loop computation

The optimal control concept has first been tested in open loop (without receding horizon). The open loop optimal control (OLOC) computations have been performed for one day ahead in summer and winter (§4.4; van Ooteghem et al., 2003a). Then the temperature integration has been added (§4.5) for good crop development, and therefore better crop quality. In the open loop computation the control input values are determined at the start of a day (once, no receding horizon) based on the initial state values  $x_0$  and the external inputs  $v$  (the weather). Open loop computations have been used in the tuning of the weight factors  $c$  in the cost function. The resulting weight factors are used in the RHOC implementation. Furthermore the open loop computations are used here to visualize the grid search and the gradient search method.

In the closed loop computation with receding horizon optimal control (RHOC), the control input trajectories are determined again for every sampling interval  $t_s$  for the receding horizon controller based on the initial state values  $x_0$  and the expected external inputs  $\tilde{v}$  (the weather prediction, see §4.3.9). The initial state values  $x_0$  for the next time interval are determined with the greenhouse-with-crop model, where instead of the weather prediction  $\tilde{v}$ , the actual weather  $v$  is used. Since these external inputs are different from the ones on which the computation was first based ( $v \neq \tilde{v}$ ), this will cause the state values  $x$  to deviate from the expected state values.

#### 4.3.11 Grid search and gradient search

The grid search method uses the initial guess for the control inputs as described in §4.3.7 with the state dependent control input bounds given in §4.3.8. This results in discrete values for the control inputs  $vp_h$  and  $Ap_{csd}$  ( $\{-1 -0.5 0 0.5 1 1.5 2\}$  and  $\{0 0.5 1 1.5 2\}$ , respectively). Each control input trajectory consists of  $\frac{t_f}{t_{s,u}} = 48$  values. Every control input trajectory  $u_{grid}^*$  is constant over the whole control horizon  $t_f$ , unless this constant value is overruled by the state dependent control input bounds. This method is used for the computation of the control input values at every full hour. At the intermediate half an hour (the sampling interval  $t_s$  is 30 min) the control input values found in the previous optimization are used. The optimal control input trajectories  $u_{grid}^*$  correspond to the minimum cost function value  $J_{grid}$  found with the grid search method. This grid search method is a (rather rough) global minimization method.

The gradient search method uses the conjugate gradient algorithm as described by Pagurek and Woodside (1968). The optimal control input trajectories  $u_{grad}^*$  correspond to the minimum cost function value  $J_{grad}$  found with the gradient search method. Since the model used in this research is highly non-linear, this non-linear iterative conjugate gradient method cannot guarantee that the global minimum is found. A wisely chosen starting point for the control input values  $u^*$  increases the probability that the global minimum for the cost function value  $J$  is found. The results  $u_{grid}^*$  of the grid search method are therefore used as an initial guess for the control input values. Resetting the algorithm from time to time will further increase this probability. By default the control input results of the previous optimization (shifted over the sampling time  $t_s$ ) are used as the initial guess for the next time interval. At every full hour the control inputs  $u_{grid}^*$  are determined again, and whenever the cost function value  $J_{grid}$  is lower than  $J_{grad}$ , these control inputs are used as the new initial guess, thus reinitializing the gradient search. This gradient search method is a local minimization method. The combination of the gradient search method with the grid search method (reset) is meant to give less local minima results.

The year-round RHOC computation has first been performed with the grid search method (§4.6; van Ooteghem et al., 2004a, 2005a). This was done to get an idea of the year-round values with a fast computation (about 8 hours). These results were used to determine the aquifer energy content curve (§4.3.5.2). Then the gradient search method was applied (§4.7; van Ooteghem et al., 2006), which was more time consuming (about 8 days).

## 4.4 Open loop optimal control ( $\mathcal{PI}$ )

This paragraph describes the open loop optimal control (OLOC) trajectories for a day in winter and in summer without temperature integration. These control input trajectories were determined as a first test of the feasibility of the optimal control method proposed here for the solar greenhouse. It is based on Van Ooteghem et al. (2003a,b).

The open loop computation gives the control input values that are determined at the start of a day based on the initial state values and the expected external inputs (weather). For the weather prediction  $\tilde{v}$  the actual weather  $v$  is used (from the *SELYear* data, one-hourly values). First the grid search method is used to find good initial values for the control inputs  $u_{grid}^*$ , which gives the corresponding cost function value  $J_{grid}$ . Then the gradient search method is

used to further improve the cost function value. This gives the control inputs  $u_{grad}^*$  with the corresponding cost function value  $J_{grad}$ .

The open loop optimal control trajectories are computed over a control horizon  $t_f$  of one day. This is a computation without temperature integration, so the temperature integral is not used in the cost function. The bounds for the temperature of the indoor air  $T_a$  (see table 4.1) are then closer together than for the optimal control with temperature integration. The results for two days are evaluated, one in winter (February 1) and one in summer (August 1). These two days have been selected based on their difference in weather data, to make sure that the optimal control settings (i.e., the weight factors  $c$  in the cost function) work well for a wide range of weather conditions.

#### 4.4.1 Weather data

Weather data is needed for the external inputs. The actual weather  $v$  — based on the *SELYear* data — is used here. The weather data is given in the figure 4.12a and figure 4.12b for the winter and the summer day respectively. It can be seen that the weather data shows large differences: on the summer day there is more radiation  $I_o$ , a higher temperature  $T_o$  and a lower relative humidity  $RH_o$  during daytime compared to the winter day. The  $\text{CO}_2$  concentration  $CO_{2o}$  of the outdoor air is equal to  $320 \mu\text{mol}[\text{CO}_2] \text{ mol}^{-1}[\text{air}]$ .

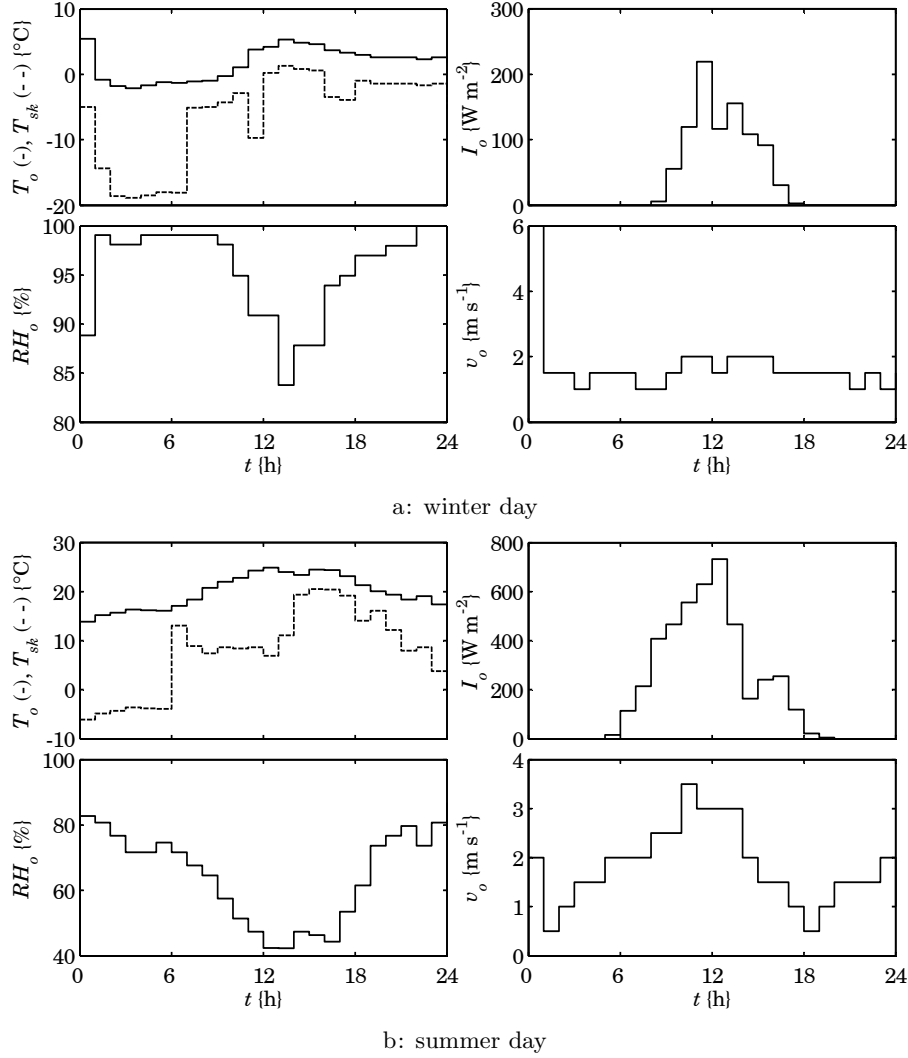
#### 4.4.2 Results open loop optimal control grid search (*PI*)

The control inputs  $u_{grid}^*$  are determined with the grid search method with state dependent control input bounds (see §4.3.7, §4.3.8 and §4.3.11). The optimal control input values  $u_{grid}^*$  correspond to the minimum cost function value  $J_{grid}$ . In figure 4.13 the resulting cost function values are given for the winter and the summer day.

From figure 4.13 it can be seen that the best initial values for the control inputs are not the same for winter and summer. Based on a grid of  $5 \times 7$  values, the best control input combination is found. They are denoted with a star ( $\star$ ) in figure 4.13:

$$\begin{aligned} \text{winter: } vp_h &= 1.5 \text{ and } Ap_{csd} = 0.5 \\ \text{summer: } vp_h &= -1.0 \text{ and } Ap_{csd} = 2.0 \end{aligned}$$

which yields the cost function values  $J_{grid} = 9.54$  for the winter day and  $J_{grid} = -20.30$  for the summer day.

Figure 4.12: Weather data  $v$ 

The following can be observed for the winter day:

- The combined heating valve position  $vp_h = 1.5$  corresponds to the valve positions  $vp_{hp}^* = 1$ ,  $vp_l = vp_u = 0.5$  and  $vp_{he}^* = 0$ . This means that the greenhouse is heated with the heat pump, and additional heat is supplied by the boiler. The heat exchanger is off.
- The combined window aperture  $Ap_{csd} = 0.5$  corresponds to the window apertures  $Ap_{lsd} = 0.5$  and  $Ap_{wsd} = 0$ . This means that the lee-side window is partly opened. Ventilation with heat recovery is used ( $op_{vhr} = 1$ ),

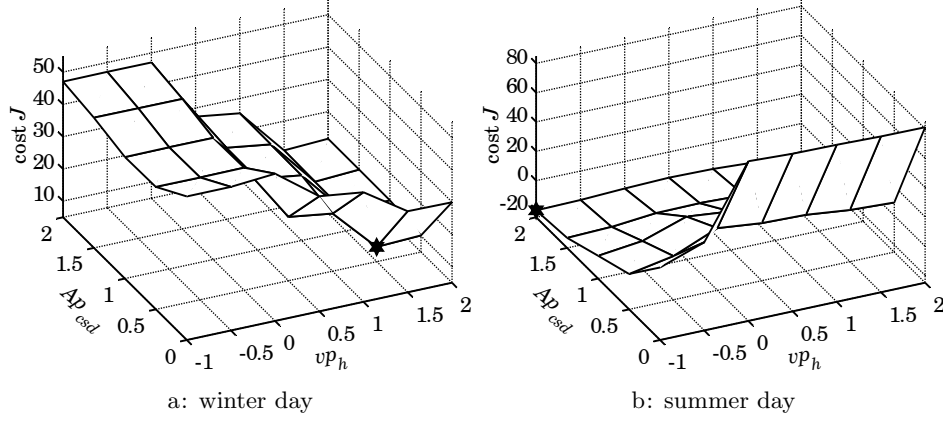


Figure 4.13: Cost function values  $J_{grid}$  (grid of  $5 \times 7$  values),  $\mathcal{PI}$

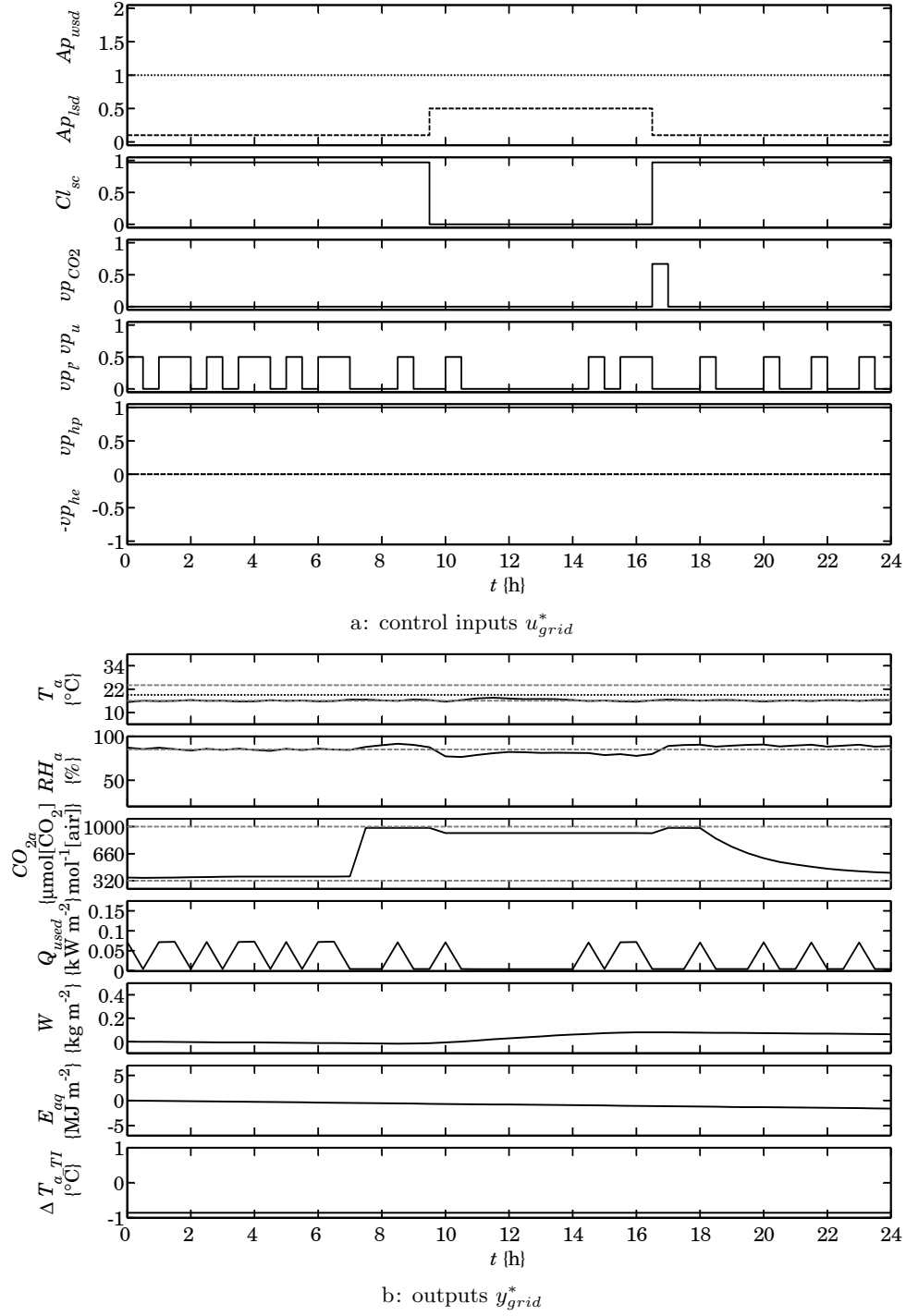
since the greenhouse is heated ( $vp_h > 0$ ), which means there is less heat loss due to this ventilation compared to normal ventilation.

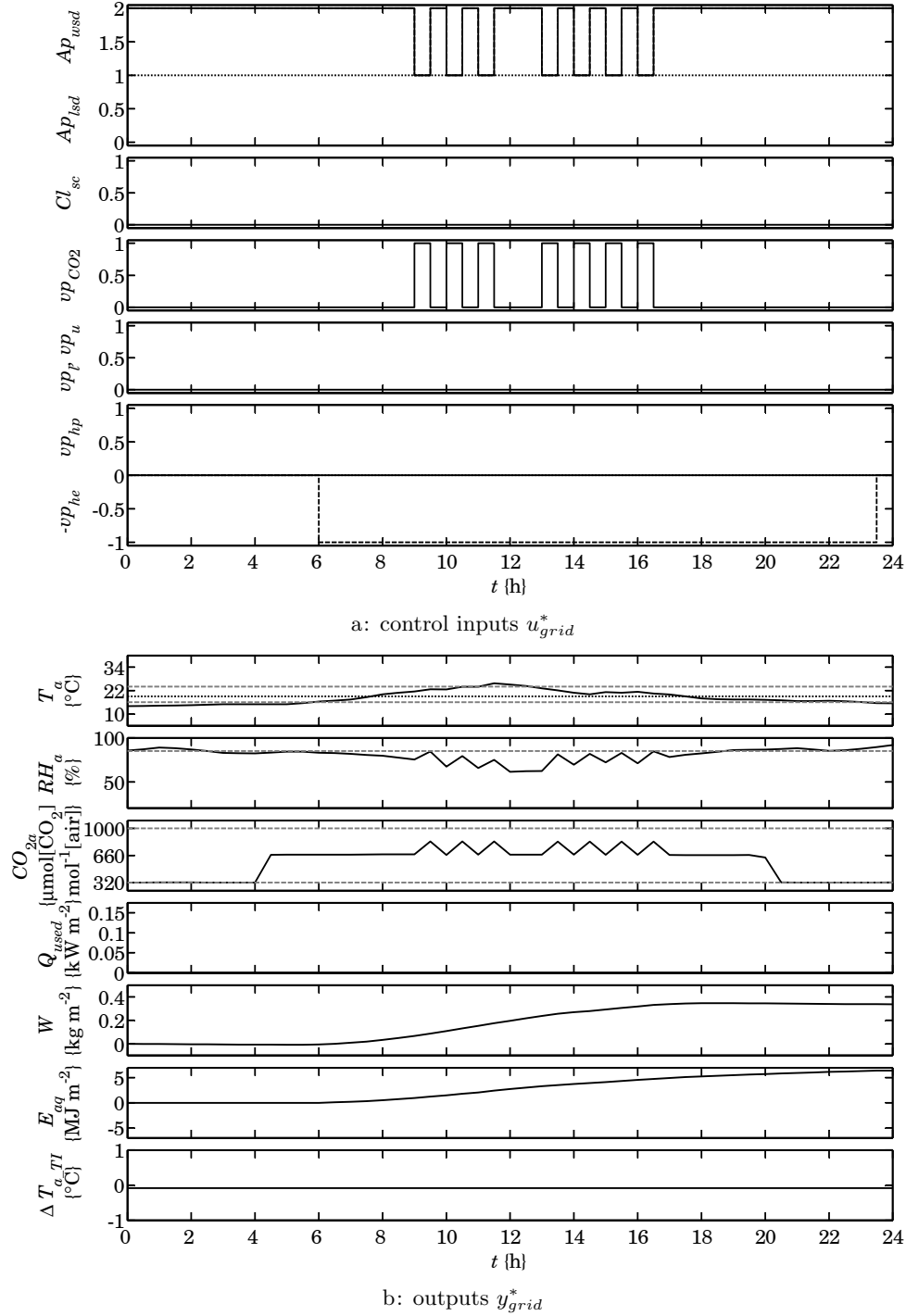
and for the summer day:

- The combined heating valve position  $vp_h = -1$  corresponds to the valve positions  $vp_{hp}^* = 0$ ,  $vp_l = vp_u = 0$  and  $vp_{he}^* = 1$ . This means that the greenhouse is cooled with the heat exchanger. The heat pump and the boiler are off.
- The combined window aperture  $Ap_{csd} = 2$  corresponds to the window apertures  $Ap_{lsc} = 1$  and  $Ap_{wsd} = 1$ . This means that the windows are fully opened on both sides. Ventilation with heat recovery is not used ( $op_{vhr} = 0$ ), since the greenhouse is cooled ( $vp_h \leq 0$ ).

In the figures 4.14a and 4.15a the control inputs  $u_{grid}^*$  are given for the winter and the summer day. These figures show the window aperture (lee-  $Ap_{lsc}$  and windward-side  $Ap_{wsd}$ ), the thermal screen closure  $Cl_{sc}$ , and the valve positions for CO<sub>2</sub> supply  $vp_{CO2}$ , lower net  $vp_l$ , upper net  $vp_u$ , heat pump  $vp_{hp}$  and heat exchanger  $vp_{he}$ . When ventilation with heat recovery is used, the window aperture is given as a dashed line.

The corresponding outputs  $y_{grid}^*$  are given in the figures 4.14b and 4.15b. These figures show the terms that determine the costs. These include the temperature  $T_a$  {°C}, the relative humidity  $RH_a$  {‰}, the CO<sub>2</sub> concentration of the indoor air below the screen  $C_{a,CO2}$  {kg m<sup>-3</sup>}, the energy used  $Q_{used}$  {W m<sup>-2</sup>}, the biomass  $W$  {kg m<sup>-2</sup>}, the aquifer energy content  $E_{aq}$  and the average temperature deviation over six days  $\Delta T_{a, TI}$  {°C}.

Figure 4.14: Grid search  $\mathcal{PI}$ , winter day (2-1)

Figure 4.15: Grid search  $\mathcal{I}$ , summer day (8-1)

In these figures the influence of the state dependent control input bounds (§4.3.8) is clearly seen.

For the winter day (figure 4.14):

- The combined heating valve position  $vp_h = 1.5$  is limited to 1 when  $T_a > T_{a\min}$  according to eqn. 4.30. This means that the boiler is turned off at these times, so  $vp_l = vp_u = 0$ .
- The combined window aperture  $Ap_{csd} = 0.5$  is limited to 0.1 when  $c_{sc} = 1$  according to eqn. 4.31. This means that the ventilation is limited when the screen is closed. Ventilation with heat recovery is used for the ventilation ( $op_{vhr} = 1$ ), which is indicated by the dashed line in figure 4.14a for the window apertures.

and for the summer day (figure 4.15):

- The combined heating valve position  $vp_h = -1$  is limited to 0 when  $T_a < T_{a\min}$  according to eqn. 4.30. This means that the heat exchanger is turned off at these times, so  $vp_{he}^* = 0$ .
- The combined window aperture  $Ap_{csd} = 2$  is limited to 1 when  $T_a < T_{a\max}$  and  $RH_a < 0.9 RH_{a\max}$  according to eqn. 4.31. This means that the ventilation is limited when the temperature  $T_a$  and the relative humidity  $RH_a$  are within their bounds. Normal ventilation with the windows is used ( $op_{vhr} = 0$ ), which is indicated by the line in figure 4.14a for the window apertures.

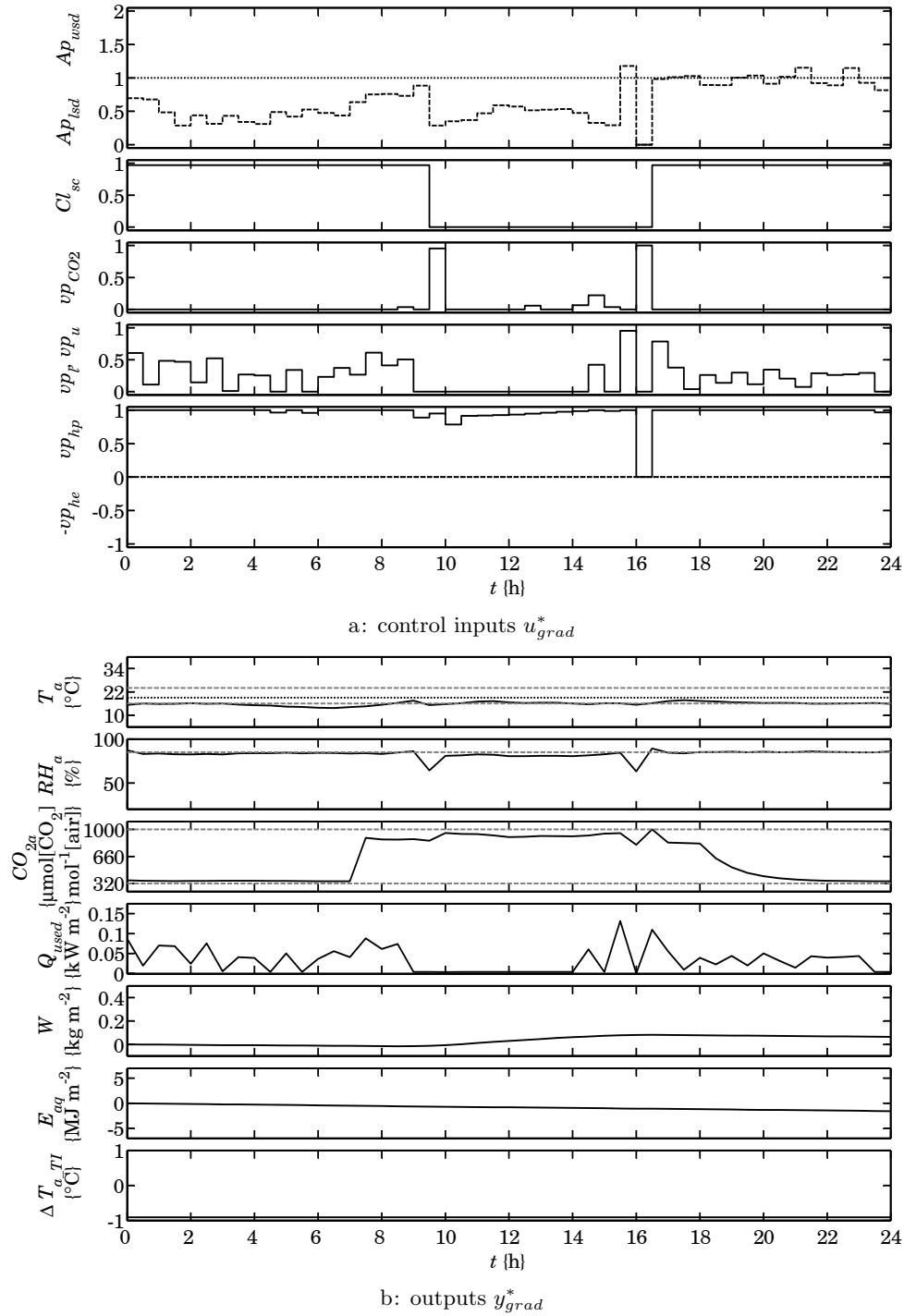
#### 4.4.3 Results open loop optimal control gradient search ( $\mathcal{PI}$ )

Now the gradient search method is used to further improve the cost function value, starting with the initial guess  $u_{grid}^*$  for the control inputs values determined with the grid search method in §4.4.2. This gives the control inputs  $u_{grad}^*$  with the corresponding cost function value  $J_{grad}$ .

In this paragraph the gradient search results are discussed for a day in winter and summer without temperature integration. It will be shown that the gradient search can further improve the grid search results.

##### 4.4.3.1 Results open loop optimal control gradient search, winter day ( $\mathcal{PI}$ )

In figure 4.16a the control inputs  $u_{grad}^*$  are given for the winter day. The dashed lines for the window aperture indicate ventilation with heat recovery. The corresponding outputs  $y_{grad}^*$  are given in figure 4.16b.

Figure 4.16: Gradient search  $\mathcal{PI}$ , winter day (2-1)

Comparing the figures 4.14a and 4.16a, the main change is seen in the window aperture  $Ap_{lsd}$  during the night. Where it was limited to 0.1 in the grid search, it is about 0.5 in the gradient search result. The valve positions for heating with the boiler  $vp_l$  and  $vp_u$  and the heat pump  $vp_{hp}$  are only slightly altered. The solar greenhouse is heated with the heat pump, and during the night the boiler is used to supply extra heat. The CO<sub>2</sub> supply keeps the CO<sub>2</sub> concentration  $CO_{2a}$  between 900 and 1000  $\mu\text{mol}[\text{CO}_2] \text{mol}^{-1}[\text{air}]$  during the day. The thermal screen is closed during the night, since the outdoor temperature  $T_o$  is low.

Comparing the figures 4.14b and 4.16b, a change is seen in the relative humidity  $RH_a$  and the energy used  $Q_{used}$ . This is more clearly seen in the values of the penalties  $L$  and the terminal costs  $\Phi$  given in table 4.2, which determine the cost function values  $J$ . The cost function value of these trajectories is  $J_{grad} = 2.93$ , which is indeed lower than the value of the grid search. In the table the costs for the temperature integral ( $\int L_{TI}$ ,  $\Phi_{TI}$ ) are also given, for later comparison with the results with temperature integration.

Table 4.2: Costs open loop  $\mathcal{PI}$ , winter day (2-1)

	$\int L_{Ta}$	$\int L_{RH_a}$	$\int L_Q$	$\Phi_W$	$\Phi_{TI}$	$J$
grid	0.40	9.51	4.50	-4.88	21.50	9.54
gradient	1.69	1.03	5.18	-4.97	22.57	2.93

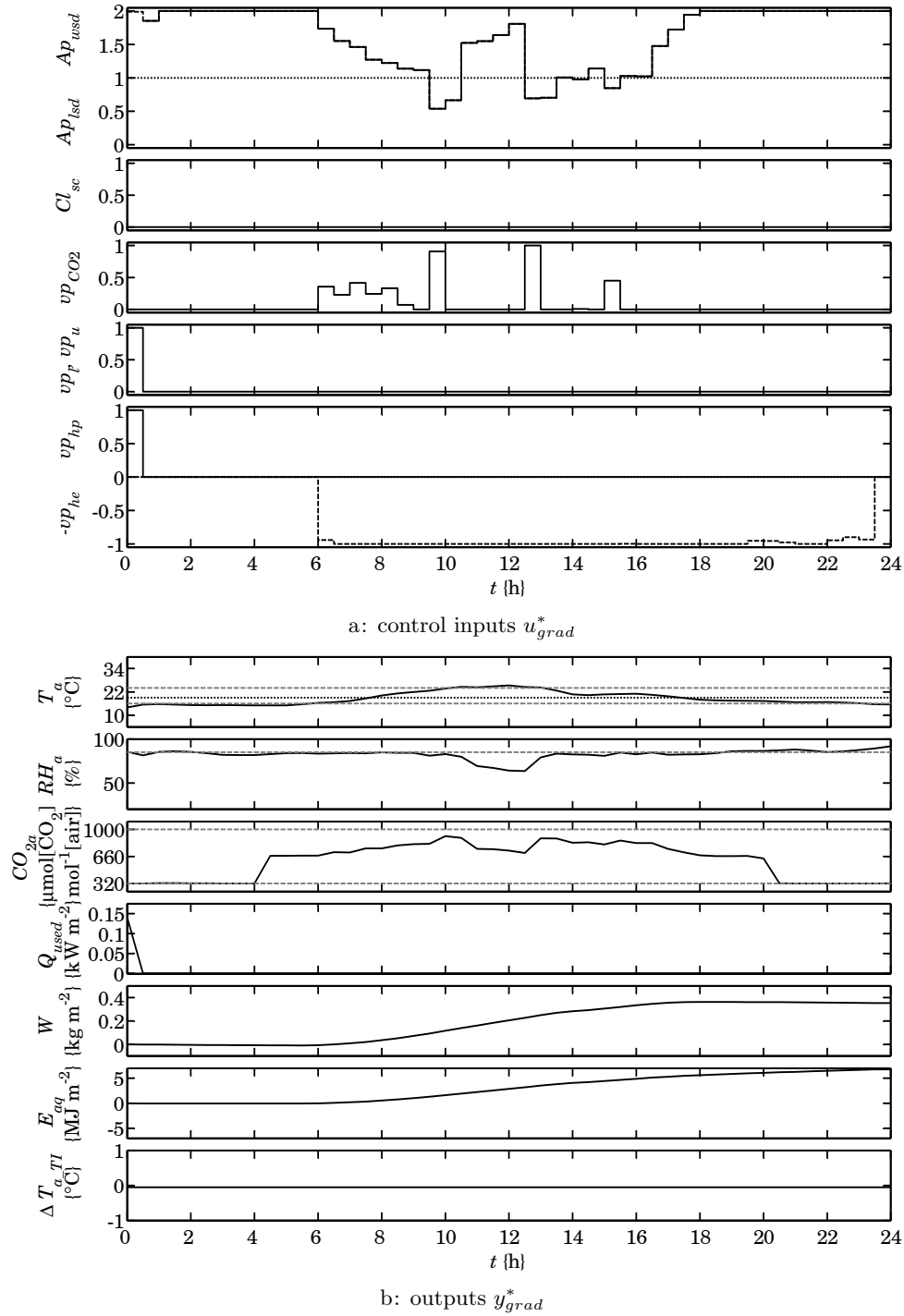
$\int L_{TI} = 0$  and  $\int L_{aq} = 0$

From the costs given in table 4.2 it can be seen that the output trajectories are changed to decrease the penalty for the relative humidity  $RH_a$ . It is important to keep the relative humidity  $RH_a$  below its upper bound  $RH_{a\max}$ , since this decreases the risk for diseases and fungi. This requires more heat input, which slightly increases the penalty  $\int L_Q$ . The temperature  $T_a$  decreases below its lower bound  $T_{a\min}$  more often, which increases the penalty  $\int L_{Ta}$ .

#### 4.4.3.2 Results open loop optimal control gradient search, summer day ( $\mathcal{PI}$ )

In figure 4.17a the control inputs  $u_{grad}^*$  are given for the summer day. The corresponding outputs  $y_{grad}^*$  are given in figure 4.17b.

Comparing the figures 4.15a and 4.17a, only small changes are seen. The valve positions for heating with the boiler  $vp_l$  and  $vp_u$  and the heat pump  $vp_{hp}$ , and for cooling with the heat exchanger  $vp_{he}$  are only slightly altered.

Figure 4.17: Gradient search  $\mathcal{PI}$ , summer day (8-1)

The heat exchanger is used to cool the greenhouse during the day. It is still used after 19 o'clock to decrease the temperature since this decreases the dark respiration  $r_c$ , which thus increases the biomass  $W$ . The  $\text{CO}_2$  supply keeps the  $\text{CO}_2$  concentration  $CO_{2a}$  between 660 and 900  $\mu\text{mol}[\text{CO}_2] \text{mol}^{-1}[\text{air}]$  during the day. The thermal screen is open, since the outdoor temperature  $T_o$  is high. Ventilation is used to decrease the relative humidity  $RH_a$  during the night, and to decrease the temperature  $T_a$  during the day.

Comparing the figures 4.15b and 4.17b, a small change is seen in the relative humidity  $RH_a$ . The values of the penalties  $L$ , the terminal costs  $\Phi$  and the cost function values  $J$  are given in table 4.3. The cost function value of these trajectories is  $J_{grad} = -22.75$ , which is lower than the value of the grid search.

Table 4.3: Costs open loop  $\mathcal{PI}$ , summer day (8-1)

	$\int L_{Ta}$	$\int L_{RH_a}$	$\int L_Q$	$\Phi_W$	$\Phi_{TI}$	$J$
grid	1.98	3.56	0.00	-25.83	2.11	-20.30
gradient	1.32	2.57	0.46	-27.09	1.25	-22.75

$\int L_{TI} = 0$  and  $\int L_{aq} = 0$

From the costs given in table 4.3 it can be seen that the output trajectories are changed to decrease the penalty for the relative humidity. The solar greenhouse is heated with the heat pump and the boiler at 0 o'clock since the temperature  $T_a$  is below its lower bound at that time. This increases the penalty  $\int L_Q$ . The temperature  $T_a$  increases above its upper bound  $T_{a\max}$  at 12 o'clock, although the ventilation is almost at its maximum, and cooling is at its maximum. The total biomass production is also increased.

#### 4.4.3.3 General results open loop optimal control, winter and summer day ( $\mathcal{PI}$ )

The photosynthesis rate is lower on the winter day compared to the summer day due to less solar radiation. This causes less  $\text{CO}_2$  consumption and a lower biomass increase  $\Delta W$ . A higher biomass increase could be achieved on the winter day by increasing the temperature  $T_a$ , but the decrease of the terminal cost  $\Phi_W$  that can be achieved does not outweigh the energy penalty  $\int L_Q$  for heating.

While there is sunlight, the CO<sub>2</sub> supply  $vp_{CO_2}$  is opened, unless it is limited by the ventilation. With high solar radiation  $I_o$  this results in a large increase of the biomass  $W$ . This growth implies a high crop photosynthesis rate  $P_{cg}$  and therewith a high use of CO<sub>2</sub>, resulting in a lower CO<sub>2</sub> concentration  $CO_{2a}$ .

A temperature increase causes a decrease in relative humidity  $RH_a$ . A higher temperature  $T_a$  during the day causes a higher photosynthesis rate  $P_{cg}$  and a lower temperature during the night causes a lower dark respiration rate  $r_c$ . This increases the net photosynthesis rate of the canopy  $\Phi_{m.a.c.CO_2}$ , and therefore the biomass increase  $\Delta W$ .

#### 4.4.4 Conclusions open loop optimal control (*PI*)

The open loop optimal control without temperature integration has been tested with weather data of a winter and a summer day. From the open loop optimal control results found, it can be concluded that

- Optimal control of the solar greenhouse is feasible.
- Although the model is non-linear and complex, rational optimal control solutions can be found.
- The control and state trajectories can be interpreted easily, since the internal variables have physical meaning.
- The use of a pre-computation of the constant initial optimal control values can be used to obtain control trajectories that are more likely to be globally optimal.
- The results of the optimal control strongly depend on the weather conditions; therefore reliable forecasts are needed.
- The boiler, heat pump and heat exchanger are used only if it yields a profit in the optimal control cost function. This causes temperature and relative humidity to be close to their bounds.
- The use of the solar greenhouse elements (heat pump, heat exchanger and ventilation with heat recovery) results in lower energy costs and a higher biomass increase.

### 4.5 Open loop optimal control (*TI*)

This paragraph describes the open loop optimal control trajectories for a day in summer and in winter with temperature integration. These control input trajectories were determined to indicate the difference between the control without and with temperature integration. It is based on Van Ooteghem

et al. (2004b,a, 2005b). The temperature integration was added to ensure proper crop development during all development stages. It is used as a descriptive method for long-term temperature effects on crop development. The underlying assumption is that crop development is determined by the average temperature, rather than the momentary temperature at a specific time.

Including the temperature integral of course changes the weight factor  $c_{TI}$ , which was equal to zero in the version without temperature integral. Furthermore wider bounds are used in the cost function (see table 4.1) for the temperature  $T_a$ , since the temperature integral is intended to ensure that an average temperature is kept. This extra margin allows additional freedom for the optimal control. The procedure is basically the same as in §4.4. A slight difference is found in the definition of the state dependent control input bounds (see §4.3.8). The weather data for the winter and the summer day are the same as before (see §4.4.1).

#### 4.5.1 Results open loop optimal control grid search (TI)

The control inputs  $u_{grid}^*$  are determined with the grid search method with state dependent control input bounds (see §4.3.7 and §4.3.8). In figure 4.18 the resulting cost function values are given for the winter and the summer day. These figures are similar to the figures without temperature integration (figure 4.13).

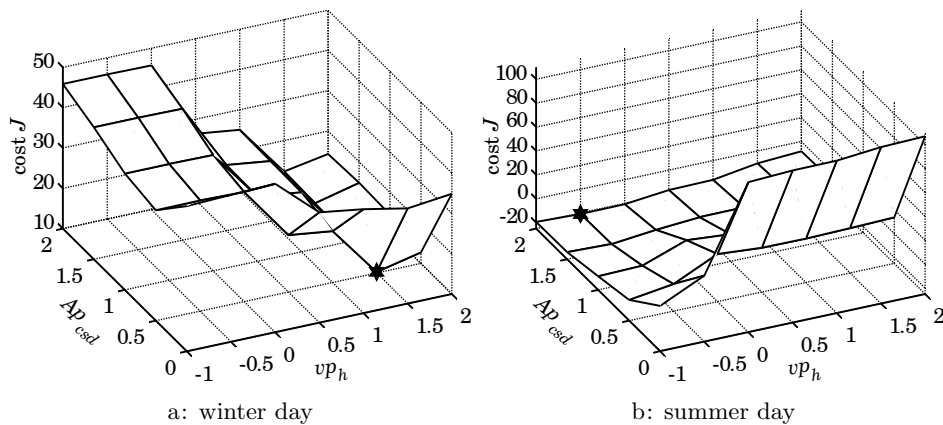


Figure 4.18: Cost function values  $J_{grid}$  (grid of  $5 \times 7$  values), TI

The best control input combinations found are denoted with a star ( $\star$ ) in figure 4.18:

$$\begin{aligned} \text{winter: } vp_h &= 1.5 \text{ and } Ap_{csd} = 0.5 \\ \text{summer: } vp_h &= -0.5 \text{ and } Ap_{csd} = 2.0 \end{aligned}$$

which yields the cost function values  $J_{grid} = 10.26$  for the winter day and  $J_{grid} = -20.79$  for the summer day. Note that the cost function value in winter is higher than without temperature integration (10.26 vs. 9.54). This is due to the fact that an average value for the temperature  $T_a$  must be achieved.

The following can be observed for the winter day:

- The combined heating valve position  $vp_h = 1.5$  corresponds to the valve positions  $vp_{hp}^* = 1$ ,  $vp_l = vp_u = 0.5$  and  $vp_{he}^* = 0$ . This means that the greenhouse is heated with the heat pump, and additional heat is supplied by the boiler. The heat exchanger is off.
- The combined window aperture  $Ap_{csd} = 0.5$  corresponds to the window apertures  $Ap_{lsd} = 0.5$  and  $Ap_{wsd} = 0$ . This means that the lee-side window is partly opened. Ventilation with heat recovery is used ( $op_{vhr} = 1$ ), since the greenhouse is heated ( $vp_h > 0$ ), which means there is less heat loss due to this ventilation compared to normal ventilation.

and for the summer day:

- The combined heating valve position  $vp_h = -0.5$  corresponds to the valve positions  $vp_{hp}^* = 0$ ,  $vp_l = vp_u = 0$  and  $vp_{he}^* = 0.5$ . This means that the greenhouse is cooled with the heat exchanger. The heat pump and the boiler are off.
- The combined window aperture  $Ap_{csd} = 2$  corresponds to the window apertures  $Ap_{lsd} = 1$  and  $Ap_{wsd} = 1$ . This means that the windows are fully opened on both sides. Ventilation with heat recovery is not used ( $op_{vhr} = 0$ ), since the greenhouse is cooled ( $vp_h \leq 0$ ).

In the figures 4.19a and 4.20a the control inputs  $u_{grid}^*$  are given for the winter and the summer day. The corresponding outputs  $y_{grid}^*$  are given in the figures 4.19b and 4.20b. In these figures the influence of the state dependent control input bounds (§4.3.8) is clearly seen.

For the winter day (figure 4.19):

- The combined heating valve position  $vp_h = 1.5$  is limited to 1 when  $T_a > T_{aref}$  according to eqn. 4.30. This means that the boiler is turned off at these times, so  $vp_l = vp_u = 0$ . The reference temperature for the temperature integral  $T_{aref} = 19^\circ\text{C}$  is shown as a dashed line in the  $T_a$  sub-figure in figure 4.19b.

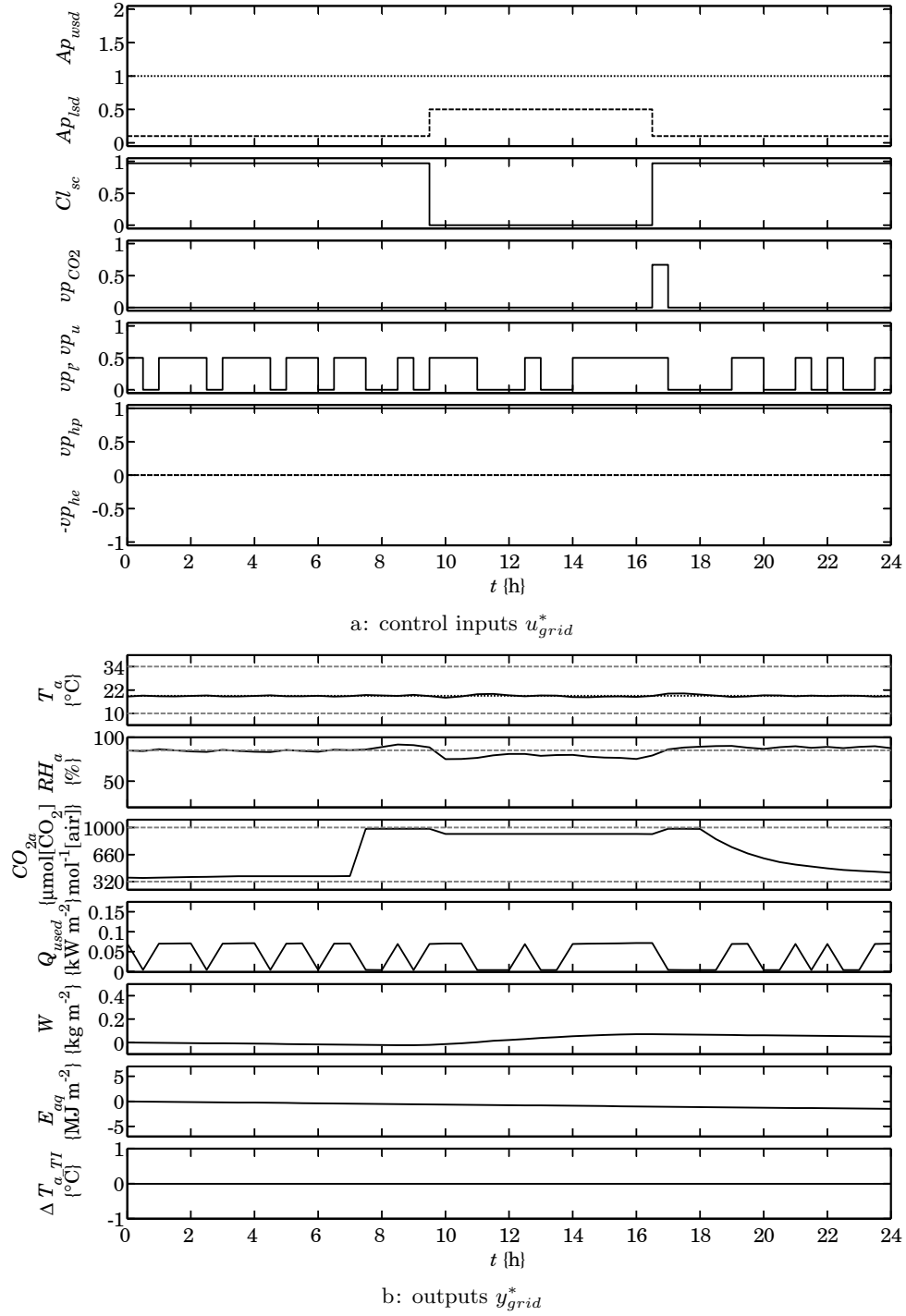
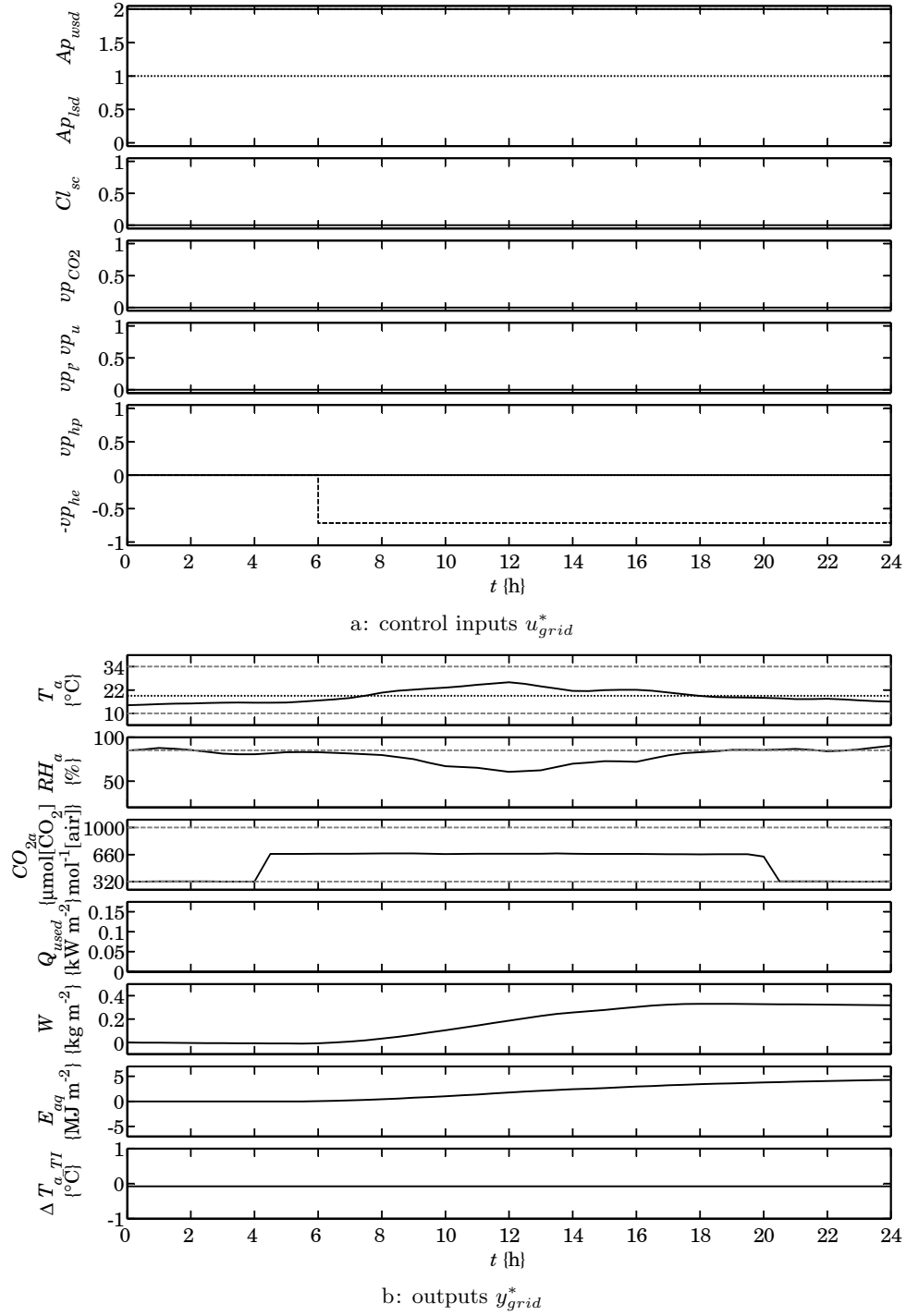


Figure 4.19: Grid search TI, winter day (2-1)

Figure 4.20: Grid search  $TI$ , summer day (8-1)

- The combined window aperture  $Ap_{csd} = 0.5$  is limited to 0.1 when  $c_{sc} = 1$  according to eqn. 4.31. This means that the ventilation is limited when the screen is closed. Ventilation with heat recovery is used for the ventilation ( $op_{vhr} = 1$ ), which is indicated by the dashed line in figure 4.19a for the window apertures.

and for the summer day (figure 4.20):

- The combined heating valve position  $vp_h = -0.5$  not limited. The real valve position for the heat exchanger  $vp_{he}$  is computed from  $vp_{he}^*$  according to eqn. 3.192, which gives:  $vp_{he}^* = 0.5 \Rightarrow vp_{he} = 0.715$ . The valve position  $vp_{he}$  is limited to 0 from 0 to 6 o'clock, since the water temperature  $T_{in\_he}$  entering the heat exchanger (not shown) is smaller than  $T_{aq,h}$  (see §3.8.4.2). This means that the heat exchanger cannot decrease this temperature any further, therefore the heat exchanger is turned off at these times, so  $vp_{he}^* = 0$ .
- The combined window aperture  $Ap_{csd} = 2$  would be limited to 1 when  $T_a < T_{aref}$  and  $RH_a < 0.9 RH_{a\max}$  according to eqn. 4.31. This is never the case here. Normal ventilation with the windows is used ( $op_{vhr} = 0$ ), which is indicated by the line in figure 4.19a for the window apertures.

### 4.5.2 Results open loop optimal control gradient search (TI)

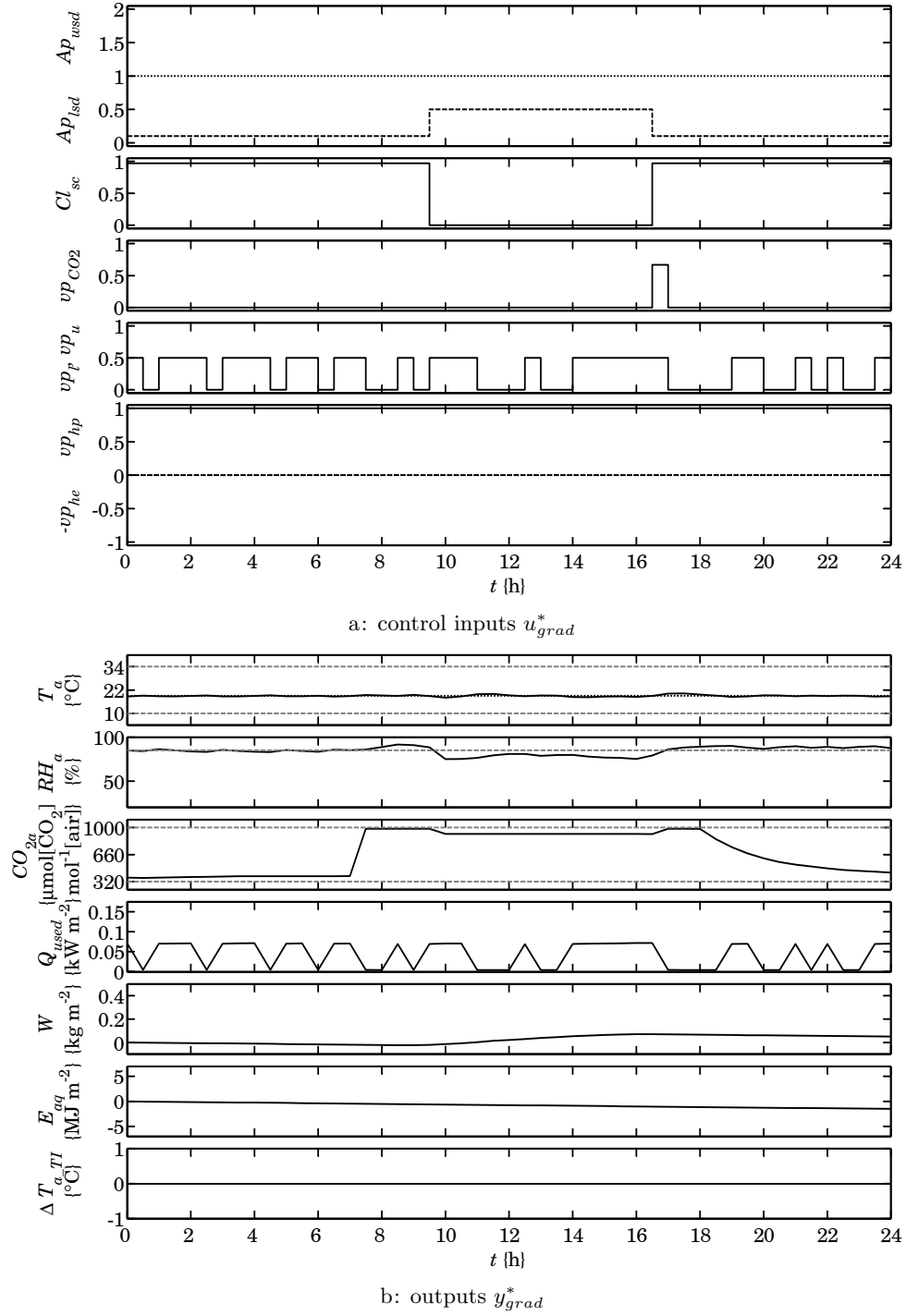
Now the gradient search method is used to further improve the cost function value, starting with the initial guess  $u_{grid}^*$  for the control inputs values determined with the grid search method in §4.5.1. This gives the control inputs  $u_{grad}^*$  with the corresponding cost function value  $J_{grad}$ .

In this paragraph the gradient search results are discussed for a day in winter and summer with temperature integration. The differences between the control with and without temperature integration will be examined.

#### 4.5.2.1 Results open loop optimal control gradient search, winter day (TI)

In figure 4.21a the control inputs  $u_{grad}^*$  are given for the winter day. The dashed lines for the window aperture indicate ventilation with heat recovery. The corresponding outputs  $y_{grad}^*$  are given in figure 4.21b.

Comparing the figures 4.19a and 4.21a, no change is seen. The solar greenhouse is heated with the heat pump, and the boiler is used to supply extra heat. The CO<sub>2</sub> supply keeps the CO<sub>2</sub> concentration  $CO_{2a}$  between 900 and

Figure 4.21: Gradient search  $TI$ , winter day (2-1)

1000  $\mu\text{mol}[\text{CO}_2] \text{ mol}^{-1}[\text{air}]$  during the day. The thermal screen is closed during the night, since the outdoor temperature  $T_o$  is low.

Comparing the figures 4.19b and 4.21b, no change is seen. The values of the penalties  $L$ , the terminal costs  $\Phi$  and the cost function values  $J$  are given in table 4.4. The cost function value of these trajectories is  $J_{grad} = 10.26$ , which is equal to the value of the grid search.

Table 4.4: Costs open loop TI, winter day (2-1)

	$\int L_{Ta}$	$\int L_{RH_a}$	$\int L_Q$	$\Phi_W$	$\Phi_{TI}$	$J$
grid	0.00	7.64	6.36	-3.86	0.12	10.26
gradient	0.00	7.64	6.36	-3.86	0.12	10.26
$\int L_{TI} = 0$ and $\int L_{aq} = 0$						

From the costs given in table 4.4 it can be seen that the input and output trajectories are not changed. This indicates that the results of the grid search were already very good.

#### 4.5.2.2 Results open loop optimal control gradient search, summer day (TI)

In figure 4.22a the control inputs  $u_{grad}^*$  are given for the summer day. The corresponding outputs  $y_{grad}^*$  are given in figure 4.22b.

Comparing the figures 4.20a and 4.22a, the main change is seen in the window apertures  $Ap_{lsd}$  and  $Ap_{wsd}$  during the day, which are now partly closed. This increases the  $\text{CO}_2$  supply  $vp_{\text{CO}_2}$ , which is otherwise limited by this window aperture. No heating is used. The heat exchanger is used to cool the greenhouse during the day. It is still used after 19 o'clock to decrease the temperature since this decreases the dark respiration  $r_c$ , which thus increases the biomass  $W$ . The  $\text{CO}_2$  supply keeps the  $\text{CO}_2$  concentration  $\text{CO}_{2a}$  between 660 and 800  $\mu\text{mol}[\text{CO}_2] \text{ mol}^{-1}[\text{air}]$  during the day. The thermal screen is open, since the outdoor temperature  $T_o$  is high. Ventilation is used to decrease the relative humidity  $RH_a$  during the night, and to decrease the temperature  $T_a$  during the day.

Comparing the figures 4.20b and 4.22b, the main change is seen in the  $\text{CO}_2$  concentration  $\text{CO}_{2a}$  during the day. The values of the penalties  $L$ , the terminal costs  $\Phi$  and the cost function values  $J$  are given in table 4.5. The cost function value of these trajectories is  $J_{grad} = -23.71$ , which is lower than the value of the grid search.

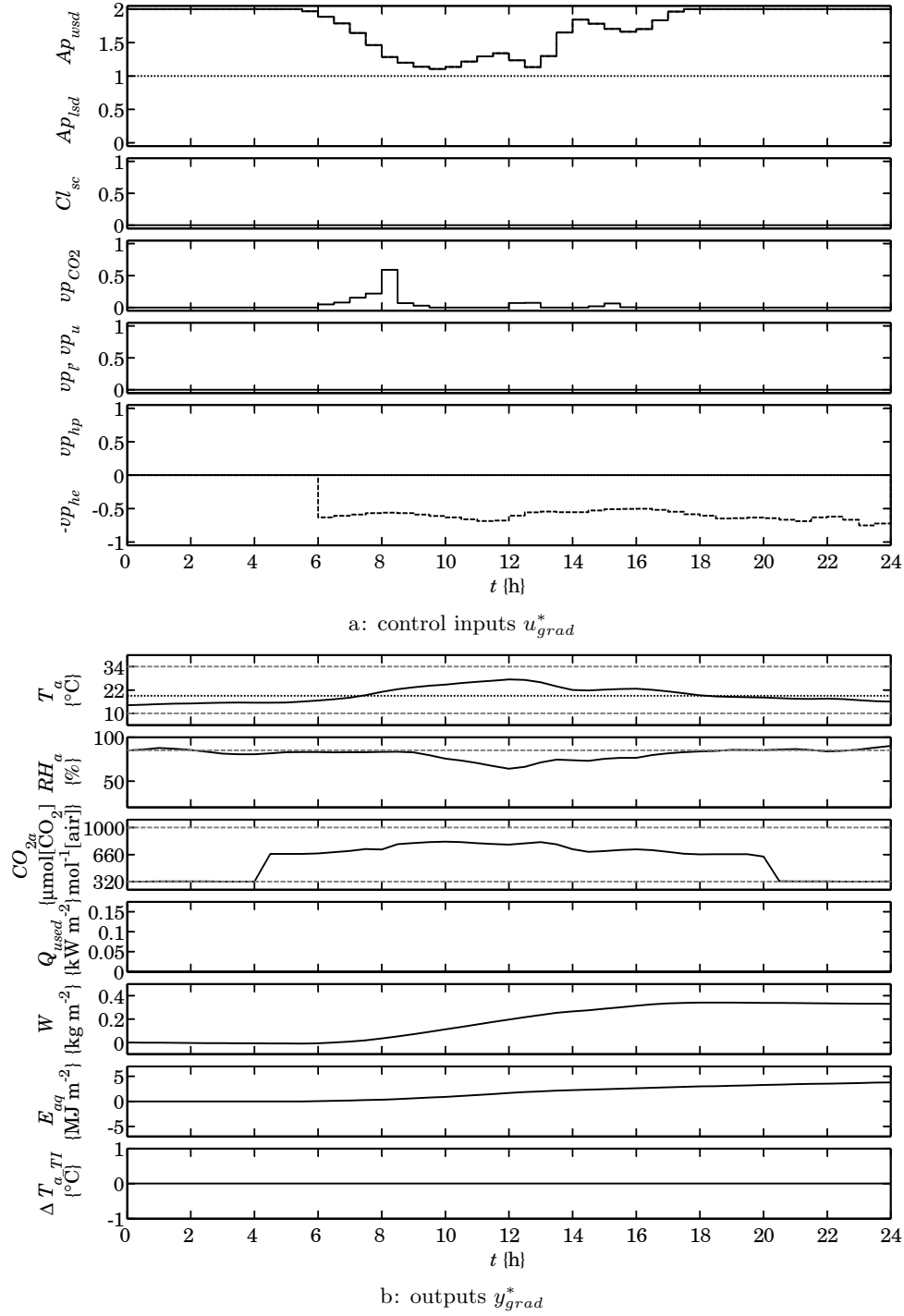


Figure 4.22: Gradient search TI, summer day (8-1)

Table 4.5: Costs open loop *TI*, summer day (8-1)

	$\int L_{Ta}$	$\int L_{RH a}$	$\int L_Q$	$\Phi_W$	$\Phi_{TI}$	$J$
grid	0.00	1.74	0.00	-24.50	1.97	-20.79
gradient	0.00	1.63	0.00	-25.34	0.00	-23.71

$\int L_{TI} = 0$  and  $\int L_{aq} = 0$

From the costs given in table 4.5 it can be seen that the output trajectories are changed to decrease the terminal cost for the temperature integral  $\Phi_{TI}$  and the penalty for the relative humidity  $\int L_{RH a}$ . The terminal cost for the biomass increase  $\Phi_W$  is decreased (higher biomass increase  $\Delta W$ ) due to the higher  $\text{CO}_2$  concentration  $\text{CO}_{2a}$ .

#### 4.5.2.3 General results open loop optimal control, winter and summer day (*TI*)

For the winter day, the results found with the gradient search and the grid search method are equal. The gradient search method cannot improve these results any more, which indicates that the grid search results are already very good.

For the summer day, the  $\text{CO}_2$  concentration is higher in the results with the gradient search compared to the grid search method. This results in a higher biomass increase  $\Delta W$ . The  $\text{CO}_2$  supply valve is controlled by a proportional controller, which is a function of the window apertures  $Ap_{l_{sd}}$  and  $Ap_{w_{sd}}$ . The gradient search decreases the window aperture during the day, which leads to a higher  $\text{CO}_2$  concentration.

#### 4.5.3 Conclusions open loop optimal control (*TI*)

The general idea of the temperature integral is that for good crop development an average reference temperature value must be achieved over a longer period of time. If this reference temperature is not achieved (e.g., the temperature is too low for a longer period of time) crop development is inhibited. This would lead to a low quality product that cannot be sold. It is therefore important that the temperature integral demands are fulfilled.

In the tables 4.6a and 4.6b the costs of the gradient search for the winter and the summer day are given without and with temperature integration. The bounds for the temperature integral penalty  $\int L_{TI}$  and the aquifer energy content penalty  $\int L_{aq}$  are never crossed, so these penalties are zero.

Table 4.6: Costs open loop gradient search,  $\mathcal{AI}$  versus  $TI$

a: winter day						
	$\int L_{Ta}$	$\int L_{RH a}$	$\int L_Q$	$\Phi_W$	$\Phi_{TI}$	$J$
$\mathcal{AI}$	1.69	1.03	5.18	-4.97	22.57	2.93
$TI$	0.00	7.64	6.36	-3.86	0.12	10.26
$\int L_{TI} = 0$ and $\int L_{aq} = 0$						
b: summer day						
	$\int L_{Ta}$	$\int L_{RH a}$	$\int L_Q$	$\Phi_W$	$\Phi_{TI}$	$J$
$\mathcal{AI}$	1.32	2.57	0.46	-27.09	1.25	-22.75
$TI$	0.00	1.63	0.00	-25.34	0.00	-23.71
$\int L_{TI} = 0$ and $\int L_{aq} = 0$						

In the version with temperature integration the bounds for the temperature penalty  $\int L_{Ta}$  are wider. This allows additional freedom for the temperature  $T_a$  to fluctuate, with an average temperature  $T_{aref} = 19^\circ\text{C}$  over six days. The temperature bounds are never crossed, so the penalty  $\int L_{Ta} = 0$ .

The temperature integral is added to ensure good crop development, and therefore better crop quality. It can be seen in the tables 4.6a and 4.6b that in the version with temperature integration the terminal cost  $\Phi_W$  for the biomass increase is higher compared to the version without temperature integration. This indicates that the biomass increase  $\Delta W$  is smaller. This is due to more dark respiration  $r_c$  in the version with temperature integration, since the average temperature is higher. This shows that the temperature integration has a significant negative effect on biomass increase. The term  $\Phi_W$  however can be very misleading in this context. All penalties should be taken into account, since they all indicate an influence on the crop growth and development, especially  $\Phi_{TI}$ . The balance between all these penalties and terminal costs is very important and can be adjusted with the weight factors  $c$  in table 4.1. According to the definition of the cost function, the version without temperature integration would lead to a crop that cannot be sold due to the low quality.

In winter (see table 4.6a) the cost function value  $J$  is higher with than without temperature integration. In the version without temperature integration the deviation from  $19^\circ\text{C}$  is quite large. The temperature  $T_a$  keeps to its lower

bound (16°C), which gives the terminal cost  $\Phi_{TI} = 22.57$ . This means that the temperature  $T_a$  is actually too low, which is bad for crop development. In the version with temperature integration the terminal cost is  $\Phi_{TI} = 0.12$ . The temperature is allowed to fluctuate around 19°C (with much wider bounds), giving an average temperature closer to 19°C, which is better for crop development. To obtain this temperature the greenhouse needs to be heated more, which increases  $\int L_Q$ . The upper humidity bound is exceeded more frequently.

In summer (see table 4.6b) the cost function value  $J$  is lower with than without temperature integration. In the version without temperature integration the deviation from 19°C is much smaller than in winter ( $\Phi_{TI} = 1.25$  vs. 22.57). The temperature  $T_a$  is at its lower bound during the night, and at its upper bound during the day, which gives the terminal cost  $\Phi_{TI} = 1.25$ . In the version with temperature integration the terminal cost is  $\Phi_{TI} = 0.00$ . The control uses the wider bounds for the temperature  $T_a$  to allow it to fluctuate more. The greenhouse no longer needs heating ( $\int L_Q = 0$ ). The upper humidity bound is exceeded less frequently.

## 4.6 Receding horizon optimal control, grid search (*TI*)

The receding horizon optimal controller (see §4.3.3) solves an optimal control problem for each sampling interval  $t_s$  of the receding horizon controller. The control input trajectories  $u^*$  consist of two inputs ( $vp_h$  and  $Ap_{csd}$ ) of 48 values each. This means that the optimal control problem has to optimize 96 values. For every sampling interval the full simulation over the control horizon  $t_f$  of one day has to be done a large number of times. The simulation of the associated optimal closed loop control system is therefore very time consuming in general. To drastically limit simulation time, the optimal control problem to be solved by the receding horizon optimal controller is highly simplified using the grid search method (see §4.3.11).

In the grid search method, the cost function values are determined for a grid of  $5 \times 7$  discrete constant control input values as described in §4.3.7. State dependent control input bounds (§4.3.8) are used to adjust the control input values, to push the optimal control solutions into the correct direction, thus leading to time varying control inputs. As a result the solution of the simplified optimal control problem is obtained after only 35 simulations. For the cost function the version with temperature integration is used. This method is used for year-round computations to test the RHOC concept and obtain a better

insight in the profit of the solar greenhouse design (van Ooteghem et al., 2004a, 2005a). The computations took about 8 hours. These results were also used to determine the aquifer energy content curve (§4.3.5.2).

#### 4.6.1 Results RHOC grid search, year-round

The results of the year-round RHOC computations are given in figure 4.23.

Figure 4.23a shows the window aperture (lee-  $Ap_{lsc}$  and windward-side  $Ap_{wsd}$ ), the thermal screen closure  $Cl_{sc}$ , and the valve positions for CO<sub>2</sub> supply  $vp_{CO2}$ , lower net  $vp_l$ , upper net  $vp_u$ , heat pump  $vp_{hp}$  and heat exchanger  $vp_{he}$ . When ventilation with heat recovery is used, the window aperture is given as a dashed line.

Figure 4.23b shows the terms that determine the costs. These include the temperature  $T_a$  {°C}, the relative humidity  $RH_a$  {%}, the CO<sub>2</sub> concentration of the indoor air below the screen  $C_{a,CO2}$  {kg m<sup>-3</sup>}, the energy used  $Q_{used}$  {W m<sup>-2</sup>}, the biomass  $W$  {kg m<sup>-2</sup>}, the aquifer energy content  $E_{aq}$  and the average temperature deviation over six days  $\Delta T_{a,TI}$  {°C}, which lead to the resulting cost function values  $J$ .

Looking at the optimal control inputs (figure 4.23a) it can be seen that:

- The window aperture ( $Ap_{lsc}$ ,  $Ap_{wsd}$ ) is higher in spring and summer than in fall and winter. In fall and winter ventilation with heat recovery is used to decrease energy loss due to ventilation.
- The screen closure  $Cl_{sc}$  (not optimized, depends on weather conditions) is used in fall and winter to decrease energy loss.
- The CO<sub>2</sub> supply ( $vp_{CO2}$ ) (not optimized, depends on window aperture) is used during the day to supply CO<sub>2</sub>, and closed during the night.
- The solar greenhouse is heated during fall and winter with the heat pump ( $vp_{hp}$ ) in combination with the boiler ( $vp_l$ ,  $vp_u$ ), mainly to increase the temperature. In spring and summer the heat pump is used, mainly to decrease the relative humidity.
- The solar greenhouse is cooled during spring and summer with the heat exchanger ( $vp_{he}$ ), in combination with ventilation by opening the windows.

Looking at the optimal control results (figure 4.23b) it can be seen that:

- The temperature  $T_a$  stays within its bounds all year. The average temperature deviation  $\Delta T_{a,TI}$  only shows small deviations from zero in summer, but never reaches its bounds [-6, 6].
- The relative humidity  $RH_a$  exceeds its upper bound, but the deviation is kept within limits.

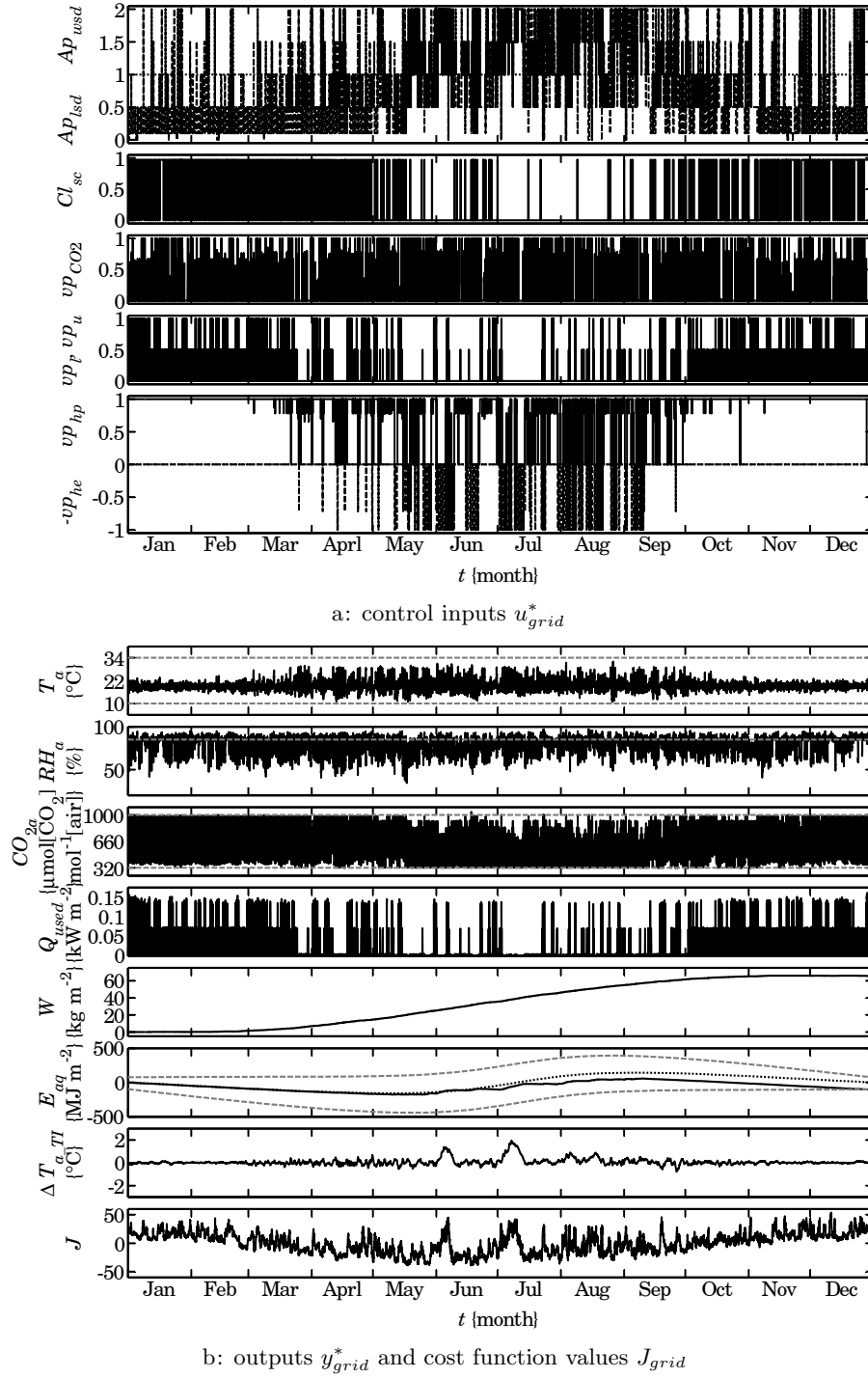


Figure 4.23: Computation RHOC with grid search, year-round

- The energy used  $Q_{used}$  is directly related to the control inputs for the heat pump and the boiler. The energy use is high in fall and winter and low in spring and summer.
- The main biomass increase  $\Delta W$  is found in spring and summer. This is mainly due to the high radiation in these seasons.
- The resulting cost function value  $J$  is lower in spring and summer than in fall and winter. This is mainly due to the lower energy use and the higher biomass increase.
- The aquifer energy content  $E_{aq}$  stays within its bounds up till the last 15 days of the year.

These computations were also performed without the penalty  $L_{aq}$  for the aquifer energy content ( $c_{aq} = 0$ ). The resulting curve for  $E_{aq}$  is used in §4.3.5 to determine the aquifer energy content reference curve. The results of that computation were the same as given here, except for the last 15 days, where the aquifer energy content  $E_{aq}$  exceeds its bounds. In the version with penalty  $L_{aq}$  the greenhouse is then heated with the boiler alone — without the heat pump — to increase the aquifer energy content  $E_{aq}$ , such that the bounds are no longer exceeded. This results in a slight increase of the energy use  $Q_{used}$ .

#### 4.6.2 Solar versus non-solar greenhouse

To get a sense of the influence of the solar greenhouse elements (heat pump, heat exchanger, ventilation with heat recovery, cooling net, aquifer), a non-solar greenhouse is introduced. The non-solar greenhouse is basically the solar greenhouse without the solar greenhouse elements. The CO<sub>2</sub> supply is still assumed to be independent of boiler operation. This gives the following changes in the greenhouse model:

- The aquifer is removed, so all terms relating to the aquifer (e.g.  $E_{aq}$ ) are zero.
- The heat pump is removed, so the valve position of the heat pump  $vp_{hp} = 0$ .
- The heat exchanger is removed, so the valve position of the heat exchanger  $vp_{he} = 0$ .
- The upper cooling net is removed, so all exchange coefficients with the upper cooling net are zero.
- Ventilation with heat recovery is removed, so the option ventilation heat recovery  $op_{vhr} = 0$ .

The optimal control is for the main part identical to the control used for the solar greenhouse. The combined valve position  $vp_h$  can now only take values between 1 and 2, since  $vp_{hp} = 0$  and  $vp_{he} = 0$ . This also changes one of the

rules for the state dependent control input bounds. The control input bound on the combined heating valve position (see eqn. 4.30)  $vp_h$  [1,2] is now defined by

$$\mathcal{TI}, TI \quad vp_{h \max}(t) = 1 \quad T_{a \max} \leq T_a \quad (4.33)$$

which means that there is no heating with the boiler if temperature  $T_a$  is above its upper bound  $T_{a \max}$ .

These results are given in table 4.7. The main influence of the solar greenhouse elements is found in the gas use  $\Phi_{gas}$ , the biomass increase  $\Delta W$ , the CO<sub>2</sub> supply  $\Phi_{m\_CO2}$ , the ventilation flow  $\Phi_{as\_o}$  and the heat exchange by natural ventilation  $Q_{as\_o}$ .

Table 4.7: Comparison RHOC grid search, solar and non-solar greenhouse

	$\Phi_{gas}$ {m <sup>3</sup> m <sup>-2</sup> }	$\Delta W$ {kg m <sup>-2</sup> }	$\Phi_{m\_CO2}$ {kg m <sup>-2</sup> }	$\Phi_{as\_o}$ {m <sup>3</sup> m <sup>-2</sup> }	$Q_{as\_o}$ {W m <sup>-2</sup> }
<i>solar</i>	22.5=19.7+2.8	65.4	118.6	30.5·10 <sup>4</sup>	31.1·10 <sup>7</sup>
<i>solar</i>	53.6	64.8	107.3	28.9·10 <sup>4</sup>	152.0·10 <sup>7</sup>
<i>solar</i> <i>solar</i>	42%	101%	110%	106%	20%

$\Phi_{gas}$  is given as: total gas use = gas use by boiler + gas use by heat pump

From the results in table 4.7 it can be seen that the solar greenhouse in comparison with the non-solar greenhouse — with grid search

- uses much less gas  $\Phi_{gas}$  (42%); a decrease of 58%!
- has about the same biomass increase  $\Delta W$  (101%)
- uses more CO<sub>2</sub>  $\Phi_{m\_CO2}$  (110%)
- uses more ventilation  $\Phi_{as\_o}$  (106%) with much less energy loss to the environment due to ventilation and leakage  $Q_{as\_o}$  (20%)

The gas use decrease of 58% is caused by the aquifer with heat pump and heat exchanger and by the ventilation with heat recovery both. The biomass increase is the same, since the climate conditions (radiation, temperature, relative humidity and CO<sub>2</sub> concentration) are about the same. The CO<sub>2</sub> use corresponds to the ventilation flow (more ventilation flow leads to more CO<sub>2</sub> use). The ventilation with heat recovery decreases the heat loss by ventilation by 80%.

### 4.6.3 Conclusions RHOC grid search, year-round

The receding horizon optimal control has been tested with year-round weather data. Although the grid search method is a simplified version of optimal control, the results of the year-round computations are very promising.

From the results, it can be concluded that

- Receding horizon optimal control of the solar greenhouse is feasible. Although the model is non-linear and complex, rational optimal control solutions can be found.
- The heat pump and the heat exchanger are valuable additions to the greenhouse control system. The greenhouse is heated with the heat pump year-round, while in fall and winter the boiler is needed to supply additional heat. The heat exchanger is used to cool the greenhouse in spring and summer, thus harvesting energy for the aquifer.
- The use of the solar greenhouse elements (heat pump, heat exchanger and ventilation with heat recovery) results in less gas use and less energy loss to the environment with slightly more CO<sub>2</sub> use. The biomass increase is about the same, since this mainly depends on radiation, temperature and CO<sub>2</sub> concentration.
- Ventilation with heat recovery significantly decreases the energy loss due to ventilation.
- Temperature stays within its bounds, and the temperature integral requirements are well met. Relative humidity exceeds its bound; while the optimal control is doing everything it can (heating, ventilating) to decrease it.
- The use of the grid search method instead of the gradient search method gives a fast indication of the optimal control possibilities (computation time of about 8 hours).

## 4.7 Receding horizon optimal control, gradient search (*TI*)

Instead of the grid search method, the ‘real’ optimal control is now used. Starting from the initial guess for the control input values with state dependent control input bounds (the results of the grid search), the control input trajectories are computed by solving the optimal control problem in eqn. 4.11. The receding horizon control principle is explained in §4.3.3. The weather prediction  $\tilde{v}$  that is used to compute the state predictions is not equal to the actual weather  $v$  that is used to compute the actual state values.

The optimization is done with a conjugate gradient method (Pagurek and Woodside, 1968), searching for the best possible control inputs minimizing the cost function. This method has proven to be effective for conventional greenhouse control and several other applications (van Willigenburg et al., 2000).

#### 4.7.1 Results RHOC gradient search, year-round

The year-round results are split up per season to get a better view of the results:

- winter (12-21 – 3-19)
- spring (3-20 – 6-20)
- summer (6-21 – 9-22)
- fall (9-23 – 12-20)

The results of the cold seasons (fall and winter) and the warm seasons (spring and summer) are presented together, since they show similar results. The layout of the figures is the same as in §4.6.1.

Since it is difficult to judge the control input values and the outputs for the different seasons from the figures, average values and ranges are given in tables 4.8a and 4.8b. These values are all taken over the whole season.

##### 4.7.1.1 Results RHOC gradient search, fall and winter

The results of the RHOC computations with gradient search for fall and winter are given in the figures 4.24 and 4.25. The heat pump ( $vp_{hp}$ ) is used to increase temperature and reduce humidity. The boiler ( $vp_l$ ,  $vp_u$ ) is used to supply additional heat to the greenhouse, since the capacity of the heat pump is limited. The thermal screen ( $Cl_{sc}$ ) is closed almost every night, and sometimes stays closed during daytime if outdoor temperature and radiation are low. The heat exchanger ( $vp_{he}$ ) is seldom used. Ventilation ( $Ap_{l_{sd}}$ ,  $Ap_{w_{sd}}$ ) is used to reduce humidity. When ventilation is used, it is mainly ventilation with heat recovery ( $op_{vhr}$ , indicated by dashed lines for  $Ap_{l_{sd}}$  and  $Ap_{w_{sd}}$ ). Normal ventilation is only used when the heat exchanger is used. The CO<sub>2</sub> supply ( $vp_{CO_2}$ ) is only opened during daytime if the CO<sub>2</sub> concentration  $CO_{2a}$  is low and there is little ventilation. The temperature  $T_a$  seldom exceeds its bounds. At times of high radiation, temperature is allowed to rise, since this yields a higher biomass increase. The average temperatures are 19.22°C (fall) and 19.11°C (winter), which are very close to the reference temperature  $T_{aref}$

Table 4.8: RHOC solar greenhouse with gradient search, averages and ranges

a: averages of control input values								
	$Ap_{lstd}$	$Ap_{wsd}$	$op_{vhr}^\dagger$	$Cl_{sc}$	$vp_{CO2}$	$vp_l, vp_u$	$vp_{hp}$	$vp_{he}$
winter	0.56	0.20	92%	0.72	0.09	0.35	0.89	0.02
spring	0.74	0.27	69%	0.25	0.11	0.09	0.62	0.15
summer	0.87	0.50	61%	0.05	0.12	0.07	0.54	0.28
fall	0.62	0.23	92%	0.51	0.09	0.29	0.88	0.01
year-round	0.70	0.30	78%	0.37	0.10	0.20	0.73	0.12
b: ranges of output values								
	$T_a$		$RH_a$		$CO_{2a}$		$Q_{used}$	$\Delta W$
	min	max	min	max	min	max	max	max
winter	5.7	35.9	36.3	96.6	320.0	1001.0	165.9	3.8
spring	10.2	38.4	37.4	94.4	320.5	1000.8	150.4	28.9
summer	11.4	30.3	49.1	96.7	320.6	1024.1	148.6	27.5
fall	4.9	32.6	39.4	93.3	320.5	1000.7	158.4	5.9

of 19°C. The average temperature deviation  $\Delta T_{a, TI}$  is small. The relative humidity  $RH_a$  frequently exceeds its bound. At high relative humidity, the optimal control tries to decrease it by ventilation and heating with the heat pump and the boiler. The biomass increase  $\Delta W$  is fairly low compared to spring and summer, since there is little radiation.

#### 4.7.1.2 Results RHOC gradient search, spring and summer

The results of the RHOC computations with gradient search for spring and summer are given in the figures 4.26 and 4.27. The heat pump ( $vp_{hp}$ ) is used to increase temperature and reduce humidity. The boiler ( $vp_l, vp_u$ ) is used less often than in fall and winter. The thermal screen ( $Cl_{sc}$ ) is closed less often after the first half of May, since outdoor temperature and radiation increase. The heat exchanger ( $vp_{he}$ ) is frequently used to decrease the temperature. Ventilation ( $Ap_{lstd}, Ap_{wsd}$ ) is used to reduce humidity. Compared to fall and winter the ventilation with heat recovery ( $op_{vhr}$ ) is used less often, so more normal ventilation is used. Slightly more ventilation is used than in fall and winter, the heat exchanger is now used to reduce the temperature. The CO<sub>2</sub> supply ( $vp_{CO2}$ ) is only opened during daytime if the CO<sub>2</sub> concentration  $CO_{2a}$  is low

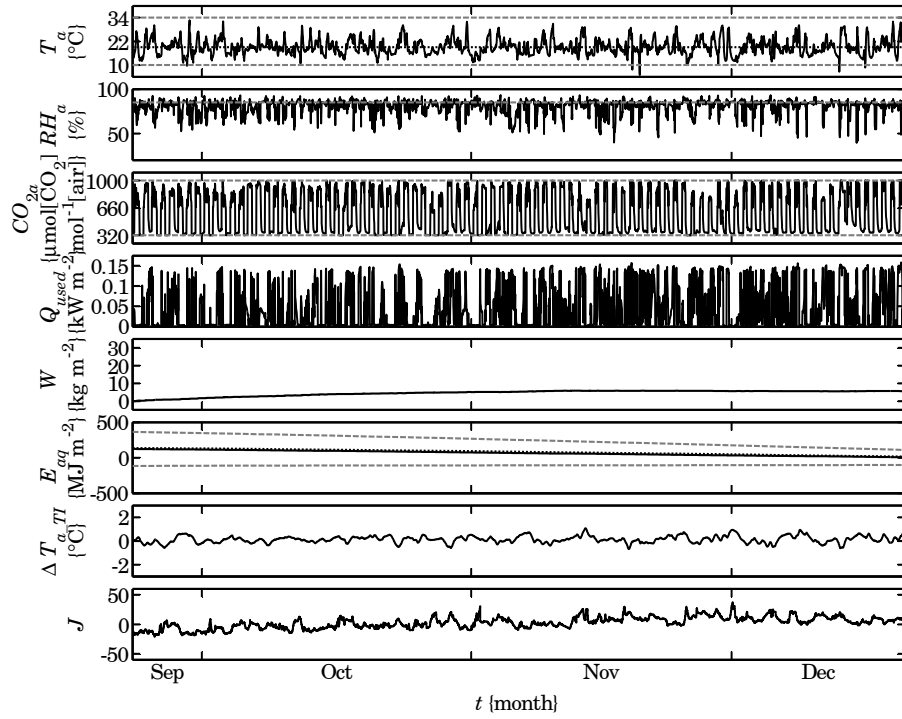
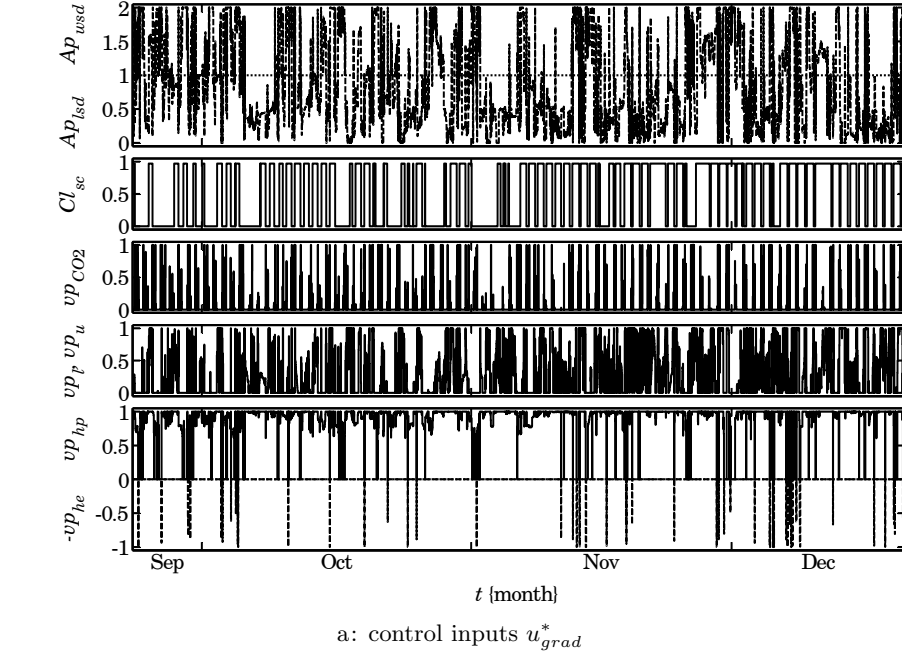


Figure 4.24: Computation RHOC with gradient search, fall

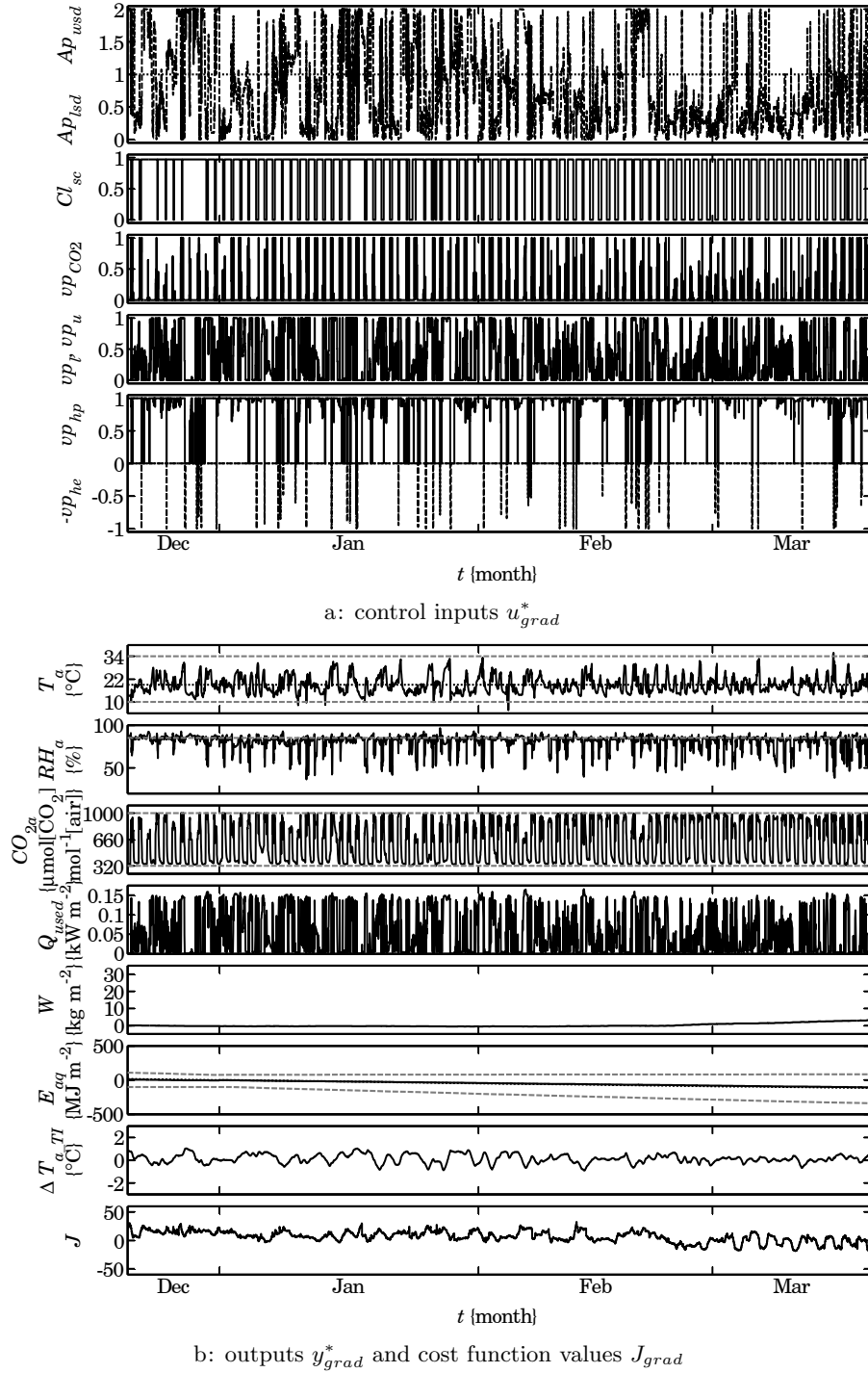


Figure 4.25: Computation RHOC with gradient search, winter

and there is little ventilation. The temperature  $T_a$  seldom exceeds its bounds. At times of high radiation, temperature is allowed to rise, since this yields a higher biomass increase. The average temperatures are 19.10°C (spring) and 19.29°C (summer), which are very close to the reference temperature  $T_{aref}$  of 19°C. The average temperature deviation  $\Delta T_{a, TI}$  is small. At the beginning of June and July the deviation increases to 1.5 and 1.9 respectively, since the average temperature was too high. At these times the heat exchanger and ventilation are used to cool the greenhouse. The relative humidity  $RH_a$  frequently exceeds its bound. At high relative humidity, the optimal control tries to decrease it by ventilation and heating with the heat pump and the boiler. The biomass increase  $\Delta W$  is much higher than in fall and winter, since there is more radiation.

#### 4.7.1.3 General results receding horizon optimal control, year-round

The thermal screen ( $Cl_{sc}$ ) is closed depending on the outdoor temperature and radiation. This can lead to closure of the thermal screen during the day in fall and winter. In the second half of spring and in summer, the thermal screen rarely closes. The windows ( $Ap_{lsc}$ ,  $Ap_{wsd}$ ) are mainly opened to decrease humidity, since the temperature can be decreased with the heat exchanger. In summer they are used to decrease temperature. The heat pump ( $vp_{hp}$ ) is used year-round, either to increase temperature or to decrease humidity. The boiler ( $vp_l$ ,  $vp_u$ ) is used to further increase temperature or to further decrease humidity in fall and winter. The heat exchanger ( $vp_{he}$ ) is used in spring and summer to decrease temperature. CO<sub>2</sub> supply ( $vp_{CO_2}$ ) is used whenever there is radiation. When the windows are opened, the CO<sub>2</sub> supply is decreased. In the second half of spring and in summer, the uptake by the crop of CO<sub>2</sub> leads to low CO<sub>2</sub> concentrations in the greenhouse.

Temperature  $T_a$  remains within its bounds relatively well, exceeding the upper bound of 34°C sometimes during daytime. Relative humidity  $RH_a$  exceeds its bound quite frequently, although the optimal control is doing everything it can (heating, ventilating) to decrease it. The main biomass increase  $\Delta W$  is found in spring and summer, which is obvious due to higher radiation in these seasons. The main gas use is found in fall and winter due to the low outdoor radiation and temperature. The average temperature deviation  $\Delta T_{a, TI}$  over six days never reaches its bounds of  $\pm 6^\circ\text{C}$ ; the maximum deviation is 2°C. The reference temperature of 19°C is well met in all seasons.

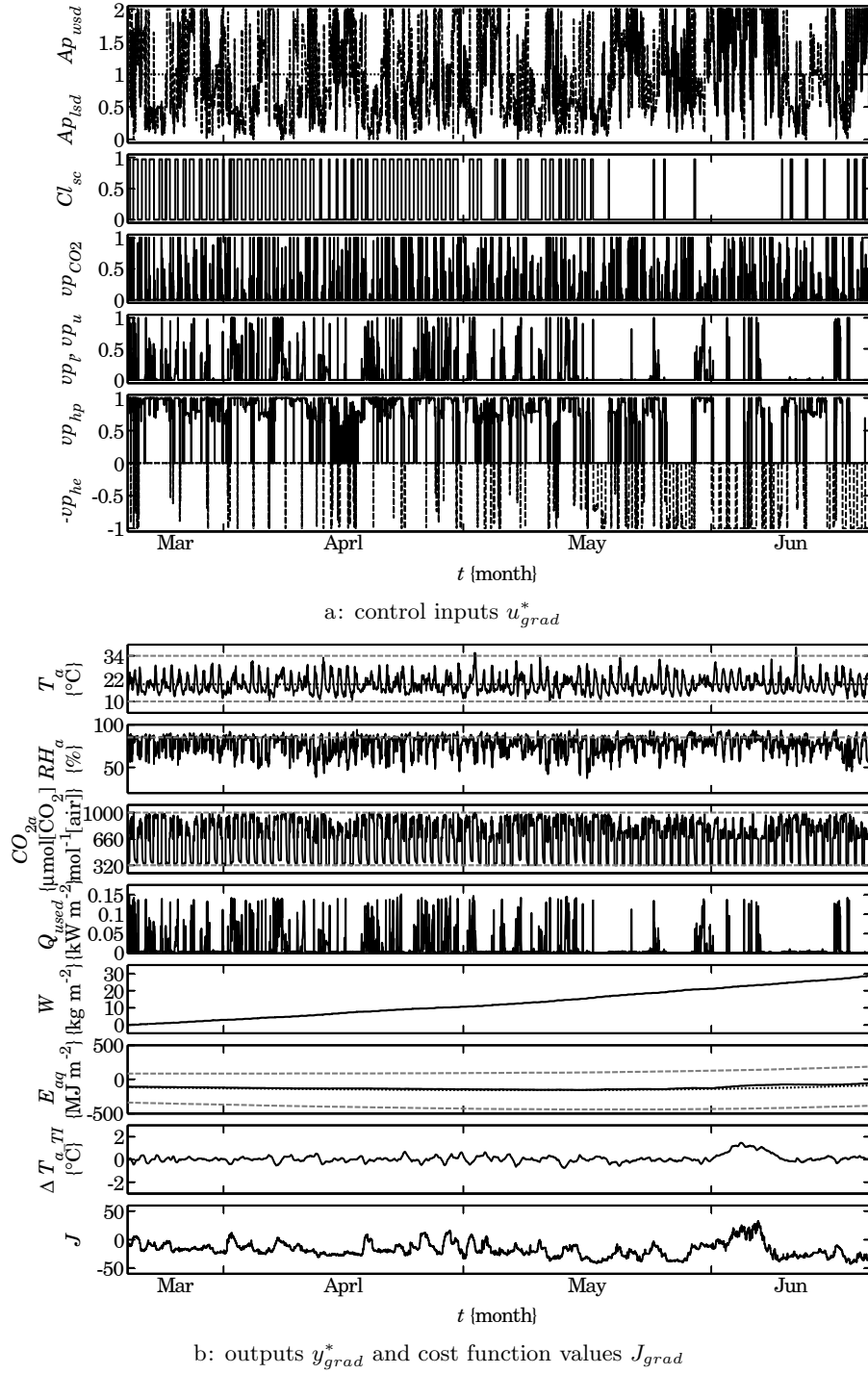


Figure 4.26: Computation RHOC with gradient search, spring

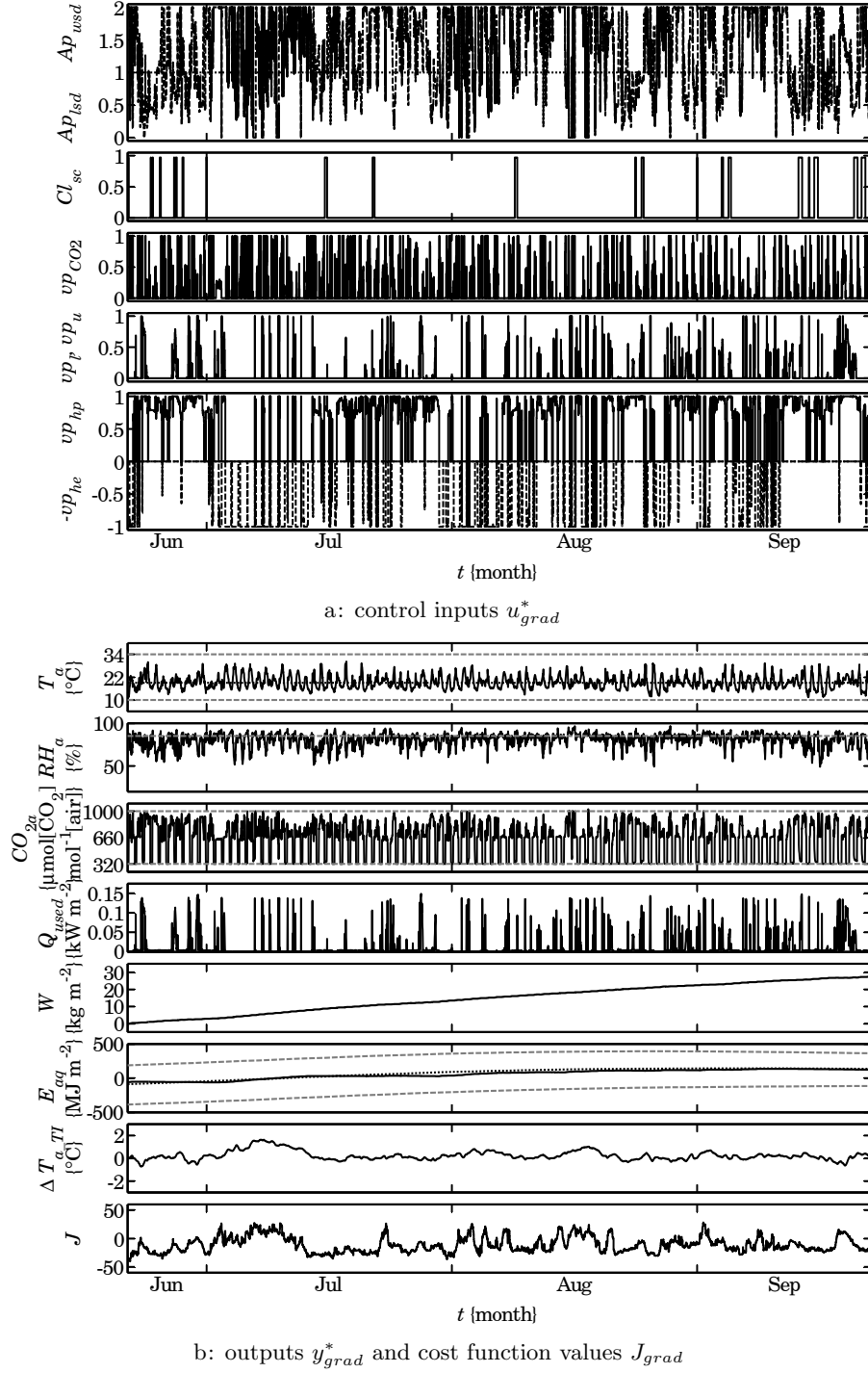


Figure 4.27: Computation RHOC with gradient search, summer

#### 4.7.2 Conclusions RHOC gradient search, year-round

The receding horizon optimal control results have been computed with year-round weather data for the solar greenhouse. The results of the computations consist of the optimal control inputs and the corresponding states, outputs and costs. The outputs are defined here as all variables in the greenhouse-with-crop model. The costs and the most interesting outputs with respect to resource use and yield for the solar greenhouse are examined.

The results are given in table 4.9. Table 4.9a presents the actual obtained resource use and yield, while the tables 4.9b and 4.9c present the penalties, terminal costs and cost function values.

There are two ways of presenting the costs, such as penalties, terminal costs and cost function values. The values reported in table 4.9b are the averages over the whole season of the costs integrated over a day ( $t_f$ ) evaluated at each half hour ( $t_s$ ) using the weather predictions  $\tilde{v}$ . These are, of course, the values used in the optimization. However, at the end of the year-round computation it is possible to evaluate what the real costs integrated over a day have been, given the actual weather  $v$ . These values can be computed from the states realized in the greenhouse as a result of the computed optimal control inputs  $u^*$  and the actual weather  $v$ . The values are called a posteriori, and are given in table 4.9c. The reason for doing this is to see in what respect the realized costs deviate from the ones expected during the optimization. This is important if the a priori results are going to be used as a prediction of the costs for a presentation tool for the grower.

The a priori values (table 4.9b) can differ from the a posteriori values (table 4.9c). The deviation is partly due to the fact that the a priori results are open loop results whereas the a posteriori results are closed loop (feedback) results, and partly due to the difference between the real and the predicted weather. The main deviations are found in the penalty  $\int L_Q$  and in the terminal cost  $\Phi_{TI}$ , while for the other costs the deviations are smaller. The a posteriori penalties  $\int L_Q$  for energy use are much higher in fall and winter, which indicates that more energy is used than initially expected. The a posteriori terminal cost  $\Phi_{TI}$  for the temperature integral is much higher in all seasons, which indicates that the realized average temperature over a period of six days is different from what was initially expected. This was likely to happen, since  $\Phi_{TI}$  is a soft terminal constraint: any deviation of the average temperature from the target value  $T_{aref} = 19^\circ\text{C}$  at time  $t_f$  (the end of the receding horizon) is penalized. When the horizon is shifted, this terminal constraint is no longer imposed in the cost function, because it is shifted in time

Table 4.9: RHOC solar greenhouse with gradient search, results and costs

a: results, a posteriori values						
	$\Phi_{gas}$ {m <sup>3</sup> m <sup>-2</sup> }	$\Delta W$ {kg m <sup>-2</sup> }	$\Phi_{m\_CO2}$ {kg m <sup>-2</sup> }	$\Phi_{as\_o}$ {m <sup>3</sup> m <sup>-2</sup> }	$Q_{as\_o}$ {W m <sup>-2</sup> }	
winter	12.1=11.3+0.8	3.2	32.9	9.6·10 <sup>4</sup>	12.8·10 <sup>7</sup>	
spring	3.4= 2.9+0.5	28.8	42.8	9.3·10 <sup>4</sup>	15.4·10 <sup>7</sup>	
summer	2.6= 2.1+0.5	27.5	50.3	13.5·10 <sup>4</sup>	9.4·10 <sup>7</sup>	
fall	9.8= 9.0+0.8	5.6	34.2	8.2·10 <sup>4</sup>	9.9·10 <sup>7</sup>	
year-round	27.9=25.3+2.6	65.1	160.2	40.6·10 <sup>4</sup>	47.5·10 <sup>7</sup>	
$\Phi_{gas}$ is given as: total gas use = gas use by boiler + gas use by heat pump						
b: average costs, a priori values						
	$\int L_{Ta}$	$\int L_{RH a}$	$\int L_Q$	$\Phi_W$	$\Phi_{TI}$	$J$
winter	0.01	3.20	5.90	−3.25	0.83	6.69
spring	0.00	2.04	1.79	−24.26	2.71	−17.72
summer	0.00	2.64	1.32	−22.65	7.69	−10.99
fall	0.00	2.84	4.58	−5.49	0.83	2.76
year-round	0.00	2.67	3.35	−14.14	3.08	−5.04
$\int L_{TI} = 0$ and $\int L_{aq} = 0$						
c: average costs, a posteriori values						
	$\int L_{Ta}$	$\int L_{RH a}$	$\int L_Q$	$\Phi_W$	$\Phi_{TI}$	$J$
winter	0.01	2.72	8.36	−2.52	7.65	16.23
spring	0.01	3.45	2.21	−23.60	7.28	−10.65
summer	0.00	5.73	1.69	−22.23	10.44	−4.37
fall	0.05	3.21	6.76	−4.81	7.44	12.65
year-round	0.02	3.80	4.69	−13.52	8.22	3.21
$\int L_{TI} = 0$ and $\int L_{aq} = 0$						

along with the receding horizon. It is therefore unlikely that it will be maintained in the receding horizon approach. These deviations in  $\Phi_{TI}$  strongly affect the cost function value  $J$ , which is higher in all seasons.

It is, of course, of interest to know the consequences of these deviations. First, it should be said that in general  $\Phi_{TI}$  will never be equal to zero. To maintain  $\Phi_{TI} = 0$  at all times would mean either to keep the temperature constant, or to have a fixed periodic symmetrical pattern. Since the temperature integral is meant as a primitive means to ensure proper crop development and crop

quality, deviations might result in less development or quality, but the extent of this is unknown. This holds for any control with temperature integration.

From the a posteriori costs it can be seen that

- The temperature penalty is always low, which indicates that the temperature bounds are seldom exceeded.
- The relative humidity bound is exceeded most frequently in summer.
- The energy penalty (and thus the energy use) is much higher in fall and winter than in spring and summer, since in these seasons the greenhouse needs to be heated.
- The terminal cost for the biomass increase is low in fall and winter and high in spring and summer. This shows that the main crop growth is found in the seasons with high radiation, irrespective of temperature and humidity conditions in the greenhouse.
- The terminal cost for the temperature integral — indicating how well the average temperature equals the reference temperature  $T_{aref}$  (19°C) over a period of 6 days — is higher in summer compared to the other seasons. The average temperature over the whole season is however close to the reference temperature  $T_{aref}$ .
- The aquifer energy content  $E_{aq}$  stays within its bounds all year.
- The resulting cost function value  $J$  is lower in spring and summer than in fall and winter. This is mainly due to the lower energy use and the higher biomass increase.

## 4.8 Comparisons

In this paragraph three comparisons are made. First the influence of the optimal control search method is evaluated in §4.8.1. It will be shown that the grid search solutions are already close to the optimal solution, and that these results can be further improved by the gradient search method. Furthermore the deviation between the a priori and a posteriori results shows that the predicted costs and yield in a presentation tool for the grower need to be interpreted carefully, since the real (a posteriori) results may deviate from the predicted (a priori) results.

Subsequently a comparison of the solar and the non-solar greenhouse is presented in §4.8.2 for all seasons. From these results it can be concluded that overall the solar greenhouse performs better than the non-solar greenhouse in all seasons.

Finally the influence of the separate solar greenhouse elements on the final results is investigated in §4.8.3. Here it is found that the gas use reduction due to the ventilation with heat recovery is even higher than with the use of the heat pump, heat exchanger and aquifer. The CO<sub>2</sub> supply separate from the boiler increases the biomass production, while it seriously increases the CO<sub>2</sub> use.

Unless it is otherwise stated, the weather  $v$  is not equal to the weather prediction  $\tilde{v}$  in the year-round computations.

#### 4.8.1 Gradient search versus grid search

The gradient search method was meant to improve the control inputs found by the grid search method, leading to optimal control inputs. In the gradient search the optimal control values can take all possible values, while in the grid search only a few discrete values are used.

In the tables 4.10a, 4.10b and 4.10c the year-round results and the associated costs (a priori and a posteriori) of the grid search (§4.6.1) and the gradient search (§4.7.1) method are given.

The results presented in table 4.10 may serve to elucidate some of the special features of optimal control. By studying the table, a better understanding is obtained on how optimality is achieved, and what factors influence the result.

First, looking at the difference between the a priori grid search and gradient search costs in table 4.10b, it can be seen that the cost function value  $J$  is lower with the gradient method ( $J_{grad} = -5.04$  vs.  $J_{grid} = 0.36$ ). This was to be expected, because the gradient method has the freedom to search further for the optimum, as it can exploit the full continuous range of the control input values.

Although a better optimum is achieved, at first sight the results of the gradient search may look strange, because it uses more gas, more CO<sub>2</sub> and more ventilation compared to the grid search (table 4.10a).

Table 4.10b shows the a priori costs, which reveal what is going on. In the quest for a better optimum, the gradient search method realizes a much lower humidity penalty  $\int L_{RH} a$ , which means that the relative humidity bound of 85% is exceeded less frequently. To accomplish this the greenhouse is heated and ventilated more often ( $Q_{as.o}$ ), leading to a higher gas use ( $\Phi_{gas}$  and  $\int L_Q$ ), and more energy loss to the environment ( $\Phi_{as.o}$ ). More ventilation furthermore leads to a higher CO<sub>2</sub> loss to the environment, and therefore more CO<sub>2</sub> supply

Table 4.10: Comparison RHOC grid and gradient search

a: results, a posteriori values							
	$\Phi_{gas}$ $\{\text{m}^3 \text{m}^{-2}\}$	$\Delta W$ $\{\text{kg m}^{-2}\}$	$\Phi_{m\_CO2}$ $\{\text{kg m}^{-2}\}$	$\Phi_{as\_o}$ $\{\text{m}^3 \text{m}^{-2}\}$	$Q_{as\_o}$ $\{\text{W m}^{-2}\}$		
grid	22.5=19.7+2.8	65.4	118.6	30.5·10 <sup>4</sup>	31.1·10 <sup>7</sup>		
gradient	27.9=25.3+2.6	65.1	160.2	40.6·10 <sup>4</sup>	47.5·10 <sup>7</sup>		
<u>gradient</u> grid	124%	100%	135%	133%	153%		
$\Phi_{gas}$ is given as: total gas use = gas use by boiler + gas use by heat pump							
b: average costs, a priori values							
	$\int L_{Ta}$	$\int L_{RH a}$	$\int L_Q$	$\int L_{aq}$	$\Phi_W$	$\Phi_{TI}$	$J$
grid	0.00	6.54	3.61	0.02	−13.77	3.97	0.36
gradient	0.00	2.67	3.35	0.00	−14.14	3.08	−5.04
$\int L_{TI} = 0$							
c: average costs, a posteriori values							
	$\int L_{Ta}$	$\int L_{RH a}$	$\int L_Q$	$\int L_{aq}$	$\Phi_W$	$\Phi_{TI}$	$J$
grid	0.00	6.80	3.80	0.02	−13.48	6.73	3.87
gradient	0.02	3.80	4.69	0.00	−13.52	8.22	3.21
$\int L_{TI} = 0$							

( $\Phi_{m\_CO2}$ ) is needed. This shows that the relative humidity has a strong effect on gas use. This result is in accordance with the results of Tap (2000).

Apparently, in the current cost function, the value adhered to the penalty for humidity is such that it gets priority over energy saving. Whether or not this is justified depends on the underlying idea that violating this penalty increases the risk for diseases and fungi. The nice thing about optimal control is that it allows freedom to individual growers to make their own judgement, and to adjust the weights in the cost function according to their entrepreneurship and experience.

Comparing the costs for the grid search and the gradient search in table 4.10b it can be seen that the differences in the temperature penalty  $\int L_{Ta}$  and the terminal cost  $\Phi_{TI}$  of the temperature integral are small. This indicates that the rules used for temperature in the state dependent input bounds are quite good. The improvement made with the gradient search for the relative humidity penalty  $\int L_{RHa}$  is much larger. It is more difficult to improve the rules for the

relative humidity in the state dependent input bounds, since it is related to both absolute humidity and temperature.

The discussion above dealt with the so called a priori costs (table 4.10b). These are the values obtained during the optimization using the predicted weather  $\tilde{v}$ . Once the controls are computed, they are applied to the greenhouse using the actual weather  $v$ , which in this case was the *SEL*year weather data. Since the actual weather deviates from the predicted weather, the actually attained temperatures, humidities and other states deviate from what was expected. From these actually attained state values the costs are computed afterwards, which gives the a posteriori costs in table 4.10c. Here the difference between the grid search and the gradient search is reversed from some terms: the penalty  $\int L_Q$  for energy use and the terminal cost  $\Phi_{TI}$  for the temperature integral are higher instead of lower. As a result the cost function value  $J$  is only slightly lower with the gradient method ( $J_{grad} = 3.21$  vs.  $J_{grid} = 3.87$ ).

All a posteriori costs in table 4.10 are higher than the a priori costs. This indicates that — on a year-round scale — the actual results are not quite as good as initially expected. Recall that the a priori results are open loop results, and the a posteriori results are closed loop (feedback) results. As explained before (§4.7.2), the open loop results will always differ from the closed loop results. The deviation between the a priori and a posteriori results with respect to the penalties  $\int L$  is partly due to the difference between the predicted weather  $\tilde{v}$  and the actual weather  $v$ , which again stresses the importance of accurate weather predictions. It must be noted that the ‘lazy man weather prediction’ as used in this thesis is not a very accurate weather prediction. The main deviation in the terminal cost  $\Phi_{TI}$  is due to the fact that it is a soft terminal constraint: any deviation from the target value at the end of the receding horizon is penalized. The terminal constraint will no longer be maintained when the receding horizon is shifted. The same principle holds for the terminal cost  $\Phi_W$ , but since the biomass increase  $\Delta W$  mainly responds to solar radiation  $I_o$ , which is shifted over a day in the weather prediction  $\tilde{v}$ , the deviation is small.

Note that it is assumed here in all computations that the model is a perfect representation of the process, since the initial state  $x_0$  is computed with the model. If the control is implemented in a greenhouse, the measurements will differ from the model results, which also requires feedback control to correct this.

### 4.8.2 Solar versus non-solar greenhouse: seasonal influences

In figure 4.28 the results of the receding horizon optimal control with gradient search method and temperature integration of the solar and the non-solar greenhouse are compared per season.

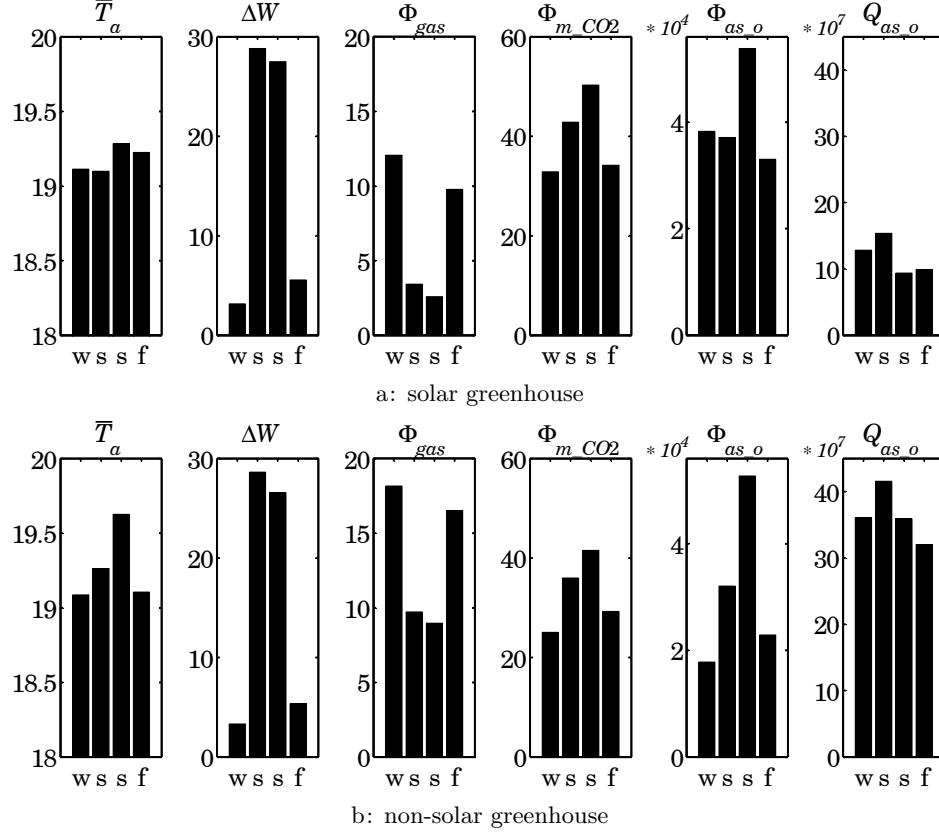


Figure 4.28: Results per season;  $\bar{T}_a$  {°C},  $\Delta W$  {kg m<sup>-2</sup>},  $\Phi_{gas}$  {m<sup>3</sup> m<sup>-2</sup>},  $\Phi_{m\_CO2}$  {kg m<sup>-2</sup>},  $\Phi_{as\_o}$  {m<sup>3</sup> m<sup>-2</sup>},  $Q_{as\_o}$  {W m<sup>-2</sup>}

In the solar greenhouse compared to the non-solar greenhouse (figure 4.28)

- the average temperature  $\bar{T}_a$  is closer to  $T_{aref} = 19^\circ\text{C}$
- the biomass increase  $\Delta W$  is about the same
- the gas use  $\Phi_{gas}$  is lower
- the CO<sub>2</sub> use  $\Phi_{m\_CO2}$  is higher
- the ventilation flow  $\Phi_{as\_o}$  is higher, with much less energy loss  $Q_{as\_o}$

The higher CO<sub>2</sub> use in the solar greenhouse is due to the higher ventilation, which is used to decrease humidity. The energy loss due to ventilation is lower

since ventilation with heat recovery is used. The biomass increase is the same since the same  $\text{CO}_2$  regime is used. The better average temperature in the solar greenhouse is probably due to the fact that it has more means to control the climate.

With respect to the differences per season the only difference is found in the ventilation flow  $\Phi_{as_o}$ . In the solar greenhouse the ventilation flow is much higher in winter, spring and fall. This is due to the ventilation with heat recovery, which is used to decrease humidity with less heat loss. Since in the non-solar greenhouse ventilation means heat loss, it is used less in the colder seasons.

In figure 4.29 the corresponding costs are given. The penalties  $\int L_{TI}$  and  $\int L_{aq}$  are not given because both are equal to zero.

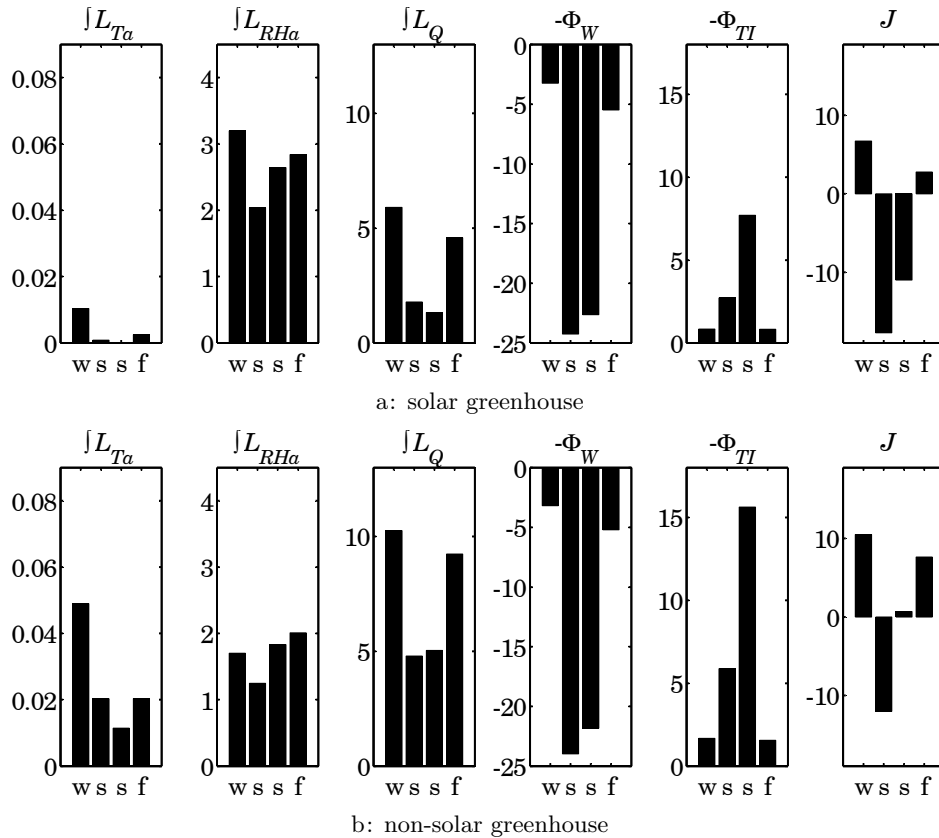


Figure 4.29: Average costs per season (a priori)

In the solar greenhouse compared to the non-solar greenhouse (figure 4.29)

- the temperature penalties  $\int L_{Ta}$  are lower
- the humidity penalties  $\int L_{RH_a}$  are higher
- the energy penalties  $\int L_Q$  are lower
- the terminal cost for the biomass increase  $\Phi_W$  is about the same
- the terminal cost for the temperature integral  $\Phi_{TI}$  is lower
- the cost function value (total of penalties and costs)  $J$  is lower

The lower penalties for temperature and temperature integral in the solar greenhouse are due to the fact that it has more means to control the climate. The lower energy penalty in the solar greenhouse is due to the use of the heat pump with the aquifer instead of the boiler. The main improvement with respect to gas use is found in summer (73%) and the lowest improvement in winter (34%), which indicates that heating is mainly needed for humidity reduction, and not for temperature increase.

It must be noted that the humidity penalty is lower in the non-solar greenhouse. The underlying variables are studied to investigate why this occurs. It is found that the lower humidity  $RH_a$  is due to a lower temperature  $T_{as}$ , which leads to more condensation on the roof  $\Phi_{m.as.ri\_H2O}$  (37% more year-round). On the other hand, the terminal cost for the temperature integral increases. So if the temperature integral concept really leads to better crop development and quality, the solar greenhouse will yield better developed crops and a higher product quality.

From these results it can be concluded that overall the solar greenhouse performs better than the non-solar greenhouse in all seasons.

#### 4.8.3 Solar versus non-solar greenhouse: influence of separate solar greenhouse elements

In the receding horizon optimal control computations with the solar greenhouse all solar greenhouse elements are used. This makes it difficult to distinguish the influence of the separate solar greenhouse elements. To get an impression of the contribution of the separate elements additional computations are done in this paragraph for the RHOC with TI and gradient search.

*A* represents the solar greenhouse with all solar greenhouse elements;  
*B* represents the solar greenhouse with heat pump, heat exchanger and aquifer, but without ventilation with heat recovery;  
*C* represents the solar greenhouse with ventilation with heat recovery, but without heat pump, heat exchanger and aquifer;  
*D* represents the solar greenhouse without heat pump, heat exchanger and aquifer, and without ventilation with heat recovery, which we called the non-solar greenhouse;  
*E* represents the solar greenhouse without heat pump, heat exchanger and aquifer, and without ventilation with heat recovery, but with CO<sub>2</sub> supply from the boiler. This means that CO<sub>2</sub> supply is now dependent on boiler operation, and eqn. 3.18 is used instead of eqn. 3.17 to compute the CO<sub>2</sub> supply.

These different cases are listed here.

	heat pump, heat exchanger, aquifer	ventilation with heat recovery	CO <sub>2</sub> from boiler
<i>A</i> ( <i>solar</i> )	+	+	–
<i>B</i>	+	–	–
<i>C</i>	–	+	–
<i>D</i> ( <i>̄solar</i> )	–	–	–
<i>E</i>	–	–	+

In the tables 4.11a, 4.11b and 4.11c the results and the associated costs (a priori and a posteriori) are given for the different cases.

In table 4.11a a number of cases are compared to investigate the influence of the separate solar greenhouse elements. The main results of these comparisons are described here.

The use of the heat pump, heat exchanger and aquifer (compare *B–D*) leads to:

- lower gas use  $\Phi_{gas}$  (77%)
- higher CO<sub>2</sub> use  $\Phi_{m\_CO2}$  (111%)
- less ventilation  $\Phi_{as\_o}$  (97%) and  $Q_{as\_o}$  (94%)

The heat pump was intended to decrease the gas use by heating the greenhouse with water from the aquifer, which decreases the gas use by 23%. Less ventilation is used since the greenhouse can be cooled with the heat exchanger, so the windows are opened less. This increases the CO<sub>2</sub> use, since this is made

Table 4.11: Comparison RHOC separate solar greenhouse elements

a: results, a posteriori values

	$\Phi_{gas}$ {m <sup>3</sup> m <sup>-2</sup> }	$\Delta W$ {kg m <sup>-2</sup> }	$\Phi_{m\_CO2}$ {kg m <sup>-2</sup> }	$\Phi_{as\_o}$ {m <sup>3</sup> m <sup>-2</sup> }	$Q_{as\_o}$ {W m <sup>-2</sup> }
<i>A</i>	27.9=25.3+2.6	65.1	160.2	40.6·10 <sup>4</sup>	47.5·10 <sup>7</sup>
<i>B</i>	41.1=38.3+2.8	65.2	145.6	30.6·10 <sup>4</sup>	136.3·10 <sup>7</sup>
<i>C</i>	39.7	63.6	128.0	40.1·10 <sup>4</sup>	60.0·10 <sup>7</sup>
<i>D</i>	53.3	63.9	131.8	31.4·10 <sup>4</sup>	145.6·10 <sup>7</sup>
<i>E</i>	57.9	46.6	45.5	34.2·10 <sup>4</sup>	149.2·10 <sup>7</sup>
<i>B-D</i>	77%	102%	111%	97%	94%
<i>C-D</i>	74%	100%	97%	128%	41%
<i>D-E</i>	92%	137%	289%	92%	98%
<i>A-D</i>	52%	102%	122%	129%	33%
<i>A-E</i>	48%	139%	352%	118%	32%

$\Phi_{gas}$  is given as: total gas use = gas use by boiler + gas use by heat pump

b: average costs, a priori values

	$\int L_{Ta}$	$\int L_{RHa}$	$\int L_Q$	$\Phi_W$	$\Phi_{TI}$	$J$
<i>A</i>	0.00	2.67	3.35	-14.14	3.08	-5.04
<i>B</i>	0.01	2.80	5.01	-14.26	3.16	-3.28
<i>C</i>	0.01	2.28	5.79	-13.62	6.21	0.67
<i>D</i>	0.03	1.69	7.27	-13.77	6.31	1.52
<i>E</i>	0.02	1.62	8.41	-10.01	5.59	5.64

$\int L_{TI} = 0$  and  $\int L_{aq} = 0$

c: average costs, a posteriori values

	$\int L_{Ta}$	$\int L_{RHa}$	$\int L_Q$	$\Phi_W$	$\Phi_{TI}$	$J$
<i>A</i>	0.02	3.80	4.69	-13.52	8.22	3.21
<i>B</i>	0.11	4.53	6.91	-13.31	8.75	6.99
<i>C</i>	0.04	2.98	6.67	-13.24	10.53	6.98
<i>D</i>	0.12	4.00	8.97	-13.02	11.31	11.38
<i>E</i>	0.17	3.79	9.72	-9.53	11.23	15.37

$\int L_{TI} = 0$  and  $\int L_{aq} = 0$

dependent on the window aperture. All costs decrease, except the penalty  $\int L_{RH_a}$  for the humidity. This is mainly due to the windows being opened less.

The use of ventilation with heat recovery (compare  $C-D$ ) leads to:

- lower gas use  $\Phi_{gas}$  (74%)
- more ventilation  $\Phi_{as-o}$  (128%) with less energy loss  $Q_{as-o}$  (41%)

Ventilation with heat recovery was intended to decrease the gas use by reducing the heat loss due to ventilation at times where ventilation is needed for reducing relative humidity, but not for reducing temperature. The gas use is decreased by 26%, which is quite a large reduction, even more than obtained by the heat pump. The energy loss is decreased by 59%. More ventilation is used (128%), since this can now be done with less energy loss, so less costs. More energy is needed to decrease humidity without ventilation with heat recovery, since relative humidity is decreased not by decreasing the humidity but by increasing the temperature. All costs decrease, except the terminal cost  $\Phi_W$  for the biomass increase, which is only slightly higher. This is probably due to the lower  $CO_2$  supply, which is a result of the higher ventilation flow.

Humidity must be controlled to prevent leaf and crop wetness, which may cause crop diseases. The relative humidity, which is generally used in practice, may not be a good measure for this wetness. Leaf wetness can occur at relative humidities below 80%, while they can be dry at a relative humidity of 100%. It is expected that the difference between the crop temperature  $T_c$  and the dewpoint temperature  $T_d$  (eqn. 2.73) is a better indicator for leaf and crop wetness. Since the crop temperature is a state of the model this can easily be implemented in the optimal control.

The use of  $CO_2$  supply independent of boiler operation (compare  $D-E$ ) leads to:

- lower gas use  $\Phi_{gas}$  (92%)
- higher biomass increase  $\Delta W$  (137%)
- much higher  $CO_2$  use  $\Phi_{m-CO_2}$  (289%)
- less ventilation  $\Phi_{as-o}$  (92%) with less energy loss  $Q_{as-o}$  (98%)

The total amount of  $CO_2$  supplied with  $CO_2$  supply independent of boiler operation is much higher (289%) than when it depends on boiler operation. This leads to a higher biomass increase. The boiler is used less, since it does not have to be used to produce  $CO_2$ . The windows are opened less. Most costs decrease, except the penalty  $\int L_{RH_a}$  for the humidity and the terminal cost  $\Phi_{TI}$  for the temperature integral. This is however at the expense of a large increase in the penalty  $\int L_{Ta}$  for temperature.

The use of the heat pump, heat exchanger and aquifer, ventilation with heat recovery and CO<sub>2</sub> supply independent of boiler operation (compare *A–D*, *solar–solar*) leads to:

- much lower gas use  $\Phi_{gas}$  (52%), which means 48% less gas use!
- slightly higher biomass increase  $\Delta W$  (102%)
- higher CO<sub>2</sub> use  $\Phi_{m\_CO_2}$  (122%)
- more ventilation  $\Phi_{as\_o}$  (129%) with much less energy loss  $Q_{as\_o}$  (33%)

These differences are due to the combination of the solar greenhouse elements. All costs decrease, except the penalty  $\int L_{RHa}$  for the humidity. As stated earlier in §4.8.2 this is due to more condensation on the roof and more ventilation.

The closest to a real comparison between the solar greenhouse and a conventional greenhouse (but now controlled by optimal control) can be seen when comparing *A–E*:

- lower gas use  $\Phi_{gas}$  (48%), which means 52% less gas use!
- higher biomass increase  $\Delta W$  (139%)
- much higher CO<sub>2</sub> use  $\Phi_{m\_CO_2}$  (352%)
- more ventilation  $\Phi_{as\_o}$  (118%) with much less energy loss  $Q_{as\_o}$  (32%)

This shows that it is possible to obtain a higher biomass increase (39% more) with a much lower gas use (52% less). These benefits compensate for the higher use of CO<sub>2</sub> (252% more),

In all cases the a priori values (table 4.11b) are better than the a posteriori values (table 4.11c). This means that the actual results are not quite as good as initially expected. The main increase is found in the terminal cost  $\Phi_{TI}$  for the temperature integral. This is because it is a soft terminal constraint, which has a set target value at the end of the receding horizon. When the horizon shifts, the constraint is no longer maintained. For the penalties, ( $\int L$ ) the difference between the a priori and the a posteriori values is partly due to changes occurring due to the receding horizon (horizon shifts, new information, changed control inputs) and partly due to the difference between the predicted weather  $\tilde{v}$  and the actual weather  $v$ , as stated earlier. The ‘lazy man weather prediction’ as used in this thesis is not a very accurate weather prediction. When weather predictions from meteorological institutes are used in practice, the weather deviations are expected to be smaller. This will then lead to smaller differences between the a priori and a posteriori results.

## 4.9 Conclusions and discussion

### *Why optimal control?*

By using optimal control, quantitative scientific knowledge of the greenhouse and crop is used to determine the optimal control inputs. The results found hold for the models and the cost function as they have been defined in this thesis. The advantage of using a cost function is that in the definition of the cost function all possible demands can be incorporated and weighted. In this way, the grower can define how important specific parts of the cost function are by setting the weight factors of the cost function. The influence of weight factors on the results, such as gas use and biomass increase, can be directly visualized. The underlying model is mainly a white model, so most variables have a physical meaning. Therefore the results can always be interpreted and improved relatively easy.

### *Cost function and weight factors*

Open loop computations were used to determine the weight factors for the cost function, to investigate the influence of the temperature integral on the results and to visualize the differences between the results of the grid search and the gradient search method. The weight factors are balanced such that the costs of gas use to heat the greenhouse do not outweigh, for instance, the temperature penalty too much, such that heating can be used to increase temperature. The tuning is done over single days chosen throughout the year to make sure that the weight factors hold in different seasons. An important advantage over classical greenhouse climate control is that these weight factors have a clear and evident meaning. Balancing the weight factors in the cost function is a delicate matter. In the end the choice of the weight factors depends on what the grower thinks is important. If the grower has to set these weight factors it is important that a presentation tool is available that shows the results of these settings on the long run. With the optimal control approach it is possible to show such results. It would be possible to advise the grower on these settings based on weather predictions and a reference temperature for the temperature integral. This is an interesting subject for further research.

***The solar greenhouse: does it use less gas?***

Yes, it does! A gas use reduction of 52% can be accomplished. Furthermore the total biomass weight is increased by 39%, which is partly due to the possibility to use (252% more) free CO<sub>2</sub>.

These values are based on a comparison between a non-solar greenhouse where the CO<sub>2</sub> supply depends on boiler operation with the solar greenhouse including all its enhancements. It should be noted that, unlike common practice, this non-solar greenhouse is controlled by optimal control as well. Since the same requirements were put on maintaining humidity and temperature integral, it is likely that this greenhouse uses more gas and gives a better yield than greenhouses in practice, which are controlled by classical controllers. This means that the yield improvement expected from the solar greenhouse with respect to common practice is even higher than presented here, at the expense of somewhat less gas use reduction. In all cases the constraints for crop development and crop quality are maintained far better than in current practice.

The enhancements of the solar greenhouse are:

- heat pump, heat exchanger and aquifer;
- ventilation with heat recovery;
- CO<sub>2</sub> separate from boiler operation (e.g., Shell Pernis);
- zigzag cover;
- thermal screen.

The solar greenhouse uses 27.9 m<sup>3</sup> m<sup>-2</sup> gas, 160.2 kg m<sup>-2</sup> CO<sub>2</sub>, and it produces 65.1 kg m<sup>-2</sup> biomass per year. The non-solar greenhouse with CO<sub>2</sub> from the boiler (case *E* in §4.8.3) uses 57.9 m<sup>3</sup> m<sup>-2</sup> gas, 45.5 kg m<sup>-2</sup> CO<sub>2</sub>, and it produces 46.7 kg m<sup>-2</sup> biomass per year. Other interesting values are given in table 4.11a.

The influence of the solar greenhouse elements has been investigated to analyze the effect of the separate elements.

***The solar greenhouse elements:***  
***heat pump, heat exchanger and aquifer***

With the use of the heat pump, heat exchanger and aquifer the heating can be done with less gas use, and the heat exchanger can be used for cooling, so less ventilation is needed to decrease temperature. By using these solar greenhouse elements, a gas use reduction of 23% can be accomplished. The reduction of ventilation leads to a higher CO<sub>2</sub> concentration in the greenhouse, which gives

a higher biomass increase. The coefficient of performance of the heat pump ( $COP$ , eqn. 3.177) is 5.7 for the solar greenhouse. This means that the energy delivered to the greenhouse is 5.7 times as high as the energy used by the heat pump in the form of gas.

***The solar greenhouse elements:  
ventilation with heat recovery***

The gas use reduction of the ventilation with heat recovery is 26%. This is even higher than the gas use reduction of the heat pump, heat exchanger and aquifer. The use of ventilation with heat recovery seriously reduces the heat loss due to ventilation, which leads to more ventilation to reduce humidity.

***The solar greenhouse elements:  
CO<sub>2</sub> supply separate from the boiler***

In the Netherlands, pure CO<sub>2</sub> can be retrieved from Shell Pernis / OCAP, who currently supplies about 200 growers with CO<sub>2</sub>. The CO<sub>2</sub> supply is then independent of boiler operation. When CO<sub>2</sub> supply by the boiler is used, the amount of CO<sub>2</sub> that can be supplied is much lower than in the case with CO<sub>2</sub> supply independent of boiler operation. In commercial greenhouses, CO<sub>2</sub> supply by the boiler is used in combination with a short term heat buffer. When CO<sub>2</sub> supply is needed without energy supply, the boiler is used to produce CO<sub>2</sub> and the heat surplus is stored in the short term heat buffer. Comparing the cases *D-E* it can be seen that the gas use does not differ that much, and also the penalty  $\int L_{Ta}$  is not very high, which indicates that the gas supply is not generally needed for heat supply. Furthermore the highest CO<sub>2</sub> supply is needed in summer, when the lowest gas use is found. Based on these results the use of a short term heat buffer does not seem very beneficial, since the energy stored in it is usually not needed by the greenhouse. Assuming a short term buffer and the same CO<sub>2</sub> supply as in case *D*, an extra  $131.8 - 45.5 = 86.3 \text{ kg m}^{-2}$  would have to be produced by using the boiler. This would imply an extra gas use of  $\frac{86.3}{1.78} = 48.5 \text{ m}^3 \text{ m}^{-2}$  (assuming that all stored energy can be reused without any loss). This would increase the gas use of case *E* to  $57.9 + 48.5 = 106.4 \text{ m}^3 \text{ m}^{-2}$ , which is twice the gas use of case *D*. This would increase the biomass production from 46.6 to 63.9  $\text{kg m}^{-2}$ . In the cost function used in this thesis, this profit does not outweigh the extra cost for gas use.

### ***Control inputs***

Two control inputs have been optimized by the optimal control. From these two combined inputs the valve positions for heating and cooling and the window apertures were derived.

The valve positions for heating and cooling are coupled in the combined heating valve position  $vp_h$ . Removing this coupling would yield different control input trajectories. From tests without this coupling it was found however that the optimal control often gets stuck in local minima.

The CO<sub>2</sub> supply has not been optimized, but is a function of outdoor radiation, window aperture and the actual CO<sub>2</sub> concentration. This is done to reduce computation time and for simplicity. If the CO<sub>2</sub> supply must be included in the optimal control, penalties have to be defined that hold costs for supplying CO<sub>2</sub> and for emitting CO<sub>2</sub> into the environment when the windows are opened. This will cause an increase in the computation time, since then 144 instead of 96 control input values have to be computed for every receding horizon time step.

### ***The grid search and the gradient search method, a priori and a posteriori results***

A grid search method has been introduced, which gives an educated guess for the control input values. The control inputs are discretized values, and state dependent bounds are used to restrict the control inputs based on a priori knowledge of the system. The results of the grid search are used as an initial guess for the control inputs for the gradient search, thus ensuring that the values are already close to the optimum. In the open loop (one day) results it is found that the gradient search can generally improve the control inputs further. The main improvement is found in keeping the relative humidity better below its upper bound.

From the receding horizon (year-round) computations it is found that the a priori and the a posteriori<sup>⊕</sup> results of the gradient search are better than those of the grid search. The main improvement is found in the relative humidity penalty  $\int L_{RH a}$ . Since the a priori costs are open loop results and the a posteriori costs are closed loop results they will differ.

---

<sup>⊕</sup> The a priori values are open loop values computed during the receding horizon computation with the results up to that time and model predictions for the upcoming day, while the a posteriori values are closed loop values computed afterwards from the actual results (see §4.7.2).

To study this further, the results have been examined per season. The average costs are given in table 4.12 for the grid search and the gradient search method. As expected, the gradient search finds better a priori results in all seasons. The difference between the a priori and a posteriori costs is most pronounced in the terminal costs  $\Phi_{TI}$  for the temperature integral in table 4.12.

To investigate the influence of the weather prediction on the a posteriori results, a year-round computation is performed where the weather prediction  $\tilde{v}$  is equal to the actual weather  $v$ . These results are indicated with ‘gradient\*’ in table 4.12.

Table 4.12: Differences between a priori and a posteriori results

	$\int L_{RH_a}$		$\int L_Q$		$\Phi_W$		$\Phi_{TI}$		$J$	
	winter									
grid	8.60	7.67	6.74	6.92	-3.07	-2.91	1.46	4.24	13.81	16.00
gradient	3.20	2.72	5.90	8.36	-3.25	-2.52	0.83	7.65	6.69	16.23
gradient*	3.20	1.95	5.33	8.25	-3.57	-2.76	1.33	6.47	6.31	13.93
	spring									
grid	4.87	5.55	1.57	1.69	-23.78	-23.28	3.63	6.87	-13.71	-9.17
gradient	2.04	3.45	1.79	2.21	-24.26	-23.60	2.71	7.28	-17.72	-10.65
gradient*	2.71	2.10	1.15	1.63	-24.46	-24.31	1.35	3.58	-19.25	-17.01
	summer									
grid	5.57	7.63	0.88	1.07	-22.14	-21.80	8.79	10.93	-6.90	-2.16
gradient	2.64	5.73	1.32	1.69	-22.65	-22.23	7.69	10.44	-10.99	-4.37
gradient*	2.66	2.54	0.86	1.22	-22.56	-22.57	5.41	6.64	-13.63	-12.18
	fall									
grid	7.25	6.35	5.50	5.75	-5.20	-5.02	1.73	4.65	9.28	11.73
gradient	2.84	3.21	4.58	6.76	-5.49	-4.81	0.83	7.44	2.76	12.65
gradient*	2.57	1.72	4.35	6.29	-5.34	-4.88	1.19	5.28	2.77	8.41
	year-round									
grid	6.54	6.80	3.61	3.80	-13.77	-13.48	3.97	6.73	0.36	3.87
gradient	2.67	3.80	3.35	4.69	-14.14	-13.52	3.08	8.22	-5.04	3.21
gradient*	2.78	2.08	2.88	4.28	-14.21	-13.87	2.35	5.49	-6.20	-2.02

black = a priori values; grey = a posteriori values

gradient\* = gradient search, in which  $\tilde{v} = v$

$\int L_{TI} = 0$ ,  $\int L_{Ta}$  and  $\int L_{aq}$  are very small

Although the gradient\* version uses the actual weather for both the prediction and the actual results, the a priori and a posteriori costs differ. In the receding horizon principle, the actual states will be equal to the predicted states when there is no disturbance for the open loop (a priori) results. However, when

the horizon is shifted, new weather information becomes available, which may cause the optimal control to change the control inputs, leading to different closed loop (a posteriori) results.

Comparing the a posteriori and the a priori costs it is found that:

- The a posteriori terminal cost  $\Phi_{TI}$  for the temperature integral is much higher in all seasons. This is due to the fact that it is a soft terminal constraint, which will always deviate from the target value ( $T_{aref} = 19^\circ\text{C}$ ) when the receding horizon is shifted. As expected, the deviations with actual weather (gradient\*) are smaller than with predicted weather (gradient).
- All a posteriori costs are higher, except for the relative humidity penalty  $\int L_{RH_a}$ : in all seasons (gradient\*), in winter and fall (grid search) and in winter (gradient). The relative humidity penalty is much higher a posteriori than a priori in summer for the grid and the gradient search, while it is smaller for the gradient\* search.
- For the gradient search with and without weather prediction, the a posteriori penalties for energy use  $\int L_Q$  are much higher in winter and fall, causing a higher year-round energy use than initially anticipated.
- The deviation between the a priori and a posteriori costs for the gradient\* search are entirely due to the fact that the a priori costs are open loop results, and the a posteriori costs are closed loop (feedback) results. The influence of the weather prediction is the highest on the relative humidity penalty  $\int L_{RH_a}$  and the terminal cost  $\Phi_{TI}$  for the temperature integral.

The results indicate that part of the open loop (a priori) results are not achieved in the actual closed loop (a posteriori) results. When the a priori results are used in a presentation tool for the grower, the results should be carefully interpreted since they may be delusive.

The weather prediction is found to influence all results. Little deviation is seen in the terminal cost  $\Phi_W$  for biomass increase, since the biomass increase  $\Delta W$  mainly responds to solar radiation  $I_o$ . In the weather prediction (in this study), the solar radiation is merely shifted over a day, so that the prediction and the actual weather have practically the same radiation sum year-round. Nevertheless, with a perfect weather prediction ( $\tilde{v} = v$ ) the results are better. A real weather forecast will probably lead to larger deviations in the biomass increase than the weather prediction used here.

The difference between the a priori costs of the version with and without weather prediction ( $J = -5.04$  vs.  $-6.20$ ) is due to the difference between the weather prediction and the actual weather. This difference is found to be quite

small compared to the influence of the terminal constraint on the temperature integral.

The difference between the a priori and the a posteriori costs of the gradient\* search ( $J = -6.20$  vs.  $-2.02$ ) is entirely due to the receding horizon concept, since  $\tilde{v} = v$ . The only cost that can change much when the horizon is shifted is the soft terminal constraint of the temperature integral. The optimal control inputs are adjusted when the horizon is shifted to minimize the terminal cost of the temperature integral. Since the difference in the costs is quite large, it is important to further investigate this effect in further research.

When applying a temperature integral it is very important to have little uncertainty in the weather predictions. It must be noted that the ‘lazy man weather prediction’ as used in this thesis is not a very accurate one, so the deviations between the forecasted and the actual weather are probably smaller in practice, which will also lead to smaller differences between the a priori and a posteriori results. Better weather predictions are available from meteorological institutes. These should be used in a real implementation of this optimal control.

The results also indicate that the weather prediction may nullify the benefits obtained with the gradient method over the grid search method. In view of these uncertainties, it can be stated that the grid search method is sufficiently accurate for practical computations. Since the grid search method is entirely rule based, one might argue that the rule based methods currently used by the growers may not be that bad. The grid search method however also uses an optimization strategy. Furthermore it gives more insight in the influence of control inputs on energy use and crop growth compared to the methods currently used. The results of the gradient method compared to the grid search method do call for better weather predictions. There is uncertainty in the weather predictions and there might be uncertainty in the model. In further research the influence of these uncertainties on the cost function value should be investigated.

In the receding horizon optimal control with the gradient method, the control inputs are reinitialized when the grid search result is better. The control inputs  $u_{grid}^*$  of the grid search method are determined again at every full hour. If the cost function value  $J_{grid}$  is lower than  $J_{grad}$ , these control inputs are used as the initial guess (see §4.3.11).

During one year the control inputs can be reinitialized 8760 times (every 60 min). In table 4.13 the number of times (#) and the percentage of times (%) that the gradient search controls are reset to the grid search controls are given.

Table 4.13: Reinitialization control inputs

	$A$	$B$	$C$	$D$	$E$	$A^*$
#	1127	879	598	707	636	288
%	13	10	7	8	7	3
$A^* = A$ , in which $\tilde{v} = v$						

These percentages (up to 13% for the solar greenhouse) indicate that the reset of the gradient search is required quite often. Since the gradient search method is a local minimization method, it is likely that the global optimum is not found when the reinitialization is not used. The grid search method is a (rough) global minimization method, which enhances the possibility that a result close to the global minimum is found. In first tests of the optimal control the reinitialization was not used, and it was clear from the results that the gradient search got stuck in local minima quite often, leading to poor optimization results. The effect of the deviation between the weather prediction  $\tilde{v}$  and the actual weather  $v$  on the number of reinitializations is large ( $A$  versus  $A^*$ , 13% versus 3%). Along with the other conclusions in this paragraph, this indicates that the high number of reinitializations is probably due the terminal cost for the temperature integral.

### ***The temperature integral***

The temperature integral concept used in this thesis was specifically designed for the solar greenhouse by Körner and Challa (2003). The temperature integral makes it possible to use wider bounds for the temperature while attaining an average reference temperature over a certain number of days. This reference temperature and the number of days could be set by the grower depending on the crop stage. Although it is being used by most growers, the temperature integral is a feeble concept. It is used to describe the long-term effect on crop development and quality, but its relation to the physical or physiological background is remote. One can argue that it is, in fact, a poor man's solution to bypass a real crop development model. In this research it is assumed that the temperature integral rules can be used as a good model for crop development. The wider bounds for the temperature (compared to the case without temperature integration) make it possible to use less energy while keeping an

average temperature. The temperature integral is penalized by two terms in the cost function: a terminal cost  $\Phi_{TI}$  for long-term crop processes, and a penalty  $\int L_{TI}$  for short-term crop processes.

In the current study the temperature integral is clipped at a history of five days, which means that all information before that time is abruptly forgotten. This is unlikely to be a good model of a biophysical process and moreover raises difficult implementation issues. In future research, if a temperature integral is to be used, a forgetting factor should be incorporated to prevent this abrupt clipping.

It is shown that the deviation between the a posteriori and a priori terminal cost  $\Phi_{TI}$  for the temperature integral is quite large. Since it is a soft terminal constraint, it will deviate from the target value  $T_{aref}$  when the receding horizon is shifted. It might therefore be better to reduce its influence in the cost function by decreasing its weight and using more narrow temperature bounds. This would however annul some of the advantages achieved in this thesis. Therefore it is very important that further research is performed to develop a (preferably simple) crop development model that shows the sensitivity of crop development to temperature in the different development stages instead of concentrating on temperature integration.

The terminal cost  $\Phi_{TI}$  is a function of the average temperature deviation  $\Delta T_{a-TI}(t_f)$  over 6 days between the greenhouse air temperature  $T_a$  and the reference temperature  $T_{aref}$ . For the solar greenhouse this temperature deviation is smaller than  $0.5^\circ\text{C}$  during 80% of the time. This indicates that — although the terminal cost  $\Phi_{TI}$  is large — the average temperature over 6 days is still close to the reference temperature  $T_{aref}$ . Decreasing the weight in the cost function will cause this average temperature to deviate more.

In the optimization results it is found that the penalty  $\int L_{TI}$  for the average temperature deviation  $\Delta T_{a-TI}$  is always equal to zero, which means that the boundary values of  $\pm 6$  K are never crossed. For the different cases that have been computed the maximum value of  $|\Delta T_{a-TI}| = 3.45$  K is found for the non-solar greenhouse (case *D*), while the minimum value of  $|\Delta T_{a-TI}| = 1.63$  K is found for the solar greenhouse with  $\tilde{v} = v$ . The penalty was meant to control the fast crop processes, such as photosynthesis and respiration. From the results it can be concluded that these processes were already sufficiently controlled by the optimal control of the biomass increase, which means that this penalty can be omitted.

### ***Biomass increase***

When looking at the optimal control results of the solar greenhouse one is inclined to focus on the biomass increase  $\Delta W$  and the terminal cost  $\Phi_W$  related to it. It is very important to note that most of the penalties and terminal costs:  $\int L_{Ta}$  (temperature),  $\int L_{RH_a}$  (relative humidity),  $\int L_{TI}$  and  $\Phi_{TI}$  (temperature integral) represent terms that are important for crop growth and development. Only the penalties  $\int L_Q$  (gas use) and  $\int L_{aq}$  (aquifer energy content) are not directly crop related. When the biomass increase is high, but the temperature integral rules are not met, this will lead to bad crop development and a low quality crop. An example of this effect is seen in the comparison of the open loop optimal control with and without temperature integral in §4.5.3, where the temperature integral was shown to have a significant negative effect on biomass increase. In judging the results of this thesis not only the biomass increase but also the crop related penalties should be judged. The optimal control balances all these aspects that are important for greenhouse and crop management.

### ***Relative humidity***

It is found that relative humidity has a strong effect on gas use. During spring and summer the heating is mainly used to decrease humidity, not to increase temperature. If the humidity bound can be increased, this will give a direct cost reduction, since less heating is needed.

Relative humidity is used as a measure to indicate leaf and crop wetness, as these may cause crop diseases and fungi. This is current greenhouse practice. Relative humidity may however not be a good measure for this wetness, since leaf and crop wetness can occur at relative humidities below 80%, while they can be dry at a relative humidity of 100%. The dewpoint temperature (eqn. 2.73) is probably a better indicator of wetness. When the crop temperature  $T_c$  is lower than the dewpoint temperature  $T_d$ , condensation will take place. The crop temperature is a lumped temperature over the whole greenhouse, so a safety margin must be taken into account to correct for temperature variations throughout the greenhouse (e.g., 2°C). Then wetness is expected when  $T_c \leq T_d + 2^\circ\text{C}$ . Since the crop temperature is a state of the model this can easily be implemented in the optimal control.

In figure 4.30 the indoor air temperature  $T_a$ , humidity  $C_{a,H2O}$  and relative humidity  $RH_a$  are shown for two days in summer (22 and 23 June, solar greenhouse with RHOC), together with the crop temperature  $T_c$ , the dewpoint temperature  $T_d$ , and their difference  $\Delta T_{cd} = T_c - T_d$ . The bounds for relative humidity (85%) and temperature difference (2°C) are indicated with dashed lines. It is indicated with a star (★) where the relative humidity is higher than 85%.

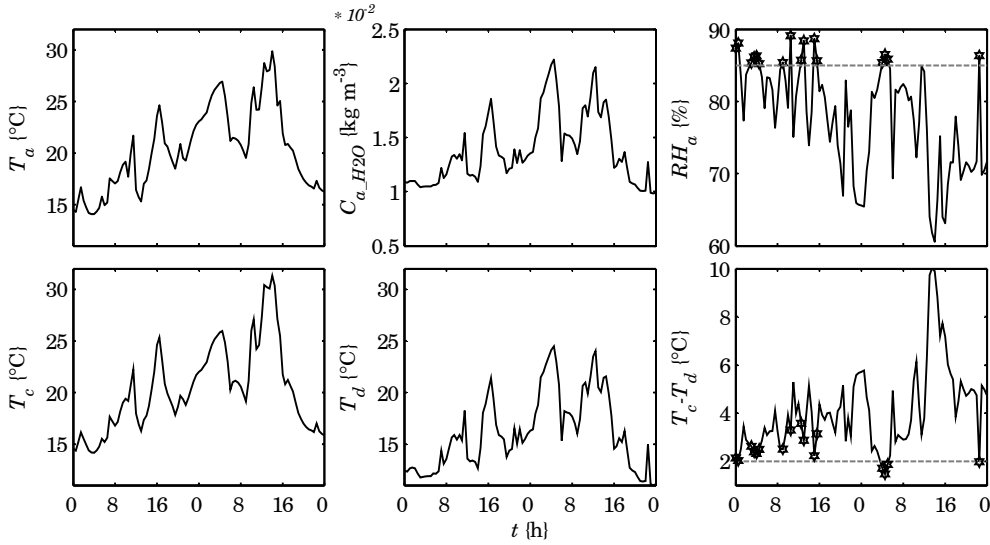


Figure 4.30: Relative humidity and dewpoint temperature

Although relative humidity and temperature difference are clearly related, it is obvious from the figure that a relative humidity  $RH_a$  above 85% does not always mean that the temperature difference  $\Delta T_{cd}$  is less than 2°C. In particular, while the relative humidity is higher than 85% on the first day, the temperature difference is above 2°C (no wetness). This method incorporates the crop temperature, while with relative humidity only the water content and the temperature of the indoor air are used.

In table 4.14 an overview is given of the results for the solar greenhouse with RHOC. A comparison is made between the cases where the relative humidity was above its bound, and where the temperature difference was below its bound.

From this table it can be seen that the relative humidity gives a stricter bound than the temperature difference (16 + 11 = 27% vs. 1 + 11 = 12%). Based on the temperature difference bound, relative humidity could be allowed to exceed its bound in 59% (16% out of 27%) of these cases, without leaf and crop

Table 4.14: Relative humidity and dewpoint temperature

	$RH_a < 85\%$	$RH_a \geq 85\%$
$\Delta T_{cd} > 2^\circ\text{C}$	72%	16%
$\Delta T_{cd} \leq 2^\circ\text{C}$	1%	11%

wetness! From the results for the temperature difference it is also seen that this bound is exceeded while the relative humidity is below 85% in 8% (1% out of 12%) of the cases, which indicates that leaf and crop wetness occurred while the relative humidity was below its bound.

### ***The aquifer***

The government demands that the aquifer runs approximately energy neutral year-round. Since we are looking only one day ahead (control horizon  $t_f$ ) the implementation of this demand in the RHOC cost function was not that straightforward. A solution has been found in defining a reference curve for the year-round aquifer energy content with the heat pump and heat exchanger capacities as used in the solar greenhouse. Bounds have been defined for this reference curve, which were then used in the cost function. From the results of the year-round computations with the gradient search method it is found that the aquifer energy content stays within its bounds all year. The aquifer energy content  $E_{aq}$  is equal to  $-6.1 \text{ MJ m}^{-2}$  at the end of the year, which means that slightly more energy was retrieved from the aquifer than was stored. This value is still very well within the bounds (see figure 4.4). The amount of energy stored in and retrieved from the aquifer is well balanced, which suggests that the capacities for the heat pump and the heat exchanger are chosen correctly.

The penalty  $\int L_{aq}$  for the year-round aquifer energy content  $E_{aq}$  is equal to zero in all computations with the aquifer present, except for the grid search optimization. In the grid search the energy content  $E_{aq}$  drops below its lower bound during the last 15 days of the year (see figure 4.23b). This indicates that the heat pump would use more energy from the aquifer than allowed. The heating is subsequently done with the boiler. This shows that the aquifer penalty in the optimal control does what it is supposed to do: control the aquifer energy content.

### *Other new greenhouse concepts*

A large number of innovative greenhouses have been designed and some even built in the past 10 years:

- the energy efficient greenhouse;
- the greenhouse of the future (*de kas van de toekomst*);
- the closed greenhouse (*de gesloten kas*, Themato, Innogrow);
- the greenhouse as an energy source (*de kas als energiebron, de energieproducerende kas*);
- the solar greenhouse.

The concepts show differences, but the general idea is the same: we have to use less energy. Further research has to be done to combine the most promising results to get the ultimate ‘super greenhouse’. The willingness to work together and the knowledge to make it work is there. Facilities to test the opportunities are very important but expensive. Hopefully in the future such facilities will be made available. Only then Dutch growers can truly benefit from the promising results obtained from this and other research into optimal greenhouse climate management.

## References

- G.P.A. Bot (1983). *Greenhouse climate: from physical processes to a dynamic model*. Ph.D. thesis, Wageningen Agricultural University, Wageningen, The Netherlands. 240 p.
- J.J.G. Breuer and N.J. van de Braak (1989). Reference year for Dutch greenhouses. *Acta Horticulturae*, 248, pp. 101–108.
- T. de Jong (1990). *Natural ventilation of large multi-span greenhouses*. Ph.D. thesis, Wageningen Agricultural University, Wageningen, The Netherlands.
- H.F. de Zwart (1996). *Analyzing energy-saving options in greenhouse cultivation using a simulation model*. Ph.D. thesis, Wageningen Agricultural University, Wageningen, The Netherlands. 236 p.
- T.G. Doeswijk and K.J. Keesman (2005). Adaptive weather forecasting using local meteorological information. *Biosystems Engineering*, 91(4), pp. 421–431.
- G.D. Farquhar, S. von Caemmerer, and J.A. Berry (1980). A biochemical model of photosynthetic CO<sub>2</sub> assimilation in leaves of C<sub>3</sub> species. *Planta*, 149, pp. 78–90.

- L. Heesen (1997). *Definitie, gevoeligheidsanalyse en evaluatie van een dynamisch model van het kas-gewasproductieproces*. M.Sc. thesis, Wageningen Agricultural University, Wageningen, The Netherlands. (in Dutch).
- E. Heuvelink (1996). *Tomato growth and yield: quantitative analysis and synthesis*. Ph.D. thesis, Wageningen Agricultural University, Wageningen, The Netherlands. 326 p.
- O. Körner (2003). *Crop based climate regimes for energy saving in greenhouse cultivation*. Ph.D. thesis, Wageningen University, Wageningen, The Netherlands.
- O. Körner and H. Challa (2003). Design for an improved temperature integration concept in greenhouse cultivation. *Computers and Electronics in Agriculture*, 39(1), pp. 39–59.
- O. Körner, H. Challa, and R.J.C. van Ooteghem (2002). Modelling temperature effects on crop photosynthesis at high radiation in a solar greenhouse. *Acta Horticulturae*, 593, pp. 137–144.
- O. Körner and R.J.C. van Ooteghem (2003). Chapter 2.4: Simulating crop gross photosynthesis at high temperatures. In: *Crop based climate regimes for energy saving in greenhouse cultivation*, pp. 75–90, Ph.D. thesis, Wageningen University, Wageningen, The Netherlands.
- L. Lukasse, A.-J. van der Voort, and J. de Kramer-Cuppen (2006). Optimal climate control to anticipate future weather and energy tariffs. In: *4<sup>th</sup> IFAC/CIGR workshop, Control applications in post-harvest and processing technology (CAPPT)*, Potsdam, Germany. March 26–29.
- E.M. Nederhoff (1994). *Effects of CO<sub>2</sub> concentration on photosynthesis, transpiration and production of greenhouse fruit vegetable crops*. Ph.D. thesis, Wageningen Agricultural University, Wageningen, The Netherlands. 213 p.
- B. Pagurek and C.M. Woodside (1968). The conjugate gradient method for optimal control problems with bounded control variables. *Automatica*, 4, pp. 337–349.
- G. Shina and I. Seginer (1989). Optimal management of tomato growth in greenhouses. *Acta Horticulturae*, 248, pp. 307–313.
- C. Stanghellini (1987). *Transpiration of greenhouse crops — an aid to climate management*. Ph.D. thesis, Wageningen Agricultural University, Wageningen, The Netherlands. 150 p.
- R.F. Tap (2000). *Economics-based optimal control of greenhouse tomato crop production*. Ph.D. thesis, Wageningen Agricultural University, Wageningen, The Netherlands.
- R.F. Tap, L.G. van Willigenburg, and G. van Straten (1996). Receding horizon optimal control of greenhouse climate using the lazy man weather prediction. In: *Proceedings of the 13th IFAC World Congress, San Francisco, USA*.

- June 30–July 5, paper 4a-013.
- B.N.J. van Dongen (2004). *Zonnekas tussen theorie en praktijk*. B.Sc. thesis, (MRS034), Wageningen University, Wageningen, The Netherlands. 21 p.
- E.J. van Henten (1994). *Greenhouse climate management: an optimal control approach*. Ph.D. thesis, Wageningen Agricultural University, Wageningen, The Netherlands. 329 p.
- E.J. van Henten and J. Bontsema (1991). Optimal control of greenhouse climate. In: *Mathematical and Control Applications in Agriculture and Horticulture*, vol. 1, pp. 27–32. IFAC Workshop Series.
- R.J.C. van Ooteghem (2003a). EET-project De Zonnekas: gewasproductie met duurzame in plaats van fossiele energie, deelproject 3a, WU-deel. Internal report, Wageningen University, Wageningen, The Netherlands. (in Dutch).
- R.J.C. van Ooteghem (2003b). The solar greenhouse model; extension of the greenhouse with crop model. Internal report, Wageningen University, Wageningen, The Netherlands.
- R.J.C. van Ooteghem, J.D. Stigter, L.G. van Willigenburg, and G. van Straten (2003a). Optimal control of a solar greenhouse. In: *Proceedings of the European Control Conference (ECC) 2003*, University of Cambridge, Cambridge, United Kingdom. September 1–4.
- R.J.C. van Ooteghem, J.D. Stigter, L.G. van Willigenburg, and G. van Straten (2003b). Optimal control of a solar greenhouse. In: *22<sup>nd</sup> Benelux Meeting on Systems and Control*, p. 41, Lommel, Belgium. Editors: J. Swevers and C. Lauwerys, March 19–21.
- R.J.C. van Ooteghem, J.D. Stigter, L.G. van Willigenburg, and G. van Straten (2004a). Receding horizon optimal control of a solar greenhouse. In: *GreenSys2004, International Symposium on Sustainable greenhouse systems*, Catholic University Leuven, Leuven, Belgium. Editors: G. van Straten, G.P.A. Bot, W.T.M. van Meurs, and L.M.F. Marcelis, September 12–16.
- R.J.C. van Ooteghem, J.D. Stigter, L.G. van Willigenburg, and G. van Straten (2004b). Receding horizon optimal control of a solar greenhouse. In: *23<sup>rd</sup> Benelux Meeting on Systems and Control*, p. 85, Helvoirt, The Netherlands. March 17–19.
- R.J.C. van Ooteghem, L.G. van Willigenburg, and G. van Straten (2005a). Receding horizon optimal control of a solar greenhouse. *Acta Horticulturae (ISHS)*, 691, pp. 797–806.
- R.J.C. van Ooteghem, L.G. van Willigenburg, and G. van Straten (2005b). Receding horizon optimal control of a solar greenhouse. In: *24<sup>rd</sup> Benelux Meeting on Systems and Control*, p. 91, Houffalize, Belgium. March 22–24.

- R.J.C. van Ooteghem, L.G. van Willigenburg, and G. van Straten (2006). Receding horizon optimal control of a solar greenhouse. In: *25<sup>th</sup> Benelux Meeting on Systems and Control*, p. 90, Heeze, The Netherlands. Editors: B. de Jager and G. Meinsma, March 13–15.
- L.G. van Willigenburg, E.J. van Henten, and W.T.M. van Meurs (2000). Three time-scale receding horizon optimal control in a greenhouse with a heat storage tank. In: *Proceedings of the Agricontrol 2000 Conference*, Wageningen, The Netherlands.

# Summary

Intensive crop production in greenhouse horticulture in the Netherlands requires a high input of fossil energy of about 10% of the total national consumption (in 2004). Several initiatives have been taken by universities, research institutes and industry to investigate methods to reduce energy use. This has resulted in new greenhouse designs and new methods for control.

The Dutch climate has cool summers and mild winters, which is favourable for greenhouse crop production. All greenhouses collect solar energy. If the solar energy could be stored during the warm periods and retrieved during the colder periods, a large gas use reduction could be achieved. This notion led to the solar greenhouse project. Participants in this project were industry, the former IMAG-DLO<sup>⊗</sup> and the chairs of Physics, Horticultural Production Chains, and Systems and Control.

Within the solar greenhouse project, the goal was arrive at a greenhouse and control design for optimal crop production with sustainable instead of fossil energy. A number of researchers have been working together on this project. A new greenhouse design has been proposed that minimizes external energy demand. This solar greenhouse design is integrated with climate control to obtain optimal crop growth conditions. Model based receding horizon optimal control is used to maximize solar energy use, minimize fossil energy consumption and obtain optimal crop growth conditions.

---

<sup>⊗</sup> This part of IMAG-DLO currently belongs to the Greenhouse Technology group of Plant Research International.

This thesis describes the optimal control design for the solar greenhouse. Optimal control uses optimization algorithms to minimize a criterion that describes the desired goal. This criterion is a measure that can be computed based on model simulations of the involved dynamic processes.

In the optimal control design the proposed goal must be quantified. The goal is constructed from a number of subgoals (the gas use and the crop yield, development and quality), which are united in the so called cost function. The importance of each subgoal is weighed against the other subgoals. With proposed control input trajectories and a weather prediction, the cost function value can be computed from the greenhouse and crop conditions (temperature, relative humidity, crop biomass increase, gas use etc.). The control inputs consist of actuator settings, such as window apertures and valve positions of, for instance, the boiler. Changing these trajectories will result in different greenhouse and crop conditions, and thus a different cost function value. The control inputs are changed to achieve the minimum cost function value. The corresponding greenhouse and crop conditions are then considered optimal.

A cost function can only be computed if the underlying processes that determine the gas use and the crop yield, development and quality are known. It is therefore necessary to have a good model that gives an accurate description of the dynamic response of both the greenhouse as well as the crop to the control inputs (actuator settings) and external inputs (weather conditions). The crop model describes the crop biophysical processes (photosynthesis, respiration, evapotranspiration) and the temperature integral in response to the indoor greenhouse conditions. The temperature integral is used in this thesis as an indicator of crop development and quality. The greenhouse model describes the physical relations to derive the indoor greenhouse conditions from the outdoor weather conditions and the control inputs. To reduce the energy use, larger temperature fluctuations will be allowed by the optimal control, which may lead to temperature and humidity extremes beyond the operating range of currently existing models.

The research objectives addressed in this thesis are therefore as follows:

- Design a greenhouse-with-crop model for the solar greenhouse suitable for optimal control purposes.
- Validate the model for a conventional greenhouse (since data is available for a conventional greenhouse, and not for the solar greenhouse).
- Design an optimal controller for the solar greenhouse that minimizes gas use and maximizes crop production.

## Model of crop biophysics (chapter 2)

The model of the crop biophysics has been developed based on partly existing submodels of photosynthesis, respiration, evaporation and temperature integration. A number of photosynthesis models have been compared. A new crop photosynthesis model has been designed based on a detailed biochemical leaf photosynthesis model (Farquhar et al., 1980) with Gaussian integration over the crop layers (Goudriaan and van Laar, 1994; Heuvelink, 1996) and a variable stomatal and boundary layer resistance to CO<sub>2</sub> diffusion (Stanghellini, 1987). This model has been validated by Körner and van Ooteghem (Körner and van Ooteghem, 2003; Körner et al., 2001a,b, 2002, 2003, 2007a,b) and showed good accordance with measured data. Temperature integration has been used as a descriptive method for long-term temperature effects on crop development, based on the research by Körner and Challa (2003). Although no particular crop has been chosen in the crop model development, the production of a tomato crop has been assumed in the submodels for the evapotranspiration and the temperature integral. With different parameters in these submodels, the crop could be changed to, for instance, sweet pepper or rose.

## Solar greenhouse model (chapter 3)

As compared to a conventional greenhouse, the solar greenhouse is extended with some extra elements:

- Improved roof cover: for increased solar radiation and less heat loss.
- Ventilation with heat recovery: to reduce humidity with less heat loss.
- Aquifer: for long-term storage of warm and cool water.
- Heat exchanger: to cool the greenhouse with cool water from the aquifer.
- Heat pump: to heat the greenhouse with warm water from the aquifer.

The model of the solar greenhouse has been developed based on the conventional greenhouse model by Heesen (1997), who exploited the research by Van Henten (1994), De Zwart (1996), De Jong (1990) and Bot (1983). The original model only described a simple greenhouse with a single glass cover, and without a thermal screen.

To make it suitable for the solar greenhouse, this model has been modified to include a thermal screen, a double glass cover and a cooling net. Submodels have been designed for the heat pump, the heat exchanger and the aquifer. The model parts that were too elaborate or computationally heavy for use in an optimal control context were simplified. The crop biophysics

model has been included to obtain a correct description of the water and carbon dioxide levels in the greenhouse, leading to a greenhouse-with-crop model. The complete solar greenhouse-with-crop model is described by 16 states, 9 control inputs (actuators) and 6 external inputs (weather). The conventional greenhouse model (without the solar greenhouse elements) has been validated with measured greenhouse data. Sensitivity analysis has been performed to retrieve the uncertain model parameters. Parameter estimation was used to match the data to the model. Only a few parameters of the conventional greenhouse model needed calibration. The conventional greenhouse-with-crop model showed good accordance with the data.

## Optimal control of a solar greenhouse (chapter 4)

Optimal control is a form of model predictive control. Model predictive control has the advantage that specific knowledge that is incorporated in a dynamic model can be directly used, whereas in other control system designs this knowledge is not, or only partly, used. Moreover, all variables in the greenhouse-with-crop model can be used in the cost function that defines the control objectives in a quantitative and explicit way. The control objectives have been defined as:

1. Minimize gas use.
2. Maximize crop biomass increase.
3. Take care of good crop development and disease free conditions.
4. Make sure that the aquifer use complies with government regulations.

The objectives 1 and 2 are directly related to variables in the model. Objective 3 is translated to bounds for the temperature, the relative humidity and the temperature integral. Objective 4 has required some extra attention since the government regulations are based on year-round requirements, and the control horizon used in the optimal control is only one day. Preliminary computations were done to obtain a trajectory of the aquifer energy content over a year. This trajectory was subsequently used to create bounds that could be used in the cost function. All objectives are combined in the cost function.

It was found that if the actual control inputs were optimized, the optimal control often got stuck in local minima. From the 9 control inputs, 7 are optimized. By smart a combination of of these actual control inputs, this number can be reduced to 2 control inputs that are optimized by the optimal control, which also reduces the computation time. This combination of the control inputs is meant to rule out control actions that are not supposed to

take place at the same time (e.g. heating and cooling). These two control inputs determine the actual control inputs.

The conjugate gradient search method is used to search for the optimal control inputs. This local minimization method is robust and reasonably efficient with respect to computation time. This method requires a good initial guess for the control inputs to prevent the result from moving to a local minimum. A good initial guess for the control inputs is found with the grid search method, a rough global minimization method that was specifically designed during this research for this optimal control problem. The grid search method uses only a small number of discrete constant trajectories for the control inputs. State dependent control input bounds are used to prevent behaviour that is known beforehand to be non-optimal (for instance, cooling when the temperature is below its minimum temperature). These state dependent control input bounds are based on knowledge of the greenhouse-with-crop system. The discrete bounded control inputs that lead to the lowest cost function value are the results of the grid search optimization.

### Open loop computations, winter and summer day

Open loop optimal control computations have been performed for a day in winter and in summer, both with and without temperature integration. These computations were used

- to determine the weight factors for the cost function with and without temperature integration;
- to validate if the grid search results were indeed a good initial guess;
- to review the influence of temperature integration on the results.

The weight factors were balanced such that the costs of gas use to heat the greenhouse did not outweigh, for instance, the temperature penalty too much, so that heating could be used to increase temperature. Single days in different seasons were used for the tuning to make sure that the weight factors would apply in different seasons. The balance of the weight factors in the cost function depends on what the grower thinks is important. The optimal control approach described in this thesis can be used in the future to develop a presentation tool for the grower that visualizes the effect of the chosen controller settings on the expected results.

It was found that the grid search results were already quite good. The gradient search could further improve the results of the grid search. Specifically the relative humidity was improved by the gradient search.

Comparing the versions without and with temperature integration it was found that the latter version yielded a lower crop biomass increase. This indicates that the temperature integration can have a negative effect on biomass increase. However also crop development and quality should be taken into account, which are determined by the penalties and terminal costs for temperature, relative humidity and the temperature integral. The optimal control balances all these aspects. Accordingly the version without temperature integration might yield a low quality crop that cannot be sold.

### **Closed loop RHOC computations, year-round**

Closed loop year-round computations with a receding horizon optimal controller were performed using the grid search and the gradient search method. The year-round computation took 8 days with the gradient search method and only 8 hours with the grid search method. To our best knowledge this is the first time that year-round RHOC computations have been performed with a physical greenhouse model.

#### ***Gradient search versus grid search***

The grid search method has been used to get a first feel for the optimal control results. A comparison has been made between the solar and the non-solar greenhouse. The non-solar greenhouse was assumed to be the same as the solar greenhouse, but without the heat pump, heat exchanger and ventilation with heat recovery. These first results showed that the aquifer could be operated year-round, and a large decrease in gas use (of 58%) could be achieved.

Next the conjugate gradient search method was used. As expected, the gradient search resulted in lower cost function values than the grid search, which showed that the grid search results could be further improved. Again, as in the open loop computations, the main improvement was found in the relative humidity penalty.

#### ***A priori versus a posteriori***

The a priori costs are the costs that are computed a priori by the receding horizon optimal control system. These are the minimal costs expected based on all available information available at the time of the computation of the control actions. The a posteriori costs are the actually accomplished costs of

the receding horizon optimal control algorithm. When the controller actions are going to be presented to the grower via a kind of presentation tool, only the a priori costs are available. It is therefore relevant to have an indication of the deviation between the a priori and the a posteriori results.

The deviation between the a priori and a posteriori results (in the computations in this thesis) is partly due to the receding horizon and partly due to the difference between the real and the predicted weather (when these are different). To investigate the influence of the weather prediction, a simple weather prediction for the upcoming day has been developed based on the ‘lazy man weather prediction’, where the weather of the previous day is taken as the prediction with a correction based on current weather measurements.

A comparison was made for the situation in which the weather prediction is equal to the actual weather. The difference between the a priori and the a posteriori costs was quite large. This difference arises because the inclusion at the next control interval of new information at the end of the horizon forces the receding horizon controller to modify the control trajectory away from the trajectory first believed to be optimal when the new information was not yet available. It appears that the terminal cost for the temperature integral is the main cause for the change of the control inputs. A large penalty is used for this soft terminal constraint, that penalizes based on the average temperature over 6 days. This is compensated by wider bounds for the temperature itself, which gives more room for the optimization. Due to this large penalty, the average temperature over 6 days is very close to the reference temperature of 19°C. The results also indicate that it is, in fact, impossible to satisfy the temperature integral demands at every instant.

The difference in the a priori costs for the situation in which the weather prediction was equal and unequal to the actual weather was minor. This difference is due to the deviation between the actual and the predicted weather. This indicates that the sensitivity of the *expected* results for the weather prediction is small. This indicates that the influence of the weather prediction on the *expected* results is small. The difference in the a posteriori costs that result from the control actions computed with actual weather and from control actions computed with the weather prediction was much larger. This shows that the influence of the weather prediction on the *actual* results is still significant. It must be noted that the ‘lazy man weather prediction’ as used in this thesis is not a very accurate weather prediction on a time scale of one whole day.

***Influence of solar greenhouse elements:  
heat pump, heat exchanger and aquifer,  
ventilation with heat recovery,  
CO<sub>2</sub> supply independent of boiler operation***

The influence of the separate solar greenhouse elements has been investigated. It was found that the use of the heat pump, heat exchanger and aquifer gave a significant gas use reduction (of 23%). The use of ventilation with heat recovery gave an even higher gas use reduction (of 26%). CO<sub>2</sub> supply independent of boiler operation led to a much higher crop biomass increase (of 37%) with a small gas use reduction (of 8%) at the expense of much more CO<sub>2</sub> use (of 189%).

If the same amount of CO<sub>2</sub> would have to be produced by using the boiler, this would lead to a significant increase of gas use. In common greenhouse practice the heat surplus is stored in a short term heat buffer. Under the circumstances computed in this thesis for the conventional greenhouse this stored heat was hardly needed for greenhouse heating or dehumidification, which implies that the use of a short term heat buffer under these circumstances would not be very beneficial.

The government demands that the aquifer runs approximately energy neutral year-round. With a control horizon of one day, the implementation of this demand in the RHOC cost function was not that straightforward. A solution was found in defining a reference curve for the aquifer energy content. Bounds were defined for this reference curve, which were then used in the cost function. From the year-round computations it has been found that the aquifer energy content stayed within its bounds all year.

***Relative humidity***

It has been found that relative humidity has a strong effect on gas use. During spring and summer the heating is mainly used to decrease humidity, not to increase temperature. A direct cost reduction could be achieved when the humidity bound could be increased to a value higher than 85%.

In current greenhouse practice the relative humidity is used as a measure for leaf and crop wetness, since this can cause crop diseases and fungi. Relative humidity is however not a good measure for wetness. Leaves can be wet, for instance, at a relative humidity below 80%, while they can be dry at a relative humidity of 100%. A new approach has been proposed that uses the dewpoint

temperature of the crop. This temperature is probably a better indicator of wetness, since it is a direct measure for condensation. It has been shown that the use of the dewpoint temperature gives less strict bounds, which is expected to lead to less gas use. This can be easily implemented in the receding horizon optimal controller because the crop temperature is a state of the model.

### ***Solar greenhouse versus conventional greenhouse***

When the solar greenhouse is compared to a conventional greenhouse, without all solar greenhouse elements (such as: heat pump, heat exchanger, ventilation with heat recovery, CO<sub>2</sub> supply independent of boiler operation), both controlled by optimal control, it is found that the gas use is decreased by 52%, with a 39% higher crop biomass increase.



# Samenvatting

De intensieve gewasproductie in de glastuinbouw in Nederland vereist een hoog gebruik van fossiele energie van ongeveer 10% van de totale nationale consumptie (in 2004). Verschillende initiatieven zijn genomen door universiteiten, onderzoeksinstituten en de industrie voor het onderzoeken van methoden om het energieverbruik te verminderen. Dit heeft geresulteerd in nieuwe kasontwerpen en nieuwe regelmethoden.

Het Nederlandse klimaat met koele zomers en milde winters is gunstig voor de gewasproductie in kassen. Alle kassen slaan zonne-energie op. Als de zonne-energie opgeslagen zou kunnen worden gedurende de warme periodes en teruggewonnen tijdens de koudere periodes, dan zou een grote vermindering van het gasverbruik kunnen worden bereikt. Deze notie leidde tot het zonnekasproject. Deelnemers in dit project waren de industrie, het voormalige IMAG-DLO<sup>⊗</sup> en de leerstoelgroepen Natuurkunde, Tuinbouwproductieketens, en Meet-, Regelen en Systeemtechniek.

In het zonnekasproject, was het doel te komen tot een kas- en regelaarontwerp voor optimale gewasproductie met duurzame in plaats van fossiele energie. Een aantal onderzoekers heeft samengewerkt aan dit project. Een nieuw kasontwerp is voorgesteld dat de externe energiebehoefte minimaliseert. Dit zonnekasontwerp is geïntegreerd met de klimaatregeling voor het verkrijgen van optimale omstandigheden voor de gewasgroei. Een modelgebaseerde wijkende horizon optimale regeling wordt gebruikt om de benutting van zonne-energie te maximaliseren, het gebruik van fossiele energie te minimaliseren en de optimale omstandigheden voor de gewasgroei te verkrijgen.

Dit proefschrift beschrijft het ontwerp van de optimale regelaar voor de zonnekas. De optimale regeling gebruikt optimaliseringsalgoritmen om een criterium

---

<sup>⊗</sup> Dit deel van IMAG-DLO behoort nu tot de groep Greenhouse Technology van Plant Research International.

te minimaliseren dat het gewenste doel beschrijft. De waarde van het criterium wordt berekend uit modelsimulaties van de betreffende dynamische processen.

In het optimale regelaarontwerp moet het gewenste doel worden gekwantificeerd. Het doel wordt geconstrueerd uit een aantal subdoelen (het gasverbruik en de gewasopbrengst, -ontwikkeling en -kwaliteit), die verenigd zijn in de zogenoemde kostenfunctie. Het belang van elk subdoel wordt gewogen tegen andere subdoelen. Met een voorgesteld verloop van de sturingen en een weersvoorspelling kan de waarde van de kostenfunctie worden berekend uit de kas- en gewasomstandigheden (temperatuur, relatieve luchtvochtigheid, toename van biomassa, gasverbruik enz.). De sturingen bestaan uit actuator-instellingen, zoals vensteropeningen en klepposities van, bijvoorbeeld, de ketel. Het veranderen van het verloop hiervan zal resulteren in andere kas- en gewasomstandigheden, en dus ook een andere waarde voor de kostenfunctie. De sturingen worden aangepast totdat de waarde van de kostenfunctie minimaal is. De bijbehorende kas- en gewasomstandigheden worden dan optimaal geacht.

Een kostenfunctie kan alleen berekend worden als de onderliggende processen die het gasverbruik en de gewasopbrengst, -ontwikkeling en -kwaliteit bepalen, bekend zijn. Het is daarom noodzakelijk om een goed model te hebben dat een nauwkeurige beschrijving van het dynamische gedrag van zowel de kas als het gewas op de sturingen (actuator-instellingen) en de externe ingangen (weersomstandigheden) geeft. Het gewasmodel beschrijft de biofysische processen van het gewas (fotosynthese, onderhoudsademhaling, verdamping) en de temperatuurintegraal als functie van het klimaat in de kas. De temperatuurintegraal wordt gebruikt in dit proefschrift als indicator voor de gewasontwikkeling en -kwaliteit. Het kasmodel beschrijft de fysieke relaties om het klimaat in de kas te bepalen uit de weersomstandigheden en de sturingen. Om het energieverbruik te verminderen, zullen grotere fluctuaties in de temperatuur toegestaan worden door de optimale regeling, wat zal leiden tot temperatuur- en luchtvochtigheidswaarden buiten het normale werkgebied van de bestaande modellen.

De onderzoeksdoelstellingen in dit proefschrift zijn:

- Ontwerp een kas-met-gewas model voor de zonnekas dat geschikt is voor optimale regeling.
- Valideer het model voor een conventionele kas (aangezien er gegevens beschikbaar zijn voor een conventionele kas, en niet voor de zonnekas).
- Ontwerp een optimale regelaar voor de zonnekas die het gasverbruik minimaliseert en de gewasproductie maximaliseert.

## Model van de gewasbiofysica (hoofdstuk 2)

Het model van de gewasbiofysica is ontwikkeld gebaseerd op gedeeltelijk bestaande submodellen van fotosynthese, onderhoudsademhaling, verdamping en temperatuurintegratie. Een aantal fotosynthesemodellen is vergeleken. Een nieuw model voor de gewasfotosynthese is ontworpen op basis van een gedetailleerd biochemisch model van de bladfotosynthese (Farquhar et al., 1980) met Gaussische integratie over de gewaslagen (Goudriaan en van Laar, 1994; Heuvelink, 1996) en een variabele stomataire en grenslaag weerstand voor CO<sub>2</sub> diffusie (Stanghellini, 1987). Dit model is gevalideerd door Körner en van Ooteghem (Körner en van Ooteghem, 2003; Körner et al., 2001a,b, 2002, 2003, 2007a,b) en bleek goed overeen te komen met de gemeten data. Temperatuurintegratie is gebruikt als beschrijvende methode voor lange-termijn gevolgen van temperatuur op de gewasontwikkeling, gebaseerd op het onderzoek van Körner en Challa (2003). Hoewel geen specifiek gewas gekozen is tijdens de ontwikkeling van het gewasmodel, is de productie van een tomatengewas verondersteld in de submodellen voor de verdamping en de temperatuurintegraal. Met andere parameters in deze submodellen zou het gewas veranderd kunnen worden in, bijvoorbeeld, paprika of roos.

## Model van de zonnekas (hoofdstuk 3)

In vergelijking met een conventionele kas, is de zonnekas uitgebreid met enkele extra elementen:

- Beter kasdek: voor verhoogde zon-instraling en minder warmteverlies.
- Ventilatie met warmteterugwinning: voor het verminderen van de luchtvochtigheid met minder warmteverlies.
- Aquifer: voor de lange-termijn opslag van warm en koud water.
- Warmtewisselaar: voor het koelen van de kas met koud water van de aquifer.
- Warmtepomp: voor het verwarmen van de kas met warm water van de aquifer.

Het model van de zonnekas is een verdere ontwikkeling van het conventionele kasmodel van Heesen (1997), dat gebruik maakte van het onderzoek van Van Henten (1994), De Zwart (1996), De Jong (1990) en Bot (1983). Het originele model beschreef slechts een eenvoudige kas met een kasdek van enkel glas, en zonder energiescherm.

Om het geschikt te maken voor de zonnekas zijn aan dit model een energiescherm, een dubbel glas kasdek en een koelnet toegevoegd. Er zijn submodellen ontworpen voor de warmtepomp, de warmtewisselaar en de aquifer. De modeldelen die te gedetailleerd of rekentechnisch te zwaar waren voor gebruik in een optimale regeling werden vereenvoudigd. Het model van de gewasbiofysica is opgenomen om een correcte beschrijving te verkrijgen van de water- en koolstofdioxideconcentraties in de kas, waardoor een model van de kas-met-gewas wordt verkregen. Het volledige zonnekas-met-gewas model wordt beschreven door 16 toestanden, 9 stuuringangen (actuatoren) en 6 externe ingangen (het weer). Het conventionele kasmodel (zonder de zonnekas-elementen) is gevalideerd met gemeten kasdata. Een gevoeligheidsanalyse is uitgevoerd om de onzekere modelparameters te vinden. Parameterschatting werd gebruikt om het model af te stemmen op de data. Slechts een paar parameters van het conventionele kasmodel dienden gekalibreerd te worden. Het conventionele kas-met-gewasmodel toonde goede overeenstemming met de data.

## Optimale regeling van een zonnekas (hoofdstuk 4)

Optimale regeling is een vorm van modelvoorspellende regeling. Modelvoorspellende regeling heeft als voordeel dat specifieke kennis die in het model aanwezig is direct gebruikt kan worden, terwijl deze kennis bij andere regelingen niet, of slechts ten dele, gebruikt wordt. Bovendien kunnen alle variabelen in het kas-met-gewas model gebruikt worden in de kostenfunctie die de regeldoelen kwantitatief en expliciet beschrijft. De regeldoelen zijn gedefinieerd als:

1. Minimaliseer gasverbruik.
2. Maximaliseer biomassa-toename van het gewas.
3. Zorg voor goede gewasontwikkeling en ziektevrije omstandigheden.
4. Zorg ervoor dat het gebruik van de aquifer voldoet aan de regels die door de overheid zijn opgesteld.

De doelen 1 en 2 zijn direct gerelateerd aan modelvariabelen. Doel 3 is vertaald naar grenzen voor de temperatuur, de relatieve luchtvochtigheid en de temperatuurintegraal. Doel 4 vereiste wat extra aandacht, aangezien de overheidsregels gebaseerd zijn op jaarrond-eisen, en de regelhorizon die gebruikt wordt in de optimale regeling slechts een dag is. Berekeningen werden vooraf uitgevoerd om het verloop van de energie-inhoud van de aquifer gedurende het jaar te bepalen. Dit verloop werd vervolgens gebruikt om grenzen te definiëren die gebruikt konden worden in de kostenfunctie. Alle doelen zijn gecombineerd in de kostenfunctie.

De optimale regeling bleek vaak te eindigen in lokale minima als de feitelijke sturingen geoptimaliseerd werden. Van de 9 sturingen worden er 7 geoptimaliseerd. Door het slim combineren van deze feitelijke sturingen kan dit aantal verminderd worden tot 2 sturingen die geoptimaliseerd worden door de optimale regeling, wat tevens de rekentijd verkort. Deze combinatie van de sturingen is bedoeld om sturingen die niet tegelijkertijd behoren plaats te vinden (bijv. verwarmen en koelen) uit te sluiten. Deze twee sturingen bepalen de feitelijke sturingen.

De geconjugeerde gradiënt-zoekmethode is gebruikt om te zoeken naar de optimale sturingen. Deze lokale minimalisatiemethode is robuust en redelijk efficiënt met betrekking tot rekentijd. Deze methode heeft een goede initiële aanname voor de sturingen nodig om te voorkomen dat het resultaat naar een lokaal minimum loopt. Een goede initiële aanname voor de sturingen wordt gevonden met de zogenaamde raster-zoekmethode, een grove globale minimalisatiemethode die specifiek voor deze optimale regeling werd ontworpen gedurende dit onderzoek. De raster-zoekmethode gebruikt een klein aantal discrete constante trajecten voor de sturingen. Toestandsafhankelijke grenzen zijn gebruikt voor de sturingen om gedrag te voorkomen waarvan op voorhand bekend is dat dit niet optimaal is (bijvoorbeeld, koelen als de temperatuur beneden de minimumtemperatuur is). Deze toestandsafhankelijke grenzen voor de sturingen zijn gebaseerd op kennis van het kas-met-gewas systeem. De discrete begrensde sturingen die leiden tot de laagste kostenfunctie-waarde zijn het resultaat van de raster-optimalisatie.

## Open lus berekeningen, winter en zomer dag

Open lus berekeningen met optimale regeling zijn uitgevoerd voor een dag in de winter en in de zomer, zowel met als zonder temperatuurintegratie. Deze berekeningen werden gebruikt

- om de gewichtsfactoren voor de kostenfunctie met en zonder temperatuurintegratie te bepalen;
- om te valideren of de resultaten van de raster-zoekmethode inderdaad een goede eerste aanname waren;
- om de invloed van temperatuurintegratie op de resultaten te bekijken.

De gewichtsfactoren zijn zodanig gewogen dat bijvoorbeeld de kosten van gasverbruik om de kas te verwarmen niet zwaarder gewogen werden dan de temperatuurstraf, zodat de verwarming gebruikt kan worden om de temperatuur te verhogen. Enkele dagen in verschillende seizoenen werden gebruikt voor het bepalen van de weegfactoren om ervoor te zorgen dat de gewichtsfactoren

toepasbaar zijn in verschillende seizoenen. De balans tussen de gewichtsfactoren in de kostenfunctie hangt af van wat de tuinder belangrijk vindt. De optimale regeling die in dit proefschrift wordt beschreven kan in de toekomst worden gebruikt om een presentatieprogramma te ontwikkelen voor de tuinder waarmee de verwachte resultaten van de gekozen regelaarinstellingen worden gevisualiseerd.

Er werd vastgesteld dat de resultaten van de raster-zoekmethode reeds vrij goed waren. Met de gradiënt-zoekmethode konden de resultaten van de raster-zoekmethode nog verder verbeterd worden. Vooral de relatieve luchtvochtigheid werd verbeterd door de gradiënt-zoekmethode.

Uit de vergelijking van de versies zonder en met temperatuurintegratie bleek dat laatstgenoemde een lagere biomassa-toename opleverde. Dit wijst erop dat de temperatuurintegratie een negatief effect kan hebben op de biomassa-toename. Nochtans moet ook rekening gehouden worden met de gewasontwikkeling en -kwaliteit, die bepaald worden door de straffen en eindkosten voor temperatuur, relatieve luchtvochtigheid en temperatuurintegraal. De optimale regeling weegt al deze aspecten tegen elkaar af. Zodoende zou de versie zonder temperatuurintegratie een lage gewaskwaliteit kunnen opleveren die niet geschikt is voor de verkoop.

### **Gesloten lus RHOC berekeningen, jaarrond**

Gesloten lus jaarrond-berekeningen zijn uitgevoerd met een wijkende horizon optimale regelaar (RHOC, receding horizon optimal controller) gebruik makend van de raster- en de gradiënt-zoekmethode. De jaarrond-berekening duurde 8 dagen met de gradiënt-zoekmethode en slechts 8 uur met de raster-zoekmethode. Zover we weten is dit de eerste keer dat jaarrond RHOC berekeningen zijn uitgevoerd met een fysisch kasmodel.

### ***Gradiënt-zoekmethode versus raster-zoekmethode***

De raster-zoekmethode is gebruikt om een eerste beeld te krijgen van de resultaten van de optimale regelaar. Er is een vergelijking gemaakt tussen de zonnepark en de niet-zonnepark. Voor de niet-zonnepark is aangenomen dat deze gelijk is aan de zonnepark, maar dan zonder de warmtepomp, warmtewisselaar en ventilatie met warmteterugwinning. Deze eerste resultaten lieten zien dat de aquifer jaarrond gebruikt kon worden, en een grote vermindering van het gasverbruik (van 58%) kon worden behaald.

Vervolgens werd de geconjugeerde gradiënt-zoekmethode gebruikt. Zoals verwacht, resulteerde de gradiënt-methode in lagere kostenfunctie-waarden dan de raster-methode, wat aantoonde dat de resultaten van de raster-methode verder verbeterd konden worden. Wederom, zoals bij de open lus berekeningen, bleek de grootste verbetering haalbaar bij de straf voor de relatieve luchtvochtigheid.

### ***A priori versus a posteriori***

De a priori kosten zijn de kosten die a priori berekend worden door het wijkende horizon optimale regelsysteem. Dit zijn de minimale verwachte kosten gebaseerd op alle aanwezige informatie op het moment dat de regelacties berekend worden. De a posteriori kosten zijn de feitelijk behaalde kosten van het wijkende horizon optimale regel-algoritme. Als de regelacties via een presentatieprogramma gepresenteerd gaan worden aan de tuinder, dan zijn alleen de a priori kosten beschikbaar. Daarom is het relevant om een indicatie te hebben van het verschil tussen de a priori en de a posteriori resultaten.

Het verschil tussen de a priori en de a posteriori resultaten (in de berekeningen in dit proefschrift) is deels het gevolg van de wijkende horizon en deels het gevolg van het verschil tussen het echte en het voorspelde weer (als deze verschillen). Om het effect van de weersvoorspelling te onderzoeken is een eenvoudige weersvoorspelling voor de komende dag ontwikkeld gebaseerd op het 'lazy man' principe, waarbij het weer van de voorgaande dag wordt gebruikt als voorspelling met een correctie gebaseerd op metingen van de echte weersomstandigheden.

Er is een vergelijking gemaakt voor de situatie waarbij de weersvoorspelling gelijk was aan het echte weer. Het verschil tussen de a priori en de a posteriori kosten was relatief groot. Dit verschil ontstaat doordat het meenemen van nieuwe informatie aan het eind van de horizon de wijkende horizon regelaar dwingt om de stuurtrajecten aan te passen ten opzicht van de stuurtrajecten die eerst optimaal geacht werden, voordat deze nieuwe informatie bekend was. Het schijnt dat de eindstraf voor de temperatuurintegraal de hoofdoorzaak is voor de aanpassing van de sturingen. Er wordt een zware straf gebruikt voor deze zachte eindlimiet, die straft op basis van een 6-daags gemiddelde van de temperatuur. Dit wordt gecompenseerd door wijdere grenzen voor de temperatuur zelf, wat de optimalisatie meer ruimte geeft. Door deze zware straf is de gemiddelde temperatuur over 6 dagen zeer dicht bij de referentietemperatuur van 19°C. Uit de resultaten blijkt verder dat het feitelijk onmogelijk is om op elk tijdstip te voldoen aan de temperatuurintegraal-eisen.

Het verschil tussen de a priori kosten voor de situatie waarbij de weersvoorspelling gelijk en ongelijk is aan het echte weer was klein. Dit verschil is het gevolg van de afwijking tussen de werkelijke en de voorspelde weersomstandigheden. Dit geeft aan dat de gevoeligheid van de *verwachte* resultaten voor de weersvoorspelling gering is. Het verschil tussen de a posteriori kosten die ontstaan met de sturingen berekend met echt weer en met de sturingen berekend met de weersvoorspelling was veel groter. Hieruit blijkt dat de invloed van de weersvoorspelling op de *werkelijke* resultaten toch belangrijk is. Hierbij moet opgemerkt worden dat de ‘lazy man’ weersvoorspelling zoals deze is toegepast in dit proefschrift niet erg nauwkeurig is op een tijdschaal van een hele dag.

***Invloed van de zonnepanelen:***

***warmtepomp, warmtewisselaar en aquifer,  
ventilatie met warmteterugwinning,  
CO<sub>2</sub> toevoer onafhankelijk van ketelgebruik***

De invloed van de afzonderlijke zonnepanelen is onderzocht. Hieruit bleek dat het gebruik van de warmtepomp, warmtewisselaar en aquifer een significante afname van het gasverbruik opleverde (van 23%). Het gebruik van ventilatie met warmteterugwinning gaf nog een grotere afname van het gasverbruik (van 26%). CO<sub>2</sub> toevoer onafhankelijk van ketelgebruik leidde tot een hogere biomassa-toename (van 37%) met een kleine afname van het gasverbruik (van 8%) ten koste van veel meer CO<sub>2</sub> verbruik (van 189%).

Indien dezelfde hoeveelheid CO<sub>2</sub> geproduceerd zou moeten worden door het stoken van de ketel, dan zou dit leiden tot een significante toename van het gasverbruik. Het warmteoverschot dat daardoor ontstaat wordt in de huidige kaspraktijk opgeslagen in een korte-termijn warmtebuffer. Onder de omstandigheden die zijn doorgerekend in dit proefschrift voor de conventionele kas is deze opgeslagen warmte nauwelijks nodig is voor het verwarmen of ontvochtigen van de kas, waaruit blijkt dat het gebruik van een korte-termijn warmtebuffer onder deze omstandigheden weinig zinvol is.

De overheid eist dat de aquifer jaarrond ongeveer energie-neutraal draait. Met een regelhorizon van een dag was de implementatie van deze eis niet zo eenvoudig. Een oplossing werd gevonden door het definiëren van een referentiecurve voor de energie-inhoud van de aquifer. Voor deze referentiecurve zijn grenzen gedefinieerd, die vervolgens gebruikt zijn in de kostenfunctie. Uit de jaarrond-berekeningen is gebleken dat de aquifer het hele jaar binnen zijn grenzen bleef.

### ***Relatieve luchtvochtigheid***

Er is gebleken dat de relatieve luchtvochtigheid een sterk effect heeft op het gasverbruik. Gedurende de lente en de zomer wordt de verwarming met name gebruikt om de luchtvochtigheid te verlagen, en niet om te temperatuur te verhogen. Als de vochtgrens verhoogd zou kunnen worden boven de 85%, dan zou dit een directe kostenverlaging opleveren.

In de huidige kaspraktijk wordt de relatieve luchtvochtigheid gebruikt als een maat voor de natheid van bladeren en gewas, aangezien dit gewasziekten en schimmelvorming kan veroorzaken. Relatieve luchtvochtigheid is echter geen goede maat voor natheid. De bladeren kunnen nat zijn bij bijvoorbeeld een relatieve luchtvochtigheid onder 80%, terwijl ze droog kunnen zijn bij een relatieve luchtvochtigheid van 100%. Een nieuwe aanpak is voorgesteld waarbij gebruik gemaakt wordt van de dauwpuntstemperatuur van het gewas. Deze temperatuur is waarschijnlijk een betere indicator voor natheid, aangezien deze een directe maat is voor condensatie. Er is aangetoond dat het gebruik van de dauwpuntstemperatuur minder strikte grenzen oplevert, wat naar verwachting leidt tot een lager gasverbruik. Dit kan eenvoudig geïmplementeerd worden in de wijkende horizon optimale regeling aangezien de gewastemperatuur een toestand is van het model.

### ***Zonnekas versus conventionele kas***

Als de zonnekas wordt vergeleken met de conventionele kas, zonder alle zonnekas-elementen (zoals: warmtepomp, warmtewisselaar, ventilatie met warmteterugwinning, CO<sub>2</sub> toevoer onafhankelijk van ketelgebruik), beide geregeld met de optimale regeling, dan wordt gevonden dat het gasverbruik is verlaagd met 52%, met een 39% hogere biomassa-toename.



# Dankwoord

Eindelijk . . . het proefschrift is af! Het onderzoek naar de regeling van kassen was een beetje stilgevallen na de promoties van Eldert van Henten en Frank Tap. Met het zonnekasproject kwam hier verandering in. Ik had net mijn M.Sc. gehaald, en Gerrit kwam vragen of ik niet het regelgedeelte van dit project op mij wilde nemen om daarop te promoveren. Na diep nagedacht te hebben (ik had net mijn M.Sc. afstudeerverslag af) heb ik hier ja op gezegd.

Ik wist niks van kassen toen ik met het onderzoek begon. De projectbesprekingen met de projectmedewerkers van het voormalige IMAG-DLO<sup>⊗</sup>, en de leerstoelgroepen Natuurkunde, Tuinbouwproductieketens en Meet-, Regel- en Systeemtechniek waren in het begin moeilijk te volgen omdat ik de terminologie van de standaard praktijkregeling met termen als stooktemperatuur, minimum buistemperatuur, ventilatietemperatuur, stralingsafhankelijke lichtcorrecties en droogstoken niet kende.

Met het AIO-groepje (Oliver Körner, Jouke Kampen, An Saye en ik) zijn we vervolgens aparte besprekingen gaan houden, waarin we elkaar goed verder konden helpen. Vooral met Oliver heb ik vervolgens intensief samengewerkt om tot een goed model van de gewasbiofysica te komen, eerst in het Engels (met een beetje Duits), later in het Nederlands.

Nu het proefschrift klaar is, wil ik iedereen bedanken die direct of indirect een bijdrage aan dit werk heeft geleverd. Met name mijn promotor Gerrit van Straten en mijn co-promotor Gerard van Willigenburg hebben een belangrijke rol gespeeld bij de totstandkoming van dit proefschrift dankzij hun commentaar, adviezen en de — vaak pittige — inhoudelijke discussies. Gerrit met de meer perfectionistische insteek, en Gerard voor de grote lijn bleek een prima combinatie te zijn. Verder bedank ik hier Gerard Bot, de leider van het zonne-

---

<sup>⊗</sup> Dit deel van IMAG-DLO hoort tegenwoordig bij de Greenhouse Technology group van Plant Research International.

kasproject, die een onuitputtelijke bron van kasinformatie is, en Hans Stigter, die ook een tijdje mijn dagelijkse begeleider is geweest.

In het zonnekasproject heb ik veel gehad aan de inhoudelijke bijdragen van Hugo Challa, Oliver Körner, Ep Heuvelink, Jan Goudriaan, Bert van 't Ooster, Feije de Zwart, Gert-Jan Swinkels, Cecilia Stanghellini, Jan Kornet en Wim van Meurs. Ook de afstudeerstudenten Elco Oost, Jaap de Bruin en Barry van Dongen en stagiair Hendrik Wouters bij PRIVA hebben een waardevolle bijdrage aan dit onderzoek geleverd.

Verder wil ik natuurlijk al mijn collega's van de leerstoelgroep Meet-, Regel- en Systeemtechniek (MRS) bedanken, die — ieder vanuit hun eigen vakgebied — een bijdrage hebben geleverd aan het onderzoek, en samen zorgen voor een fijne werksfeer. Kees, Ton, Kees de G., Karel en Wilko: bedankt! Marja zorgt met haar lach (en heel af en toe wat gemopper op vervelende computer-applicaties) voor de gezelligheid en de persoonlijke noot. En natuurlijk nog enkele ex-collega's die niet vergeten mogen worden: Gert van Dijk (Hydrionline), Jan Bontsema en Geerten Lenters.

Ook wil ik de AIO's (Tijmen, Martijn, Mohamad, Timo, Hady, Zita, Bas en Dirk) en oud-AIO's (Stefan, Irineo, Ronald, Ilse) bedanken voor de discussies tijdens de koffie- en lunchpauzes over onderzoek en allerlei andere zaken. Met name mijn kamergenoten Bas (toen nog bezig met een afstudeervak) en Tijmen (met zijn afstudeerders en stagairs) wil ik bedanken voor de gezellige tijd en de tips en trucs.

Verder wil ik de meiden van JazzDance Wageningen bedanken, de dansgroep waar ik inmiddels al 11 jaar met veel plezier dans. Verder speciale dank aan de geweldige meiden van de dansproductiegroep e-motion (Jantiene, Gonne, Lisa, Maaike, Renske, Linda, Anne, Petra), de ex-emotions (Emilie, Irene, Tamara, Mignon) en de choreograaf en motor achter de groep: Carsten Sasse. Met deze semi-professionele dansgroep heb ik inmiddels door heel Nederland gedanst. Ik ben trots dat ik daar deel van uit mag maken.

Als laatste bedank ik het thuisfront. Pap en mam, jullie hebben mij altijd met plezier zien leren: dit was echt het laatste studieproject! Mijn broer Dennis, die met mij de paragraaf over temperatuurintegratie (§2.4) op oudejaarsavond 2005 heeft herschreven. Pa en ma van Geesink, Ewald en Monique, Angelique en Marco, jullie waren altijd geïnteresseerd in mijn vorderingen. En natuurlijk Frank, voor je gezelschap en mentale steun tijdens de nachtelijke programmeersessies, de cappuccino, de schouderklopjes en het aanhoren van mijn verhalen: zonder jouw steun was dit proefschrift er nooit gekomen.

*Rachel*

# Curriculum Vitae

## Personal details

<i>Full name</i>	Rachel Joanna Catharina van Ooteghem
<i>Date of birth</i>	13 August 1969
<i>Place of birth</i>	Maastricht, The Netherlands
<i>Citizenship</i>	Dutch
<i>Gender</i>	Female

## Education

<i>1981–1985</i>	MAVO, Mater Misericordiæ in Cadier en Keer
<i>1985–1987</i>	HAVO, Sint-Maartenscollege in Maastricht
<i>1987–1992</i>	HTO Heerlen, Technische Natuurkunde, differentiatie Besturingstechnologie
<i>1994–1995</i>	Hogeschool van Arnhem en Nijmegen / University of Hertfordshire (United Kingdom), Post-hoger beroepsonderwijs, Meet-, Regel- en besturingstechniek
<i>1996–1998</i>	University of Hertfordshire (United Kingdom), Master of Science, Control Systems Engineering M.Sc. thesis: <i>Flexible control design for canned meat sterilization</i>
<i>1999–2007</i>	Wageningen University, Ph.D. student Ph.D. thesis: <i>Optimal control design for a solar greenhouse</i>

## Working experience

<i>1993–1999</i>	Practical teacher, Systems and Control group, Wageningen University
<i>1999–2006</i>	Ph.D. student, Solar Greenhouse Project, Systems and Control group, Wageningen University

## Computer skills

<i>Operating systems</i>	Windows, DOS
<i>Programming languages</i>	Matlab, Fortran 77, HTML, Pascal, Turbo Pascal, BASIC, TUTsim, PSI/c
<i>Applications</i>	L <sup>A</sup> T <sub>E</sub> X, Word, Excel, Visio

## Languages

<i>Dutch</i>	native
<i>English</i>	good
<i>German</i>	good

## Hobbies

<i>Jazzdance</i>	Danceproduction-group e-motion, JazzDance Wageningen
<i>Scuba diving</i>	Advanced diver

## List of publications

- R.J.C. van Ooteghem (2000). Flexible control design for canned meat sterilization. In: *19<sup>th</sup> Benelux Meeting on Systems and Control*, p. 70, Mierlo, The Netherlands. March 1–3.
- O. Körner, H. Challa and R.J.C. van Ooteghem (2001a). Modelling temperature effects on crop photosynthesis at high radiation in a solar greenhouse. In: *Joint meeting on modeling for the 21<sup>st</sup> century: Agronomic and greenhouse crop models; ISHS symposium*.
- O. Körner, H. Challa and R.J.C. van Ooteghem (2001b). Modelling temperature effects on crop photosynthesis at high radiation in a solar greenhouse. In: *Workshop Modelling for the 21st century: Agronomic and greenhouse crop models; Joined meeting of International Society of Horticultural Science (ISHS) and Biological Systems Simulation Group (BSSG)*, Beltsville, Maryland, USA. March 25–29.
- O. Körner, H. Challa and R.J.C. van Ooteghem (2002). Modelling temperature effects on crop photosynthesis at high radiation in a solar greenhouse. *Acta Horticulturae*, 593, pp. 137–144.
- R.J.C. van Ooteghem (2002). New heating model. Internal report, Wageningen University, Wageningen, The Netherlands.

- O. Körner, H. Challa and R.J.C. van Ooteghem (2003). Chapter 2.1: Modelling temperature effects on crop photosynthesis. In: *Crop based climate regimes for energy saving in greenhouse cultivation*, pp. 29–36, Ph.D. thesis, Wageningen University, Wageningen, The Netherlands.
- O. Körner and R.J.C. van Ooteghem (2003). Chapter 2.4: Simulating crop gross photosynthesis at high temperatures. In: *Crop based climate regimes for energy saving in greenhouse cultivation*, pp. 75–90, Ph.D. thesis, Wageningen University, Wageningen, The Netherlands.
- R.J.C. van Ooteghem (2003a). EET-project De Zonnekas: gewasproductie met duurzame in plaats van fossiele energie, deelproject 3a, WU-deel. Internal report, Wageningen University, Wageningen, The Netherlands. (in Dutch).
- R.J.C. van Ooteghem (2003b). The solar greenhouse model; extension of the greenhouse with crop model. Internal report, Wageningen University, Wageningen, The Netherlands.
- R.J.C. van Ooteghem, J.D. Stigter, L.G. van Willigenburg and G. van Straten (2003a). Optimal control of a solar greenhouse. In: *22<sup>nd</sup> Benelux Meeting on Systems and Control*, p. 41, Lommel, Belgium. Editors: J. Swevers and C. Lauwerys, March 19–21.
- R.J.C. van Ooteghem, J.D. Stigter, L.G. van Willigenburg and G. van Straten (2003b). Optimal control of a solar greenhouse. In: *Proceedings of the European Control Conference (ECC) 2003*, University of Cambridge, Cambridge, United Kingdom. September 1–4.
- T.H. Gieling, F.J.M. Corver, H.J.J. Janssen, G. van Straten, R.J.C. van Ooteghem and G.J. van Dijk (2004). Hydrion-line, towards a closed system for water and nutrients: feedback control of water and nutrients in the drain. In: *GreenSys2004, International Symposium on Sustainable greenhouse systems*, Catholic University Leuven, Leuven, Belgium. Editors: G. van Straten, G.P.A. Bot, W.T.M. van Meurs and L.M.F. Marcelis, September 12–16.
- R.J.C. van Ooteghem, J.D. Stigter, L.G. van Willigenburg and G. van Straten (2004a). Receding horizon optimal control of a solar greenhouse. In: *23<sup>rd</sup> Benelux Meeting on Systems and Control*, p. 85, Helvoirt, The Netherlands. March 17–19.
- R.J.C. van Ooteghem, J.D. Stigter, L.G. van Willigenburg and G. van Straten (2004b). Receding horizon optimal control of a solar greenhouse. In: *GreenSys2004, International Symposium on Sustainable greenhouse systems*, Catholic University Leuven, Leuven, Belgium. Editors: G. van Straten, G.P.A. Bot, W.T.M. van Meurs and L.M.F. Marcelis, September 12–16.

- T.H. Gieling, F.J.M. Corver, H.J.J. Janssen, G. van Straten, R.J.C. van Ooteghem and G.J. van Dijk (2005a). Hydrion-line, towards a closed system for water and nutrients: feedback control of water and nutrients in the drain. *Acta Horticulturae (ISHS)*, 691, pp. 259–266.
- T.H. Gieling, F.J.M. Corver, H.J.J. Janssen, G. van Straten, R.J.C. van Ooteghem and G.J. van Dijk (2005b). Il controllo delle soluzioni di drenaggio nelle colture a ciclo chiuso in serra (Closed systems for water and nutrients in greenhouses: feedback control). In: *Workshop: I sistemi di coltivazione a ciclo chiuso per le colture ortofloricole*, p. 6, Università di Pisa, Pisa, Italy. October 21 (in Italian).
- G. van Straten, G.J. van Dijk, R.J.C. van Ooteghem, T.H. Gieling, H.J.J. Janssen and W.F. Mulckhuijs (2005). Identification for ion-based fertigation control in soilless greenhouse cultivation. In: *Preprints of the 16<sup>th</sup> IFAC World Congress*, Prague, Czech Republic. July 3–8.
- R.J.C. van Ooteghem, L.G. van Willigenburg and G. van Straten (2005a). Receding horizon optimal control of a solar greenhouse. *Acta Horticulturae (ISHS)*, 691, pp. 797–806.
- R.J.C. van Ooteghem, L.G. van Willigenburg and G. van Straten (2005b). Receding horizon optimal control of a solar greenhouse. In: *24<sup>th</sup> Benelux Meeting on Systems and Control*, p. 91, Houffalize, Belgium. March 22–24.
- R.J.C. van Ooteghem, L.G. van Willigenburg and G. van Straten (2006). Receding horizon optimal control of a solar greenhouse. In: *25<sup>th</sup> Benelux Meeting on Systems and Control*, p. 90, Heeze, The Netherlands. Editors: B. de Jager and G. Meinsma, March 13–15.
- O. Körner, Q. Niu and R.J.C. van Ooteghem (2007). Simulations of high temperature and CO<sub>2</sub> effects on greenhouse crop photosynthesis. In preparation.
- R.J.C. van Ooteghem (2007). *Optimal control design for a solar greenhouse*. Ph.D. thesis, Wageningen University, Wageningen, The Netherlands. 304 p. (this thesis).

# References

- B. Acock, D.A. Charles-Edwards, D.J. Fitter, D.W. Hand, L.J. Ludwig, J.W. Wilson, and A.C. Withers (1978). The contribution of leaves from different levels within a tomato crop to canopy net photosynthesis: an experimental examination of two canopy models. *Journal of experimental botany*, 29, pp. 815–827.
- R. Baldick, A. Kahng, A. Kennings, and I. Markov (1999). Function smoothing with applications to VLSI layout. In: *ASP-DAC*, pp. 225–228, IEEE Computer Society, Los Alamitos, CA, USA. Asia and South Pacific Design Automation Conference 1999 (ASP-DAC 99).
- K. Bernaerts and J.F. van Impe (2004). Data-driven approaches to the modelling of bioprocesses. *Transactions of the institute of measurement and control*, 26(5), pp. 349–372.
- G.P.A. Bot (1983). *Greenhouse climate: from physical processes to a dynamic model*. Ph.D. thesis, Wageningen Agricultural University, Wageningen, The Netherlands. 240 p.
- G.P.A. Bot (2001). Developments in indoor sustainable plant production with emphasis on energy saving. *Computers and Electronics in Agriculture*, 30, pp. 151–165.
- J.J.G. Breuer, H.F. de Zwart, and G.P.A. Bot (1999). Aspecten warmtepompen. IMAG-DLO, nota 99–130, Wageningen, The Netherlands. (in Dutch).
- J.J.G. Breuer and N.J. van de Braak (1989). Reference year for Dutch greenhouses. *Acta Horticulturae*, 248, pp. 101–108.
- S.C. de Graaf (2006). *Low nitrate lettuce cultivations in greenhouses: optimal control in the presence of measurable disturbances*. Ph.D. thesis, Wageningen Agricultural University, Wageningen, The Netherlands. 138 p.
- T. de Jong (1990). *Natural ventilation of large multi-span greenhouses*. Ph.D. thesis, Wageningen Agricultural University, Wageningen, The Netherlands.
- A.N.M. de Koning (1988). More efficient use of base load heating with a temperature integrating control programme; effect on development, growth and production of tomato. *Acta Horticulturae*, 229, pp. 233–237.

- H.F. de Zwart (1996). *Analyzing energy-saving options in greenhouse cultivation using a simulation model*. Ph.D. thesis, Wageningen Agricultural University, Wageningen, The Netherlands. 236 p.
- A. Defant and F. Defant (1958). *Physikalische Dynamik der Atmosphäre*. Akademische Verlagsgesellschaft, Frankfurt, Germany. (in German).
- T.G. Doeswijk and K.J. Keesman (2005). Adaptive weather forecasting using local meteorological information. *Biosystems Engineering*, 91(4), pp. 421–431.
- A. Elings, F.L.K. Kempkes, R.C. Kaarsemaker, M.N.A. Ruijs, N.J. van de Braak, and T.A. Dueck (2005). The energy balance and energy-saving measures in greenhouse tomato cultivation. *Acta Horticulturae (ISHS)*, 691, pp. 67–74.
- J.R. Evans and G.D. Farquhar (1991). *Modeling crop photosynthesis: from biochemistry to canopy*, chapter 1: Modelling canopy photosynthesis from the biochemistry of the C<sub>3</sub> chloroplast, pp. 1–15. Madison, Wisconsin, USA. Editors: K.J. Boote and R.S. Loomis, CSSA special publication no. 19.
- G.D. Farquhar (1988). Models relating subcellular effects of temperature to whole plant responses. In: *Plants and temperature*, vol. 42, pp. 395–409. Society for experimental biology; Editors: S.P. Long and F.I. Woodward.
- G.D. Farquhar and S. von Caemmerer (1982). Modelling of photosynthetic response to environmental conditions. In: *Encyclopedia of plant physiology, New series; Physiological Plant Ecology II*, vol. 12B, pp. 549–587, Springer-Verlag, Heidelberg, Germany. Editors: O.L. Lange, P.S. Nobel, and H. Ziegler.
- G.D. Farquhar, S. von Caemmerer, and J.A. Berry (1980). A biochemical model of photosynthetic CO<sub>2</sub> assimilation in leaves of C<sub>3</sub> species. *Planta*, 149, pp. 78–90.
- W. Ferrel (1885). Annual report of the chief signal officer of the army to the secretary of war for the year 1886. Appendix 24, Washington DC.
- T.H. Gieling, F.J.M. Corver, H.J.J. Janssen, G. van Straten, R.J.C. van Ooteghem, and G.J. van Dijk (2004). Hydrion-line, towards a closed system for water and nutrients: feedback control of water and nutrients in the drain. In: *GreenSys2004, International Symposium on Sustainable greenhouse systems*, Catholic University Leuven, Leuven, Belgium. Editors: G. van Straten, G.P.A. Bot, W.T.M. van Meurs, and L.M.F. Marcelis, September 12–16.
- T.H. Gieling, F.J.M. Corver, H.J.J. Janssen, G. van Straten, R.J.C. van Ooteghem, and G.J. van Dijk (2005a). Hydrion-line, towards a closed system for water and nutrients: feedback control of water and nutrients in the drain. *Acta Horticulturae (ISHS)*, 691, pp. 259–266.

- T.H. Gieling, F.J.M. Corver, H.J.J. Janssen, G. van Straten, R.J.C. van Ooteghem, and G.J. van Dijk (2005b). Il controllo delle soluzioni di drenaggio nelle colture a ciclo chiuso in serra (Closed systems for water and nutrients in greenhouses: feedback control). In: *Workshop: I sistemi di coltivazione a ciclo chiuso per le colture ortofloricole*, p. 6, Università di Pisa, Pisa, Italy. October 21 (in Italian).
- J. Goudriaan (1987). *Simulatie van gewasgroei*. Wageningen Agricultural University, the Netherlands. (in Dutch).
- J. Goudriaan and H.H. van Laar (1994). *Modelling potential crop growth process*, vol. 2. Kluwer academic publishers, Dordrecht, the Netherlands. 238 p.
- H. Gijzen (1994). Ontwikkeling van een simulatiemodel voor transpiratie en wateropname en van een integraal gewasmodel. AB-DLO, rapport 18, Wageningen, The Netherlands. (in Dutch).
- H. Gijzen, E. Heuvelink, H. Challa, E. Dayan, L.F.M. Marcelis, S. Cohen, and M. Fuchs (1998). Hortisim: a model for greenhouse crops and greenhouse climate. *Acta Horticulturae*, 456, pp. 441–450.
- L. Heesen (1997). *Definitie, gevoeligheidsanalyse en evaluatie van een dynamisch model van het kas-gewasproductieproces*. M.Sc. thesis, Wageningen Agricultural University, Wageningen, The Netherlands. (in Dutch).
- E. Heuvelink (1996). *Tomato growth and yield: quantitative analysis and synthesis*. Ph.D. thesis, Wageningen Agricultural University, Wageningen, The Netherlands. 326 p.
- I. Ioslovich and I. Seginer (1998). Approximate seasonal optimization of the greenhouse environment for a mulit-state-variable tomato model. *Transactions of the ASAE*, 41(4), pp. 1139–1149.
- O. Körner (2003). *Crop based climate regimes for energy saving in greenhouse cultivation*. Ph.D. thesis, Wageningen University, Wageningen, The Netherlands.
- O. Körner and H. Challa (2003). Design for an improved temperature integration concept in greenhouse cultivation. *Computers and Electronics in Agriculture*, 39(1), pp. 39–59.
- O. Körner, H. Challa, and R.J.C. van Ooteghem (2001a). Modelling temperature effects on crop photosynthesis at high radiation in a solar greenhouse. In: *Joint meeting on modeling for the 21<sup>st</sup> century: Agronomic and greenhouse crop models; ISHS symposium*.
- O. Körner, H. Challa, and R.J.C. van Ooteghem (2001b). Modelling temperature effects on crop photosynthesis at high radiation in a solar greenhouse. In: *Workshop Modelling for the 21st century: Agronomic and greenhouse crop models; Joined meeting of International Society of Horticultural Sci-*

- ence(*ISHS*) and *Biological Systems Simulation Group (BSSG)*, Beltsville, Maryland, USA. March 25–29.
- O. Körner, H. Challa, and R.J.C. van Ooteghem (2002). Modelling temperature effects on crop photosynthesis at high radiation in a solar greenhouse. *Acta Horticulturae*, 593, pp. 137–144.
- O. Körner, H. Challa, and R.J.C. van Ooteghem (2003). Chapter 2.1: Modelling temperature effects on crop photosynthesis. In: *Crop based climate regimes for energy saving in greenhouse cultivation*, pp. 29–36, Ph.D. thesis, Wageningen University, Wageningen, The Netherlands.
- O. Körner, Q. Niu, and E. Heuvelink (2007a). Quantification of temperature and CO<sub>2</sub> effects on crop photosynthesis. In preparation.
- O. Körner, Q. Niu, and R.J.C. van Ooteghem (2007b). Simulations of high temperature and CO<sub>2</sub> effects on greenhouse crop photosynthesis. In preparation.
- O. Körner and R.J.C. van Ooteghem (2003). Chapter 2.4: Simulating crop gross photosynthesis at high temperatures. In: *Crop based climate regimes for energy saving in greenhouse cultivation*, pp. 75–90, Ph.D. thesis, Wageningen University, Wageningen, The Netherlands.
- L. Lukasse, A.-J. van der Voort, and J. de Kramer-Cuppen (2006). Optimal climate control to anticipate future weather and energy tariffs. In: *4<sup>th</sup> IFAC/CIGR workshop, Control applications in post-harvest and processing technology (CAPPT)*, Potsdam, Germany. March 26–29.
- J.L. Monteith and M.H. Unsworth (1990). *Principles of environmental physics*. Edward Arnold, London, United Kingdom, 2<sup>nd</sup> edition. 291 p.
- A. Munack (1991). *Biotechnology, a multi-volume comprehensive treatise, Measuring, modelling and control*, vol. 4, chapter 8: Optimization of sampling, pp. 252–264. VCH, Weinheim, Germany. Editors: H.-J. Rehm, G. Reed, A. Pühler, and P. Stadler.
- E.M. Nederhoff (1994). *Effects of CO<sub>2</sub> concentration on photosynthesis, transpiration and production of greenhouse fruit vegetable crops*. Ph.D. thesis, Wageningen Agricultural University, Wageningen, The Netherlands. 213 p.
- B. Pagurek and C.M. Woodside (1968). The conjugate gradient method for optimal control problems with bounded control variables. *Automatica*, 4, pp. 337–349.
- W.H. Press, B.P. Flannery, S.A. Teukolsky, and W.T. Vetterling (1986). *Numerical recipes*. Cambridge University Press, Cambridge, United Kingdom, 2<sup>nd</sup> edition. 291 p.
- I. Seginer, C. Gary, and M. Tchamitchian (1994). Optimal temperature regimes for a greenhouse crop with a carbohydrate pool: a modelling study. *Scientia Horticulturae*, 60, pp. 55–80.

- G. Shina and I. Seginer (1989). Optimal management of tomato growth in greenhouses. *Acta Horticulturae*, 248, pp. 307–313.
- N. Sigrimis, A. Anastasiou, and N. Rerras (2000). Energy saving in greenhouses using temperature integration: a simulation survey. *Computers and Electronics in Agriculture*, 26(1), pp. 321–341.
- Smithsonian Meteorological Tables (1966). Washington D.C., 6<sup>th</sup> (revised) edition. Editor: R.J. List.
- E.M. Sparrow and R.D. Cess (1970). *Radiation heat transfer*. Brooks/Cole Publishers, Belmont, U.S.A., rev. ed. edition. 340 p.
- C.J.T. Spitters (1986). Separating the diffuse and direct component of global radiation and its implications for modeling canopy photosynthesis. Part II. Calculation of canopy photosynthesis. *Agricultural and forest meteorology*, 38, pp. 231–242.
- C. Stanghellini (1987). *Transpiration of greenhouse crops — an aid to climate management*. Ph.D. thesis, Wageningen Agricultural University, Wageningen, The Netherlands. 150 p.
- J.A. Stoffers (1989). Tuinbouwtechnische aspecten van de druppelprofieling bij kasverwarmingsbuis. Intern rapport, IMAG-DLO, Wageningen, The Netherlands. (in Dutch), 24 p.
- R.F. Tap (2000). *Economics-based optimal control of greenhouse tomato crop production*. Ph.D. thesis, Wageningen Agricultural University, Wageningen, The Netherlands.
- R.F. Tap, L.G. van Willigenburg, and G. van Straten (1996). Receding horizon optimal control of greenhouse climate using the lazy man weather prediction. In: *Proceedings of the 13th IFAC World Congress, San Francisco, USA*. June 30–July 5, paper 4a-013.
- A.J. Udink ten Cate (1983). *Modeling and (adaptive) control of greenhouse climates*. Ph.D. thesis, Wageningen Agricultural University, Wageningen, The Netherlands.
- J.A.M. van den Bosch (1998). Opportunities and bottlenecks for model applications in practice. *Acta Horticulturae*, 456, pp. 505–508.
- A. van der Knijff, J. Benninga, C. Reijnders, and J. Nienhuis (2006). Energie in de glastuinbouw van nederland; ontwikkelingen in de sector en op de bedrijven tot en met 2004. Rapport 3.06.02, LEI, Den Haag, The Netherlands. (in Dutch), 77 p.
- B.N.J. van Dongen (2004). *Zonnekas tussen theorie en praktijk*. B.Sc. thesis, (MRS034), Wageningen University, Wageningen, The Netherlands. 21 p.
- E.J. van Henten (1994). *Greenhouse climate management: an optimal control approach*. Ph.D. thesis, Wageningen Agricultural University, Wageningen, The Netherlands. 329 p.

- E.J. van Henten and J. Bontsema (1991). Optimal control of greenhouse climate. In: *Mathematical and Control Applications in Agriculture and Horticulture*, vol. 1, pp. 27–32. IFAC Workshop Series.
- A.J.M. van Kimmenade (1986). *Warmteleer voor technici*. Educaboek B.V., Culemborg, the Netherlands. 576 p.
- R.J.C. van Ooteghem (2000). Flexible control design for canned meat sterilization. In: *19<sup>th</sup> Benelux Meeting on Systems and Control*, p. 70, Mierlo, The Netherlands. March 1–3.
- R.J.C. van Ooteghem (2002). New heating model. Internal report, Wageningen University, Wageningen, The Netherlands.
- R.J.C. van Ooteghem (2003a). EET-project De Zonnekas: gewasproductie met duurzame in plaats van fossiele energie, deelproject 3a, WU-deel. Internal report, Wageningen University, Wageningen, The Netherlands. (in Dutch).
- R.J.C. van Ooteghem (2003b). The solar greenhouse model; extension of the greenhouse with crop model. Internal report, Wageningen University, Wageningen, The Netherlands.
- R.J.C. van Ooteghem (2007). *Optimal control design for a solar greenhouse*. Ph.D. thesis, Wageningen University, Wageningen, The Netherlands. 304 p. (this thesis).
- R.J.C. van Ooteghem, J.D. Stigter, L.G. van Willigenburg, and G. van Straten (2003a). Optimal control of a solar greenhouse. In: *Proceedings of the European Control Conference (ECC) 2003*, University of Cambridge, Cambridge, United Kingdom. September 1–4.
- R.J.C. van Ooteghem, J.D. Stigter, L.G. van Willigenburg, and G. van Straten (2003b). Optimal control of a solar greenhouse. In: *22<sup>nd</sup> Benelux Meeting on Systems and Control*, p. 41, Lommel, Belgium. Editors: J. Swevers and C. Lauwerys, March 19–21.
- R.J.C. van Ooteghem, J.D. Stigter, L.G. van Willigenburg, and G. van Straten (2004a). Receding horizon optimal control of a solar greenhouse. In: *GreenSys2004, International Symposium on Sustainable greenhouse systems*, Catholic University Leuven, Leuven, Belgium. Editors: G. van Straten, G.P.A. Bot, W.T.M. van Meurs, and L.M.F. Marcelis, September 12–16.
- R.J.C. van Ooteghem, J.D. Stigter, L.G. van Willigenburg, and G. van Straten (2004b). Receding horizon optimal control of a solar greenhouse. In: *23<sup>rd</sup> Benelux Meeting on Systems and Control*, p. 85, Helvoirt, The Netherlands. March 17–19.
- R.J.C. van Ooteghem, L.G. van Willigenburg, and G. van Straten (2005a). Receding horizon optimal control of a solar greenhouse. *Acta Horticulturae (ISHS)*, 691, pp. 797–806.

- 
- R.J.C. van Ooteghem, L.G. van Willigenburg, and G. van Straten (2005b). Receding horizon optimal control of a solar greenhouse. In: *24<sup>rd</sup> Benelux Meeting on Systems and Control*, p. 91, Houffalize, Belgium. March 22–24.
- R.J.C. van Ooteghem, L.G. van Willigenburg, and G. van Straten (2006). Receding horizon optimal control of a solar greenhouse. In: *25<sup>th</sup> Benelux Meeting on Systems and Control*, p. 90, Heeze, The Netherlands. Editors: B. de Jager and G. Meinsma, March 13–15.
- G. van Straten, G.J. van Dijk, R.J.C. van Ooteghem, T.H. Gieling, H.J.J. Janssen, and W.F. Mulckhuijse (2005). Identification for ion-based fertigation control in soilless greenhouse cultivation. In: *Preprints of the 16<sup>th</sup> IFAC World Congress*, Prague, Czech Republic. July 3–8.
- A. van Strien (1988). *Klimaat in een enkel- en dubbeldekskas — metingen en simulaties*. M.Sc. thesis, Wageningen Agricultural University, Wageningen, The Netherlands. (in Dutch), 2 dl.
- L.G. van Willigenburg, E.J. van Henten, and W.T.M. van Meurs (2000). Three time-scale receding horizon optimal control in a greenhouse with a heat storage tank. In: *Proceedings of the Agricontrol 2000 Conference*, Wageningen, The Netherlands.
- E. Walter and L. Pronzato (1997). *Identification of parametric models*. Springer, Masson, Great Britain. 159 p.



# Appendix A

## List of figures and tables

### List of figures

1.1	Gas use, production and energy efficiency index . . . . .	2
1.2	Smoothing function, original and smoothed functions . . . . .	10
1.3	Examples smoothing function, original and smoothed function . . .	12
2.1	Stomatal resistance parameters $f_I$ , $f_{T_c}$ , $f_{CO_2}$ and $f_{H_2O}$ . . . . .	17
2.2	Photosynthesis parameters $J_{\max}$ and $\Gamma$ as a function of crop temperature $T_c$ . . . . .	27
2.3	Leaf stomatal resistance to $CO_2$ $R_{s,CO_2}$ as a function of $T_c$ , $CO_{2a}$ , $I_o$ and $RH_a$ . . . . .	28
2.4	Leaf boundary layer resistance to $CO_2$ $R_{b,CO_2}$ as a function of $v_a$ , $ T_c - T_a $ and $l_f$ . . . . .	29
2.5	Photosynthesis rate $P_g$ as a function of $I_o$ , $CO_{2a}$ and $T_c$ with variable resistances . . . . .	32
2.6	Photosynthesis rate $P_g$ as a function of $I_o$ , $CO_{2a}$ and $T_c$ with fixed resistances . . . . .	33
2.7	Dark respiration rate $r_D$ as a function of $T_c$ . . . . .	34
2.8	Temperature trajectory $T_a$ for temperature integral . . . . .	36
2.9	Temperature deviation $T_a - T_{aref}$ , temperature integral $S_T$ and predicted average temperature deviation $\Delta T_{a,TI}$ at time $t$ . . . . .	37
3.1	Greenhouse configuration . . . . .	58
3.2	States $x$ , external inputs $v$ and control inputs $u$ in the solar greenhouse . . . . .	64

3.3	States $x$ , external input $v$ and control input $u$ in the carbon dioxide model . . . . .	67
3.4	States $x$ and external input $v$ in the water vapour model . . . . .	70
3.5	States $x$ and external inputs $v$ in the thermal model . . . . .	75
3.6	Heating with boiler, condenser and heat pump . . . . .	102
3.7	Cooling with heat exchanger . . . . .	103
3.8	Configuration and energy transport heat pump . . . . .	107
3.9	Configuration and energy transport heat exchanger . . . . .	111
3.10	Estimation: control inputs $u$ , data set 040323 . . . . .	122
3.11	Estimation: external inputs $v$ , data set 040323 . . . . .	122
3.12	Estimation: measured and simulated states $x$ , data set 040323 . . . . .	123
3.13	Validation: measured and simulated states $x$ , data set 040617 . . . . .	124
3.14	Validation: measured and simulated states $x$ , data set 040910 . . . . .	125
3.15	Soil temperature $T_s$ original and simplified model, subsoil temperature $T_{s2}$ and estimation error . . . . .	136
3.16	Roof temperatures $T_{ri}$ and $T_{ro}$ original and simplified model, energy absorbed by indoor side of the roof $\Sigma Q_{i,ri}$ and temperature deviation . . . . .	140
4.1	Example receding horizon optimal control . . . . .	155
4.2	Energy extraction and supply for the aquifer with $SEL_{year}$ . . . . .	163
4.3	Energy extraction and supply for the aquifer with $SEL_{year}$ , computed and estimated curves . . . . .	164
4.4	Aquifer energy content with $SEL_{year}$ , computed and estimated curve and bounds . . . . .	165
4.5	Relations control inputs . . . . .	166
4.6	Combined heating valve position $vp_h$ . . . . .	168
4.7	Combined window aperture $Ap_{csd}$ . . . . .	169
4.8	Bounds for combined heating valve position $vp_h$ . . . . .	172
4.9	Bounds for combined window aperture $Ap_{csd}$ . . . . .	173
4.10	$SEL_{year}$ weather data $v$ . . . . .	174
4.11	Weather data with predictions for August 1 . . . . .	175
4.12	Weather data $v$ . . . . .	179
4.13	Cost function values, $\mathcal{PI}$ . . . . .	180
4.14	Grid search $\mathcal{PI}$ , winter day . . . . .	181
4.15	Grid search $\mathcal{PI}$ , summer day . . . . .	182
4.16	Gradient search $\mathcal{PI}$ , winter day . . . . .	184
4.17	Gradient search $\mathcal{PI}$ , summer day . . . . .	186
4.18	Cost function values, $TI$ . . . . .	189
4.19	Grid search $TI$ , winter day . . . . .	191
4.20	Grid search $TI$ , summer day . . . . .	192

4.21	Gradient search $TI$ , winter day . . . . .	194
4.22	Gradient search $TI$ , summer day . . . . .	196
4.23	Computation RHOC with grid search, year-round . . . . .	201
4.24	Computation RHOC with gradient search, fall . . . . .	207
4.25	Computation RHOC with gradient search, winter . . . . .	208
4.26	Computation RHOC with gradient search, spring . . . . .	210
4.27	Computation RHOC with gradient search, summer . . . . .	211
4.28	Results per season . . . . .	218
4.29	Average costs per season . . . . .	219
4.30	Relative humidity and dewpoint temperature . . . . .	235

## List of tables

1.1	Examples smoothing function . . . . .	12
2.1	Photosynthesis model, general parameters . . . . .	20
2.2	Photosynthesis parameters $J_{\max}$ and $\Gamma$ . . . . .	27
2.3	Greenhouse and crop parameters . . . . .	31
2.4	Model $CG1$ . . . . .	42
2.5	Model $CG2$ . . . . .	43
2.6	Model $CG3$ . . . . .	45
2.7	Model $CG4$ . . . . .	47
3.1	Notational conventions . . . . .	62
3.2	States, control inputs and external inputs . . . . .	63
3.3	Initial values states . . . . .	121
3.4	Average deviation and standard deviation between simulation and measurement . . . . .	123
3.5	View factors . . . . .	130
3.6	View factor values with screen open and closed . . . . .	131
4.1	Cost function: weight factors and bounds . . . . .	157
4.2	Costs open loop $\mathcal{PI}$ , winter day . . . . .	185
4.3	Costs open loop $\mathcal{PI}$ , summer day . . . . .	187
4.4	Costs open loop $TI$ , winter day . . . . .	195
4.5	Costs open loop $TI$ , summer day . . . . .	197
4.6	Costs open loop gradient search, $\mathcal{PI}$ versus $TI$ . . . . .	198
4.7	Comparison RHOC grid search, solar and non-solar greenhouse . .	203
4.8	RHOC solar greenhouse with gradient search, averages and ranges	206

4.9	RHOC solar greenhouse with gradient search, results and costs . .	213
4.10	Comparison RHOC grid and gradient search . . . . .	216
4.11	Comparison RHOC separate solar greenhouse elements . . . . .	222
4.12	Differences between a priori and a posteriori results . . . . .	229
4.13	Reinitialization control inputs . . . . .	232
4.14	Relative humidity and dewpoint temperature . . . . .	236
B.1	List of parameters . . . . .	280

## Appendix B

# List of variables and parameters

Here a list of variables and parameters is given for easy reference. For all variables and parameters used in this thesis either the equation number or the value is given.

Table B.1: List of parameters

name	value	unit	contents
$\alpha_{a,c}$	eqn. 3.40	$\text{W m}^{-2} \text{K}^{-1}$	heat transfer coefficient from indoor air below screen to canopy
$\alpha_{a,s}$	eqn. 3.52	$\text{W m}^{-2} \text{K}^{-1}$	heat transfer coefficient from indoor air below screen to soil
$\alpha_{a,sc}$	eqn. 3.60	$\text{W m}^{-2} \text{K}^{-1}$	heat transfer coefficient from indoor air below screen to screen
$\alpha_{a,s-r_i}$	eqn. 3.55	$\text{W m}^{-2} \text{K}^{-1}$	heat transfer coefficient from indoor air above screen to roof indoor side
$\alpha_{as,sc}$	eqn. 3.62	$\text{W m}^{-2} \text{K}^{-1}$	heat transfer coefficient from indoor air above screen to screen
$\alpha_{l,a}$	eqn. 3.43	$\text{W m}^{-2} \text{K}^{-1}$	heat transfer coefficient from lower net to indoor air below screen
$\alpha_{ro,o}$	eqn. 3.57	$\text{W m}^{-2} \text{K}^{-1}$	heat transfer coefficient from roof outdoor side to outdoor air
$\alpha_{sun}$	eqn. 2.52	rad	azimuth of the sun
$\alpha_{u,a}$	eqn. 3.46	$\text{W m}^{-2} \text{K}^{-1}$	heat transfer coefficient from upper net to indoor air below screen
$\alpha_{uc,a}$	eqn. 3.49	$\text{W m}^{-2} \text{K}^{-1}$	heat transfer coefficient from upper cooling net to indoor air below screen
$\beta_{c,Is}$	eqn. 3.126	—	reflection coefficient shortwave radiation by canopy
$\beta_{c,Is\infty}$	0.12	—	reflection coefficient shortwave radiation by canopy of a dense stand
$\beta_{dif}$	$\frac{1-\sqrt{1-\delta}}{1+\sqrt{1-\delta}}$	—	reflection coefficient canopy diffuse PAR
$\beta_{dir}$	$\frac{2}{1+\frac{k_{dif}BL}{k_{dir}BL}} \cdot \beta_{dif}$	—	reflection coefficient canopy direct PAR
$\beta_{l,Is}$	0.83	—	reflection coefficient shortwave radiation by lower net
$\beta_{s,Is}$	0.58	—	reflection coefficient shortwave radiation by soil (white foil)
$\beta_{sc,Is}$	0.05	—	reflection coefficient shortwave radiation by screen
$\beta_{sun}$	eqn. 2.49	rad	elevation of the sun
$\beta_{u,Is}$	0.83	—	reflection coefficient shortwave radiation by upper net
$\gamma$	$\frac{22}{180} \cdot \pi$	rad	angle of the roof with the horizontal plane
$\Gamma$	eqn. 2.27	$\mu\text{mol}[\text{CO}_2] \text{mol}^{-1}$	$\text{CO}_2$ compensation concentration in the absence of dark respiration
$\delta$	0.15	—	scattering coefficient
$\delta_{sun}$	eqn. 2.48	rad	declination of the sun
$\Delta I_{a,scr}$	20	$\text{W m}^{-2}$	delta value for switch screen condition $C_{sc,Io}$
$\Delta p_{c,H2Om}$	0.01 ( $p_{c,H2Os} - p_{a,H2O}$ )	mbar	saturation deficit crop
$\text{°}$	control input, $\text{°}$ external input, $\text{°}$ state and $\text{°}$ computed value		

Continued on next page

Table B.1 List of parameters – continued from previous page

name	value	unit	contents
$\Delta p_{x,H2O}$	eqn. 2.65	$N\,m^{-2}$	saturation deficit between object $x$ and air
$\Delta t$	60	s	sampling time of the data
$\Delta T_{a,TI}$	eqn. 2.46	K	predicted average temperature deviation between indoor air and reference
$\Delta T_{cd}$	$T_c - T_d$	K	temperature difference; indicator for leaf wetness
$\Delta T_{max\_he}$	eqn. 3.269	K	maximum temperature difference for heat transfer, heat exchanger
$\Delta T_{max\_hp-c}$	eqn. 3.253	K	maximum temperature difference for heat transfer, cold side heat pump
$\Delta T_{max\_hp-h}$	eqn. 3.251	K	maximum temperature difference for heat transfer, hot side heat pump
$\Delta T_{mc\_hp}$	eqn. 3.250	K	mean temperature difference for heat transfer, cold side heat pump
$\Delta T_{mh\_hp}$	eqn. 3.249	K	mean temperature difference for heat transfer, hot side heat pump
$\Delta T_{min\_he}$	eqn. 3.270	K	minimum temperature difference for heat transfer, heat exchanger
$\Delta T_{min\_hp-c}$	eqn. 3.254	K	minimum temperature difference for heat transfer, cold side heat pump
$\Delta T_{min\_hp-h}$	eqn. 3.252	K	minimum temperature difference for heat transfer, hot side heat pump
$\Delta T_{m\_he}$	eqn. 3.268	K	average temperature difference for heat transfer of heat exchanger
$\Delta T_{o\_scr}$	2	K	delta value for switch screen condition $C_{sc}T_o$
$\Delta W$		$kg[b.m.]m^{-2}[soil]$	total biomass increase over a period of time
$\Delta X$	$X - X_s$ ; see eqn. 1.2	–	difference for sigmoid smoothing function $\Sigma$
$\epsilon$	eqn. 3.200	–	error to minimize in model parameter fit
$\varepsilon$	eqn. 2.25	$mg[CO_2]J^{-1}$	light use efficiency by photorespiration
$\zeta$	4.59	$\mu mol[photons]J^{-1}$	conversion factor from J to photons
$\eta_{boil}$	0.95; see eqn. 3.20	–	efficiency of the boiler
$\eta_{c,Is}$	$0.752(1 - Cl_{sc})^\ddagger$ ; eqn. 3.125	–	absorption coefficient shortwave radiation by canopy
$\eta_{hp}$	0.4	–	efficiency of the heat pump
$\eta_{l,Is}$	$0.030(1 - Cl_{sc})^\ddagger$ ; eqn. 3.123	–	absorption coefficient shortwave radiation by lower net

<sup>‡</sup> control input, <sup>\*</sup> external input, <sup>°</sup> state and <sup>‡</sup> computed value

Continued on next page

Table B.1 List of parameters – continued from previous page

name	value	unit	contents
$\eta_{ri-Is}$	eqn. 3.114	–	absorption coefficient shortwave radiation by roof indoor side
$\eta_{ro-Is}$	0.02; see eqn. 3.115	–	absorption coefficient shortwave radiation by roof outdoor side
$\eta_{s-Is}$	$0.147(1 - Cl_{sc})^\dagger$ ; eqn. 3.129	–	absorption coefficient shortwave radiation by soil
$\eta_{sc-Is}$	$0.42 Cl_{sc}^\dagger$ ; eqn. 3.117	–	absorption coefficient shortwave radiation by screen
$\eta_{u-Is}$	$0.085(1 - Cl_{sc})^\dagger$ ; eqn. 3.119	–	absorption coefficient shortwave radiation by upper net
$\eta_{uc-Is}$	$0.085(1 - Cl_{sc})^\dagger$ ; eqn. 3.121	–	absorption coefficient shortwave radiation by upper cooling net
$\eta_{ohr}$	0.9	–	efficiency factor ventilation with heat recovery
$\Theta$	0.7	–	degree of curvature $P_{n\max}$
$\Theta_{\max}$	$\frac{40}{180} \cdot \pi$	rad	maximum angle window aperture
$\theta$	see §3.9.2	–	parameter values for parameter estimation and sensitivity analysis
$\bar{\theta}$	see eqn. 3.275	–	nominal parameter values for sensitivity analysis
$\theta_{he}$	see eqn. 4.16	–	parameter values for estimation heat exchanger energy curve $E_{he}$
$\theta_{hp}$	see eqn. 4.17	–	parameter values for estimation heat pump energy curve $E_{hp}$
$\lambda_a$	$24 \cdot 10^{-3}$	$W m^{-1} K^{-1}$	thermal conductivity air
$\lambda_{concrete}$	1.7	$W m^{-1} K^{-1}$	thermal conductivity concrete
$\lambda_{gh}$	52	°	latitude location greenhouse
$\lambda_s$	$0.86^\dagger$ ; see eqn. 3.225	$W m^{-1} K^{-1}$	thermal conductivity soil
$\lambda_{soil}$	0.85	$W m^{-1} K^{-1}$	thermal conductivity soil
$\nu$	see eqn. 2.43	–	time step integration temperature integral
$\rho_a$	$1.29 \cdot \frac{T_0}{T_a}$	$kg m^{-3}$	density air below screen
$\bar{\rho}_a$	$1.29 \cdot \frac{2T_0}{T_a + T_{as}}$	$kg m^{-3}$	average density air below and above screen
$\rho_{as}$	$1.29 \cdot \frac{T_0}{T_{as}}$	$kg m^{-3}$	density air above screen
$\rho_c$	700	$kg m^{-3}$	density crop
$\rho_{chl}$	0.45	$g[Chl] m^{-2}[leaf]$	superficial chlorophyll density
$\rho_{CO2}$	1.98	$kg m^{-3}$	density $CO_2$ at temperature $T_0$
$\rho_{CO2T}$	eqn. 2.36	$kg m^{-3}$	density $CO_2$ at temperature $T$

<sup>†</sup> control input, <sup>\*</sup> external input, <sup>°</sup> state and <sup>#</sup> computed value

Continued on next page

Table B.1 List of parameters – continued from previous page

name	value	unit	contents
$\rho_{H2O}$	998	$\text{kg m}^{-3}$	density water
$\rho_r$	2500	$\text{kg m}^{-3}$	density (roof) glass
$\rho_s$	see eqn. 3.226	$\text{kg m}^{-3}$	density soil
$\rho_{sand}$	1600	$\text{kg m}^{-3}$	density sand
$\rho_{sc}$	1500	$\text{kg m}^{-3}$	density screen material (PVC)
$\sigma$	$5.67051 \cdot 10^{-8}$	$\text{W m}^{-2} \text{K}^{-4}$	Stefan-Boltzmann constant
$\zeta$	see eqn. 1.2	–	slope of sigmoid smoothing function $\Sigma$
$\Sigma$	1.2	–	sigmoid smoothing function
$\tau$	see eqn. 2.43	s	time for simulating over horizon $t_f$ for temperature integral
$\tau_{atm}$	eqn. 2.55	–	atmospheric transmission
$\tau_{c,II}$	eqn. 3.73	–	transmittance of longwave radiation by the canopy
$\tau_{c,Is}$	eqn. 3.127	–	transmittance of shortwave radiation by the canopy
$\tau_{dif}$	$e^{-k_{dif} \cdot LAI}$	–	transmittance diffuse PAR
$\tau_{difR}$	0.78 (solar), 0.55 (conv.)	–	transmittance of diffuse shortwave radiation by the roof
$\tau_{dir}$	$e^{-k_{dir} \cdot LAI}$	–	transmittance direct PAR total
$\tau_{dir,BL}$	$e^{-k_{dir,BL} \cdot LAI}$	–	transmittance direct PAR and black leaves
$\tau_{dir,R}$	eqn. 2.64	–	transmittance of direct shortwave radiation by the roof
$\tau_{r,Is}$	eqn. 3.109	–	transmittance of shortwave radiation by the roof
$\tau_{sc,Is}$	eqn. 3.110	–	transmittance of shortwave radiation by the screen
$\tau_{sc,Is0}$	0.8	–	transmittance of shortwave radiation by the screen if it is fully closed
$\varphi_D$	eqn. 3.279	–	D-criterion Fisher information matrix
$\varphi_E$	eqn. 3.280	–	modified E-criterion Fisher information matrix
$\varphi_{gh}$	4.2	o	longitude location greenhouse
$\Phi$	eqn. 4.3	cost	terminal costs for cost function $J$
$\Phi_{\Delta T_{Isd}}$	eqn. 3.156	$\text{m}^3 \text{s}^{-1}$	volume flow air from air above screen to outdoor air through the windows, lee-side (ventilation)
$\Phi_{\Delta T_{usd}}$	eqn. 3.157	$\text{m}^3 \text{s}^{-1}$	volume flow air from air above screen to outdoor air through the windows, windward-side (ventilation)
$\Phi_{a,as}$	eqn. 3.145	$\text{m}^3 \text{s}^{-1}$	volume flow air from below screen to above screen

▷ control input, \*external input, °state and #computed value

Continued on next page

Table B.1 List of parameters – continued from previous page

name	value	unit	contents
$\Phi_{as-o}$	eqn. 3.150	$\text{m}^3 \text{s}^{-1}$	volume flow air from air above screen to outdoor air (ventilation)
$\Phi_{boil}$	eqns. 3.173 and 3.196	$\text{m}^3 \text{s}^{-1}$	volume flow water through the boiler
$\Phi_{gas}$	eqn. 3.20	$\text{m}^3 [\text{gas}] \text{s}^{-1}$	flow gas needed by boiler
$\Phi_{in-l}$	eqn. 3.162	$\text{m}^3 \text{s}^{-1}$	volume flow water into the lower heating net
$\Phi_{in-u}$	eqn. 3.168	$\text{m}^3 \text{s}^{-1}$	volume flow water into the upper heating net
$\Phi_{in-uc}$	eqn. 3.185	$\text{m}^3 \text{s}^{-1}$	volume flow water into the upper cooling net
$\Phi_{leak}$	eqn. 3.151	$\text{m}^3 \text{s}^{-1}$	volume flow air from air above screen to outdoor air due to leakage (ventilation)
$\Phi_{m-a-as-CO2}$	eqn. 3.26	$\text{kg}[\text{CO}_2] \text{s}^{-1}$	mass flow rate carbon dioxide from indoor air below screen to indoor air above screen
$\Phi_{m-a-as-H2O}$	eqn. 3.36	$\text{kg}[\text{H}_2\text{O}] \text{s}^{-1}$	mass flow rate water vapour from air below screen to air above screen
$\Phi_{m-a-c-CO2}$	eqn. 3.21	$\text{kg}[\text{CO}_2] \text{s}^{-1}$	mass flow rate carbon dioxide from indoor air to canopy (net photosynthesis rate canopy)
$\Phi_{m-a-sc-H2O}$	eqn. 3.31	$\text{kg}[\text{H}_2\text{O}] \text{s}^{-1}$	mass flow rate water vapour from indoor air below screen to screen (condensation)
$\Phi_{m-a-uc-H2O}$	eqn. 3.29	$\text{kg}[\text{H}_2\text{O}] \text{s}^{-1}$	mass flow rate water vapour from indoor air below screen to upper cooling net (condensation)
$\Phi_{m-as-o-CO2}$	eqn. 3.25	$\text{kg}[\text{CO}_2] \text{s}^{-1}$	mass flow rate carbon dioxide from indoor air above screen to outdoor air
$\Phi_{m-as-o-H2O}$	eqn. 3.35	$\text{kg}[\text{H}_2\text{O}] \text{s}^{-1}$	mass flow rate water vapour from indoor air above screen to outdoor air
$\Phi_{m-as-ri-H2O}$	eqn. 3.27	$\text{kg}[\text{H}_2\text{O}] \text{s}^{-1}$	mass flow rate water vapour from indoor air above screen to roof indoor side (condensation)
$\Phi_{m-as-sc-H2O}$	eqn. 3.32	$\text{kg}[\text{H}_2\text{O}] \text{s}^{-1}$	mass flow rate water vapour from indoor air above screen to screen (condensation)
$\Phi_{m-c-a-H2O}$	eqn. 2.1	$\text{kg}[\text{H}_2\text{O}] \text{s}^{-1}$	mass flow rate water vapour from canopy to indoor air (transpiration)
$\Phi_{m-CO2}$	$5 \cdot 10^{-5} A_s$ (solar), $0.4 \cdot 10^{-5} A_s$ (conv.)	$\text{kg}[\text{CO}_2] \text{s}^{-1}$	maximum mass flow rate carbon dioxide supply
$\Phi_{m-in-a-CO2 \max}$	eqn. 3.19	$\text{kg}[\text{CO}_2] \text{s}^{-1}$	maximum mass flow rate carbon dioxide supply by the boiler

<sup>▷</sup> control input, <sup>\*</sup> external input, <sup>°</sup> state and <sup>‡</sup> computed value

Continued on next page

Table B.1 List of parameters – continued from previous page

name	value	unit	contents
$\Phi_{m.in.a-CO_2}$	eqn. 3.17	$\text{kg}[\text{CO}_2] \text{ s}^{-1}$	mass flow rate carbon dioxide supply
$\Phi_{pump.boil}$	$1.62 \cdot 10^{-3}$	$\text{m}^3 \text{ s}^{-1}$	maximum volume flow water from the boiler
$\Phi_{pump.he}$	$5.7 \cdot 10^{-3}$	$\text{m}^3 \text{ s}^{-1}$	maximum volume flow water through the heat exchanger
$\Phi_{pump.hp}$	$1.5 \cdot 10^{-3}$	$\text{m}^3 \text{ s}^{-1}$	maximum volume flow water through the heat pump
$\Phi_{pump.l}$	$1.62 \cdot 10^{-3}$	$\text{m}^3 \text{ s}^{-1}$	maximum volume flow water into the lower heating net
$\Phi_{pump.u}$	$1.08 \cdot 10^{-3}$	$\text{m}^3 \text{ s}^{-1}$	maximum volume flow water into the upper heating net
$\Phi_{pump.uc}$	$6 \cdot 10^{-3}$	$\text{m}^3 \text{ s}^{-1}$	maximum volume flow water into the upper cooling net
$\Phi_{Tl}$	eqn. 4.5	cost	terminal cost temperature integral
$\Phi_W$	eqn. 4.4	cost	terminal cost biomass increase
$\Phi_{win}$	eqn. 3.152	$\text{m}^3 \text{ s}^{-1}$	volume flow air from air above screen to outdoor air through the windows (ventilation)
$\Phi_{wind}$	eqn. 3.153	$\text{m}^3 \text{ s}^{-1}$	volume flow air from air above screen to outdoor air through the windows, wind induced (ventilation)
$\psi$	eqn. 2.26	$\mu\text{mol}[\text{e}^-] \text{ J}^{-1}$	conversion factor from J to $\mu\text{mol}[\text{e}^-]$
$A_c$	$18816^\#$ ; eqn. 3.39	$\text{m}^2$	surface area canopy
$A_{he}$	2500	$\text{m}^2$	surface area for heat transfer of heat exchanger
$A_{hp}$	500	$\text{m}^2$	surface area for heat transfer of heat pump
$A_l$	$614.05^\#$ ; eqn. 3.42	$\text{m}^2$	surface area lower net
$A_{csd}$	$\triangleright$ see §4.3.6.1	[0,2]	(control input) combined window aperture; combination of $A_{plsd}$ and $A_{pwsd}$
$A_{plsd}$	$\triangleright$	[0,1]	(control input) window aperture lee-side
$A_{psy}$	eqn. 2.72	$\text{K}^{-1}$	psychrometric coefficient
$A_{pwsd}$	$\triangleright$	[0,1]	(control input) window aperture windward-side
$A_r$	$3382.28^\#$ ; eqn. 3.54	$\text{m}^2$	surface area roof
$A_s$	$3136^\#$ ; eqn. 3.51	$\text{m}^2$	surface area soil
$A_{sc}$	$3136^\#$ ; eqn. 3.59	$\text{m}^2$	surface area screen
$ASRQ$	1.2	$\text{kg}[\text{CH}_2\text{O}] \text{ kg}[\text{d.w.}]^{-1}$	conversion factor from dry weight to $\text{CH}_2\text{O}$
$a_T$	see eqn. 3.181	–	parameter of a fourth order equation for $T_{out.hp}$
$A_u$	$337.12^\#$ ; eqn. 3.45	$\text{m}^2$	surface area upper net
$A_{uc}$	$2456.19^\#$ ; eqn. 3.48	$\text{m}^2$	surface area upper cooling net

 $\triangleright$  control input,  $^\#$  external input,  $^\circ$  state and  $^\dagger$  computed value

Continued on next page

Table B.1 List of parameters – continued from previous page

name	value	unit	contents
$b_T$	see eqn. 3.181	–	parameter of a fourth order equation for $T_{out\_hp}$
$c_1$	see eqn. 3.180	–	intermediate variable for computing $T_{aq\_c\_hp}$
$C_{a\_CO_2}$	°eqn. 3.1	kg[CO <sub>2</sub> ] m <sup>-3</sup>	(state) CO <sub>2</sub> concentration indoor air below screen
$C_{a\_H_2O}$	°eqn. 3.3	kg[H <sub>2</sub> O] m <sup>-3</sup>	(state) H <sub>2</sub> O concentration indoor air below screen
$C_{as\_CO_2}$	°eqn. 3.2	kg[CO <sub>2</sub> ] m <sup>-3</sup>	(state) CO <sub>2</sub> concentration indoor air above screen
$C_{as\_H_2O}$	°eqn. 3.4	kg[H <sub>2</sub> O] m <sup>-3</sup>	(state) H <sub>2</sub> O concentration indoor air above screen
$C_{c\_H_2O_s}$	see eqn. 2.68	kg[H <sub>2</sub> O] m <sup>-3</sup>	saturation concentration water vapour at crop temperature
$c$	see table 4.1	cost day <sup>-1</sup> unit <sup>-1</sup>	weight factors cost function
$c_{c,s}$	$\frac{30}{44}$	kg[CH <sub>2</sub> O] kg[CO <sub>2</sub> ] <sup>-1</sup>	conversion factor from CO <sub>2</sub> to CH <sub>2</sub> O
$c_f$	1	–	fraction of produced biomass material for dry weight
$c_{he}$	see eqn. 3.190	–	intermediate variable for computing $T_{aq\_h\_he}$
$Cl_{sc}$	$\triangleright$	[0,1]	(control input) thermal screen closure
$c_{isd0}$	$1.26730 \cdot 10^{-4}$	–	ventilation function coefficient lee-side
$c_{isd1}$	$4.71176 \cdot 10^{-2}$	–	ventilation function coefficient lee-side
$c_{isd2}$	$3.77646 \cdot 10^{-2}$	–	ventilation function coefficient lee-side
$c_{isd3}$	$1.21774 \cdot 10^{-2}$	–	ventilation function coefficient lee-side
$c_m$	see eqn. 3.200	–	scaling factor parameter estimation
$CO_{2a}$	$\frac{C_{a\_CO_2}}{1.83 \cdot 10^{-6}}$	μmol[CO <sub>2</sub> ] mol <sup>-1</sup>	CO <sub>2</sub> concentration indoor air below screen
$CO_{2a\_sp}$	eqn. 4.28	μmol[CO <sub>2</sub> ] mol <sup>-1</sup>	set point CO <sub>2</sub> concentration indoor air below screen
$CO_{2o}$	$\frac{C_{o\_CO_2}}{1.83 \cdot 10^{-6}}$	μmol[CO <sub>2</sub> ] mol <sup>-1</sup>	CO <sub>2</sub> concentration outdoor air
$C_{o\_CO_2}$	*	kg[CO <sub>2</sub> ] m <sup>-3</sup>	(external input) CO <sub>2</sub> concentration outdoor air
$C_{o\_H_2O}$	see §2.C.1	kg[H <sub>2</sub> O] m <sup>-3</sup>	H <sub>2</sub> O concentration outdoor air
$C_{sc\_H_2O_s}$	see eqn. 2.68	kg[H <sub>2</sub> O] m <sup>-3</sup>	saturation concentration water vapour at screen temperature
$COP$	eqn. 3.177	WW <sup>-1</sup>	coefficient of performance heat pump
$\cos\alpha$	eqn. 2.53	–	cosine of the solar azimuth
$c_{p\_a}$	1000	J kg <sup>-1</sup> K <sup>-1</sup>	specific heat capacity of air
$c_{p\_H_2O}$	4186	J kg <sup>-1</sup> K <sup>-1</sup>	specific heat capacity of water
$c_{p\_r}$	840	J kg <sup>-1</sup> K <sup>-1</sup>	specific heat capacity of (roof) glass
$c_{p\_sand}$	800	J kg <sup>-1</sup> K <sup>-1</sup>	specific heat capacity sand

$\triangleright$  control input, \* external input, ° state and  $\dagger$  computed value

Continued on next page

Table B.1 List of parameters – continued from previous page

name	value	unit	contents
$c_{p-sc}$	1500	$\text{J kg}^{-1} \text{K}^{-1}$	specific heat capacity screen material (PVC)
$C_{ri-H_2O_s}$	eqn. 2.68	$\text{kg}[\text{H}_2\text{O}]\text{m}^{-3}$	saturation concentration water vapour at roof indoor side temperature
$c_{s1}$	eqn. 2.67	–	saturation pressure coefficient
$c_{s2}$	eqn. 2.67	–	saturation pressure coefficient
$c_{s3}$	eqn. 2.67	–	saturation pressure coefficient
$c_{sc}$	eqns. 3.140, 3.195	$\{0,1\}$	screen condition (open or closed)
$c_{sc-I}$	eqn. 3.141	$\{0,1\}$	screen condition due to solar radiation
$c_{sc-I0}$	eqn. 3.142	$\{0,1\}$	previous screen condition due to solar radiation
$c_{sc-T}$	eqn. 3.143	$\{0,1\}$	screen condition due to temperature outdoor air
$c_{sc-T0}$	eqn. 3.144	$\{0,1\}$	previous screen condition due to temperature outdoor air
$c_T$	see eqn. 3.181	–	parameter of a fourth order equation for $T_{out,hp}$
$c_{Tr1}$	see eqn. 3.242	–	parameter of equation for $T_{ro}$
$c_{Tr2}$	see eqn. 3.242	–	parameter of equation for $T_{ro}$
$c_{Tr3}$	see eqn. 3.242	–	parameter of equation for $T_{ro}$
$c_{Tr4}$	see eqn. 3.242	–	parameter of equation for $T_{ro}$
$c_{Tr5}$	see eqn. 3.242	–	parameter of equation for $T_{ro}$
$c_{Tsk}$	0.6	–	clouded fraction of the sky
$C_{uc-H_2O_s}$	eqn. 2.68	$\text{kg}[\text{H}_2\text{O}]\text{m}^{-3}[\text{air}]$	saturation concentration water vapour at upper cooling net temperature
$c_w$	0.6	–	discharge coefficient through windows
$c_{usd0}$	$5.91362 \cdot 10^{-4}$	–	ventilation function coefficient windward-side
$c_{usd1}$	$7.08828 \cdot 10^{-2}$	–	ventilation function coefficient windward-side
$c_{usd2}$	$4.48621 \cdot 10^{-2}$	–	ventilation function coefficient windward-side
$c_{usd3}$	$2.42856 \cdot 10^{-2}$	–	ventilation function coefficient windward-side
$C_{x-H_2O}$	see eqn. 2.69	$\text{kg}[\text{H}_2\text{O}]\text{m}^{-3}[\text{air}]$	concentration water vapour at temperature $T_x$
$C_{x-H_2O_s}$	eqn. 2.68	$\text{kg}[\text{H}_2\text{O}]\text{m}^{-3}[\text{air}]$	saturation concentration water vapour at temperature $T_x$
$dayNR$	[1,365]	–	day number
$d_l$	0.051	m	outer diameter lower net pipe

<sup>▷</sup> control input, <sup>\*</sup> external input, <sup>°</sup> state and <sup>#</sup> computed value

Continued on next page

Table B.1 List of parameters – continued from previous page

name	value	unit	contents
$d_r$	0.004	m	thickness roof glass
$d_{ra}$	0.01	m	air cavity roof (between inner and outer glass cover)
$d_s$	0.65	m	thickness soil layer
$d_{sc}$	$0.5 \cdot 10^{-3}$	m	thickness screen material
$d_T$	see eqn. 3.181	–	parameter of a fourth order equation for $T_{out\_hp}$
$d_u$	0.028	m	outer diameter upper net pipe
$d_{uc}$	0.051	m	outer diameter upper cooling net pipe
$d_{x_s}$	1.247	m	distance between centers of upper soil layer and subsoil layer
$E_{aq}$	°eqn. 3.16	$\text{J m}^{-2}[\text{soil}]$	(state) aquifer energy content
$E_{aq}^*$	eqn. 4.18	$\text{J m}^{-2}[\text{soil}]$	aquifer energy content reference curve
$E_{aq0}$	see eqn. 4.13	$\text{J m}^{-2}[\text{soil}]$	initial value accumulated aquifer energy content
$E_{aq \max}$	eqn. 4.20	$\text{J m}^{-2}[\text{soil}]$	aquifer energy content reference maximum bound
$E_{aq \min}$	eqn. 4.19	$\text{J m}^{-2}[\text{soil}]$	aquifer energy content reference minimum bound
$E_c$	$1 - \tau_{c\_II}$	–	emission coefficient canopy
$E_C$	59356	$\text{J mol}^{-1}$	activation energy $K_C$ Rubisco carboxylation
$E_D$	66405	$\text{J mol}^{-1}$	activation energy $r_D$ dark respiration rate
$E_{he}$	eqn. 4.14	$\text{J m}^{-2}[\text{soil}]$	energy extracted from the greenhouse by the heat exchanger and stored in the aquifer
$E_{hp}$	eqn. 4.15	$\text{J m}^{-2}[\text{soil}]$	energy supplied to the greenhouse by the heat pump and retrieved from the aquifer
$E_J$	37000	$\text{J mol}^{-1}$	activation energy $J_{\max}$ maximum electron transport rate
$E_l$	0.95	–	emission coefficient lower net
$E_M$	39017	$\text{J mol}^{-1}$	activation energy $K_M$ Michaelis Menten constant
$E_O$	35948	$\text{J mol}^{-1}$	activation energy $K_O$ Rubisco oxygenation
$E_{ri}$	0.95	–	emission coefficient roof indoor side
$E_{ro}$	0.95	–	emission coefficient roof outdoor side
$E_s$	0.7	–	emission coefficient soil
$E_{sc}$	0.9	–	emission coefficient screen
$E_{sk}$	1	–	emission coefficient sky

▷ control input, \*external input, °state and #computed value

Continued on next page

Table B.1 List of parameters – continued from previous page

name	value	unit	contents
$E_{sky\_clear}$	eqn. 3.198	–	emission coefficient (fictive) of clear sky
$e_T$	see eqn. 3.181	–	parameter of a fourth order equation for $T_{out\_hp}$
$E_t$	87.0	$\mu\text{mol}[\text{CO}_2]\text{g}^{-1}[\text{Chl}]$	total concentration of enzyme sites
$E_u$	0.95	–	emission coefficient upper net
$E_{uc}$	0.95	–	emission coefficient upper cooling net
$E_{VC}$	58520	$\text{J mol}^{-1}$	activation energy $V_C$ max maximum carboxylation rate
$F_p$	0.3	–	fraction PAR absorbed by non-photosynthetic tissues
$F$	eqn. 3.278	–	Fisher information matrix
$\tilde{F}$	eqn. 3.281	–	Fisher information matrix of the relative sensitivities
$f_a$	1	–	infiltration factor $\Phi_{leak}$
$F_{c,sc}$	eqn. 3.105	–	view factor from canopy to screen
$f_{clear}$	eqn. 2.61	–	apparent fraction clear
$f_{CO_2}$	eqn. 2.6	–	$\text{CO}_2$ dependency $R_{s\_H2O}$
$f_{CO_2\_gas}$	1.78; see eqn. 3.20	$\text{kg}[\text{CO}_2]\text{m}^{-3}[\text{gas}]$	conversion factor from $\text{m}^3[\text{gas}]$ to $\text{kg}[\text{CO}_2]$
$f_{CO_2ia}$	0.67	–	fraction $\text{CO}_2$ inside compared to outside stomata
$f_{dif}$	eqn. 2.57	–	fraction diffuse radiation in outdoor shortwave solar radiation
$f_{dif1}$	eqn. 2.58	–	intermediate variable for computation $f_{dif}$
$f_{dif2}$	eqn. 2.59	–	intermediate variable for computation $f_{dif}$
$f_{difpar}$	eqn. 2.60	–	fraction diffuse radiation in PAR radiation
$f_{H2O}$	eqn. 2.7	–	$\text{H}_2\text{O}$ dependency $R_{s\_H2O}$
$f_l$	eqn. 2.4	–	radiation dependency $R_{s\_H2O}$
$F_{Lc}$	eqn. 3.68	–	view factor from lower net to canopy
$F_{Lr\ddot{i}}$	eqn. 3.72	–	view factor from lower net to roof indoor side
$F_{Ls}$	eqn. 3.70	–	view factor from lower net to soil
$F_{Lsc}$	eqn. 3.75	–	view factor from lower net to screen
$f_{isd}$	eqn. 3.154	–	ventilation function lee-side
$f_{OC}$	0.21	–	ratio $\frac{V_{O\max}}{V_C\max}$
$f_{par}$	eqn. 2.62	–	fraction par in outdoor shortwave solar radiation
$F_{ri,c}$	eqn. 3.99	–	view factor from roof indoor side to canopy

▷ control input, \*external input, °state and °computed value

Continued on next page

Table B.1 List of parameters – continued from previous page

name	value	unit	contents
$F_{Ti-ro}$	eqn. 3.101	–	view factor from roof indoor side to roof outdoor side
$F_{To-sk}$	eqn. 3.103	–	view factor from roof outdoor side to sky
$F_{s-c}$	eqn. 3.93	–	view factor from soil to canopy
$F_{sc-ri}$	eqn. 3.107	–	view factor from screen to roof indoor side
$F_{s-l}$	eqn. 3.209	–	view factor from soil to lower net
$f_{SLA}$	$\tau_{dirBL}(l_1)$	–	fraction sunlit leaf area
$F_{s-ri}$	eqn. 3.95	–	view factor from soil to roof indoor side
$F_{s-sc}$	eqn. 3.97	–	view factor from soil to screen
$F_{s-u}$	eqn. 3.210	–	view factor from soil to upper net
$F_{s-uc}$	eqn. 3.211	–	view factor from soil to upper cooling net
$f_{TC}$	eqn. 2.5	–	temperature dependency $R_{s,H2O}$
$F_{u-c}$	eqn. 3.77	–	view factor from upper net to canopy
$F_{uc-c}$	eqn. 3.85	–	view factor from upper cooling net to canopy
$F_{uc-ri}$	eqn. 3.89	–	view factor from upper cooling net to roof indoor side
$F_{uc-s}$	eqn. 3.87	–	view factor from upper cooling net to soil
$F_{uc-sc}$	eqn. 3.91	–	view factor from upper cooling net to screen
$F_{u-ri}$	eqn. 3.81	–	view factor from upper net to roof indoor side
$F_{u-s}$	eqn. 3.79	–	view factor from upper net to soil
$F_{u-sc}$	eqn. 3.83	–	view factor from upper net to screen
$f_{w-CO2}$	eqn. 3.24	kg[b.m.] kg <sup>-1</sup> [CO <sub>2</sub> ]	conversion factor from CO <sub>2</sub> to crop weight
$f_{wsd}$	eqn. 3.155	–	ventilation function windward-side
$g$	9.81	m s <sup>-2</sup>	gravity
$H$	220000; see eqn. 2.34	J mol <sup>-1</sup>	constant for temperature dependency $J_{\max}$
$h_1$	see eqn. 3.180	–	intermediate variable for computing $T_{aq-c.hp}$
$h_g$	4.5	m	height greenhouse gutter
$hour$	[0,23]	–	hour of the day
$h_r$	$h_g + 0.5 w_s \cdot \tan(\gamma)$	m	height greenhouse ridge
$H_u$	$35.17 \cdot 10^6$ ; see eqn. 3.20	J m <sup>-3</sup> [gas]	(high) combustion value gas
$I_A$	see eqn. 2.12	W m <sup>-2</sup>	absorbed radiation

<sup>▷</sup>control input, <sup>\*</sup>external input, <sup>°</sup>state and <sup>‡</sup>computed value

Continued on next page

Table B.1 List of parameters – continued from previous page

name	value	unit	contents
$I_{A\_dif}$	eqn. 2.21	$W m^{-2}$	radiation absorbed by the crop, diffuse flux
$I_{A\_dir}$	eqn. 2.23	$W m^{-2}$	radiation absorbed by the crop, direct flux
$I_{A\_ppd}$	eqn. 2.24	$W m^{-2}$	radiation absorbed by the crop, direct flux perpendicular on direct beam
$I_{A\_shd}$	eqn. 2.20	$W m^{-2}$	radiation absorbed by the crop, shaded part
$I_{A\_sun}$	eqn. 2.19	$W m^{-2}$	radiation absorbed by the crop, sunlit part
$I_{A\_tdir}$	eqn. 2.22	$W m^{-2}$	radiation absorbed by the crop, total direct flux
$I_{c\_s}$	$\frac{Q_{rad-c}}{A_s}$	$W m^{-2}$	heat absorbed by canopy (shortwave radiation absorption)
$I_o$	*	$W m^{-2}$	(external input) outdoor shortwave solar radiation
$I_{o\_high}$	60#	$W m^{-2}$	high boundary value for switch screen condition $C_{sc.I_o}$
$I_{o\_low}$	20#	$W m^{-2}$	low boundary value for switch screen condition $C_{sc.I_o}$
$I_{o\_scr}$	40	$W m^{-2}$	mean value for switch screen condition $C_{sc.I_o}$
$I_{P\_dif}$	$\tau_{difR} \cdot \tau_{sc.I_s} \cdot I_{P\_dif_o}$	$W m^{-2}$	diffuse PAR inside greenhouse
$I_{P\_dif_o}$	$f_{difpar} \cdot I_{P_o}$	$W m^{-2}$	diffuse PAR outside greenhouse
$I_{P\_dir}$	$\tau_{dirR} \cdot \tau_{sc.I_s} \cdot I_{P\_dir_o}$	$W m^{-2}$	direct PAR inside greenhouse
$I_{P\_dir_o}$	$I_{P_o} - I_{P\_dif_o}$	$W m^{-2}$	direct PAR outside greenhouse
$I_P$	$f_{par} \cdot \tau_{difR} \cdot \tau_{sc.I_s} \cdot I_o$	$W m^{-2}$	PAR inside greenhouse
$I_{P_o}$	$f_{par} \cdot I_o$	$W m^{-2}$	PAR outside greenhouse
$J$	eqn. 4.2	cost	cost function value
$J_{grad}$	see eqn. 4.2	cost	cost function value conjugate gradient search method
$J_{grid}$	see eqn. 4.2	cost	cost function value grid search method
$J_{min}$	see eqn. 4.2	cost	minimum (optimal) cost function value
$J_{max}$	eqn. 2.34	$\mu mol[e^-] m^{-2} [leaf] s^{-1}$	maximum electron transport rate
$J_{max25}$	467 $\rho_{chl}$	$\mu mol[e^-] m^{-2} [leaf] s^{-1}$	maximum electron transport rate at 25°C
$k_\nu$	see eqn. 2.45, 3.200	–	discrete time step summation
$k_{a\_sc.H2O}$	eqn. 3.33	$m s^{-1}$	mass transfer coefficient of water vapour from air below screen to screen
$k_{as\_ri.H2O}$	eqn. 3.28	$m s^{-1}$	mass transfer coefficient of water vapour from air above screen to roof indoor side

▷ control input, \*external input, °state and #computed value

Continued on next page

Table B.1 List of parameters – continued from previous page

name	value	unit	contents
$k_{as-sc.H2O}$	eqn. 3.34	$m\ s^{-1}$	mass transfer coefficient of water vapour from air above screen to screen
$k_{a-uc.H2O}$	eqn. 3.30	$m\ s^{-1}$	mass transfer coefficient of water vapour from air below screen to upper cooling net
$k_C$	2.5	$s^{-1}$	turnover number of RuP2 (carboxylase)
$K_C$	eqn. 2.28	$\mu bar$	Michaelis Menten constant Rubisco carboxylation ( $CO_2$ )
$K_{C25}$	310	$\mu bar$	Michaelis Menten constant Rubisco carboxylation ( $CO_2$ ) at 25°C
$k_{c-a.H2O}$	eqn. 2.2	$m\ s^{-1}$	mass transfer coefficient of water vapour from crop to air below screen
$k_{c-ll}$	0.64	–	extinction coefficient for longwave radiation by the canopy
$k_{c-ls}$	0.48	–	extinction coefficient for shortwave radiation by the canopy
$k_{dif}$	$k_{difBL} \cdot \sqrt{1 - \delta}$	–	extinction coefficient diffuse PAR
$k_{difBL}$	0.8	–	extinction coefficient diffuse PAR and black leaves
$k_{dir}$	$k_{dirBL} \cdot \sqrt{1 - \delta}$	–	extinction coefficient direct PAR
$k_{dirBL}$	$\frac{s_{lo}}{sin\beta}$	–	extinction coefficient direct PAR and black leaves
$k_{he}$	250	$W\ m^{-2}\ K^{-1}$	heat transfer coefficient heat exchanger
$k_{hp}$	250	$W\ m^{-2}\ K^{-1}$	heat transfer coefficient heat pump
$K_M$	eqn. 2.41	$\mu bar$	effective Michaelis Menten constant carboxylation
$K_O$	eqn. 2.29	mbar	Michaelis Menten constant Rubisco oxygenation ( $O_2$ )
$K_{O25}$	155	mbar	Michaelis Menten constant Rubisco oxygenation ( $O_2$ ) at 25°C
$L$	eqn. 4.6	cost $s^{-1}$	penalty function for cost function $J$
$l_1$	{1, 2, 3}	–	summation counter for integration over canopy depth
$L_1$	2.25	m	window length
$l_2$	{1, 2, 3}	–	summation counter for correction $I_{A\_ppd}$ for canopy depth
$L_2$	1	m	window height
$LAI$	3	$m^2[leaf]\ m^{-2}[soil]$	leaf area index
$LAI_l$	eqn. 2.15	$m^2[leaf]\ m^{-2}[soil]$	leaf area index at layer $l_1$
$L_{aq}$	see eqn. 4.6	cost $s^{-1}$	penalty function accumulated energy content aquifer
$Le$	0.89	–	Lewis number for water vapour in air
$l_f$	0.035	m	mean leaf width

<sup>▷</sup> control input, <sup>\*</sup> external input, <sup>°</sup> state and <sup>†</sup> computed value

Continued on next page

Table B.1 List of parameters – continued from previous page

name	value	unit	contents
$l_l$	$2(l_s - 2 + 0.75) = 109.5^\#$	m	length of one loop of the lower net
$L_Q$	eqn. 4.9	cost s <sup>-1</sup>	penalty function gas use
$L_{RHa}$	see eqn. 4.6	cost s <sup>-1</sup>	penalty function relative humidity indoor air
$l_s$	56	m	length of the greenhouse span
$L_{Ta}$	see eqn. 4.6	cost s <sup>-1</sup>	penalty function temperature indoor air
$L_{TI}$	see eqn. 4.6	cost s <sup>-1</sup>	penalty function temperature integral
$l_u$	$2(l_s - 2 + 0.75) = 109.5^\#$	m	length of one loop of the upper net
$l_{uc}$	$2(l_s - 2 + 0.75) = 109.5^\#$	m	length of one loop of the upper cooling net
$L_{win\_lsd}$	eqn. 3.158	m	length of vertical projection of windows opening lee-side
$L_{win\_usd}$	eqn. 3.159	m	length of vertical projection of windows opening windward-side
$M_{CO2}$	$44 \cdot 10^{-3}$	kg mol <sup>-1</sup>	molar mass CO <sub>2</sub>
$M_{H2O}$	$18 \cdot 10^{-3}$	kg mol <sup>-1</sup>	molar mass water
$n_l$	2.5	–	number of pipes of the lower net per greenhouse span
$n_s$	14	–	number of greenhouse spans
$n_{secs}$	86400	s day <sup>-1</sup>	number of seconds in a day
$n_{secs\_yr}$	$86400 \cdot 365 = 31536000$	s year <sup>-1</sup>	number of seconds in a year
$n_u$	2.5	–	number of pipes of the upper net per greenhouse span
$n_{uc}$	2.5	–	number of pipes of the upper cooling net per greenhouse span
$n_{win}$	$n_s \cdot n_{wins}$	–	total number of windows per greenhouse span side
$n_{wins}$	12	–	number of windows per greenhouse span side
$op_{vhr}$	$\triangleright$	{0,1}	(control input) option ventilation heat recovery
$p_{a,H2O}$	$p_{a,H2O,s} \cdot \frac{RH_a}{100}$	N m <sup>-2</sup>	vapour pressure indoor air below screen
$p_{a,H2O_s}$	see eqn. 2.66	N m <sup>-2</sup>	saturation vapour pressure indoor air below screen
$p_{bar}$	101325	N m <sup>-2</sup>	atmospheric pressure
$p_{C1}$	$-7.2956 \cdot 10^{-5}$	–	coefficient for computation $COP$
$p_{C2}$	$6.9194 \cdot 10^{-3}$	–	coefficient for computation $COP$
$p_{C3}$	$-3.1741 \cdot 10^{-3}$	–	coefficient for computation $COP$
$p_{C4}$	$1.7438 \cdot 10^{-2}$	–	coefficient for computation $COP$
$P_{cg}$	eqn. 3.22	kg[CO <sub>2</sub> ] m <sup>-2</sup> [soil] s <sup>-1</sup>	gross assimilation rate canopy

 $\triangleright$  control input, \* external input, ° state and  $^\#$  computed value

Continued on next page

Table B.1 List of parameters – continued from previous page

name	value	unit	contents
$p_{c,H2O_s}$	see eqn. 2.66	$N\ m^{-2}$	saturation vapour pressure crop
$p_{da}$	6.4	–	parameter for computation $f_{dif}$ (de Bilt, the Netherlands)
$p_{db}$	0.22	–	parameter for computation $f_{dif}$ (de Bilt, the Netherlands)
$p_{dc}$	0.35	–	parameter for computation $f_{dif}$ (de Bilt, the Netherlands)
$p_{dd}$	0.15	–	parameter for computation $f_{dif}$ (de Bilt, the Netherlands)
$P_g$	eqn. 2.10	$mg[CO_2]\ m^{-2}[leaf]\ s^{-1}$	gross assimilation rate canopy
$P_{g\_L}$	eqn. 2.16	$mg[CO_2]\ m^{-2}[leaf]\ s^{-1}$	gross leaf assimilation rate
$P_{g\ max}$	eqn. 2.30	$mg[CO_2]\ m^{-2}[leaf]\ s^{-1}$	maximum gross assimilation rate
$P_{g\_shd}$	eqn. 2.18	$mg[CO_2]\ m^{-2}[leaf]\ s^{-1}$	gross leaf assimilation rate shaded part
$P_{g\_sun}$	eqn. 2.17	$mg[CO_2]\ m^{-2}[leaf]\ s^{-1}$	gross leaf assimilation rate sunlit part
$P_{gm}$	eqn. 2.33	$mg[CO_2]\ m^{-2}[leaf]\ s^{-1}$	maximum endogenous photosynthetic capacity
$P_{nc}$	eqn. 2.35	$mg[CO_2]\ m^{-2}[leaf]\ s^{-1}$	maximum net assimilation rate limited by $CO_2$
$P_{n\ max}$	eqn. 2.32	$mg[CO_2]\ m^{-2}[leaf]\ s^{-1}$	maximum (light saturated) net assimilation rate
$pO2i$	210	mbar	$O_2$ partial pressure inside stomata
$p_{o,H2O}$	see eqns. 2.69, 3.198	$N\ m^{-2}$	vapour pressure outdoor air
$p_{pa}$	2.9	–	parameter for computation $f_{par}$ (Wageningen and Assen, the Netherlands)
$p_{pb}$	4.9	–	parameter for computation $f_{par}$ (Wageningen and Assen, the Netherlands)
$p_{pc}$	0.51	–	parameter for computation $f_{par}$ (Wageningen and Assen, the Netherlands)
$p_{pe}$	0.84	–	parameter for computation $f_{par}$ (Wageningen and Assen, the Netherlands)
$p_{pf}$	0.033	–	parameter for computation $f_{par}$ (Wageningen and Assen, the Netherlands)
$p_{T1}$	see eqn. 3.181	–	parameter combinations for equation for $T_{out\_hp}$
$p_{T2}$	see eqn. 3.181	–	parameter combinations for equation for $T_{out\_hp}$
$p_{T3}$	see eqn. 3.181	–	parameter combinations for equation for $T_{out\_hp}$
$p_{T4}$	see eqn. 3.181	–	parameter combinations for equation for $T_{out\_hp}$
$p_{T5}$	see eqn. 3.181	–	parameter combinations for equation for $T_{out\_hp}$
▷ control input, *external input, °state and †computed value			

Continued on next page

Table B.1 List of parameters – continued from previous page

name	value	unit	contents
$P_{T6}$	see eqn. 3.181	–	parameter combinations for equation for $T_{out\_hp}$
$p_w$	94	%	percentage water in total biomass
$p_{x\_H2O}$	eqns. 2.69, 2.71	$N\ m^{-2}$	vapour pressure at object temperature $T_x$
$p_{x\_H2O_s}$	eqn. 2.66	$N\ m^{-2}$	saturation vapour pressure at object temperature $T_x$
$p_{x\_w\_H2O_s}$	see eqn. 2.71	$N\ m^{-2}$	saturation vapour pressure at object temperature $T_{x\_w}$
$Q_{\Sigma l}$	see §3.B	W	energy transfer lower heating net
$Q_{a\_as}$	eqn. 3.63	W	heat transfer from indoor air below screen to indoor air above screen (convection)
$Q_{a\_c}$	eqn. 3.38	W	heat transfer from indoor air below screen to canopy (convection)
$Q_{a\_s}$	eqn. 3.50	W	heat transfer from indoor air below screen to soil (convection)
$Q_{a\_sc\_H2O}$	eqn. 3.136	W	heat transfer from indoor air below screen to screen (latent heat)
$Q_{a\_s_o}$	eqn. 3.64	W	heat transfer from indoor air above screen to outdoor air (convection, ventilation)
$Q_{a\_s\_ri\_H2O}$	eqn. 3.134	W	heat transfer from indoor air above screen to roof indoor side (latent heat)
$Q_{a\_s\_ri}$	eqn. 3.53	W	heat transfer from indoor air above screen to roof indoor side (convection)
$Q_{a\_s\_sc\_H2O}$	eqn. 3.137	W	heat transfer from indoor air above screen to screen (latent heat)
$Q_{a\_uc\_H2O}$	eqn. 3.135	W	heat transfer from indoor air below screen to upper cooling net (latent heat)
$Q_{boil}$	eqn. 3.172	W	energy transport, heat supply by boiler
$Q_c$	eqn. 3.179	W	energy transport heat pump due to the water flow on the aquifer side
$Q_{c\_a\_H2O}$	eqn. 3.138	W	heat transfer from canopy to indoor air below screen (latent heat)
$Q_{c\_sc}$	eqn. 3.104	W	heat transfer from canopy to screen (longwave radiation absorption)
$Q_F$	see eqns. 3.278, 3.281	–	weighing matrix for the Fisher information matrix
$Q_h$	eqn. 3.178	W	energy transport heat pump due to the water flow on the lower net side
$Q_{he}$	eqn. 3.189	W	energy transfer from heat exchanger to aquifer
$Q_{hp}$	eqn. 3.176	W	energy used by the heat pump
$Q_{in\_l}$	eqn. 3.160	W	energy transport due to the water flow into the lower net

▷ control input, \*external input, °state and #computed value

Continued on next page

Table B.1 List of parameters – continued from previous page

name	value	unit	contents
$Q_{in_u}$	eqn. 3.166	W	energy transport due to the water flow into the upper net
$Q_{in_{uc}}$	eqn. 3.183	W	energy transport due to the water flow into the upper cooling net
$Q_{l_a}$	eqn. 3.41	W	heat transfer from lower net to indoor air below screen (convection)
$Q_{l_c}$	eqn. 3.67	W	heat transfer from lower net to canopy (longwave radiation absorption)
$Q_{l_{ri}}$	eqn. 3.71	W	heat transfer from lower net to roof indoor side (longwave radiation absorption)
$Q_{l_s}$	eqn. 3.69	W	heat transfer from lower net to soil (longwave radiation absorption)
$Q_{l_{sc}}$	eqn. 3.74	W	heat transfer from lower net to screen (longwave radiation absorption)
$Q_{out_l}$	eqn. 3.161	W	energy transport due to the water flow out of the lower net
$Q_{out_u}$	eqn. 3.167	W	energy transport due to the water flow out of the upper net
$Q_{out_{uc}}$	eqn. 3.184	W	energy transport due to the water flow out of the upper cooling net
$Q_{rd_c}$	eqn. 3.124	W	heat absorbed by canopy (shortwave radiation absorption)
$Q_{rd_l}$	eqn. 3.122	W	heat absorbed by lower net (shortwave radiation absorption)
$Q_{rd_{ri}}$	eqn. 3.112	W	heat absorbed by roof indoor side (shortwave radiation absorption)
$Q_{rd_{ro}}$	eqn. 3.113	W	heat absorbed by roof outdoor side (shortwave radiation absorption)
$Q_{rd_s}$	eqn. 3.128	W	heat absorbed by soil (shortwave radiation absorption)
$Q_{rd_{sc}}$	eqn. 3.116	W	heat absorbed by screen (shortwave radiation absorption)
$Q_{rd_u}$	eqn. 3.118	W	heat absorbed by upper net (shortwave radiation absorption)
$Q_{rd_{uc}}$	eqn. 3.120	W	heat absorbed by upper cooling net (shortwave radiation absorption)
$Q_{ri_c}$	eqn. 3.98	W	heat transfer from roof indoor side to canopy (longwave radiation absorption)
$Q_{ri_{ro}}$	eqn. 3.133	W	heat transfer from roof indoor side to roof outdoor side (conduction)
$Q_{ri_{roL}}$	eqn. 3.100	W	heat transfer from roof indoor side to roof outdoor side (longwave radiation absorption)
$Q_{ro_o}$	eqn. 3.56	W	heat transfer from roof outdoor side to outdoor air (convection)
$Q_{ro_{sk}}$	eqn. 3.102	W	heat transfer from roof outdoor side to sky (longwave radiation absorption)
$Q_{s_c}$	eqn. 3.92	W	heat transfer from soil to canopy (longwave radiation absorption)

▷ control input, \*external input, °state and #computed value

Continued on next page

Table B.1 List of parameters – continued from previous page

name	value	unit	contents
$Q_{sc-a}$	eqn. 3.58	W	heat transfer from screen to indoor air below screen (convection)
$Q_{sc-as}$	eqn. 3.61	W	heat transfer from screen to indoor air above screen (convection)
$Q_{sc-ri}$	eqn. 3.106	W	heat transfer from screen to roof indoor side (longwave radiation absorption)
$Q_{s-ri}$	eqn. 3.94	W	heat transfer from soil to roof indoor side (longwave radiation absorption)
$Q_{s-s2}$	eqn. 3.131	W	heat transfer from upper to lower soil layer (conduction)
$Q_{s-sc}$	eqn. 3.96	W	heat transfer from soil to screen (longwave radiation absorption)
$Q_{u-a}$	eqn. 3.44	W	heat transfer from upper net to indoor air below screen (convection)
$Q_{u-c}$	eqn. 3.76	W	heat transfer from upper net to canopy (longwave radiation absorption)
$Q_{uc-a}$	eqn. 3.47	W	heat transfer from upper cooling net to indoor air below screen (convection)
$Q_{uc-c}$	eqn. 3.84	W	heat transfer from upper cooling net to canopy (longwave radiation absorption)
$Q_{uc-ri}$	eqn. 3.88	W	heat transfer from upper cooling net to roof indoor side (longwave radiation absorption)
$Q_{uc-s}$	eqn. 3.86	W	heat transfer from upper cooling net to soil (longwave radiation absorption)
$Q_{uc-sc}$	eqn. 3.90	W	heat transfer from upper cooling net to screen (longwave radiation absorption)
$Q_{u-ri}$	eqn. 3.80	W	heat transfer from upper net to roof indoor side (longwave radiation absorption)
$Q_{u-s}$	eqn. 3.78	W	heat transfer from upper net to soil (longwave radiation absorption)
$Q_{u-sc}$	eqn. 3.82	W	heat transfer from upper net to screen (longwave radiation absorption)
$Q_{used}$	eqn. 4.8	$W m^{-2}$	total amount of energy used per square meter greenhouse
$R_{b,CO_2}$	eqn. 2.39	$s m^{-1}$	leaf boundary layer resistance to diffusion of $CO_2$
$R_{b,H_2O}$	eqn. 2.8	$s m^{-1}$	leaf boundary layer resistance to diffusion of water
$R_{b,heat}$	eqn. 2.9	$s m^{-1}$	leaf boundary layer resistance to heat transport

▷ control input, \*external input, °state and #computed value

Continued on next page

Table B.1 List of parameters – continued from previous page

name	value	unit	contents
$r_c$	eqn. 3.23	$\text{kg}[\text{CO}_2] \text{ s}^{-1}$	dark respiration rate canopy
$R_{c\_CO2}$	eqn. 2.40	$\text{m}^{-1}$	leaf carboxylation resistance to diffusion of $\text{CO}_2$
$R_{CO2}$	see table 2.7	$\text{m}^{-1}$	leaf stomatal + boundary layer resistance to $\text{CO}_2$ diffusion
$R_{cut}$	2000	$\text{m}^{-1}$	leaf cuticular resistance
$r_D$	eqn. 2.11	$\text{mg}[\text{CO}_2] \text{ s}^{-1}$	dark respiration rate canopy
$r_{D\_uL}$	eqn. 2.31	$\mu\text{mol}[\text{CO}_2] \text{ m}^{-2} [\text{leaf}] \text{ s}^{-1}$	leaf dark respiration rate
$r_{D25\_uL}$	1.1	$\mu\text{mol}[\text{CO}_2] \text{ m}^{-2} [\text{leaf}] \text{ s}^{-1}$	dark respiration rate at 25°C
$R_g$	8.314	$\text{J mol}^{-1} \text{ K}^{-1}$	gas constant
$RH_a$	see eqn. 2.70	%	relative humidity indoor air below screen
$RH_{a\_max}$	85	%	upper bound relative humidity indoor air below screen
$RH_o$	see eqn. 2.70	%	relative humidity outdoor air
$RH_x$	eqn. 2.70	%	relative humidity at temperature $T_x$
$R_{min}$	82.003	$\text{m}^{-1}$	minimum internal crop resistance
$R_{s\_CO2}$	eqn. 2.38	$\text{m}^{-1}$	leaf stomatal resistance to diffusion of $\text{CO}_2$
$R_{s\_H2O}$	eqn. 2.3	$\text{m}^{-1}$	leaf stomatal resistance to diffusion of water
$R_{tot\_CO2}$	eqn. 2.37	$\text{m}^{-1}$	total resistance to diffusion of $\text{CO}_2$
$r_w$	$2.26 \cdot 10^6$	$\text{J kg}^{-1}$	heat of evaporation of water
$S$	710; see eqn. 2.34	$\text{J mol}^{-1} \text{ K}^{-1}$	constant for temperature dependency $J_{max}$
$\sin\beta$	eqn. 2.50	–	sine of solar elevation
$slo$	0.5	–	specific leaf orientation
$solarC$	eqn. 2.54	–	solar constant
$SOL_{hr}$	eqn. 2.51	h	solar time (time of the day)
$S_T$	°eqns. 3.14 and 2.43	K day	(state) temperature integral
$S_{T0}$	eqn. 2.45	K day	initial value temperature integral
$sun_{up}$	eqn. 2.56	{0,1}	parameter: sun up or down
$t$		s	time
$t_0$	see eqn. 3.275	s	initial time integration
$T_0$	273.15	–	conversion factor from °C to K
$T_{25}$	$T_0 + 25$	–	temperature of 25°C

<sup>▷</sup>control input, <sup>\*</sup>external input, <sup>°</sup>state and <sup>‡</sup>computed value

Continued on next page

Table B.1 List of parameters – continued from previous page

name	value	unit	contents
$T_a$	$^{\circ}\text{eqn. 3.5}$	K	(state) temperature indoor air below screen
$\hat{T}_a$	see eqn. 2.43	K	predicted temperature indoor air below screen
$\bar{T}_a$	see figure 4.28	K	average temperature (over a season) indoor air below screen
$T_{a\max}$	$T_0 + 24$ ( $\mathcal{PT}$ ); $T_0 + 10$ ( $TI$ )	K	upper bound temperature indoor air below screen
$T_{a\min}$	$T_0 + 16$ ( $\mathcal{PT}$ ); $T_0 + 34$ ( $TI$ )	K	lower bound temperature indoor air below screen
$T_{a\text{ref}}$	$T_0 + 19$	K	reference temperature for temperature integral
$T_{aq-c}$	$T_0 + 10$	K	desired temperature cold side aquifer
$T_{aq-c,hp}$	eqn. 3.180	K	temperature of the cooled aquifer water resulting from the heat pump
$T_{aq,h}$	$T_0 + 16$	K	desired temperature warm side aquifer
$T_{aq,h,he}$	eqn. 3.190	K	temperature of the heated aquifer water resulting from the heat exchanger
$T_{as}$	$^{\circ}\text{eqn. 3.6}$	K	(state) temperature indoor air above screen
$\bar{T}_{a,ts}$	see eqn. 2.45	K	average temperature (over $t_s = 1800$ s) indoor air below screen
$T_{boil}$	$T_0 + 90$	K	water temperature boiler
$T_c$	$^{\circ}\text{eqn. 3.7}$	K	(state) temperature crop
$T_{cond}$	$T_0 + 45$	K	water temperature condenser
$T_{cs}$	eqn. 3.256	K	water temperature cold side heat pump
$T_d$	eqn. 2.73	K	dewpoint temperature
$t_f$	$1\ n_{secs} = 86400$	s	control horizon optimal control
$T_{hs}$	eqn. 3.255	K	water temperature warm side heat pump
$T_{in,boil}$	eqn. 3.174	K	water temperature entering the boiler
$T_{in,he}$	eqn. 3.188	K	water temperature entering the heat exchanger
$T_{in,he\min}$	$T_{aq,h}$	K	minimum water temperature entering the heat exchanger
$T_{in,hp}$	eqn. 3.175	K	water temperature entering the heat pump
$T_{in,hp\max}$	$T_0 + 30.1$	K	maximum water temperature entering the heat pump
$T_{in,l}$	eqn. 3.163	K	water temperature entering the lower net
$T_{in,u}$	eqn. 3.169	K	water temperature entering the upper net
$T_{in,uc}$	eqn. 3.186	K	water temperature entering the upper cooling net

$\triangleright$  control input,  $\ast$  external input,  $^{\circ}$ state and  $\#$ computed value

Continued on next page

Table B.1 List of parameters – continued from previous page

name	value	unit	contents
$T_l$	<sup>o</sup> eqn. 3.9	K	(state) temperature lower heating net
$T_{l\_bypass}$	eqn. 3.164	K	water temperature lower net bypass
$T_{o\_high}$	$T_0 + 12^\#$	K	high boundary value for switch screen condition $C_{sc.T_o}$
$T_{o\_low}$	$T_0 + 8^\#$	K	low boundary value for switch screen condition $C_{sc.T_o}$
$T_{o\_scr}$	$T_0 + 10$	K	mean value for switch screen condition $C_{sc.T_o}$
$T_{out\_he}$	eqn. 3.191	K	water temperature leaving the heat exchanger
$T_{out\_hp}$	eqn. 3.181	K	water temperature leaving the heat pump
$T_{out\_l}$	eqn. 3.165	K	water temperature leaving the lower net
$T_{out\_u}$	eqn. 3.171	K	water temperature leaving the upper net
$T_{out\_uc}$	eqn. 3.187	K	water temperature leaving the upper cooling net
$T_o$	*	K	(external input) temperature outdoor air
$T_{o\_w}$	*	K	(external input) wet bulb temperature outdoor air
$t_p$	$5 n_{secs} = 432000$	s	days in the past for temperature integral
$T_{ri}$	<sup>o</sup> eqn. 3.12	K	(state) temperature roof indoor side
$T_{ro}$	eqn. 3.242	K	temperature roof outdoor side
$t_s$	1800	s	sampling interval receding horizon controller
$T_s$	<sup>o</sup> eqn. 3.8	K	(state) temperature soil (upper layer)
$T_{s2}$	eqn. 3.132	K	temperature soil (subsoil layer)
$T_{sc}$	<sup>o</sup> eqn. 3.13	K	(state) temperature thermal screen
$T_{sk}$	*	K	(external input) temperature sky
$t_{s\_u}$	1800	s	time interval for the optimal control inputs
$T_u$	<sup>o</sup> eqn. 3.10	K	(state) temperature upper heating net
$T_{u\_bypass}$	eqn. 3.170	K	water temperature upper net bypass
$T_{uc}$	<sup>o</sup> eqn. 3.11	K	(state) temperature upper cooling net
$T_{x\_w}$	see §2.C.2	K	wet bulb temperature of object $x$
$T_x$	see §2.C	K	temperature of object $x$
$u$	$\triangleright$	–	control inputs
$u_0$		–	initial values control inputs before optimization
$u^*$	eqn. 4.11	–	control input trajectories that minimize the cost function value $J$

<sup>o</sup>control input, \*external input, <sup>o</sup>state and <sup>#</sup>computed value

Continued on next page

Table B.1 List of parameters – continued from previous page

name	value	unit	contents
$u_{grad}^*$	see eqn. 4.11	–	control input trajectories $u^*$ with the conjugate gradient method
$u_{grid}^*$	see eqn. 4.11	–	control input trajectories $u^*$ with the grid search method
$v$	*	–	external inputs
$\tilde{v}$		–	expected external inputs
$v_a$	0.09	$\text{m s}^{-1}$	wind speed in the greenhouse
$V_a$	$14112^\#; A_s \cdot h_g$	$\text{m}^3$	volume indoor air below screen
$v_{a-as}$	$0.05; \text{eqn. 3.146}$	$\text{m s}^{-1}$	air exchange rate between air below and above screen
$V_{as}$	$1267.03^\#; A_s \cdot 0.5 (h_n - h_g)$	$\text{m}^3$	volume indoor air above screen
$V_c$	$28.22^\#; LAI \cdot A_s \cdot d_c$	$\text{m}^3$	volume canopy
$V_{C \max}$	eqn. 2.42	$\mu\text{mol}[\text{CO}_2] \text{m}^{-2} [\text{leaf}] \text{s}^{-1}$	maximum carboxylation rate
$V_{C \max 25}$	$\rho_{Chl} \cdot k_C \cdot E_t$	$\mu\text{mol}[\text{CO}_2] \text{m}^{-2} [\text{leaf}] \text{s}^{-1}$	maximum carboxylation rate at 25°C
$V_l$	$7.83^\#; n_s \cdot n_l \cdot l_l \cdot 0.25 \pi \cdot d_l^2$	$\text{m}^3$	volume lower net
$v_o$	*	$\text{m s}^{-1}$	(external input) wind speed outdoor
$V_{O \max}$	see eqn. 2.27	$\mu\text{mol}[\text{CO}_2] \text{m}^{-2} [\text{leaf}] \text{s}^{-1}$	maximum oxygenation rate
$vp_{boil}$	$\triangleright$	[0,1]	(control input) valve position boiler (conventional greenhouse)
$vp_{CO2}$	$\triangleright$	[0,1]	(control input) valve position CO <sub>2</sub> supply
$vp_h$	$\triangleright$ see §4.3.6.1	[-1,2]	(control input) combined valve position heating and cooling; combination of $vp_{he}^*$ , $vp_{hp}^*$ , $vp_l$ and $vp_u$
$vp_{he}$	eqn. 3.192	[0,1]	valve position heat exchanger, corrected range
$vp_{he}^*$	$\triangleright$	[0,1]	(control input) valve position heat exchanger
$vp_{he \min}$	0.43	[0,1]	minimum valve position heat exchanger
$vp_{hp}$	eqn. 3.182	[0,1]	valve position heat pump, corrected range
$vp_{hp}^*$	$\triangleright$	[0,1]	(control input) valve position heat pump
$vp_{hp \min}$	0.57	[0,1]	minimum valve position heat pump
$vp_l$	$\triangleright$	[0,1]	(control input) valve position lower heating net
$vp_u$	$\triangleright$	[0,1]	(control input) valve position upper heating net
$V_r$	$13.53^\#; A_r \cdot d_r$	$\text{m}^3$	volume roof (one layer of glass)
$V_s$	$2038.40^\#; A_s \cdot d_s$	$\text{m}^3$	volume soil layer
$V_{sc}$	$1.57^\#; A_{sc} \cdot d_{sc}$	$\text{m}^3$	volume screen

 $\triangleright$  control input, \* external input,  $^\circ$  state and  $^\#$  computed value

Continued on next page

Table B.1 List of parameters – continued from previous page

name	value	unit	contents
$V_u$	$2.36^\ddagger$ ; $n_s n_u l_u \cdot 0.25 \pi d_u^2$	$\text{m}^3$	volume upper net
$V_{uc}$	$7.83^\ddagger$ ; $n_s n_{uc} l_{uc} \cdot 0.25 \pi d_{uc}^2$	$\text{m}^3$	volume upper cooling net
$W$	$^\circ \text{eqn. 3.15}$	$\text{kg}[\text{b.m.}] \text{m}^{-2}[\text{soil}]$	(state) total biomass
$W_g$	$\{0.2778, 0.4444, 0.2778\}$	–	weight factor for three-point Gaussian integration
$w_s$	4	$\text{m}$	width of the greenhouse span
$x$	$^\circ$	–	states
$X$	see eqn. 1.2	–	value for smoothing function $\Sigma$
$x_0$		–	initial values states
$x_\theta$	eqn. 3.276	–	trajectories sensitivity
$\tilde{x}_\theta$	eqn. 3.277	–	trajectories relative sensitivity
$X_g$	$\{0.1127, 0.5, 0.8873\}$	–	relative depth of the canopy for three-point Gaussian integration
$x_{meas}$	see eqn. 3.200	–	measured state values
$x_{\min}$	see eqn. 4.7, table 4.1	–	lower bound variable $x$ for penalty function $L$
$x_{\max}$	see eqn. 4.7, table 4.1	–	upper bound variable $x$ for penalty function $L$
$X_s$	see eqn. 1.2	–	switching value for smoothing function $\Sigma$
$x_{sim}$	see eqn. 3.200	–	simulated state values
$y$		–	outputs
$y^*$	see eqn. 4.11	–	output trajectories resulting from control inputs $u^*$
$y_{grad}^*$	see eqn. 4.11	–	output trajectories resulting from control inputs $u_{grad}^*$ with the conjugate gradient method
$y_{grid}^*$	see eqn. 4.11	–	output trajectories resulting from control inputs $u_{grid}^*$ with the grid search method

$\ddagger$  control input,  $^*$  external input,  $^\circ$  state and  $^\#$  computed value



Dit onderzoek werd mede gefinancierd door het programma 'Ecologie, Economie en Technologie' (EET) van de ministeries van Economische Zaken (EZ), Onderwijs, Cultuur en Wetenschappen (OC&W) en Volksgezondheid, Ruimtelijk Ordening en Milieu (VROM) onder projectnummer EETK96084 (Zonnekas).